

How long will it last?

An assessment of the useful life of plastics for the
encapsulation of an alkaline electrolyser

Xiao Xu Zheng



Zero Emission Fuels

This thesis is confidential

This thesis is submitted for the degree of Master of Science

How long will it last?

An assessment of the useful life of plastics for the
encapsulation of an alkaline electrolyser

by

Xiao Xu Zheng

This thesis is submitted in partial fulfilment of the requirements for the degree of

Master of Science

in Materials Science and Engineering

at the Delft University of Technology,

to be defended publicly on Wednesday November 27th, 2019 at 10:00 AM.

Student number: 4715551

Project duration: January 1st, 2019 – November 27th, 2019

Daily supervisor: Ir. J. Van Kranendonk, ZEF B.V.

Thesis committee: Dr. A. J. Böttger, TU Delft 3ME, chair

Dr. M. A. Bessa TU Delft 3ME

Prof. dr. ir. K. M. B. Jansen, TU Delft IO

Dr. S. J. Garcia, TU Delft L&R

Prof. dr. ir. J. Van Turnhout, TU Delft 3ME

This thesis is confidential and cannot be made public until November 27th, 2019.

An electronic version of this thesis is available at <http://repository.tudelft.nl/>.



Abstract

Alkaline water electrolysis will become increasingly important for supplying the world with sufficient renewable energy, and with raw material for the chemical and pharmaceutical industry. Zero Emission Fuels B.V. (ZEF), a technology start-up based in the Netherlands, is developing a small scale alkaline electrolysis cell (AEC), which is integrated in a methanol producing micro-plant. The challenge of this project is to look into the use of polymers for the encapsulation of the ZEF AEC. The conditions of the ZEF AEC are not to be neglected. The system will run in a 30wt% KOH solution at a temperature of 90 °C and a pressure of 50 bar. Not many polymers will be able to withstand these conditions for a desired lifetime of 20 years.

Using CES EduPack, a selection of 30 potentially suitable polymers has been made, from which high density polyethylene (HDPE), 40% glass-reinforced polyphenylene sulfide (PPS-40%gf) and polysulfone (PSU) are further investigated. Based on a literature review and a simple KOH ageing test, HDPE is found unsuitable for application in the ZEF AEC. PPS-40%gf and PSU have been subjected to durability testing for a range of different conditions involving a variety of KOH concentrations (15, 30 and 45wt%), and two oxygen partial pressures (O_2 at 5 bar and air with $pO_2=20\%$) at different temperatures (90, 120 and 170 °C). The purpose of the ageing experiments is to give a better understanding of the effect of these parameters on the structure and integrity of the polymer; and to eventually be able to acquire a lifetime prediction. Extensive characterisation of the exposed samples has been carried out using different techniques, including weight measurement, tensile testing, DMA, creep-recovery testing, DSC, FTIR, XRD and SEM.

After 12 weeks of ageing, it is found that glass-filled polymers are unsuitable for application in a strong alkaline solution at elevated temperatures, due to the dissolution of the glass fibres, which leads to a reduction in mechanical and barrier properties. However, the PPS matrix and PSU are found to be resistant to thermo-oxidative and chemical degradation in the tested ageing conditions. Only subtle changes in mechanical, visco-elastic and thermal behaviour are observed, which can be assigned to the effects of physical ageing. Due to the undesirable brittle nature of PPS, it can be concluded that PSU is the most promising candidate for the long-term application in alkaline electrolysis.

Preface

Before you lies the thesis *How long will it last? An assessment of the useful life of plastics for the encapsulation of an alkaline electrolyser*. This study has been conducted in cooperation with Zero Emission Fuels B.V. (ZEF), a TU Delft technology start-up, which is in the process of radically changing the energy market, by introducing a fuel solely produced by renewable energy and carbon captured directly from the atmosphere. This thesis has been written in order to fulfil the graduation requirements of the masters programme *Materials Science and Engineering* at Delft University of Technology.

The objective of this project is to assess the suitability of polymers for the purpose of encapsulation of the ZEF alkaline electrolysis cell, which is operating in a 30wt% KOH solution at 90 °C and 50 bar pressure. The project includes assessing the mechanisms of material failure due to these conditions; a material selection process in order to select the most promising candidates; and an accelerated ageing study, in which the mechanical, thermal and visco-elastic behaviour of the polymers in an alkaline and oxidative environment are investigated.

I would like to thank my supervisors, Dr. A. J. Böttger, Prof.dr.ir J. Van Turnhout, Prof.dr.ir. K. M. B Jansen and Jan van Kranendonk, for their excellent guidance and support during this process. I also wish to thank everyone from ZEF for making this possible, in particular the founders Ulrich Starke, Jan van Kranendonk and Hessel Jongebreur. Moreover, I would like to thank Michel van den Brink, Prof.dr.ir. K. M. B Jansen, Dr. S. Garcia, Dr. S. Ghodrat, Nico Geerlofs, Ruud Hendrikx and Sander van Asperen for allowing me to use their characterisation equipment, ovens and labspace. Without it, I would not have been able to present any results. Finally, I would like to thank my friends and family. You kept me motivated, if I ever lost interest.

With that said, I hope you enjoy your reading.

Xiao Xu Zheng
Delft, November 15th, 2019

Contents

1	Introduction	1
1.1	Water electrolysis for the energy transition	1
1.2	The role of Zero Emission Fuels B.V. (ZEF)	2
1.3	The encapsulation of the alkaline electrolysis cell	4
1.4	The reliability and safety of the electrolyser	7
1.5	Objectives	8
1.6	Content of the report	9
2	Literature review	11
2.1	An introduction to polymers	11
2.2	Polymer performance parameters	13
2.3	Visco-elastic behaviour of polymers	15
2.3.1	Time-temperature superposition	16
2.3.2	Frequency-temperature superposition	17
2.4	Degradation mechanisms	18
2.4.1	Thermo-oxidative degradation	19
2.4.2	Chemical degradation	22
2.5	The reaction kinetics	23
3	Material selection	25
3.1	Preliminary screening of materials	25
3.2	Background on HDPE, PPS and PSU	31
3.2.1	High density polyethylene (HDPE)	31
3.2.2	Polyphenylene sulfide (PPS) reinforced with 40% glass fibres	32
3.2.3	Polysulfone (PSU)	34
4	Methodology	37
4.1	Samples	37
4.2	Ageing procedures	38
4.2.1	Ageing conditions	39

4.2.2	Ageing set up	41
4.3	Equipment and measurement procedures	44
4.3.1	Weight measurements	46
4.3.2	Tensile testing	46
4.3.3	Dynamic mechanical analysis (DMA)	47
4.3.4	Creep-recovery testing	47
4.3.5	Differential scanning calorimetry (DSC)	48
4.3.6	Fourier-transform infrared spectroscopy (FTIR)	48
4.3.7	X-ray diffraction (XRD)	49
4.3.8	Scanning electron microscopy (SEM)	49
5	Results and discussion PPS-40%gf	51
5.1	PPS-40%gf aged in oxygen	51
5.1.1	Tensile tests (PPS-40%gf; oxygen)	51
5.1.2	DMA tests (PPS-40%gf; oxygen)	55
5.1.3	FTIR (PPS-40%gf; oxygen)	59
5.1.4	Other measurement techniques (PPS-40%gf; oxygen)	62
5.2	Discussion: what happens to PPS-40%gf when aged in an oxygen environment?	65
5.3	PPS-40%gf aged in KOH	70
5.3.1	Tensile tests (PPS-40%gf; KOH)	70
5.3.2	DMA tests (PPS-40%gf; KOH)	73
5.3.3	SEM (PPS-40%gf; KOH)	77
5.3.4	Other measurement techniques (PPS-40%gf; KOH)	80
5.4	Discussion: what happens to PPS-40%gf when aged in KOH?	84
5.5	Concluding remarks	85
6	Results and discussion PSU	87
6.1	PSU aged in oxygen	87
6.1.1	Tensile tests (PSU; oxygen)	87
6.1.2	DMA tests (PSU; oxygen)	91
6.1.3	DSC tests (PSU; oxygen)	94
6.1.4	Creep-recovery testing (PSU; oxygen)	95
6.1.5	FTIR (PSU; oxygen)	96
6.1.6	Other measurement techniques (PSU; oxygen)	96
6.2	Discussion: what happens to PSU when aged in an oxygen environment?	99
6.3	PSU aged in KOH	101
6.3.1	Tensile tests (PSU; KOH)	101
6.3.2	Creep-recovery testing (PSU; KOH)	104

6.3.3	FTIR (PSU; KOH)	105
6.3.4	Other measurement techniques (PSU; KOH)	106
6.4	Discussion: what happens to PSU when aged in KOH?	106
6.5	Concluding remarks	107
7	Extrapolation of the results	109
7.1	Predicting the creep compliance in 20 years (PSU)	109
7.2	Extrapolation of the mechanical results (PSU)	117
7.3	Predicting the storage modulus in 20 years (PPS-40%gf)	119
7.4	Sources of errors	121
8	Conclusions and recommendations	123
8.1	Conclusions	123
8.2	Recommendations	124
8.2.1	Regarding the experiments	124
8.2.2	Other polymers	124
8.2.3	Other reinforcements	124
8.2.4	Further improvement of the material	125
8.2.5	Other degradation mechanisms	125
8.2.6	Testing the product/prototype	126
	Appendices	135
A	Datasheets PPS-40%gf and PSU	137
B	Safety assessment: ageing in pure oxygen and KOH	143
B.1	Determining the worst case scenario	143
B.2	Assessing the setup	146
B.3	Evaluating the ignition mechanisms	147
B.4	Safety assessment: KOH	147
C	Additional results PPS-40%gf	149
C.1	Additional Results PPS-40% exposed to oxygen	149
C.2	Additional Results PPS-40% exposed to KOH	162
C.3	Correction of stress-strain curves	172
C.4	Control samples	173
D	Additional results PSU	175
D.1	Additional Results PSU exposed to oxygen	175
D.2	Additional Results PSU exposed to KOH	185

D.3 PSU unaged and after 12 weeks	190
---	-----

Nomenclature

Symbols

a_T	Shift-factor
E_a	Activation energy
pO_2	Oxygen partial pressure
T_g	Glass transition temperature
T_m	Melting temperature
R	Universal gas constant

Polymer abbreviations

ABS	Acrylonitrile butadiene styrene
COC	Cyclic olefin copolymer
CPVC	Chlorinated polyvinyl chloride
ECTFE	Ethylene Chlorotrifluoroethylene
ETFE	Ethylene tetrafluoroethylene
FEP	Fluorinated ethylene propylene
HDPE	High density polyethylene
LCP	Liquid-crystal polymers
MF	Melamine formaldehyde
PA	Polyamide
PCTFE	Polychlorotrifluoroethylene

PE	Polyethylene
PEBA	Polyether block amide
PEEK	Polyether ether ketone
PEI	Polyethylenimine
PEKK	Polyetherketoneketone
PEN	Polyethylene naphthalate
PESU	Polyethersulfone
PFA	Perfluoroalkoxy alkanes
PMP	Polymethylpentene
POM	Polyoxymethylene
PP	Polypropylene
PPE	Polyphenyl ether
PPS	Polyphenyl sulfide
PPSU	Polyphenylsulfone
PSU	Polysulfone
PTFE	Polytetrafluoroethylene
PVDF	Polyvinylidene fluoride
SMA	Styrene maleic anhydride
TPO	Thermoplastic Polyolefin Elastomer
VE	Vinyl ester

Chemical abbreviations

CO ₂	Carbon dioxide
H ₂	Hydrogen
KOH	Potassium hydroxide
NaOH	Sodium hydroxide

O ₂	Oxygen
OH ⁻	Hydroxide ion

Characterisation techniques

DMA	Dynamic mechanical analysis
DSC	Differential scanning calorimetry
EDS	Energy-dispersive X-ray spectroscopy
FTIR	Fourier transform infrared spectroscopy
SEM	Scanning electron microscopy
XRD	X-ray diffraction

Other abbreviations

AEC	Alkaline electrolysis cell
KWW	Kohlrausch–Williams–Watts
TTS	Time–temperature superposition
UTS	Ultimate tensile strength
WLF	Williams–Landel–Ferry
ZEF	Zero Emission Fuels

List of Figures

1.1	Block scheme of the ZEF micro-plant	3
1.2	Visual of the ZEF micro-plant	3
1.3	Schematic of the principles of alkaline water electrolysis	5
1.4	Overview of the structure of this thesis	10
2.1	The structure of polymers	12
2.2	Visco-elastic material properties	15
2.3	Time-temperature equivalence principle	17
2.4	Pathway of the thermo-oxidation reaction	20
3.1	Material selection chart	29
3.2	Results of HDPE exposed to a 30wt% KOH solution at 90 °C	33
3.3	The formation of oxidative cross-links in PPS	34
4.1	Dimensions of the dogbone samples	37
4.2	Setup of pressurised oxygen at elevated temperatures	42
4.3	Setup of samples in a KOH solution	42
4.4	Schematic of the oxygen setup	43
4.5	Procedure of the creep-recovery tests	48
5.1	Stress-strain curves of PPS-40%gf exposed to O ₂ at 5 bar and 90 °C	52
5.2	Young's modulus over time of PPS-40%gf exposed to oxygen	53
5.3	UTS over time of PPS-40%gf exposed to oxygen	53
5.4	Strain at UTS over time of PPS-40%gf exposed to oxygen	54
5.5	Material toughness over time of PPS-40%gf exposed to oxygen	54
5.6	Storage and loss modulus of PPS-40%gf aged in O ₂ at 5 bar and 90 °C	56
5.7	Storage modulus over time of PPS-40%gf exposed to oxygen	57
5.8	Loss modulus and T _g versus time of PPS-40%gf exposed to oxygen	58
5.9	Labelled FTIR spectrum of unaged PPS-40wt%gf	60
5.10	FTIR spectra of PPS-40wt%gf aged in O ₂ at 5 bar and 120 °C	61
5.11	Stacked FTIR spectra of PPS-40wt%gf aged in O ₂ at 5 bar and 120 °C	61

5.12	XRD pattern of aged PPS-40%gf compared to unaged PPS-40%gf	63
5.13	DSC analysis of aged and unaged PPS-40%gf	64
5.14	Schematic of the change in enthalpy after isothermal ageing	67
5.15	Relaxation enthalpy in DSC curve	68
5.16	Stress-strain curves of PPS-40%gf exposed to 30wt% KOH at 90 °C	70
5.17	Young's modulus over time of PPS-40%gf exposed to KOH	71
5.18	UTS over time of PPS-40%gf exposed to KOH	71
5.19	Strain at UTS over time of PPS-40%gf exposed to KOH	72
5.20	Material toughness over time of PPS-40%gf exposed to KOH	72
5.21	DMA curves of PPS-40%gf aged in KOH 30wt% at 90 °C	74
5.22	Storage modulus over time of PPS-40%gf exposed to KOH	75
5.23	Loss modulus and T_g over time of PPS-40%gf exposed to KOH	76
5.24	SEM images of the fracture surface of PPS-40%gf exposed to KOH	78
5.25	SEM 300x magnification of the fracture surface of PPS-40%gf exposed to KOH	79
5.26	Weight over time of PPS-40%gf exposed to KOH	80
5.27	FTIR spectra of PPS-40wt%gf aged in KOH 30wt% at 90 °C	81
5.28	Stacked FTIR spectra of PPS-40wt%gf aged in KOH 30wt% at 90 °C	81
5.29	XRD pattern of PPS-40%gf exposed to KOH 30wt% 90 °C	83
6.1	Stress-strain curves of PSU exposed to O ₂ at 5 bar and 90 °C	88
6.2	Young's modulus over time of PSU exposed to oxygen	88
6.3	UTS over time of PSU exposed to oxygen	89
6.4	Strain at UTS over time of PSU exposed to oxygen	89
6.5	Material toughness over time of PSU exposed to oxygen	90
6.6	Storage and loss modulus of PSU	92
6.7	Tan delta curve of PSU	93
6.8	Image of a PSU sample after performing a DMA test	93
6.9	DSC analysis of PSU exposed to oxygen	94
6.10	Creep compliance of unaged and aged PSU	95
6.11	Labelled FTIR spectrum of unaged PSU	97
6.12	FTIR spectra of PSU aged in O ₂ at 5 bar and 120 °C	98
6.13	Stacked FTIR spectra of PSU aged in O ₂ at 5 bar and 120 °C	98
6.14	Stress-strain curves of PSU exposed to 30wt% KOH at 90 °C	101
6.15	Young's modulus over time of PSU exposed to KOH	102
6.16	UTS over time of PSU exposed to KOH	102
6.17	Strain at UTS over time of PSU exposed to KOH	103

6.18	Material toughness over time of PSU exposed to KOH	103
6.19	Creep compliance of aged and unaged PSU	104
6.20	FTIR spectra of PSU aged in KOH 30wt% at 90 °C	105
6.21	Stacked FTIR spectra of PSU aged in KOH 30wt% at 90 °C	105
6.22	Weight over time of PSU exposed to KOH	106
7.1	Creep compliance master curve and shift curve for unaged PSU	111
7.2	Creep compliance master curve of unaged PSU and a KWW fit	113
7.3	Creep compliance curve versus the stages of creep	114
7.4	TTS of creep curves of aged PSU samples	115
7.5	Comparison master and shift curves of aged PSU	116
7.6	Time-temperature superposition of strain at UTS results of PSU	118
7.7	Master curves and shift curves of PPS-40%gf aged in oxygen.	120
C.1	Weight over time of PPS-40%gf exposed to oxygen	149
C.2	Stress-strain curves of PPS-40%gf exposed oxygen	150
C.3	DMA frequency sweep of unaged PPS-40%gf	151
C.4	DMA curves of PPS-40%gf aged in air at 90 °C	152
C.5	DMA curves of PPS-40%gf aged in air at 120 °C	153
C.6	DMA curves of PPS-40%gf aged in oxygen at 5 bar and 90 °C	154
C.7	DMA curves of PPS-40%gf aged in oxygen at 5 bar and 120 °C	155
C.8	XRD pattern of unaged PPS-40%gf	156
C.9	XRD pattern of 4 different samples of unaged PPS-40%gf	157
C.10	SEM images of the fracture surface of unaged and aged PPS-40%gf	158
C.11	SEM 300x magnification of the fracture surface of unaged and aged PPS-40%gf	159
C.12	Weight over time of PPS-40%gf exposed to KOH	162
C.13	Stress-strain curves of PPS-40%gf exposed to KOH	163
C.14	DMA curves of PPS-40%gf aged in KOH 15wt% at 90 °C	164
C.15	DMA curves of PPS-40%gf aged in KOH 30wt% at 90 °C	165
C.16	DMA curves of PPS-40%gf aged in KOH 45wt% at 90 °C	166
C.17	XRD pattern of aged and unaged PPS-40%gf	167
C.18	XRD pattern of PPS-40%gf exposed to KOH	168
C.19	SEM image of a single broken fibre on the fracture surface of PPS-40%gf exposed to KOH	169
C.20	Corrected stress-strain curve of PPS-40%gf	172
C.21	Stress-strain curves of PPS-40%gf unaged and after 12 weeks of ambient conditions	173
C.22	DMA curves of unaged PPS-40%gf	174

D.1	Weight over time of PSU exposed to oxygen	175
D.2	Stress-strain curves of PSU exposed to oxygen	176
D.3	Stress-strain curves of PSU exposed to air	177
D.4	DSC curves of PSU exposed to oxygen	178
D.5	XRD pattern pf unaged PSU	179
D.6	XRD pattern of 4 different unaged PSU samples	180
D.7	XRD pattern of PSU exposed to air at 170 °C	181
D.8	SEM images of the surface of PSU	182
D.9	Weight over time of PSU exposed to KOH	185
D.10	Stress-strain curves of PSU exposed to 15, 30 and 45wt% KOH at 90 °C . .	186
D.11	DSC curves of PSU exposed to KOH	187
D.12	SEM 600x magnification of the surface of PSU exposed to KOH	187
D.13	Stress-strain curves of unaged PSU	190

List of Tables

1.1	ZEF targets for the AEC	7
3.1	Material performance parameters of the ZEF AEC	25
3.2	Material properties of HDPE, PPS-40%gf and PSU	30
3.4	Molecular formula of HDPE, PPS-40%gf and PSU	31
4.1	Overview of the ageing conditions	40
4.2	Measured KOH concentrations during ageing time	41
4.3	Overview of the characterisation techniques used	45
4.4	Weights of unaged PPS-40%gf and PSU samples	46
5.1	Results of T_g of PPS-40%gf exposed to oxygen	55
5.2	ATR-FTIR peaks expected for PPS-40%gf	59
5.3	Results of PPS-40%gf exposed to oxygen	65
5.4	Results of T_g of PPS-40%gf exposed to KOH	73
5.5	Results of PPS-40%gf exposed to KOH	84
6.1	ATR-FTIR peaks expected for PSU	96
6.2	Results of PSU exposed to oxygen	100
6.3	Results of PSU exposed to KOH	107
B.1	Energy release and pressure after deflagration reaction	146

Chapter 1

Introduction

1.1 Water electrolysis for the energy transition

After an era of using fossil fuels as our main source of energy and resource for the chemical industry, a new era is about to start in which renewable energy and resources will play a major role. Water electrolysis will become increasingly important for supplying the world with sufficient renewable energy and raw material for the chemical and pharmaceutical industry. Water electrolysis is the endothermic reaction of splitting water into oxygen and more importantly hydrogen gas.

Hydrogen gas can fulfil many functions relevant to the energy supply system. Hydrogen is an energy carrier, which can supply energy by the inverse reaction of electrolysis in fuel cells. This is very relevant in light of the fluctuating supply of solar and wind energy. Apart from being an energy carrier, hydrogen has many other uses in the chemical industry. Via the Haber-Bosch process, hydrogen is used to make ammonia for agricultural fertilisers [2]. Furthermore, hydrogen is crucial for producing carbon based fuels. Hydrogenation of carbon dioxide results in methanol and hydrocarbon derivatives, which can be used as fuel or as raw material for the production of plastics or pharmaceuticals. This reaction is described via a modified Fischer-Tropsch synthesis process [69].

Hydrogen production by electrolytical water splitting is a technique which has been known since the year 1800, when it was discovered by Nicholson and Carlisle [44]. By 1902, more than 400 electrolyzers were in operation, and by 1948, the first pressurised industrial electrolyser was built [44]. Yet, in 2014, only 1% of the global hydrogen production is produced by water electrolysis [73].

Currently, the cheapest and most common way of producing hydrogen is via steam reforming of natural gas. Steam reforming involves high temperatures of 700 to 1100 °C in which steam reacts with methane, in the presence of a metal-based catalyst, to yield hydrogen, carbon monoxide and carbon dioxide [73]. This process involves the use of

unsustainable fossil fuels and emits carbon dioxide, which is harmful for the environment. Therefore, cleaner methods of extracting hydrogen gas are being developed such as different approaches to water electrolysis, which has the advantage of being able to produce hydrogen gas using renewable energy only.

At present, there are three main types of water electrolysis. These are alkaline electrolysis, membrane electrolysis and high temperature electrolysis [74]. Alkaline electrolysis uses an alkaline solution, where the charge carrier is the hydroxide ion. In membrane electrolysis the charge is carried by protons through an acidic membrane. High temperature electrolysis or solid oxide electrolysis operates at much higher temperatures of up to 1000 °C whereby the oxide ion is the charge carrier [73].

1.2 The role of Zero Emission Fuels B.V. (ZEF)

This project is in collaboration with Zero Emission Fuels B.V. (ZEF), a technology start-up located in Delft, The Netherlands. ZEF is developing a small scale alkaline electrolysis unit as part of a larger system. This larger system represents a modular micro-plant which produces methanol from carbon dioxide and hydrogen (see Figure 1.1). The carbon dioxide is captured from the atmosphere using a direct air capture system and subsequently compressed to 50 bar. The hydrogen gas is obtained from the alkaline electrolysis cell which is connected to and powered by a solar panel. Finally, methanol is produced in the methanol synthesis reactor at elevated pressure and temperature and in the presence of certain catalysts. Each of these subsystems will together form an integrated, self-sustaining system, which is able to independently produce methanol.

What makes the ZEF approach special is that they are developing a chemical factory on a small scale, *i.e.* the size of a boiler. This micro factory is powered by a solar photovoltaic panel and is able to function fully off the grid. The small scale allows the system to be more flexible with regard to the fluctuating renewable energy input. Figure 1.2 shows a visual of the ZEF micro-plant farm.

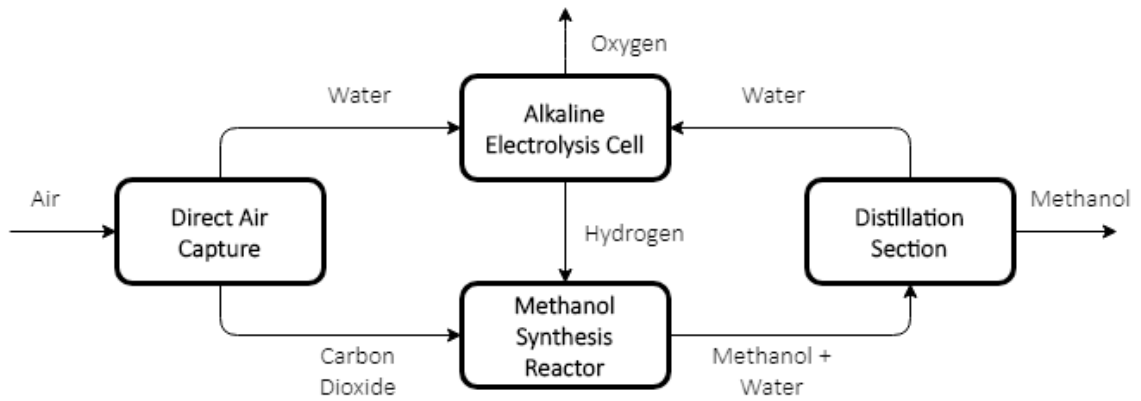


Figure 1.1: A block scheme of the ZEF micro-plant. The integration of all subsystems is self-sustaining and is powered by solar photo-voltaic panels. It functions completely off the grid. Image by courtesy of Daniel van Laake.



Figure 1.2: A visual of the ZEF micro-plant relative to the size of a human person. The micro-plant farm will consist of many rows of multiple ZEF micro-plant units (40,000 units). Image by courtesy of David van Nunen.

1.3 The encapsulation of the alkaline electrolysis cell

The topic of this thesis is the material choice for the container of the ZEF alkaline electrolysis cell (AEC), which also includes small storage compartments for the produced gases. This is challenging from a materials science perspective, since the AEC contains some of the most dangerous and corrosive substances, namely hydrogen gas (H_2), oxygen gas (O_2) and a 30wt% potassium hydroxide (KOH) solution in hostile conditions such as a pressure of 50 bar and a temperature of 90 °C. These substances have to be contained inside the electrolyser, whilst the hydrogen and oxygen gas are being kept separated.

The conditions of a pressure of 50 bar and a temperature of 90 °C stem directly from the integration of the micro-plant. The AEC produces hydrogen at a pressure of 50 bar, which is required for the methanol synthesis reactor. Having an alkaline electrolyser at this pressure eliminates the need for a compressor making the system more efficient. Furthermore, due to the reaction not being 100% effective, heat losses are generated which heat up the system. This is beneficial since the electrolysis reaction is more efficient at elevated temperatures [9]. In fact, at 2500 °C, electrical input is unnecessary since water breaks down to hydrogen and oxygen through thermolysis [9]. The AEC is capped to a temperature of 90 °C. The excess heat is used in other parts of the integrated ZEF micro-plant, such as for the desorption of carbon dioxide in the direct air-capture unit and the distillation system of methanol.

It is important to note that these operation conditions cannot be continuously maintained. The AEC is not capable of producing a continuous supply of hydrogen gas, since the AEC is directly connected and powered by a photo-voltaic panel and operates completely off the grid. During the day the solar panel provides the electricity for the reaction to take place and hydrogen is produced, whilst during the night there will be no electricity input and the reaction will stop. This means the temperature of the electrolyser will drop from 90 °C to the ambient environment temperature. The same occurs for the pressure, which will drop from 50 bar to 30-40 bar during the night.

Since ZEF has chosen to work with alkaline electrolysis, other ways of water splitting, such as membrane electrolysis and solid oxide electrolysis, are not further considered in this thesis. An alkaline electrolysis cell is characterised by the setup of two electrodes in an alkaline electrolyte solution, which is either a potassium hydroxide (KOH) or a sodium hydroxide (NaOH) solution. The electrodes are separated by a hydrophilic membrane which separates the product gases (hydrogen and oxygen) but allows the transportation of hydroxide ions [72]. Figure 1.3 shows a schematic of the principles of alkaline electrolysis and Table 1.1 lists the desired specifications of the ZEF AEC.

Normally, alkaline electrolysis is performed on a large scale with unit areas up to 4 m² and up to several 100 stacked cells [74]. However, the ZEF alkaline electrolysis unit will only have an electrode area of about 100 cm² and 18 stacked cells. The ZEF AEC design splits the function of the encapsulation in two parts: a *pressure casing* and an internal *unit*. The latter comprises of a series of injection moulded disks (called *cookies*, which represent a stack of multiple electrolysis cells with a zero gap configuration and compartments for the product gases. This series of disks is contained in a narrow fitting pressure casing which main function is to withstand the 50 bar pressure. The choice of material for the pressure casing falls outside the scope of this thesis, because the function of pressure casing can be relatively easily fulfilled by a number of materials, such as stainless steel.

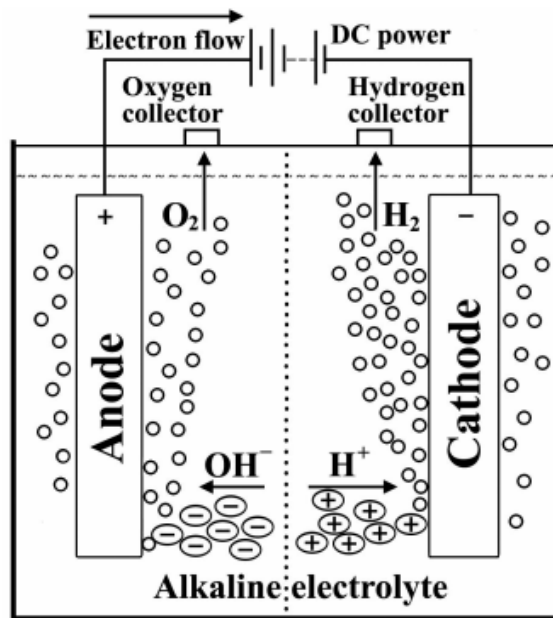


Figure 1.3: Schematic of the principles of alkaline water electrolysis [72]. Alkaline electrolysis is characterised by two electrodes, which are submersed in an alkaline electrolyte solution of KOH or NaOH. The electrodes are separated by a diaphragm, which separates the product gases, but allows the transportation of hydroxide ions (OH⁻). On the cathodic side, water is split and hydrogen gas and OH⁻ is formed. On the anodic side, OH⁻ is reacted back to water and oxygen gas is produced. The overall reaction is given by: $2\text{H}_2\text{O} \rightarrow 2\text{H}_2 + \text{O}_2$.

The material choice of the container of an alkaline electrolyser is not an extensively discussed topic in literature. The composition of the electrodes or the hydrophilic membrane are much more discussed, since these directly affect the efficiency of the electrolyser. However, the container of the electrolyser has been proven to be very relevant for the onset of a large hydrogen production system. According to Marini et al. (2012), the capital cost of alkaline electrolysis rather than the efficiency or the price of the electricity is the major limiting factor for widespread hydrogen production [50].

Currently, the material most used for the housing of advanced water electrolysis cells is monel, which is a nickel and copper alloy, or polyether ether ketone (PEEK), which is an advanced engineering thermoplast. Monel is used under extreme conditions up to 400 °C and 90 bar [30]. For example, Ganley (2009) developed a high temperature and pressure alkaline electrolysis cell constructed from a Monel alloy housing [30].

Ju et al. (2018) developed an AEC with operation conditions up to 30 bar and 80 °C. For this electrolyser, a single cell with monopolar configuration PEEK is used for the cell structure, since it is chemically stable against alkaline conditions, shows excellent mechanical resistance to high temperature and high pressure and is an electrical insulator [41]. Allebrod et al. (2013) developed an electrolyser with a PTFE liner and an inconel autoclave, which can withstand the elevated temperatures (up to 250 °C), pressures (up to 42 bar) and the extremely caustic environment [5].

Monel, inconel and PEEK are all very expensive materials. For one ZEF AEC unit, a volume of 2.3 L of material is required. This would mean a raw material cost price of about €200-300 for monel and inconel and €180-270 for PEEK [35]. For comparison, if the encapsulation would be made of HDPE, it would only cost €3.30. A raw material price of €300 may not seem significant, however, one ZEF farm, as shown in Figure 1.2, will consist of 40.000 micro-plants and therefore also 40.000 AEC units. Thus, reducing the raw material price of the material of the encapsulation can contribute significantly to reducing the capital cost of the AEC.

The relevance of this thesis lies in presenting a systematic overview of the potential candidates, including materials which have never been used before for alkaline electrolysis purposes; and in assessing the lifetime of these potential materials. Moreover, it provides the possibility of finding a cheaper material, which can be easily mass produced in order to allow for large scale use of alkaline water electrolysis for the production of hydrogen gas. Hydrogen gas will play a major role in the upcoming energy transition. To reinforce this statement, according to Steele and Heinzel (2011), conventional fuel cells use materials which have been selected more than 25 years ago. Commercialisation of fuel cells show inadequacies regarding the durability and cost of these materials [77]. Therefore, great advances have to be made regarding the materials used for fuel cells. The same goes for the inverse process, which is *water electrolysis*.

Table 1.1: The desired specifications (targets) of the ZEF alkaline electrolysis system (prototype early 2019).

ZEF Targets	
Design and cell type	bipolar zero gap configuration
Electrode area	100 cm ²
Membrane material	ZIRFON PERL [3]
Electrolyte	30wt% KOH
Operation temperature	90 °C
Operation pressure	50 bar
Operating voltage	2 V per cell
Operating current density	0.1 - 0.25 A/cm ²

1.4 The reliability and safety of the electrolyser

When developing a product, the reliability says something about whether the product can continue to perform the functions for which it is designed. For an electrolyser, this means being able to perform the water splitting for an extended period of time, *i.e.* the lifetime of the electrolyser. The product safety describes the policies designed to protect people from the risks associated with the product. There are many risks associated with running an alkaline electrolysis cell at 90 °C and 50 bar, which is powered by a noncontinuous power supply. The main risk involved is the risk of mixing of the hydrogen and oxygen gases, due to diffusion when the system is not running or due to material failure and micro-cracks in the partition between these gases. A mixture of hydrogen and oxygen is very dangerous and could lead to detonation of the whole system [60]. Under standard conditions (20 °C and atmospheric pressure) a mixture of 96% O₂ and 4% H₂ to 94% H₂ and 6% O₂ is enough to cause an explosion [60]. Therefore the material choice for the encapsulation, which separates these gases, and awareness on the durability of this material are very important to consider.

Undoubtedly, it is not economically feasible to test the reliability for several years before shipping the product. In order to be able to ensure reliability over a certain period of time with respect to the material choice, it is important to be aware of all possible failure mechanisms related to the materials involved. Failure due to design flaws is not considered in this thesis. Materials degrade/ wear-out over time, this can occur due to several mechanisms discussed in Section 2.4. Accelerated testing is a method to test the reliability of materials in a much shorter time than the lifetime of the product. This

is achieved by exposing the samples to exaggerated operation conditions. Ultimately, accelerated testing is done to obtain insights into the failure mechanisms and predict a lifetime under normal operation conditions. This testing began in the 1960's when researchers started testing materials in boiling water or steam autoclaves [26]. Over the years, material performances improved enormously, so more aggressive and diverse ageing test conditions have been developed in order to test the reliability of the material. However, it remains critical that the exaggerated stresses do not cause failure mechanisms that would not happen in normal usage conditions.

From a reliability and safety point of view, the relevance of this thesis is to provide a test method which contributes to the understanding of the mechanisms of degradation and allows for the determination of a material lifetime prediction. Furthermore, this thesis will provide valuable ageing data for the most promising polymers for application as containment of the ZEF alkaline electrolysis cell.

1.5 Objectives

The aim of this study is to, firstly, provide an overview of the different polymers which can be implemented in the encapsulation of the ZEF AEC given its operation conditions; and, secondly, to develop a method in order to be able to obtain insights into the failure mechanisms and to predict the lifetime of the material. This leads to the following research questions:

- Which polymers are theoretically suitable for the encapsulation of the ZEF alkaline electrolysis system?
- What are the main material degradation mechanisms in the conditions of the ZEF AEC?
- How do temperature, pressure and the presence of agents such as oxygen, hydrogen and 30wt% KOH affect the relevant material properties?
- How can accelerated testing be used to simulate ageing in the AEC?

1.6 Content of the report

Figure 1.4 gives an overview of the structure of this thesis. Chapter 2 provides the necessary background information in order to understand polymers and their properties. Moreover, the relevant degradation mechanisms of polymers are discussed.

Chapter 3 addresses the first objective and provides an overview of possible polymer candidates for the ZEF AEC by using a material database called CES EduPack. Three candidates are chosen and further investigated by the studying relevant literature.

The methodology of the ageing experiments is described in Chapter 4, along with the different characterisation methods, which have been used. The results and discussion follow in Chapter 5 and 6 for PPS-40%gf and PSU, respectively. Each of these chapters consist of two parts one dealing with ageing in oxygen; and the other dealing with ageing in a KOH solution.

Chapter 7 covers the extrapolation of the results of different characterisation methods. Furthermore, an overview of the sources of error in the measurements and methods of extrapolation is covered. Finally, the conclusion of this study is provided with in Chapter 8, along with further recommendations.

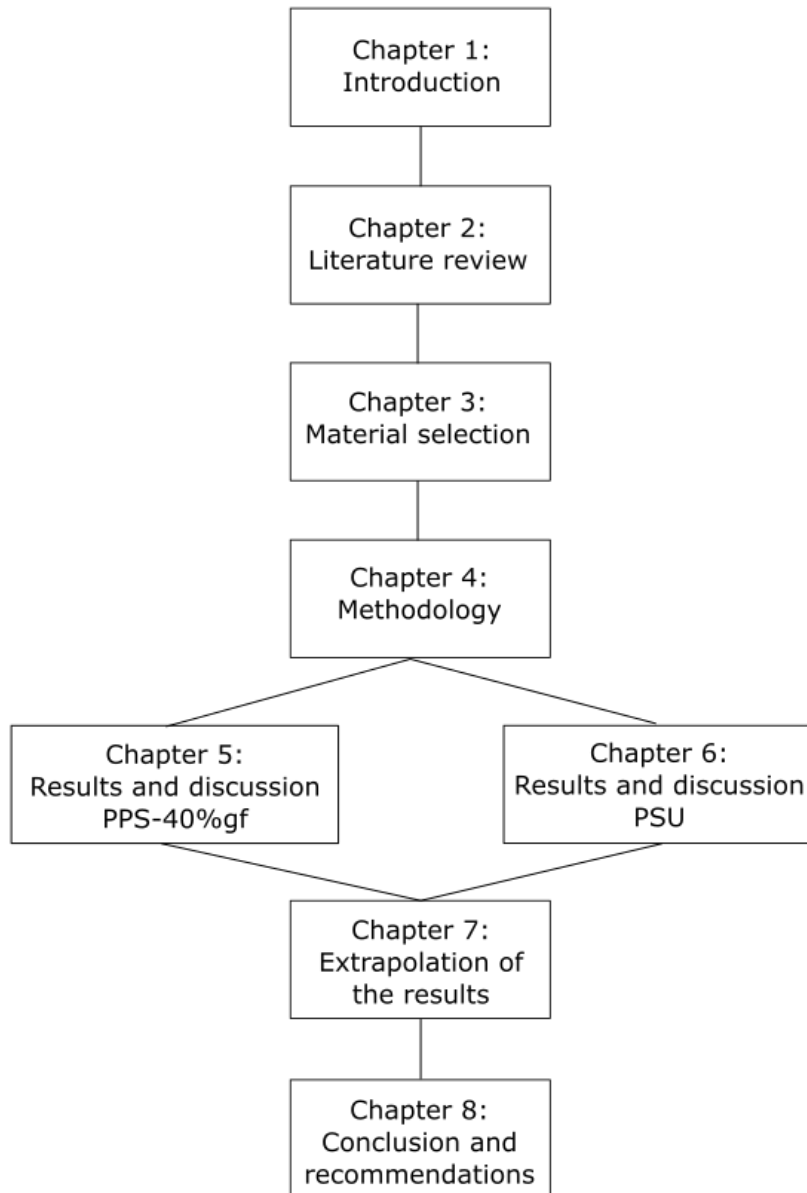


Figure 1.4: Overview of the structure of this thesis.

Chapter 2

Literature review

This chapter is devoted to providing the relevant background knowledge in order to select the polymers which may be suitable for application in the ZEF alkaline electrolysis system. Furthermore, the main material degradation mechanisms relevant to the conditions of the ZEF AEC are discussed.

2.1 An introduction to polymers

Polymers, together with metals and ceramics, are the most common types of engineering materials. Polymers consist of large chains of repeated units called monomers, which are connected together with covalent bonds. The properties of a polymer are primarily dictated by its molecular structure, which in turn is influenced by the *chemical composition* and the *morphology* of the polymer.

The *morphology* of a polymer describes the micro-scale arrangement of the chains. This arrangement can be disordered, giving rise to amorphous polymers; or linearly aligned in a periodic structure forming a crystal, resulting in semi-crystalline polymers; or there can be cross-links between the chains giving it elastomer or thermoset like properties (see Figure 2.1). Thermoplastic polymers are often semi-crystalline with an extent of crystallinity ranging from 10-80%. However, crystallinity is almost never the case for thermosetting polymers, since the cross-links inhibit the movement of the chains in a regular fashion. The crystalline areas play an important role in the structural strength of the polymer, because the strong inter-molecular forces within the crystalline region results in a very different material behaviour [45]. Crystalline regions are able to evoke higher temperature resistances, better chemical resistances, and an increased yield strength [45, 58].

Apart from the three-dimensional structure, the molecular weight of the polymer has an effect on its properties. A rule of thumb is the lower the molecular weight, the more flexible

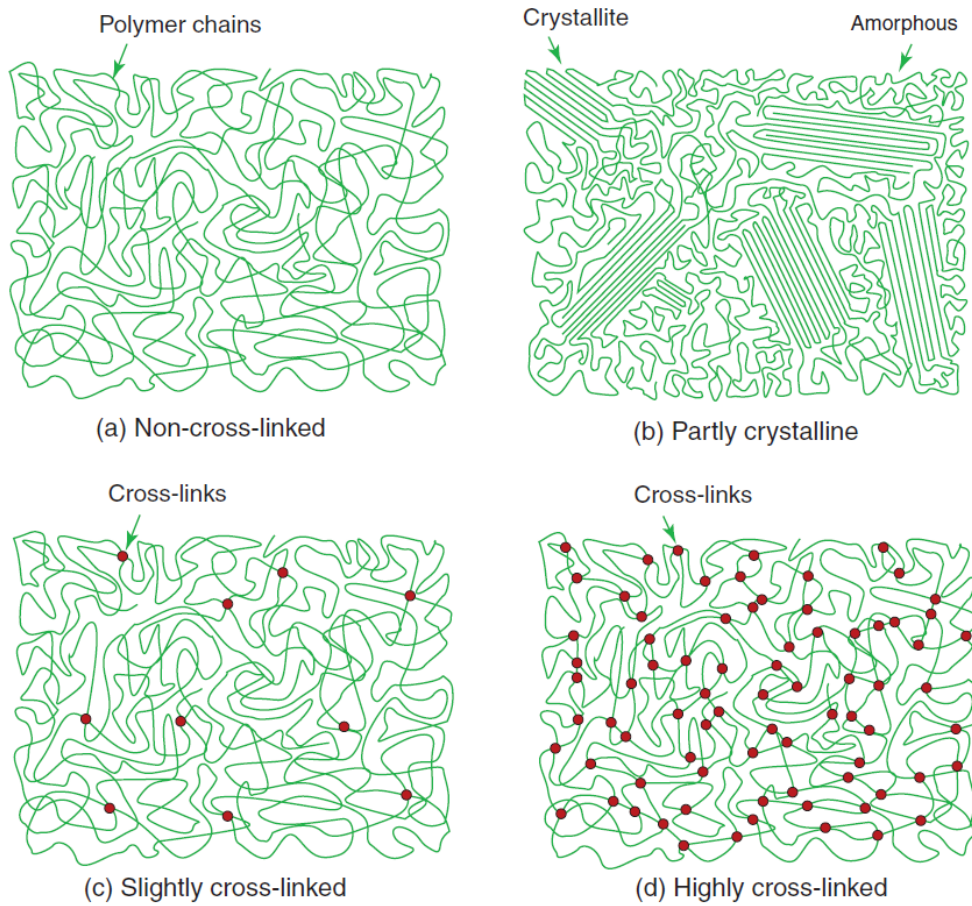


Figure 2.1: The structure of polymers [7]. (a) Chains in polymers like polypropylene form spaghetti-like tangles with a non-regular repeating pattern, the structure is amorphous. (b) Some polymers, like high density polyethylene, have the ability to form regions where the chains line up giving crystalline patches. These polymers are called semi-crystalline. (c) Elastomers have occasional cross-links between chains, but these are far apart, allowing the chains between them to stretch. (d) Heavily cross-linked polymers like epoxy inhibit chain sliding. These are thermosets.

the polymer will be, and the lower the transition temperature, viscosity and mechanical properties [1, 58].

Moreover, the *chemical composition* greatly affects polymer properties. Some functional groups or chemical elements are more stable or form stronger bonds. For example, PTFE has the same structure as HDPE, but with all the hydrogen in the side chains replaced by fluorine atoms. Since the carbon-fluorine bond is a very strong bond, in fact the fourth strongest single bond in organic chemistry [45], PTFE possesses better material properties than HDPE.

An example of a very stable functional group is the aromatic ring (or benzene ring/phenyl group), a special structure in organic chemistry, because of the positions of the single and double bonds which resonate back and forth. This cyclic, planar structure with a ring of resonating bonds give increased thermal stability compared to other geometric or connective arrangements with the same set of atoms [58].

Apart from the chemical composition of the polymer itself, the chemical interaction due to the addition of additives, such as plasticisers, flame retardants, stabilisers, antioxidants and impact modifiers, can influence the material properties of polymers. These are, however, not further considered.

2.2 Polymer performance parameters

An important performance parameter for the ZEF AEC is that the polymer retains *dimensional stability* at the operation temperature. A polymer cannot be used in conditions in which the polymer loses its dimensional stability. An important parameter of dimensional stability is the glass transition temperature (T_g). The glass transition is a process which occurs over a temperature range and only in the amorphous region of the polymer. Below the T_g the molecular motion of the polymer chains are frozen and the polymer behaves brittle and glassy. However, above the T_g molecular motions are activated, chains can slide past each other and the polymer behaves rubbery and viscous [68].

The T_g gives the onset at which a polymer loses nearly all its stiffness and starts to behave rubbery. The appearance of a rubbery plateau is the result of entanglements or cross-links. When increasing the temperature even more, the melting temperature is reached, at which the crystalline regions will start to melt. Polymers containing a significant amorphous part lose their dimensional stability at temperatures close to and above T_g [68].

In practice there are multiple ways of determining the glass transition temperature. Differential scanning calorimetry (DSC) and dynamic mechanical analysis (DMA) are two

methods to obtain the T_g . DMA gives more accurate results, but even within DMA there are multiple ways of defining the T_g . Some authors use the onset of the drop in storage modulus of the 1 Hz curve as the T_g , or the peak of the tan delta at 1 Hz or of the loss modulus at 1 Hz. The latter definition is used in this study together with the use of DSC.

For the ZEF AEC it is also important that the polymer is *tough*, since the formation of micro-cracks and the subsequent mixing and leaking of gases and chemicals can be detrimental to the AEC function. Toughness is the ability of a material to be able to absorb energy and deform plastically without fracturing. A mathematical way of obtaining the toughness of a material is by integrating the stress-strain curve. In order for a material to be classified tough, the material has to be both strong and ductile. Plasticisers can be added to a polymer in order to increase the ductility and therefore the toughness. However, plasticisers lower the hardness, strength and stiffness of the material [45].

Since the pressure casing will provide most of the mechanical strength needed to contain a pressure of 50 bar, the strength of the polymer for the encapsulation is less important. However, since toughness is a function of both strength and ductility, higher strengths are favourable.

From a chemical point of view *chemical resistance* against the strong alkaline solution and the oxidising environment in the AEC is an important property to consider. These are further discussed in Section 2.4.

Furthermore, since the polymer is in direct contact with a KOH solution and with 50 bar gas, it is important that the polymer is not soluble in this solution and that the permeability of gases or other small molecules is low. It is not expected that a polymer will dissolve into the KOH solution, since 'like dissolves like' [45]. However, the absorption of water and corrodents can result in swelling of the polymer, causing softening of the polymer. This can introduce high stresses and eventually leads to failure.

The permeability of gases or other small molecules depends on the secondary bonding of the polymer. If a molecule strongly interacts with a polymer, it will not be readily able to diffuse through it. In general, the higher the crystallinity and/or the density of the polymer, the lower the permeability, since the free volume through which the molecule must diffuse is reduced [45].

Rapid pressurisation and depressurisation of gases into and out of the material surface can lead to a phenomenon called blistering, which results in the formation of blisters on the surface [88]. This is unfavourable because it can lead to delamination of the surface and induce further degradation.

2.3 Visco-elastic behaviour of polymers

The mechanical response of polymers is of visco-elastic nature. This means that the material exhibits both viscous and elastic characteristics when the material undergoes deformation; they exhibit stress-strain characteristics that are time-dependent. Elasticity is usually a result of bond stretching, whereas viscosity is a result of the diffusion of atoms or molecules inside the material. A visco-elastic material has the following time-dependent properties: hysteresis is seen in its mechanical response; stress relaxation occurs meaning a constant strain causes decreasing stress; and creep occurs involving a constant stress that causes an increasing strain [80].

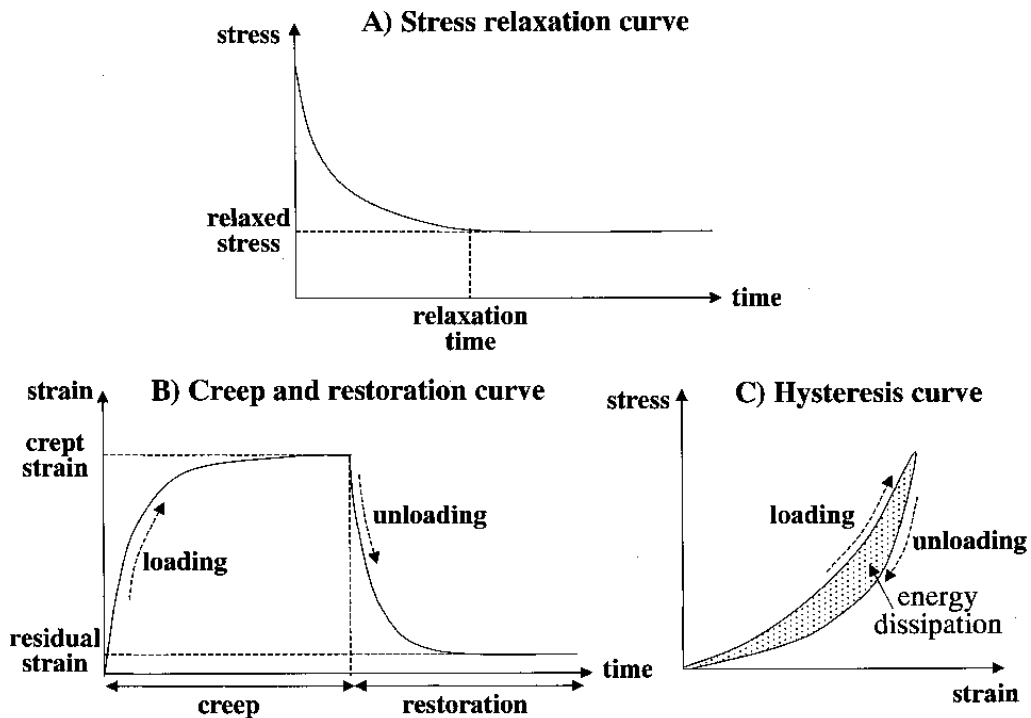


Figure 2.2: Visco-elastic material properties: (a) Stress-relaxation for a constant strain (b) creep curve at a constant stress and restoration curve and (c) the hysteresis curve, where the area enclosed by the stress-strain curve is a measure for the energy dissipation [80].

Many visco-elastic materials are linear visco-elastic. For linear visco-elastic materials it is true that the response is proportional to the input and that the Boltzmann superposition principle holds, which describes the response of a material to different loading histories [40].

Visco-elasticity can be studied using dynamic mechanical analysis, which involves applying a small oscillatory stress and measuring the resulting strain. In purely elastic materials the stress and strain are in phase and in purely viscous materials, there is a 90 degree phase lag of the strain. Visco-elastic materials have a behaviour in between. A complex dynamic modulus E^* , represents the relation between the oscillating stress and

strain, $E^* = E' + iE''$. E' represents the storage modulus, which is a measure of the elastic response of a material, *i.e.* the stored energy. E'' is the loss modulus and represents the viscous response of a material. It measures the energy dissipated as heat. Tan delta is the ratio of loss to the storage modulus and represents the phase lag of the strain to the stress. It is a measure of the energy dissipation of a material and tells us how good a material will be at absorbing energy [31].

2.3.1 Time-temperature superposition

Apart from time dependence, the modulus is also dependent on temperature. One of the observations made, is that the curves of the modulus as a function of time do not change shape as the temperature is changed, but appear only to shift along the time axis [40]. This led to the time-temperature equivalence principle, which is a characteristic of thermorheological simple materials. This means that by performing tests at multiple temperatures, it is possible to obtain information about the visco-elastic behaviour of the material at a reference temperature at much larger time scales than the experimental time scales. This is achieved by creating a master curve for the specific reference temperature along with a corresponding shift-factor curve, as shown in Figure 2.3.

The shift-factor is a basic property for thermorheological simple materials, since the same shift-factor applies to the shear modulus, bulk modulus and other visco-elastic functions of the material [40]. From the shift-factor (a_T), it is possible to obtain the apparent activation energy of the visco-elastic behaviour. It is often found that the shift-factor changes discontinuously near the glass transition. Below the T_g an Arrhenius model can be used to describe the shift-factor:

$$\ln(a_T) = \frac{-E_a}{R} \left[\frac{1}{T} - \frac{1}{T_R} \right], \quad (2.1)$$

where E_a is the activation energy, R is the gas constant (8.314 J/mol/K) and T_R is the reference temperature [40, 53]. For temperatures close to and above the T_g , the Williams-Landel-Ferry (WLF) equation can be used, which is based on the free-volume concept of polymers [87]:

$$\ln(a_T) = \frac{C_1(T - T_R)}{C_2 + T - T_R}, \quad (2.2)$$

where C_1 and C_2 are empirical constants [53]. For $T \approx T_g$ it has been found that $C_1 \approx 17.4$ and $C_2 \approx 51.5$ [40].

2.3.2 Frequency-temperature superposition

Since frequency is the inverse of time, frequency-temperature superposition can be applied by shifting different frequency curves along the frequency axis in order to obtain a master and shift-factor curve [40]. This procedure can be applied to multi-frequency DMA data of the storage and loss modulus.

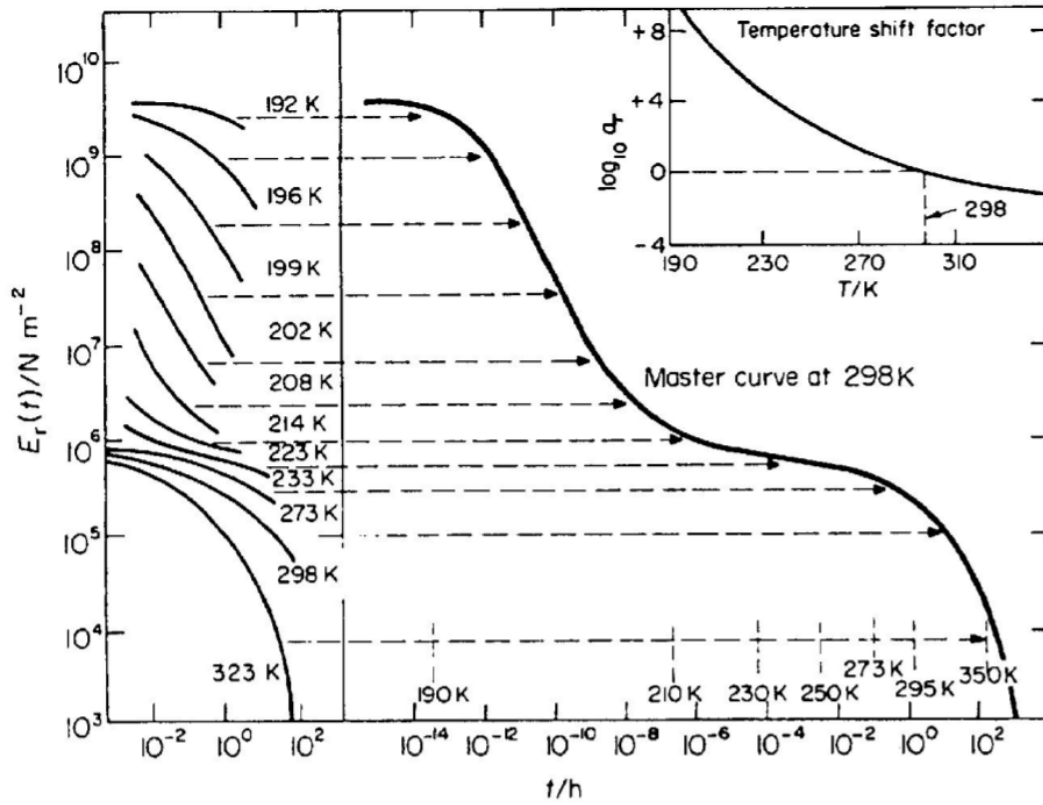


Figure 2.3: Time-temperature equivalence principle. The curves obtained in the experimental window are shifted to form a master curve for longer times and a corresponding shift-factor curve [78].

2.4 Degradation mechanisms

The scope of this thesis is to look at failure of the AEC due to failure of the plastic container. Failure of the AEC plastic container can be due to material or phenomenological causes of failure or due to human causes, which entail material mis-selection, poor design, poor processing and abuse. In order to avoid both of these causes of failure it is important to be able to perform effective product testing to identify the material and human weaknesses. In the scope of this thesis only the material weaknesses are described. Polymer degradation denotes changes in physical properties caused by chemical reactions involving bond scission in the backbone of the polymer chain. There are many different types of degradation mechanisms, which all fall into the following categories [36, 63, 88]:

- thermal degradation,
- oxidative degradation,
- radiative degradation,
- mechanical degradation,
- chemical degradation,
- and biological degradation.

Some of these forms of degradation are not relevant for the ZEF AEC, such as biological degradation and radiative degradation. This is because biological degradation requires living organisms such as bacteria and fungi, which are not present in the AEC. Radiative degradation requires a source of UV light which leads to radical formation and bond-breaking. This is also not present in the AEC, since it is a closed and shielded system.

Mechanical degradation in polymers can be in the form of environmental stress cracking, fatigue cracking or notched static rupture [88]. Environmental stress cracking is the process where organic fluids, like lubricants, adhesives or solvents accelerate crack initiation and crack growth. The fluids do not impose chemical degradation, but only accelerate the mechanism [88]. This can be problematic for the AEC, since the polymer encapsulation will contain a large body of fluid. Dynamic fatigue is caused by repeated cycles of load, for example due to cyclic thermal conditions. This can become problematic for the ZEF system, since it operates dynamically.

Finally, notched static rupture is mainly caused by stress concentrations due to processing. Although, the pressure casing will carry the pressure, meaning the polymer cookies will operate under hydro-static conditions, stress concentrations can still be present. The exact details concerning this, are dependent on the design of the AEC.

Thermal degradation is often taken together with oxidative degradation, since increasing temperature increases the rate of oxidation. Therefore the following subsections will be about thermo-oxidative degradation and chemical degradation.

2.4.1 Thermo-oxidative degradation

Thermo-oxidation is a general degradation mechanism affecting all polymers to some degree. The rate of thermo-oxidation will increase with increasing temperature. The thermo-oxidation reaction consists of three main steps, which are initiation, propagation and termination [1, 83], as shown in Figure 2.4.

Initiation: The formation of a radical by hydrogen abstraction or by homolytic scission of a carbon-carbon bond due to light or heat.

Propagation: The free radical reacts with an oxygen molecule to form a peroxy radical (ROO^*), which abstracts a hydrogen atom from another polymer chain to form a hydroperoxide (ROOH). The hydroperoxide splits into two new free radicals (RO^*) + ($^*\text{OH}$), which abstract labile hydrogens from other polymer chains.

Termination: Chain scission or recombination of two radicals which results in increase in molecular weight or cross-linking density.

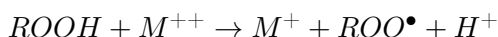
Each initiating radical can produce two new radicals. Therefore, the conversion of peroxides to hydroperoxides is the rate determining step for the chain reaction.

Apart from hydrogen abstraction, oxygen can attack residual double bonds, especially at elevated temperatures. However, it is not clear how large this effect is [1]. Oxidation nearly always affects the modulus of polymers due to oxidative cross-linking. This makes the material more brittle and therefore reduces the toughness of the material. The addition of antioxidants can protect the polymer from oxidation, since the antioxidants will react more easily with oxygen.

The effect of oxygen pressure on thermo-oxidative degradation

For thermo-oxidative degradation in polyolefins, an increase in temperature will lead to an increase in reaction rate, often in an Arrhenius type temperature dependence [34]. Apart from temperature, oxygen pressure may also play a role in the degradation rate. The effect of oxygen has been extensively investigated for polyolefins, such as PP and PE [28, 34, 65], especially for geomembrane applications [39, 66, 84]. It is well established that

or



Polyolefins, such as HDPE, are most susceptible to this reaction. The source of the metal ions can be from catalyst or stabiliser residues during processing, or from direct contact with metals or salt solutions during service. The metal ions act as sites for initial degradation, even at concentrations as low as a few ppm.

The concentration of metal ions is important for the severity of catalysis. For example, for polyethylene, copper stearates suffers reduced resistance to degradation at low concentration, whereas at high concentrations (more than 1000 ppm) the copper acts as a weak stabiliser [88].

The source of those metal ions in the ZEF AEC can originate from remnants of additives during polymer processing or perhaps from the metal ions in the electrolyte from the electrodes. Removing all remnants of additives during processing is impossible. The exact composition of the metal electrodes used for the ZEF AEC has not been established, but will most probably be a nickel alloy containing Ni, Fe, Co and in smaller quantities Zn. All of them in oxide form. These metals could potentially influence the degradation of the polymer.

Ozone induced degradation

Molecular oxygen (O_2) is an oxidising agent. This means it is able to oxidise (*i.e.* take electrons from) other substances. Molecular oxygen in air or dissolved in water has a modest oxidation potential compared with oxygen in some other states, such as ozone, atomic or singlet oxygen. Ozone (O_3) is a much stronger oxidising agent. This is due to the presence of delocalised (π) electrons, which more readily react with other molecules than localised electrons. This means that if ozone is present in the system it will most likely immediately react with the polymer and induce thermo-oxidative degradation.

The production of ozone in an alkaline electrolysis cell in normal conditions is negligible, since very high voltages and current densities are needed for the production of ozone [56]. Okoda and Naya (2011) used voltages of 12-13 V for the production of ozone water, whereas the voltage for the ZEF AEC system will stay below 2 V. Therefore, the effect of ozone can be neglected.

It is interesting to note that in the experiments of Okoda and Naya (2011) a Nafion 117 membrane was used for the production of ozone. This membrane quickly degraded in the presence of ozone, even though Nafion has excellent mechanical and thermal properties. Nafion is a sulfonated tetrafluoroethylene based fluoropolymer-copolymer. It stems from incorporating perfluorovinyl ether groups on a PTFE backbone.

2.4.2 Chemical degradation

Chemical attack leads to embrittlement and/or brittle failure due to chain scission. In combination with applied stress this can lead to stress corrosion cracking. A relevant form of chemical attack for the ZEF AEC is *hydrolysis*. Hydrolysis is any chemical reaction in which a water molecule leads to the rupture of a chemical bond [88].

The alkaline solution present in the electrolyser is a 30wt% KOH solution, which can cause an alkaline hydrolysis reaction. The hydroxyl ion, OH^- , can have two functions in a chemical reaction. It can act as a nucleophile, which is a chemical species able to donate an electron pair to form a chemical bond in relation to a reaction [82]; or it can act as catalyst with regard to the hydrolysis reaction. Numerous factors influence the hydrolysis reaction. The rate of hydrolytic degradation depends on the diffusion rate of water and the concentration of the catalyst, *i.e.* the OH^- ions [16]. The micro structure, crystallinity and chain mobility have a great effect on the diffusion of water. The hydroxyl ion has a low dielectric constant making it more difficult to penetrate the bulk material. It therefore seems that hydrolysis is largely a surface reaction. Furthermore, it has been found that hydrolysis only occurs in the amorphous regions of a polymer [29]. This is due to the fact that water is not able to penetrate the crystalline regions of the polymer.

Apart from the direct degradation effect of the hydroxyl ion, the water of the electrolyte can have an effect on the degradation of polymers. Water can cause the hydrolysis of labile bonds, and in combination with radiation it can generate hydroxyl radicals, which can promote free radicals reaction [88]. Furthermore, mechanical stresses can built up from swelling and contraction due to the absorption and desorption of water. Apart from that, water can weaken the boundary between the polymer and fibres if these are present. It can also lead to stress across the crystalline/ amorphous region due to water diffusion in polymers is controlled by and only occurs in the amorphous regions. This can result in micro-cavitation [36].

Dissolution of glass fibres in a hot alkaline solution

The PPS samples which will be tested in this thesis contain 40% glass fibres. It is therefore important to understand the behaviour of these fibres to the extreme conditions to which they are exposed. The glass fibres present in the PPS is 99% E-glass, which has the following composition: 54wt% SiO_2 , 13wt% Al_2O_3 , 21wt% $\text{CaO}+\text{MgO}$, 10wt% B_2O_3 and 2wt% $\text{Na}_2\text{O}+\text{K}_2\text{O}$ [8]. The glass fibres improve the mechanical properties of the polymer composite, but the glass transition temperature is not significantly affected [67].

Bashir et. al. (2018) investigated the kinetics of dissolution of glass fibres (E-glass) in a hot alkaline solution at 95 °C. The effects of both KOH and NaOH solutions of different concentrations (0.5 to 3 mol/L) were determined using SEM in order to measure the change in diameter of the individual fibres. It was found that the diameter reduction increases linearly with time and the dissolution rate increases with concentration. For 3.0 mol/L KOH solution the fibre diameter is almost 40% reduced, while for a 3.0 mol/L NaOH solution it is reduced by about 75% [12]. To put this into perspective: 3 mol/L is equivalent to a 15wt% KOH solution, 7 mol/L is equivalent to 30wt% KOH solution and 12 mol/L is equal to 45wt% KOH solution.

The glass dissolution process involves hydrolysis of the glass network by OH⁻ ions. An increase in concentration of the hydroxide ions theoretically leads to an increase in reaction rate and therefore dissolution. The fact that NaOH is more corrosive to the glass fibres can be explained due to the reaction products from NaOH and glass being formed more readily and more exothermic, or that the smaller Na⁺ ions have a stronger attraction to the OH⁻ ions in solution, which reduces the likelihood of the OH⁻ ions to interact with neighbouring water molecules and as a result they are more likely to come into contact with the glass [12].

2.5 The reaction kinetics

It is expected that the reaction kinetics of oxidative degradation and hydrolysis in PPS and PSU are highly complex involving multiple chemical and physical phenomena, such as phase transitions, chemical reactions, heat transfer and mass diffusion. Reaction kinetics includes information about the reaction mechanism and the rate at which the reaction takes place. For elementary reactions the chemical law of mass action can be used, which states that the rate of a chemical reaction is directly proportional to the product of the activities or concentrations of the reactants [76]. More complex reactions involving multiple steps require the rate law of step-wise reactions, which can be derived from combining the different rate laws of the various elementary reactions. In situations with consecutive reactions, the rate-determining step often determines the kinetics.

Different factors affect the reaction rate. These are the nature and physical state of the reactants, the shape and dimensions of the reaction zones, or the presence or absence of catalysts. However, the main factors influencing the reaction rate are the temperature and the concentrations (or partial pressures for gases) of the reactants, products or catalysts [76]. In general, the reaction rate increases with temperature, often following the Arrhenius law for a restricted range of the temperature. The Arrhenius law gives a linear relation between the logarithm of the rate constant (k) and the inverse of temperature (T) with a

slope equal to the activation energy (E_a) divided by the universal gas constant (R) and offset by $\ln(A)$ [76]:

$$k = Ae^{\frac{-E_a}{RT}}, \quad (2.3)$$

hence

$$\ln(k) = \frac{-E_a}{R} \left(\frac{1}{T} \right) + \ln(A). \quad (2.4)$$

In practice, however, the activation energy is greater than RT and the reaction speed increases rapidly with temperature. The influence of the concentrations of reactants, products or catalysts (or partial pressures of gases) on the reaction speed is extremely complex and varied. Sometimes equations of the following sort are encountered [76]:

$$r = k[A_1]^{\delta_1}[A_2]^{\delta_2} \dots [A_i]^{\delta_i}, \quad (2.5)$$

where r is the reaction rate, k is the temperature dependent reaction rate, $[A_i]$ are the concentrations of the reactants and δ_i are the partial orders of the reaction.

For the case of the degradation reactions occurring in the ZEF AEC, the reaction kinetics are very complex, because many different chemical reactions take place including the different steps of thermo-oxidation and hydrolysis, but also many reactions which are not known about. Moreover, there are different phases present during the degradation reaction, which includes the solid polymers, oxygen in gas form and a liquid KOH solution. This means adsorption at the gas-solid interfaces and diffusion is required to be able to transport the reactants to the right reaction zone. Therefore, trying to predict the degradation reaction rate based on modelling the reaction kinetics is difficult to do, although several studies have attempted to model thermal degradation or oxidation [25, 47, 57, 59, 70, 71]; have investigated the kinetic parameters, such as the activation energy [61, 64]; or have looked at diffusion limited oxidation modelling [62]. In this study, a more empirical approach is considered.

Chapter 3

Material selection

3.1 Preliminary screening of materials

In Section 2.2 the relevant performance parameters related to material properties have been discussed. Apart from the ones discussed, the material for the encapsulation of the ZEF AEC should be non-conductive, able to be processed with injection moulding and have a competitive cost price. Furthermore, the desired lifetime of the material should be at least 20 years in the operation conditions of the ZEF AEC. These performance parameters are summarised in Table 3.1.

Table 3.1: Performance parameters of the material for the container of the ZEF alkaline electrolysis system.

Material Requirements	
Processing Method	Suitable for injection moulding
Conductivity	Non-conductive
Permeability	Low permeability for hydrogen and oxygen gas to minimise mixing of the gases when the cell is not running and impermeable to water
Chemical stability	Resistant to the corrosive nature of the alkaline electrolyte during the operation lifetime
Oxidation stability	Resistant to oxidation during the operation lifetime
Raw material price	As low as possible
Dimensional stability	Dimensional stability at the operation temperature
Toughness	High material and fracture toughness
Material class	Thermoplastic or thermosetting polymer

From the performance parameters, the two most important initial selection criteria for the preliminary screening of material candidates are:

- resistance against strong alkalis ($\text{pH} > 10$),
- and a maximum operation temperatures of $90\text{ }^{\circ}\text{C}$ or above.

Apart from these two selection criteria, resistance against the effects of oxidation is also a very important selection criterion. However, this criterion is already incorporated into the second criterion of having a maximum operation temperature of $90\text{ }^{\circ}\text{C}$ or above, since oxidation is often involved in the degradation of polymers at elevated temperatures [63]. Moreover, it is desirable for the polymer to have a high T_g , which is also incorporated in the maximum operation temperature.

CES EduPack 2018, a material database developed by Mike Ashby of the University of Cambridge, has been used in order to compose a list of potential candidates. A material chart is produced where all polymers (thermosets and thermoplastics) are plotted with respect to their ability to resist strong alkalis and their maximum service temperature. The database consists of 702 different types of polymers, including blends, co-polymers and composites. From these 702 different types of polymers, 252 types of polymers seem to have an acceptable to excellent resistance against strong alkaline solutions and are able to withstand operation temperatures of $90\text{ }^{\circ}\text{C}$ or more. These different polymers fall in the following families of polymers, and are plotted in Figure 3.1:

- *thermoplastics*: CPVC, ECTFE, ETFE, FEP, HDPE, LCP, PA66, PTFE, PSU, PPS, PP, PMP, PFA, PESU, PEK, PEKK, PEEK, PCTFE, POM, SAN, SMA and PEBA,
- and *thermosets*: Epoxy, MF, TPO and VE.

Other polymers, such as COC, PVDF, PET, or certain types of PA and many more are not suitable, because of their limited to unacceptable use against strong alkalis, whereas EVA, ABS, AES, SBS, SMMA, PS, and many more are not suitable because of their low maximum use temperature.

It is important to note, however, that CES EduPack does not specify how long the resistance against strong alkalis is and how this is tested. Furthermore, it does not specify at which temperatures the polymer is resistant against strong alkalis. Moreover, the maximum service temperature relates to the highest temperature at which the material can be used for an extended period of time without significant problems such as oxidation, chemical change, excessive creep, loss of strength or other primary properties for which the material is normally used [35]. There is, however, no universal test for the maximum

service temperature. In CES EduPack the T_{\max} is determined via either the relative thermal index (RTI, UL 746b), which is the temperature at which 50% of electrical insulation or strength is retained after 60,000 hours, or via ASTM D794, a standard practice for determining the permanent effect of heat on plastics [24]. However, this is a very broadly defined test.

The above list includes polymers which are already used for electrolysis cells, such as the previously mentioned PEEK and PTFE, but also polymers used for the hydrophilic membrane in the electrolysis cell, such as porous PVC, polyolefins, porous PTFE, and polysulfone (PSU) [13, 72, 77]. Traditionally, asbestos cloths were used as a diaphragm in alkaline electrolysis. However, since asbestos is found to be toxic other materials have been considered such as sintered oxides. An example is Zirfon, which contains zirconium oxides bound in a polymeric binder such as polysulfone (PSU) or polytetrafluorethylene (PTFE) and coated onto a polymeric cloth based on polysulfone or polyphenylene sulfide (PPS) [3]. From these materials it is known that they must be at least in the short term (about 5 years) compatible to the operation conditions of alkaline electrolysis [3].

Apart from durability against strong alkalis and a high enough maximum service temperature, there are other constraints important for selecting the right material for the encapsulation of the ZEF AEC. One important constraint is the possibility for mass production via injection moulding. When looking at this criterion, only PTFE is deemed unsuitable from the above list. Furthermore, the polymer should be non-conductive, which is fortunately the case for all of the polymers considered.

When looking at the raw material cost-price constraints, the polymers can be subdivided into the following categories [35]:

- below 5 €/kg: Epoxy, MF, PA66, PB, HDPE, PEX, PMMA, POM, PP, PS, CPVC, SAN, SMA, VE, TPO;
- between 5 and 10 €/kg: FEP, LCP, PMP, PPS;
- between 10 and 20 €/kg: PEBA, PESU, PFA, PSU;
- and above 20€/kg: ECTFE, ETFE, PCTFE, PEEK, PEK, PEKK.

From the above categories, the polymers with a cost price below 5 €/kg, also have relatively low maximum operation temperature, meaning the chances for success for the ZEF AEC are slim. However, in collaboration with Promolding B.V., a polymer processing company which will injection mould the ZEF AEC, HDPE is considered and further investigated in Section 3.2.1. The very expensive polymers of more than 20€/kg are directly taken out of consideration. From the other two price categories, PPS and PSU seem

the most promising candidates, since they are already used in the ZIRFON membranes of the alkaline electrolysis cells for short term application. Therefore, these two polymers have been chosen to be further investigated. Table 3.2 shows an overview of the material properties of these three polymer candidates. Note, however, that PPS-40% glass filled is used. This will be elaborated upon in Section 2.4.2.

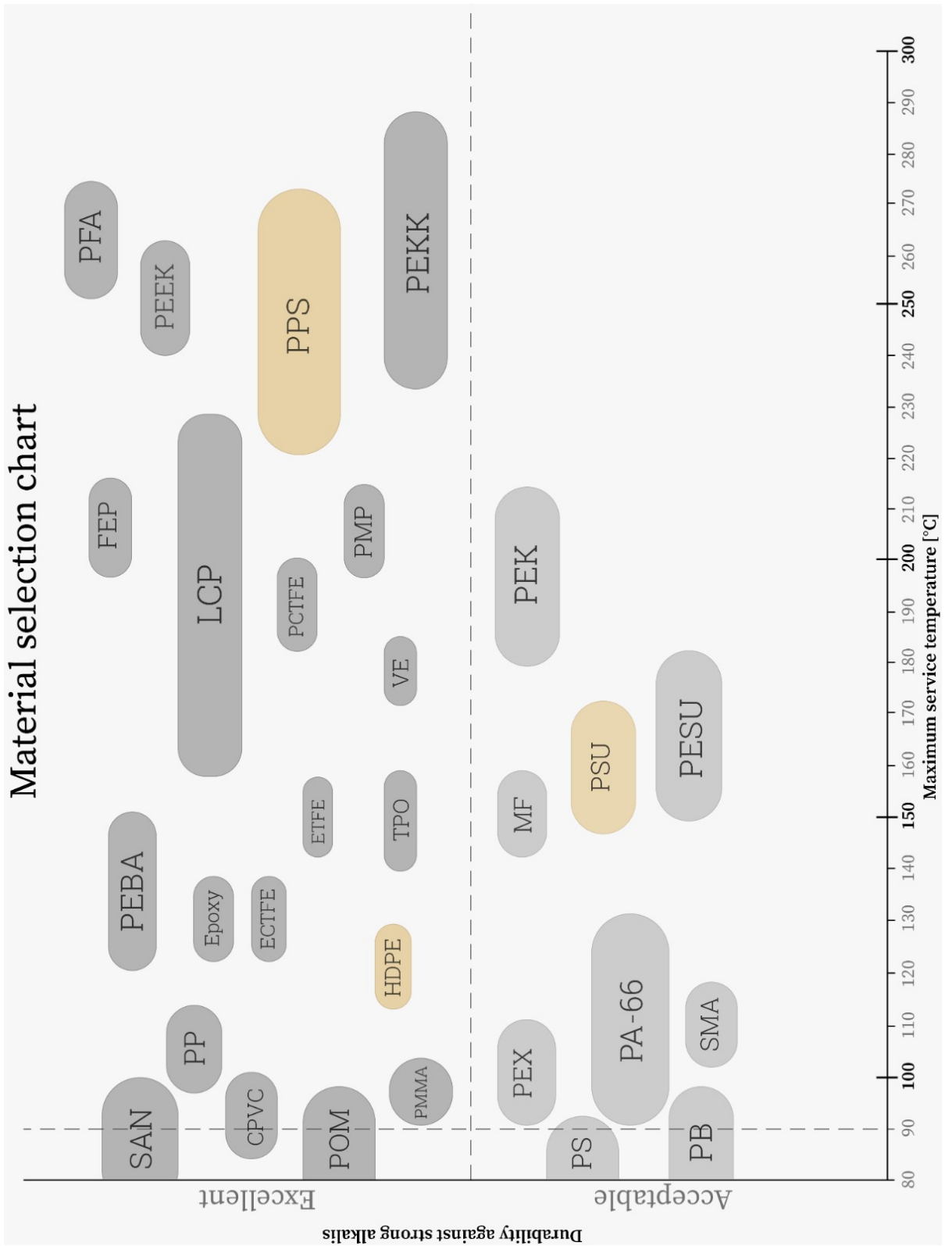


Figure 3.1: Material selection chart, information obtained from CES EduPack [35].

Table 3.2: Material properties HDPE, PPS-40%gf and PSU. This information has been taken from the software CES EduPack, 2018 [35].

Property	HDPE	PPS (40% gf)	PSU
Price (€/kg)	1.45 - 1.51	4.45 - 5.07	8.39 - 12.1
Price (€/m ³)	1390 - 1450	7120 - 8460	10300 - 15100
Physical properties			
Density (kg/m ³)	952 - 965	1600 - 1670	1230 - 1250
Mechanical Properties			
Young's modulus (GPa)	1.07 - 1.09	7.58 - 14.5	2.62 - 2.76
Yield strength (MPa)	26.2 - 31	138 - 145	75.5 - 83.3
Tensile strength (MPa)	22.1 - 31	121 - 201	95.4 - 104
Specific stiffness (MN m/kg)	1.11 - 1.14	4.64 - 8.87	2.11 - 2.23
Elongation (% strain)	1120 - 1290	0.9 - 4	40 - 80
Compressive strength (MPa)	18.6 - 24.8	145 - 301	125- 280
Bulk modulus (GPa)	2.15 - 2.26	11.4 - 12	4.2 - 4.41
Impact and fracture properties			
Fracture toughness (kJ/m ²)	1.52 - 1.82	4.56 - 6.54	1.89 - 4.69
Toughness (kJ/m ²)	2.15 - 3.04	1.83 - 4.41	1.54 - 7.08
Thermal properties			
Melting point (°C)	130 - 137	275 - 290	no data
Glass temperature (°C)	-125 - -90	81 - 97	186 - 192
Maximum service temperature (°C)	113 - 129	220 -240	147 - 172
Electrical properties			
Electrical resistivity (μΩ cm)	3 × 10 ²⁵	3 × 10 ²²	3 × 10 ²²
Absorption & permeability			
Water absorption 24 hrs (weight gain %)	0.005 - 0.01	0.004 - 0.05	0.27 - 0.33
Permeability O ₂ (cm ³ mm/(m ² .day.atm))	49.8 - 69.4	no data	59.3 - 138
Durability			
Strong alkalis	excellent	excellent	acceptable
Flammability	highly flammable	self- extinguishing	self- extinguishing
Processing			
Injection moulding	excellent	limited use	acceptable

*gf = glass-filled

3.2 Background on HDPE, PPS and PSU

Chapter 2 has given an overview of the two most important degradation mechanisms in the operation conditions of the ZEF AEC, which are thermo-oxidative degradation and chemical degradation in the form of hydrolysis. Before conducting experiments with regard to these two degradation mechanisms, a literature review is conducted to investigate the resistance of HDPE, PPS and PSU to thermo-oxidative degradation and hydrolysis.

Table 3.4: Molecular formula of HDPE, PPS-40%gf and PSU.

Molecular formula & abbreviation
$\text{---} \left(\text{---CH}_2\text{---CH}_2 \right)_n \text{---}$ <p style="text-align: center;">HDPE</p>
$\text{---} \left(\text{S---} \langle \text{benzene ring} \rangle \text{---} \right)_n \text{---}$ <p style="text-align: center;">PPS</p>
$\text{---} \left(\text{---} \langle \text{benzene ring} \rangle \text{---} \text{C} \begin{array}{c} \text{CH}_3 \\ \\ \text{CH}_3 \end{array} \text{---} \langle \text{benzene ring} \rangle \text{---} \text{O---} \langle \text{benzene ring} \rangle \text{---} \text{S} \begin{array}{c} \text{O} \\ \\ \text{O} \end{array} \text{---} \langle \text{benzene ring} \rangle \text{---} \right)_n \text{---}$ <p style="text-align: center;">PSU</p>

3.2.1 High density polyethylene (HDPE)

General Properties

Of the three options, HDPE is the cheapest option, with a raw material price of 1.45 - 1.51 €/kg as shown in Table 3.2. Despite the cheap price, HDPE shows an excellent chemical resistance against many chemicals. PE is a simple thermoplast produced via poly-addition of ethylene. When these chains do not have any branches, a higher density and a higher level of crystallinity can be obtained and the material becomes HDPE. Table 3.4 shows the chemical structure of HDPE. Moreover, the polymer is non-conductive and suitable for processing via injection moulding [35].

Degradation Resistance

Thermo-oxidative degradation seems to be the major mechanism for degradation of HDPE in the conditions of the ZEF AEC. It seems that degradation becomes significant only when the antioxidants, which protect the polymer against oxidation, are used up. This can occur due to two mechanisms: either the antioxidants have reacted with oxidising agents, and are therefore used up, or the antioxidants have leached/ diffused out of the material. A high oxygen partial pressure can lead to the antioxidants being used up much faster than in normal conditions, whilst a watery environment at higher temperatures can lead to antioxidants being easily leached out of the material. Both these scenarios are at play in the electrolyser.

Mueller & Jakob (2003) performed an experiment in which they aged HDPE at 85 °C for two years in a watery environment [54]. From the oxygen induction time measurements all antioxidants are depleted within 7 years. Hausmann & Zanzinger (2015) found that the time to failure for HDPE at 90 °C and an oxygen pressure of 50 bar is in the order of several weeks [92]. Finally, Dobkowski (2005) found that PE-LLD a lifetime has of 1 year at 100 °C [27]. These examples show that HDPE in the conditions of the ZEF AEC will most likely **not** make a lifetime of 20 years.

The role of *hydrolysis* is tested in collaboration with Promolding B.V. in a simple experiment where HDPE dog-bone shaped samples were put in a 30wt% KOH solution at 90 °C. From these tests it became clear that after about 50 days, the HDPE dogbone samples have become very brittle and lost their ability to deform plastically as shown in Figure 3.2. This confirms the **unsuitability** of HDPE for alkaline water electrolysis applications. Therefore, HDPE is **not** further considered in this study.

3.2.2 Polyphenylene sulfide (PPS) reinforced with 40% glass fibres

General Properties

Polyphenylene sulphide (PPS) is a sulphur-containing aromatic polymer. The polymer consists of aromatic rings linked by sulphides, see structure in Table 3.4. PPS is marketed under different brand names for different manufacturers. The major players are established in Asia (China and Japan), such as China Lumena New Materials and Toray Industries. In Europe, Solvay and Celanese are big manufacturers of PPS. According to their data sheets and CES EduPack [18, 35], PPS has a good thermal resistance up to 200 °C. Furthermore, it is dimensionally stable, which means that complex parts can be moulded within tight tolerances. Due to its chemical stability, it is resistant to a wide range of solvents and corrodants even at elevated temperatures. Moreover, the aromatic rings make the polymer

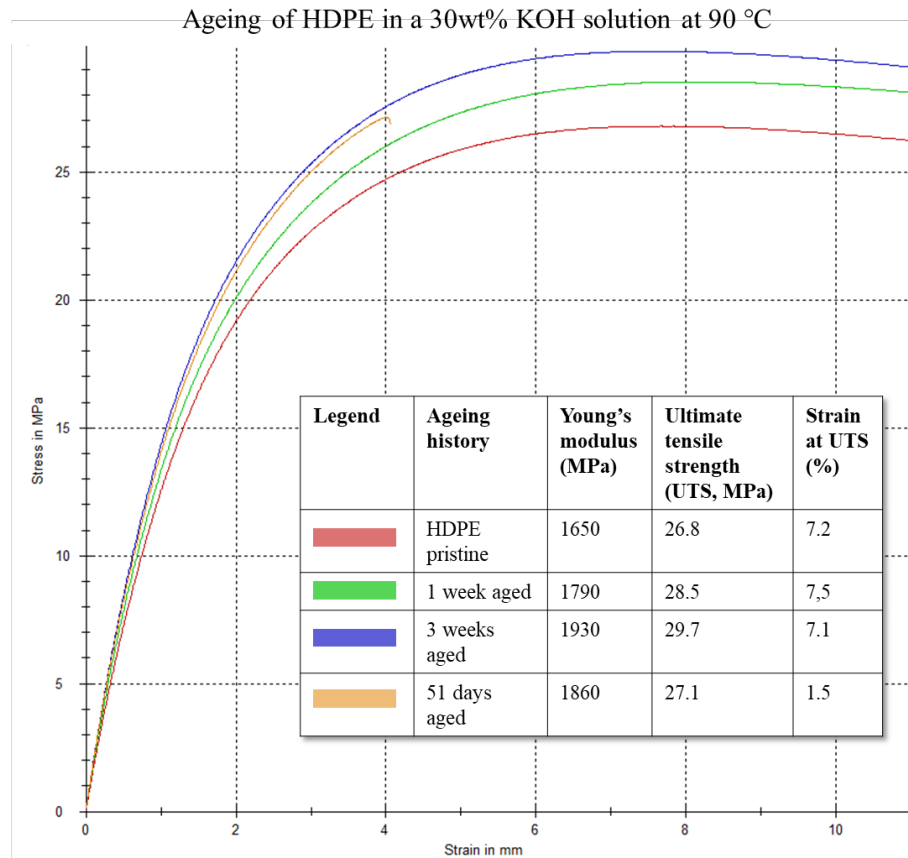


Figure 3.2: HDPE exposed to a 30wt% KOH solution at 90 °C. Experiment in collaboration with Promolding B.V.

resistant against high temperatures and give it excellent hydrolytic stability [43, 51]. With respect to these properties, PPS is a very good candidate for the liner of the ZEF AEC.

PPS is, however, very rarely used in its pure form. It is almost always mixed with fibres, such as glass or carbon fibres, or minerals and fillers in order to overcome its inherent brittleness [51]. The most general type of PPS is reinforced with 40% glass fibres. It has been discussed that glass displays poor performance against very caustic environments. This may affect the durability of glass-reinforced PPS against the conditions of the ZEF AEC. However, both CES EduPack and the manufacturer state that PPS-40%gf is resistant against alkaline solutions [35, 81]. Perhaps, dissolution is only a problem for the surface and not the bulk. Therefore, in order to investigate this, tests with PPS-40%gf have been pursued.

Degradation resistance

An application of PPS in extreme conditions is as filters in bag dedusters in coal-fired power-plants. Recently, growing interest has been shown in China leading to different PPS degradation studies [15, 37, 85]. When heated in the presence of oxygen or air to

temperatures above 250 °C, PPS will undergo cross-linking due to the oxygen reacting with the polymer chains, which is called oxidative cross-linking [46, 51, 86, 90]. This process is called curing and leads to thermoset-like properties, but also to a more brittle behaviour of the polymer. The oxidation reaction for PPS involves the generation of sulfuryl groups (-SO₂-). The low bond energy of the C-S bond results in easy oxidation of this bond [15, 89]. Hydrogen abstraction is an important mechanism for the development of cross-links. Therefore, the curing reaction is enhanced in the presence of oxygen, since oxygen is an efficient hydrogen abstractor [86]. According to Wejchan and Perkowska (1992) oxidative cross-linking occurs through the hydrogen abstraction of the phenyl group, which reacts with another phenyl group resulting in cross-links. In Figure 3.3, taken from Wejchan and Perkowska (1992), the radical is a quinone, however this could be any hydrogen abstractor such as oxygen or the thyl radical [86].

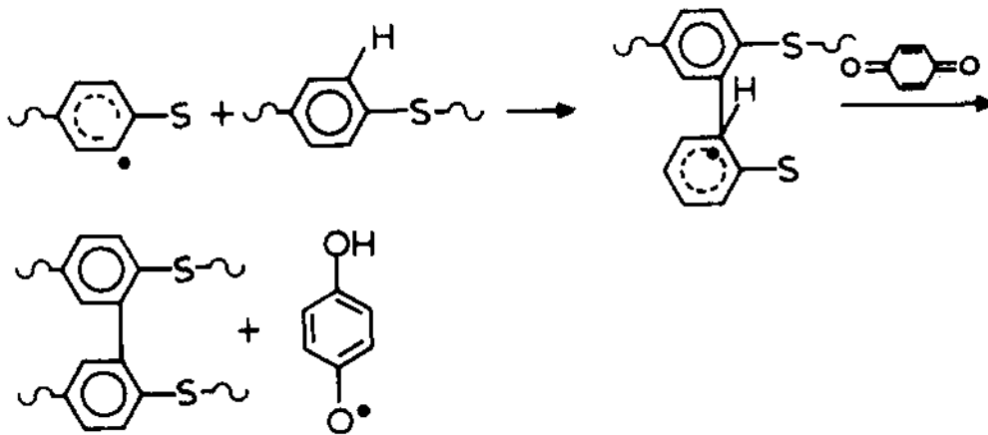


Figure 3.3: The formation of oxidative cross-links in PPS in the presence of a hydrogen abstractor. Taken from Wejchan and Perkowska (1992) [86].

3.2.3 Polysulfone (PSU)

General Properties

Polysulfone (PSU, but also abbreviated as PSF in the literature) is a rigid, amorphous high temperature thermoplastic. It has high thermal stability, good ductility, high toughness and strength and is chemical stable, making it useful for demanding engineering applications. It is also highly resistant to electrolytic solutions with a pH range from 2 to 13, and to oxidising agents [51]. The polymer is transparent in its natural state by virtue of their fully amorphous nature. PSU can be processed by injection moulding and is with a cost price of 8.39 - 12.10 €/kg the most expensive option considered.

PSU is often used for membrane applications in the food industry or as a reverse osmosis membrane, because of its excellent resistance to hydrolysis by hot water/ steam and its excellent resistance to acids and bases. It is also used as a gas separation membrane for oxygen enrichment [21], which implies good oxidation resistance.

Degradation resistance

Gesner and Kelleher (1968) found that PSU is essentially inert to both air and oxygen up to 140 °C [32]. After 8000 hours of ageing at 125 °C, the infrared spectrum was unchanged from that of the original polymer, the weight loss was less than 0.2% [32]. When aged for 6 months at 110 °C, the tensile break strength changes less than 10% and the elongation by less than 5% [32]. Yamashita et. al. (1993) found that below the glass temperature of PSU, which is between 186 and 192 °C, main chain scission and cross-linking occur simultaneously, whereas cross-linking predominates above the T_g during photodegradation [91]. Cross-linking in PSU arises due to similar mechanisms as discussed for PPS [91].

Chapter 4

Methodology

In the previous chapter, PPS and PSU are found to be very promising candidates for the encapsulation of the ZEF AEC. This chapter is concerned with the methodology of testing the durability of PPS and PSU exposed to conditions similar to that of the ZEF AEC.

The aim of the experiments is to create a better understanding of the development of the (mechanical and thermal) properties of PPS and PSU when exposed to an oxidising atmosphere or exposed to a strong alkaline solution at elevated temperatures. From the experimental data, extrapolations can be made from which the potential lifetime of the polymer can be assessed. This is further elaborated upon in the following chapters.

4.1 Samples

For the experiments dog-bone shaped samples of PPS and PSU with dimensions (length, width, and thickness) of 30.0 mm, 2.0 mm and 0.8 mm were produced by Promolding B.V., see Figure 4.1. The material was melted at 330 °C and has been processed through injection moulding with a mould temperature of 140 °C. The samples have not been subjected to any post-processing treatments.

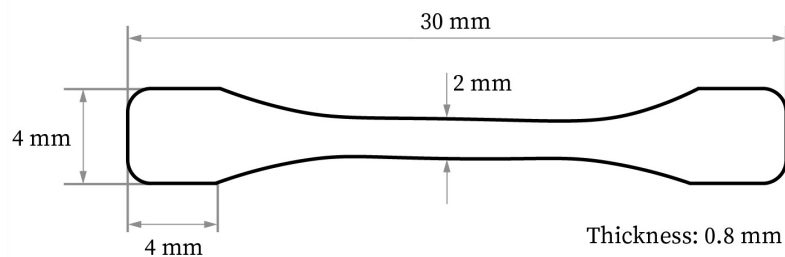


Figure 4.1: Dimensions of the PPS-40%gf and PSU dogbone samples. Gauge length 13 mm.

The **PPS** samples are the Fortron 1140L4, which is a 40% glass-reinforced grade, and will therefore from now on be denoted as *PPS-40%gf*. The glass-reinforcement is an E-glass. A mould temperature of 140 °C gives a degree of crystallinity of about 50% according to the PPS processing guide [75].

The **PSU** samples are the Udel P-1700 BK 937, which is opaque black due to the addition of 1% of carbon black. This does not affect the properties of PSU. The datasheet of PPS-40%gf and PSU are given in Appendix A.

4.2 Ageing procedures

There are essentially three approaches to assessing the service life of a material. These are from experience, from real or simulated service trials, and from accelerated testing [14].

Despite the fact that alkaline electrolysis cells have been running for over two centuries now, not much experience has accumulated and has been documented regarding the use of thermoplastic polymers in these conditions. As mentioned previously, current alkaline electrolysis systems use Zirfon membranes, which have a body made of often PSU [3]. These membranes have a predicted lifetime of at least 5 years. However, there is no public data available confirming these lifetimes, nor the testing/operation conditions. Therefore, other means -than from experience alone- have to be considered when assessing the durability and service lifetime of PPS-40%gf and PSU.

In order to reliably predict the lifetime of a material, one should expose this material to the operation conditions and track the relevant properties for a period of time which is essentially equal to the desirable lifetime. In this case this would mean ageing for 20 years. Naturally, performing durability tests for such timescales is not feasible. Therefore, accelerated ageing is performed.

Accelerated ageing is a method to mimic the operation conditions using more extreme conditions in order to be able to predict the lifetime of a material without having to wait the full lifetime [19]. This is valid for cases where we expect the *same* degradation mechanisms to occur at the service conditions as well as at the accelerated conditions. Accelerated ageing can be accomplished by exaggerating different parameters which influence the reaction rate. For example, in the case of the ZEF AEC, thermo-oxidative degradation and chemical degradation in the form of hydrolysis are expected to be the major degradation mechanisms. Therefore, it can be expected that the agents of these degradation reactions (*i.e.* the amount of available oxygen molecules and the KOH concentration) could potentially affect the rate of degradation. If this relationship is known, ageing can be accelerated by changing the oxygen partial pressure and the KOH concentration.

A more general and more widely used method of accelerated ageing is by increasing the *temperature*. This is adequately described by the Arrhenius law as shown in Equation 2.3 in Chapter 2. From this relation, a *rule of thumb* can be deduced which states that an increase of 10 °C leads to roughly a doubling of the reaction rate. For ageing this would mean that an increase of about 10 °C results in twice as fast ageing [14]. This rule of thumb can be used to obtain a sense of how long and at which temperature should be aged in order to cover a lifetime of 20 years at 90 °C. For example, in order to achieve a substantial amount of ageing in the short time period available (8-12 weeks), it is necessary to age at temperatures up to 150-160 °C. However, accelerated ageing at temperatures too far from the operation condition of 90 °C, especially if this means trespassing the glass transition temperature, can give unreliable results, because the degradation mechanisms can change. Therefore a trade off has to be made.

Moreover, in order to be able to translate the results obtained at higher temperatures to the expected results at the (lower) operation temperature, it is necessary to exactly know how the reaction rate is affected by temperature. Then, the rule of thumb does not suffice. This relationship can be obtained by performing accelerated ageing experiments for a range of temperatures. ASTM International has developed a procedure of performing accelerated ageing using elevated temperatures. They state that in order to reliably predict what happens to the material properties of a polymer after 20 years of operation, an accelerated ageing experiments at 4 different temperatures for time periods in the order of 6 months to 1 year has to be performed (ASTM D3045) [23]. For this project, however, it is not feasible to perform experiments for this type of duration. Therefore a different approach has been taken in order to obtain the desired results.

4.2.1 Ageing conditions

For the experimental ageing conditions different parameters have to be considered, which are discussed below.

Pressure

It is important to note that due to practical reasons it has **not** been possible to exactly mimic the operation conditions of the ZEF AEC ($T = 90\text{ °C}$, $P = 50\text{ bar}$ with the presence of a 30wt% KOH solution, H_2 and O_2 in gas form). Unfortunately, no high pressure lab was available in order to perform experiments at 50 bar pure oxygen. A safety assessment of working with pure oxygen has been conducted. From this assessment it has been found that it is safe to age PPS-40%gf and PSU samples at elevated temperatures in pure oxygen at *5 bar* in a regular fume-hood. The calculations are given in Appendix B.

In order to study the effect of the oxygen partial pressure (pO_2), the samples have also been subjected to ageing in atmospheric conditions where $pO_2 = 20\%$. This is a 25 times lower oxygen partial pressure than at 5 bar pure oxygen.

Temperature

Regarding temperature, it has been chosen to age at 90 °C, which is the operation temperature of the ZEF AEC, but also very close to the glass transition temperature of PPS-40%gf. A higher temperature of 120 °C has been chosen in order to induce acceleration of the degradation process. For PSU, since the glass transition temperature is very high (about 180-190 °C), it is possible to accelerate at an even higher temperature of 170 °C.

Chemical species

From literature study regarding degradation mechanisms, it became clear that the agents most likely to cause degradation of the polymer are oxygen and KOH. Hydrogen is less likely to cause significant degradation, since hydrogen is absorbed in polymers as a diatomic molecule, which is chemically inert [11].

In order to accelerate degradation due to the presence of KOH, there are two possible ways. Either by increasing the temperature or by increasing the concentration. Since the operation temperature of 90 °C is close to the boiling temperature of water, increasing the ageing temperature is only possible in a pressurised system. However, since this is not practical, ageing at different KOH concentrations has been studied. Table 4.1 gives an overview of the ageing conditions of the experiments which have been performed.

Table 4.1: An overview of the ageing conditions.

Degradation mechanism	Effect tested	Ageing condition	Ageing temperature (°C)
Thermo-oxidative degradation	Temperature	1) 5 bar oxygen	90
		2) 5 bar oxygen	120
	Oxygen partial pressure	3) air atm	90
		4) air atm	120
Extra condition for PSU	Thermo-oxidative degradation	5) air atm	170
Hydrolysis	KOH concentration	6) 15wt% KOH	90
		7) 30wt% KOH	90
		8) 45wt% KOH	90

Ageing time

The ageing experiments were conducted over a period of 4 to 12 weeks. After 5 or 6 different time moments, samples were taken out of the set up, cooled, and characterised with different measurement techniques (Section 4.3). The samples were always collected between 9:30 and 10:30 in the morning. The samples were taken out of the set up and left to cool for several hours before performing any characterisation. The KOH samples were also left to cool to room temperature and carefully wiped dry before characterisation.

4.2.2 Ageing set up

Ageing experiments in pure oxygen were conducted in a self-made oxygen tank, as shown in Figure 4.2. All other ageing experiments were conducted in an air-circulating oven. The *air* samples were aged in open beakers at either 90 °C, 120 °C or 170 °C. The *KOH* samples were contained in HDPE screw lid containers, which prevented the evaporation of liquid, as shown in Figure 4.3. However, some of the HDPE containers started leaking after 2 - 2.5 weeks of operation. These have been continuously replaced. However, after 33 days, stainless steel containers with lids have been used.

The density of the solution has been measured (using the Anton Paar DMA 5000 density meter) and refreshed regularly in order to maintain the proper KOH concentration. Table 4.2 gives an overview of the measured densities. The first row gives the actual density of a KOH solution for the different concentrations, which has been calculated with the density of KOH (2.12 g/cm³) and water (1 g/cm³). As shown the density stays within 1% of the calculated value, meaning the change in KOH concentration due to water evaporation is negligible in the bigger picture.

Table 4.2: Measured KOH concentrations during ageing time. The measurements were taken at 20 °C.

Ageing time	KOH 15wt% (g/cm ³)	KOH 30wt% (g/cm ³)	KOH 45wt% (g/cm ³)
Calculated density	1.137	1.287	1.453
0 days	1.138005	1.28838	1.45346
28 days	1.14343 (PPS) 1.15074 (PSU)	1.29999 (PPS) 1.29867 (PSU)	1.46183 (PPS) 1.46059 (PSU)
New solution after 33 days	1.14508	1.29357	1.45974

It is important to note that the density of PSU is lower than the density of the KOH-



Figure 4.2: Setup of accelerated ageing system

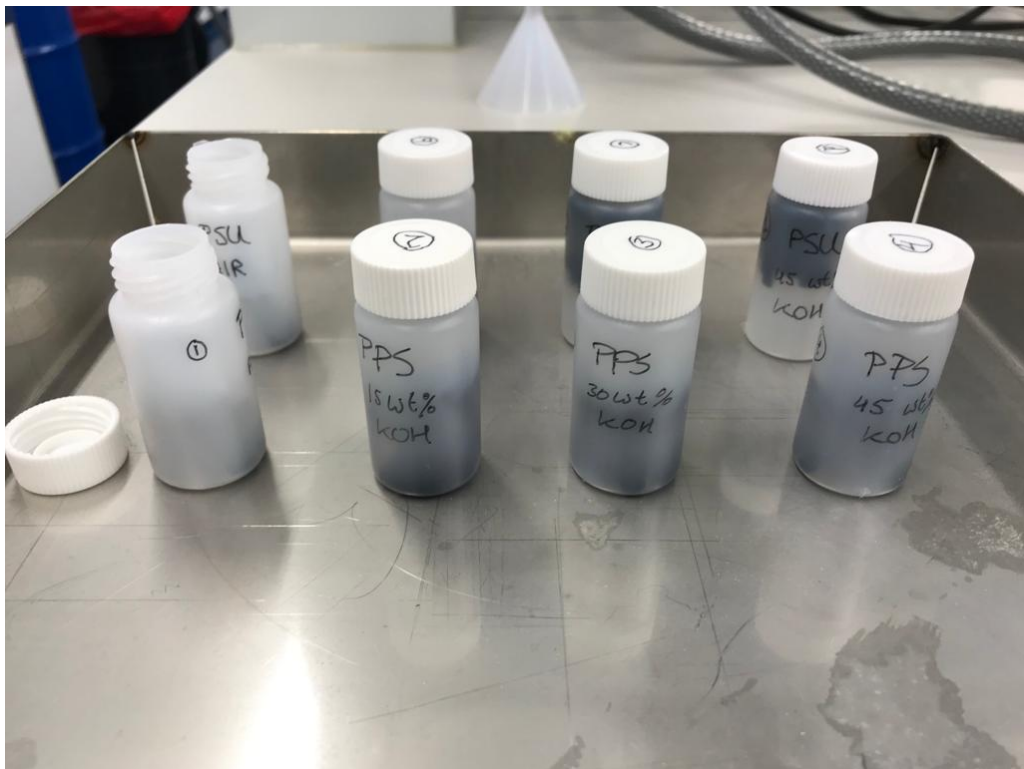


Figure 4.3: Setup of samples in a KOH solution.

solution for 30 and 45wt% KOH. This means that the PSU samples for these solutions floated. However, this is not a big problem, since the containers were small enough for all the samples to be packed vertically, meaning only a very small tip was exposed to air (Figure 4.3).

Design of the oxygen tank

As mentioned before the oxygen-samples have been aged in a self-made oxygen tank. This setup consists of four 18 mm Swagelok tubes of 50 mm long and a wall thickness of 1.5 mm, in which the samples were exposed to pressurised oxygen. The tubes were heated using two SB1 PID temperature regulators from RKC INSTRUMENT INC, which allow for ageing at two different temperatures. The setup consists of Swagelok oxygen certified needle valves and fittings, which are connected with 6 mm Swagelok tubes to an oxygen tank of 5L that contains molecular oxygen at 200 bar. The set up is shown in Figure 4.2 and 4.4.

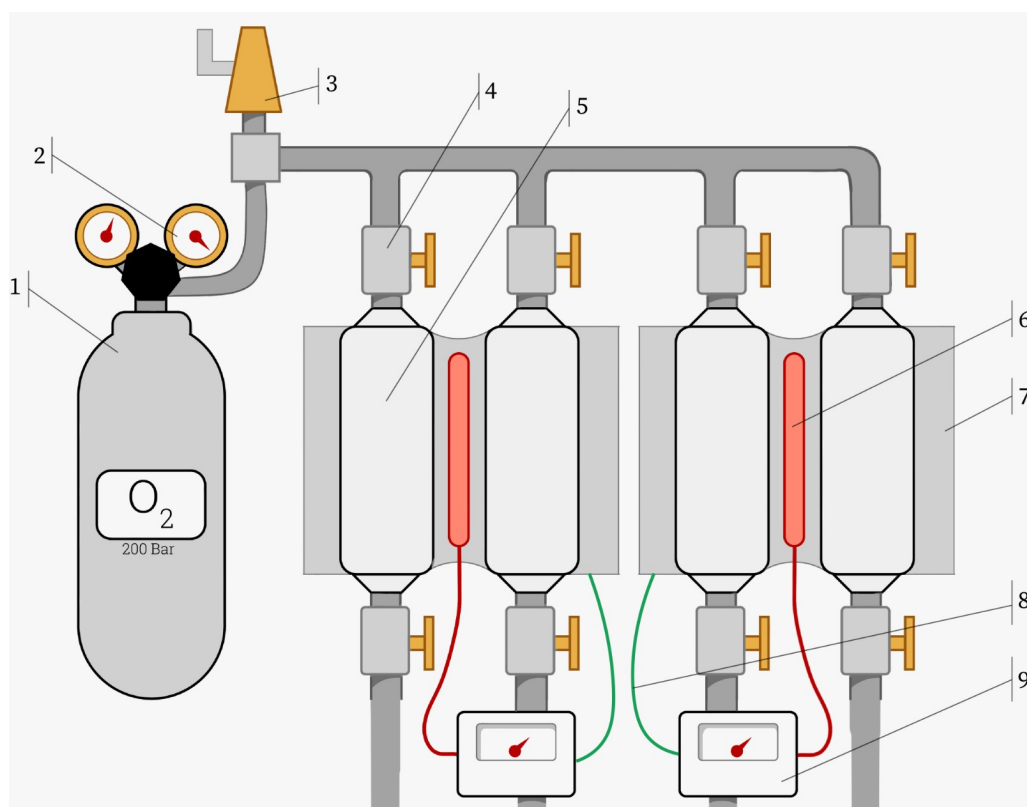


Figure 4.4: Schematic of the oxygen setup containing the following parts: 1) 5L 200 bar pure oxygen flask, 2) pressure regulator, 3) pressure relief valve set at 8 bar, 4) oxygen certified Swagelok needle valve, 5) 18 mm Swagelok tube containing the samples, 6) heating element, 7) aluminium block for heating the tubes, 8) thermocouple, and 9) SB1 PID temperature regulator from RKC INSTRUMENT INC. Heating paste has been applied between the heating element and aluminium block and between the 18 mm tubes and the aluminium block.

4.3 Equipment and measurement procedures

Degradation of polymers can lead to the breaking of primary bonds, which expresses itself in degradative symptoms such as hardening, embrittlement, softening, cracking, crazing, discoloration and alteration of properties [63]. Degradation is a gradual process and involves many different aspects, including a complex interplay of a multitude of reactions. The rate and extent of the reactions involved in polymer degradation can be monitored in different ways.

The most important performance parameters for the ZEF AEC are for the polymer to retain toughness, strength and dimensional stability. Therefore, the mechanical and thermal properties are monitored using methods such as tensile testing, dynamic mechanical testing (DMA), creep-recovery testing, and differential scanning calorimetry (DSC). Furthermore, Fourier-transform infrared spectroscopy (FTIR) is used in order to obtain information about the compositional properties. Finally, scanning electron microscopy (SEM) is used to give visual information on the fracture plane and the surface of the samples. An overview of these characterisation techniques is given in Table 4.3.

Table 4.3: An overview of the characterisation techniques used.

Measurement technique	What kind of information obtained	Suitable for		Destructive or non-destructive	Machine details
		PPS-40%gf	PSU		
Weight measurements	simple tool to obtain information regarding changes in weight	yes	yes	non-destructive	Radwaf WAX 110 balance
Tensile testing	from the stress-strain curves mechanical information regarding stiffness, strength, toughness and elongation can be obtained	yes	yes	destructive	Zwick Z010
DMA	a tool to study the visco-elastic behaviour, the storage and loss modulus are obtained from which the T_g can be derived	yes	yes ¹	destructive	TA Instruments DMA Q800
Creep-recovery testing	collects data on the visco-elastic behaviour of the polymer at very low frequencies	yes	yes	non-destructive ²	TA Instruments DMA Q800
DSC	technique to obtain the T_g	yes	yes	destructive	Perkin Elmer DSC 7
ATR-FTIR	gives insights on the presence of certain chemical groups	yes	yes	non-destructive	ThermoFisher Nicolet iS50 FT-IR
XRD	analyses crystalline structures	yes	no ³	non-destructive	Bruker D8 Advance
SEM	obtain images of the surfaces and fracture surfaces of the samples	yes	yes	non-destructive	Jeol JSM-IT100

¹However, the T_g is not well defined.

²However, due to the high temperatures internal structure and chemistry of sample may have changed.

³Since PSU is amorphous.

4.3.1 Weight measurements

Degradation in polymers could lead to chain scission and the loss of short chain polymer fragments. This could have an effect on the weight of the polymer. Weight measurements are a simple and easy tool to be able to track any differences between the unaged and aged samples. For measuring the weight an analytical RADWAG WAX 110 balance has been used. Four to five samples have been weighed and averaged for each measurement point. The error in the samples due to variation between the samples is equal to ± 0.0005 g. However, the variation of the weight measurements does not appear to be random, but is clustered around two distinct weight values, as shown in Table 4.4. For PPS-40%gf the weights of the unaged samples have values around 0.09848 and 0.09954 grams. For PSU the weights have values around 0.07471 and 0.07553 grams. This is due to the fact the samples have been injection moulded **per two**. When sorting the samples to correct for the different moulds, the variation between measurements reduces to ± 0.0001 g.

Table 4.4: Weight distribution of 10 unaged PPS-40%gf and 10 PSU samples. The error distribution is not random. The value fall within two categories, which is due to the fact they have injection moulded in set of two. For PPS-40%gf the weights of the unaged samples have values around 0.09848 and 0.09954 grams. For PSU the weights have values around 0.07471 and 0.07553 grams.

Weight unaged PPS-40%gf	Weight unaged PSU
0.09848	0.07474
0.09966	0.07457
0.09846	0.07458
0.09950	0.07548
0.09847	0.07546
0.09953	0.07553
0.09839	0.07484
0.09861	0.07554
0.09839	0.07487
0.09857	0.07475

4.3.2 Tensile testing

In order to monitor changes in mechanical properties of the polymer samples, tensile testing using the Zwick Z010 test machine with a 500 N load-cell have been performed with a test speed of 0.5 mm/min. Tensile testing subjects the dogbone shaped samples to a controlled

tension until failure. The following parameters can be obtained: ultimate tensile strength (UTS), breaking strength, maximum elongation, Young's modulus, yield strength, strain at yield and material toughness, which are further described in the results in Chapter 5 and 6. For each condition and ageing time, three samples have been subjected to the tensile tests.

4.3.3 Dynamic mechanical analysis (DMA)

Dynamic mechanical analysis is a very useful tool to study the visco-elastic behaviour of polymers. The basic principle of DMA is applying an oscillating force to a sample and analysing the material's response to that force with respect to temperature and frequency [52]. From the material's response a complex modulus (E^*) can be calculated which is composed of an elastic modulus (E') and an imaginary loss modulus (E''). The modulus measured in DMA is not exactly the same as the elastic Young's modulus of the classic stress-strain curve. The different moduli measured by DMA allows for better characterisation of the material, because the ability of the material to return or store energy (E'), and its ability to lose energy (E''), as well as the ratio of these effects ($\tan \delta$), which is called damping, can be analysed.

The peak of the 1 Hz loss modulus or the peak of the 1 Hz $\tan \delta$ curve is often used as a measure of the glass transition temperature of a polymer. In our case, the peak of the loss modulus is chosen, since the loss modulus curve is often smoother than the $\tan \delta$ curve.

For the measurements the TA Instruments DMA Q800 has been used in tensile mode. A frequency sweep was performed for 5 different frequencies (60 Hz, 31.6 Hz, 10 Hz, 3.2 Hz and 1.0 Hz) whilst the temperature increased from room temperature to 290 °C at 2.0 °C/min. The maximum amplitude is 15.0 μm in order to stay in the visco-elastic region even at elevated temperatures.

4.3.4 Creep-recovery testing

The TA Instruments DMA Q800 is also used to perform creep-recovery testing in tensile mode. Creep-recovery testing involves examining the material's response to a constant load and its behaviour on the removal of that load. It collects data on the visco-elastic behaviour of the polymer at very low frequencies.

Multi-temperature creep tests have been performed in order to be able to analyse the results with time-temperature superposition and to be able to find the apparent activation energy of creep from the shift-factor. A stress of 5 MPa is used in order to stay in the

visco-elastic region. The temperatures used are 90 °C, 110 °C, 130 °C and 150 °C. Figure 4.5 shows a graph of the testing conditions. The temperature is increased to the desired temperature, and left to equilibrate for 15 minutes. Then the 60 minute creep test starts and a stress of 5 MPa is applied, after which the sample is unloaded and left to recover for 10 minutes. The temperature increases again and after 15 minutes of equilibration and further recovery, the next creep test starts.

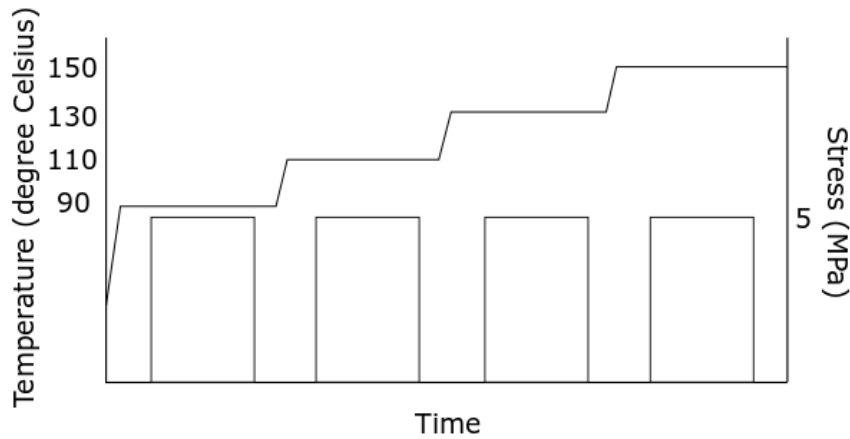


Figure 4.5: Procedure of creep-recovery test. Equilibrating at the desired temperature for 15 minutes, creep test at 5 MPa for 60 minutes, recovery for 10 minutes, followed by a temperature increase and further equilibration and recovery of 15 minutes, then again the creep test at 5 MPa for 60 minutes and so on.

4.3.5 Differential scanning calorimetry (DSC)

Differential scanning calorimetry is a technique which measures the differences in the amount of heat required to increase the temperature of a sample and that of a reference as a function of temperature. This results in a curve of heat-flux against temperature. The glass transition temperature can often be determined with DSC, since the heat capacity of the polymer is different before and after the glass transition temperature. The heat capacity of polymers is usually higher at temperatures above the T_g , resulting in a step in the curve. Other reactions such as crystallisation and melting can be shown in the curve with an exothermic valley and an endothermic peak, respectively.

For the DSC measurements, the Perkin Elmer DSC 7 has been used. The sample has been heated up from room temperature to 400 °C in steps of 10 °C per minute.

4.3.6 Fourier-transform infrared spectroscopy (FTIR)

Fourier-transform infrared spectroscopy (FTIR) is a measurement technique, which is able to obtain an infrared spectrum of the absorbed wavelengths of a solid, liquid or gas sample.

Molecules absorb specific wavelengths of light that are characteristic to their structure by the excitation of the bonds. The infrared spectrum obtained is a fingerprint of the molecular compound and can give insights in the reaction products of the induced degradation.

Unfortunately, due to circumstances, three different FTIR machines were used during the course of the project. These are the Perkin Elmer Frontier, Perkin Elmer Spectrum 100 and the ThermoFisher Nicolet iS50 FT-IR. Since, the ThermoFisher Nicolet was used for the majority of measurement, the spectra from this machine are presented in this report. The samples are measured using single reflection attenuated total reflectance (ATR) sampling. The reading is taken 2 μm below the surface. For the generation of a single spectrum, 16 scans were recorded at an optical resolution of 4 cm^{-1} and corrected for the background.

The spectra have been plotted using opensource Spectragryph software. Different references have been used in order to identify the different peaks, including infrared spectral databases, such as IRPal 2.0 and different publications of ATR-FTIR analysis of PPS and PSU [15, 22, 32, 55, 89].

4.3.7 X-ray diffraction (XRD)

X-ray diffraction is a non-destructive technique which can be used to analyse crystalline structures. The regular lattice of crystalline structures is able to diffract X-rays into many specific directions. These directions depend on the lattice spacing of the crystal structure and can be used to characterise the phases present in the sample.

The samples are fixed onto a Si510 wafer. The instrument used, is a Bruker D8 Advance diffractometer with Bragg-Brentano geometry and Lynxeye position sensitive detector. $\text{Cu K}\alpha$ radiation is used. Other parameters include: divergence slit V12, scatter screen height 5 mm, 45 kV 40 mA, detector settings LL 0.11 W 0.14, and no sample spinning. The measurements were taken with a coupled $\theta - 2\theta$ scan from 10 - 110°, with step size 0.041 * 2θ , and counting time per step 1 s. Bruker software DiffracSuite.EVA vs 5.1. is used for the data evaluation.

4.3.8 Scanning electron microscopy (SEM)

The Jeol JSM-IT100 scanning electron microscope has been used to obtain images of the surfaces and fracture surfaces of the samples. Furthermore, energy-dispersive X-ray spectroscopy (EDS) analysis has been used in order to obtain information of the elemental composition of the surface. Low vacuum mode has been used, since the samples are non-conductive, which led to lower quality images. The samples have not been coated.

Chapter 5

Results and discussion PPS-40%gf

This chapter is concerned with the results and discussion of ageing of PPS-40%gf in oxygen and KOH.

5.1 PPS-40%gf aged in oxygen

5.1.1 Tensile tests (PPS-40%gf; oxygen)

Figure 5.1 shows the stress-strain curves of unaged PPS-40%gf and PPS-40%gf exposed to oxygen at 5 bar and 90 °C for 4, 6, 8 and 12 weeks. From each stress-strain curve, four parameters are retrieved and averaged for the three measurements taken for each point. These are the Young's modulus, ultimate tensile strength (UTS), strain at UTS and material toughness.

The Young's modulus is obtained from taking the slope of the stress-strain curve between 0.2 and 0.6 % strain in order to avoid initial start up/slip effects. For the stress-strain curves in Figure 5.1 this resulted in the Young's modulus changing from an average of 7.5 to 8.8 (± 0.3) GPa. The ultimate tensile strength (UTS) is defined as the maximum strength reached, which increases from an average of 153.5 to 165.7 (± 2.5) MPa after 12 week. The strain at UTS is defined as the elongation at the point of maximum strength. However, since PPS-40%gf is a very brittle polymer the strain at UTS is equivalent to the strain at break or the maximum elongation. This parameter decreased from 2.7 to 2.4 (± 0.1) %. Finally, the material toughness is calculated as the integral of the stress-strain curve, taken from zero strain to strain at UTS. The toughness decreased slightly from 2.6 to 2.3 (± 0.2) MPa. The typical uncertainty is given within brackets and is derived from the average of the standard deviation of the three measurements over all measurements.

This procedure has been repeated for the samples aged in oxygen at 120 °C and air at 90 and 120 °C for different ageing times. The results are plotted in Figure 5.2 to 5.5, while the stress-strain curves are shown in Appendix C.1.

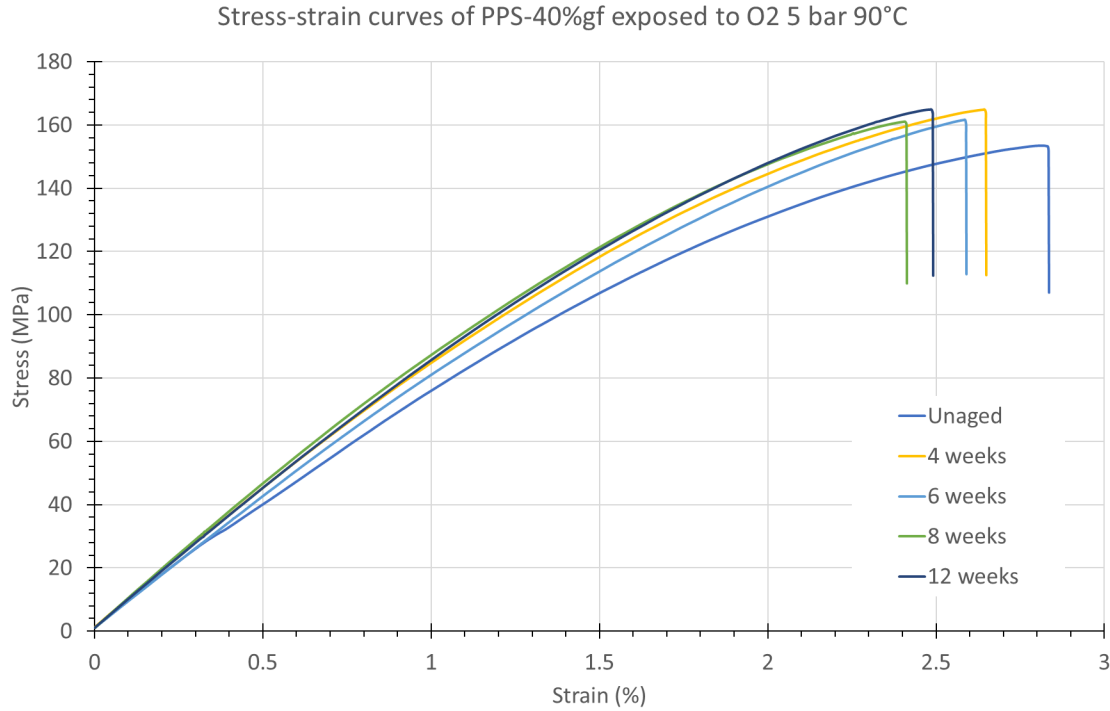


Figure 5.1: Stress-strain curves of PPS-40%gf exposed to O₂ at 5 bar and 90 °C.

All the Young's modulus curves show a dip of the modulus between 10 and 20 days of ageing. For the air 90 °C, and O₂ 90 and 120 °C curves the lower modulus could be partly due to the fact that these measurements were corrupted due to a loose grip element for which the measurements have been corrected for as shown in Appendix C.3. However, it is interesting that the air 120 °C samples also shows a slight dip in the 10 to 20 days region even though these tensile curves were not corrupted. However, since the unaged measurement was also corrupted, the position of the unaged measurement point becomes more uncertain. It can therefore **not** be confirmed that the Young's modulus has changed over time.

It is interesting that the samples aged at 120 °C all show a nearly immediate response (as short as one day) to a higher Young's modulus. This is also shown in the UTS curved in Figure 5.3 where the air and O₂ 120 °C samples show a sharp increase to about 163 MPa and seem to plateau at this strength. The samples aged at 90 °C show a slower increase in UTS and reach similar value of 160-165 MPa after about 30 days, after which the values plateau. Furthermore, it seems that the oxygen partial pressure is unimportant for the range that has been tested ($pO_2 = 0.2$ and 5 bar), since the air and O₂ 90 °C samples show the same trends and the air and O₂ 120 °C also show the same trends. The strain at UTS show a slight decrease in value of about 10% after 12 weeks (Figure 5.4). The toughness does not seem to change over time (Figure 5.5).

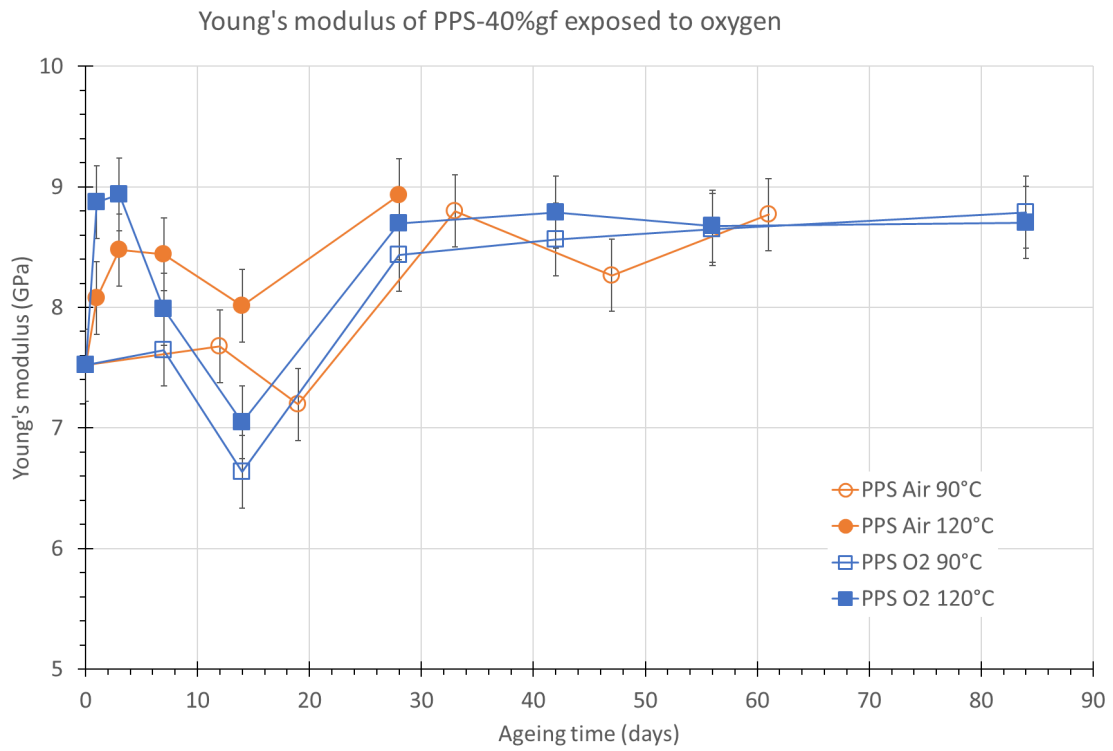


Figure 5.2: The Young's modulus over time for PPS-40%gf exposed air (orange lines) at 90 and 120 °C and oxygen at 5 bar (blue lines) at 90 and 120 °C.

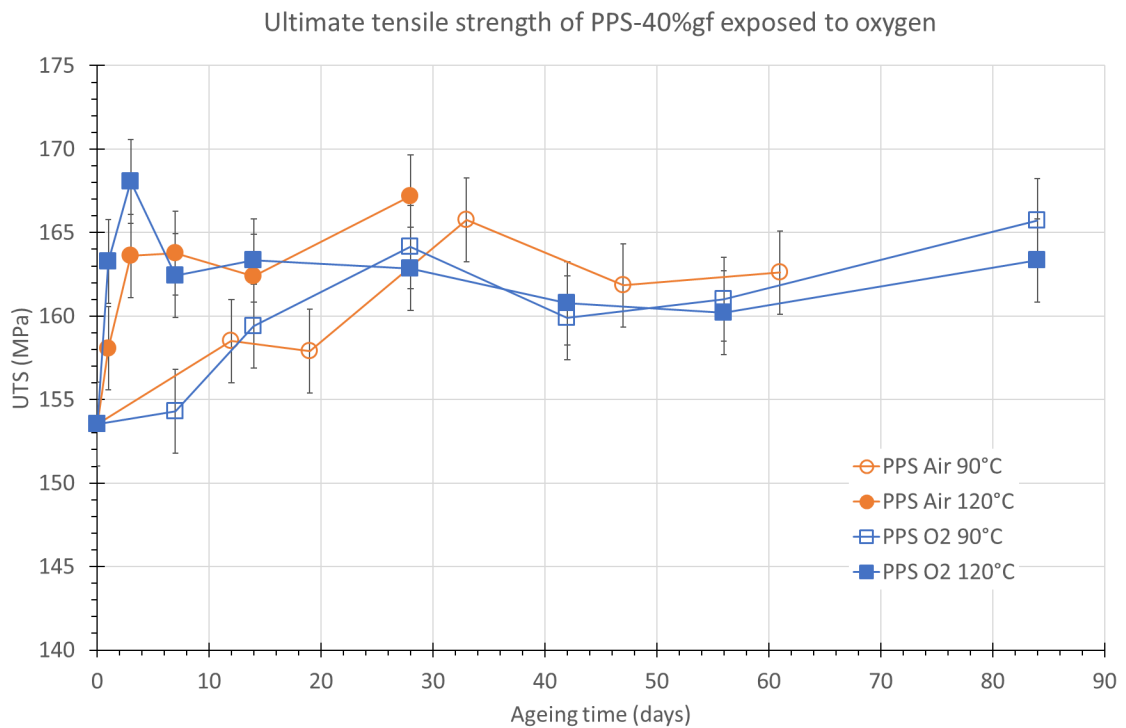


Figure 5.3: The ultimate tensile strength over time for PPS-40%gf exposed air (orange lines) at 90 and 120 °C and oxygen at 5 bar (blue lines) at 90 and 120 °C.

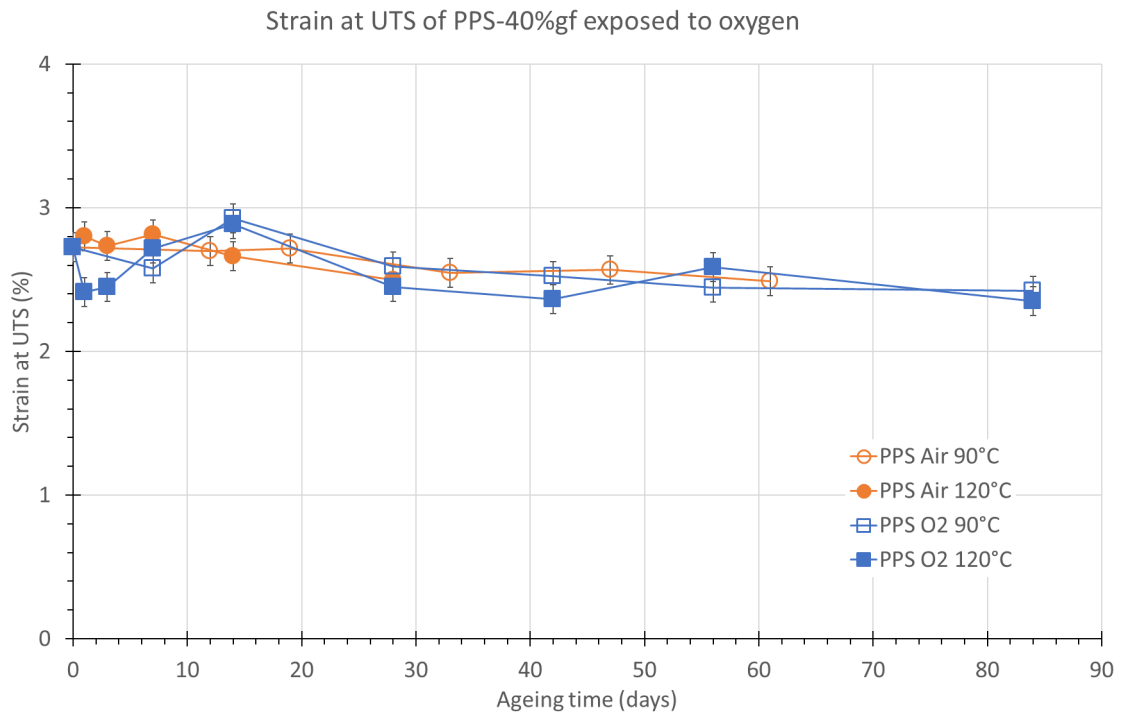


Figure 5.4: The strain at UTS over time for PPS-40%gf exposed air (orange lines) at 90 and 120 °C and oxygen at 5 bar (blue lines) at 90 and 120 °C.

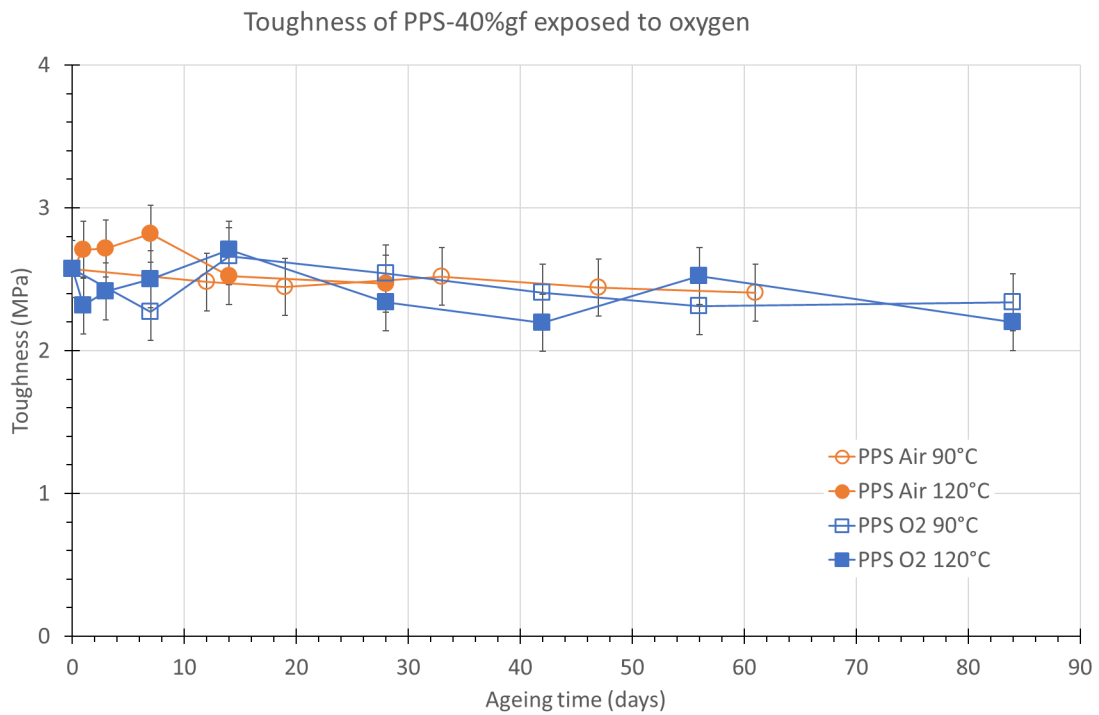


Figure 5.5: The material toughness over time for PPS-40%gf exposed air (orange lines) at 90 and 120 °C and oxygen at 5 bar (blue lines) at 90 and 120 °C.

5.1.2 DMA tests (PPS-40%gf; oxygen)

Figure 5.6 shows the storage modulus and loss modulus of the 1 Hz curve for PPS-40%gf aged in oxygen at 5 bar and 90 °C. The tan delta for the 1 Hz curves is the ratio of the loss to the storage modulus and is given in Appendix C.1. From these 1 Hz curves the storage modulus before the glass transition at 50 °C and after the glass transition at 200 °C have been determined and plotted versus ageing time. The peak of the loss modulus curve has also been determined and plotted against ageing time for both the peak value of the loss modulus itself and the corresponding temperature value. This temperature is defined as the glass transition temperature. This analysis has been applied to all the oxygen and air samples for the different ageing temperatures. The results of the storage modulus are given in Figure 5.7, whereas the peak of the loss modulus is given in Figure 5.8. Table 5.1 gives an overview of the T_g .

For the storage modulus for both the glass and the rubbery region, there is no clear trend visible over time. The loss modulus, however, shows a distinct change which is only dependent on temperature and not oxygen partial pressure as was also shown in the tensile tests. The samples aged at 120 °C, regardless of oxygen partial pressure, show a very quick drop in the loss modulus, followed by a plateau. For the 90 °C only a very small and more gradual drop is observed of about 0.2 GPa.

A similar trend is seen in the T_g values. The samples aged at 120 °C experience an almost immediate (< 1 day) increase in T_g of about 10 °C, followed by a plateau, whereas the 90 °C samples show a very gradual increase.

Table 5.1: Results of T_g of PPS-40%gf exposed to ageing in oxygen. The T_g is defined as the peak of the 1 Hz loss modulus curve.

Ageing condition	T_g (°C)							
unaged	114.66							
Air atm 90 °C	116.83	116.24	119.61	121.38	122.93			
	(12d)	(12d)	(33d)	(47d)	(61d)			
Air atm 120 °C	126.42	126.00	127.39	126.71	127.21			
	(1d)	(3d)	(7d)	(14d)	(28d)			
O ₂ 5 bar 90 °C	118.31	116.80	117.85	119.31	118.46	119.20		
	(7d)	(14d)	(28d)	(42d)	(56d)	(84d)		
O ₂ 5 bar 120 °C	125.81	126.16	128.57	127.84	131.20	136.44	132.04	132.47
	(1d)	(3d)	(7d)	(14d)	(28d)	(42d)	(56d)	(84d)

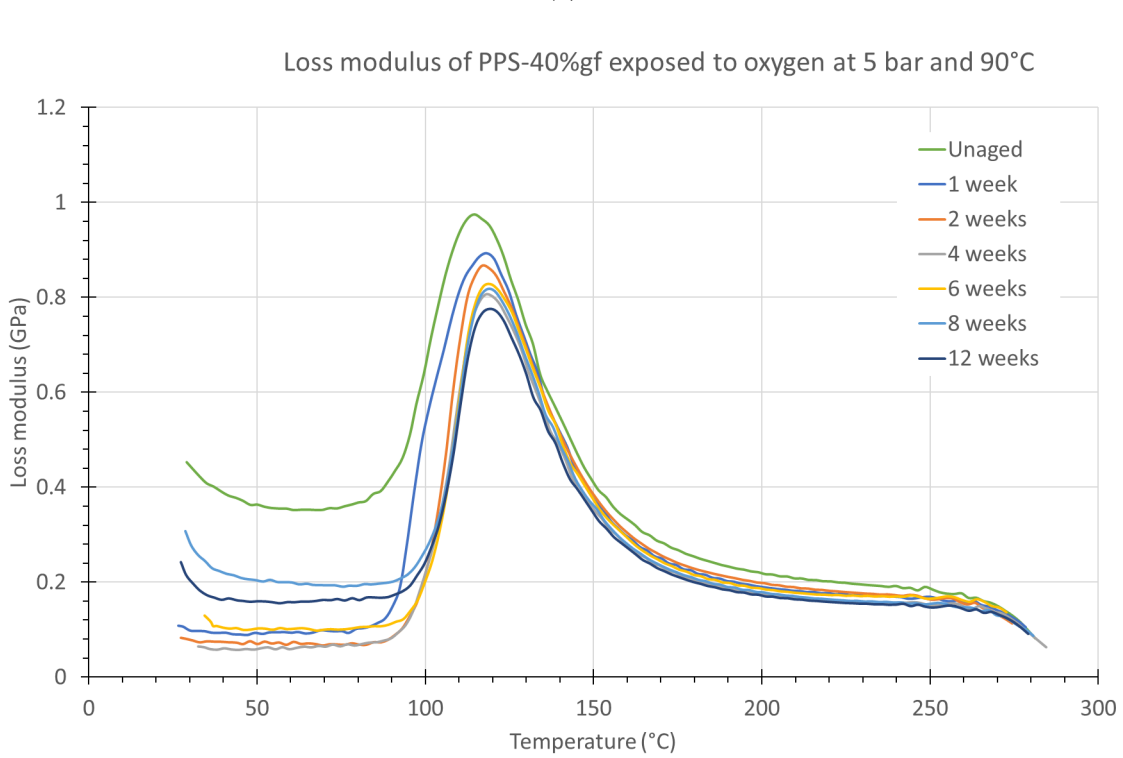
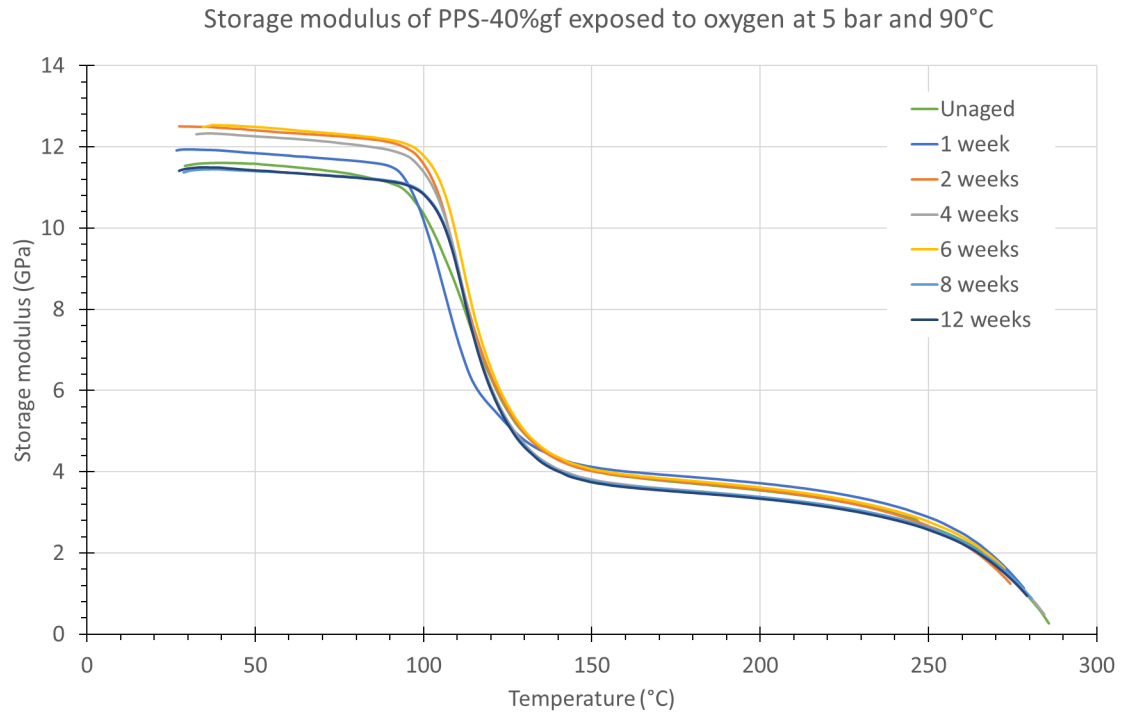


Figure 5.6: DMA curves for PPS-40%gf aged in oxygen at 5 bar and 90 °C showing (a) the storage modulus and (b) the loss modulus.

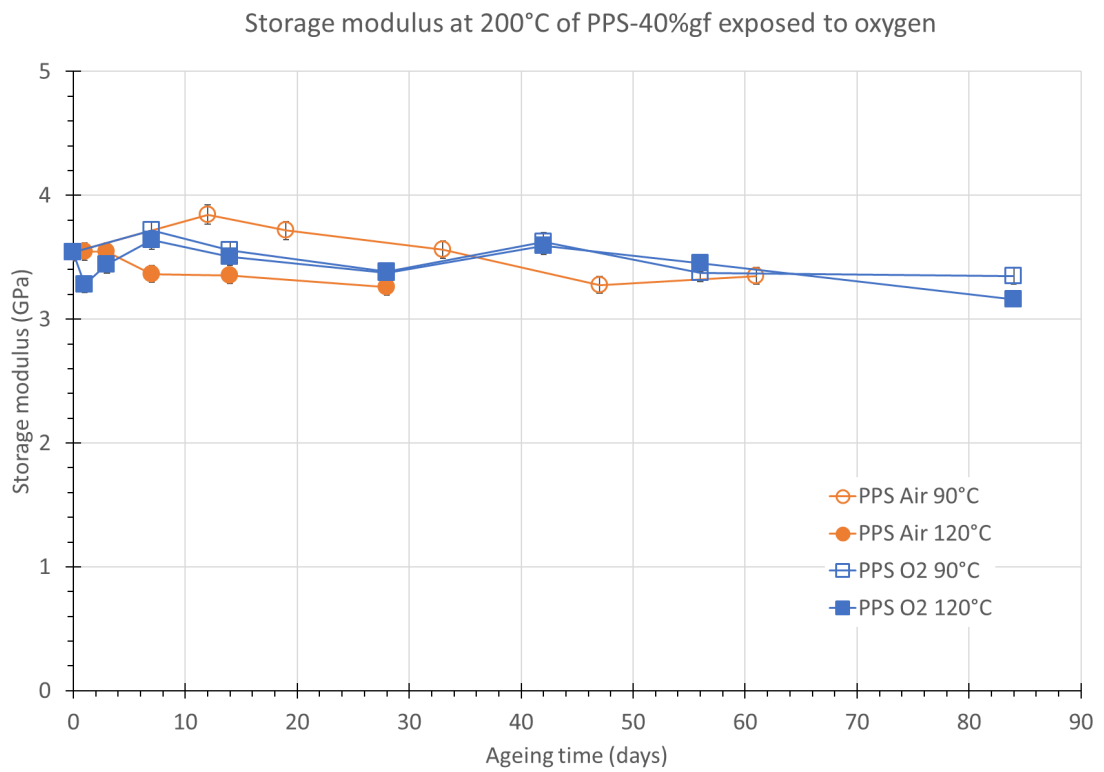
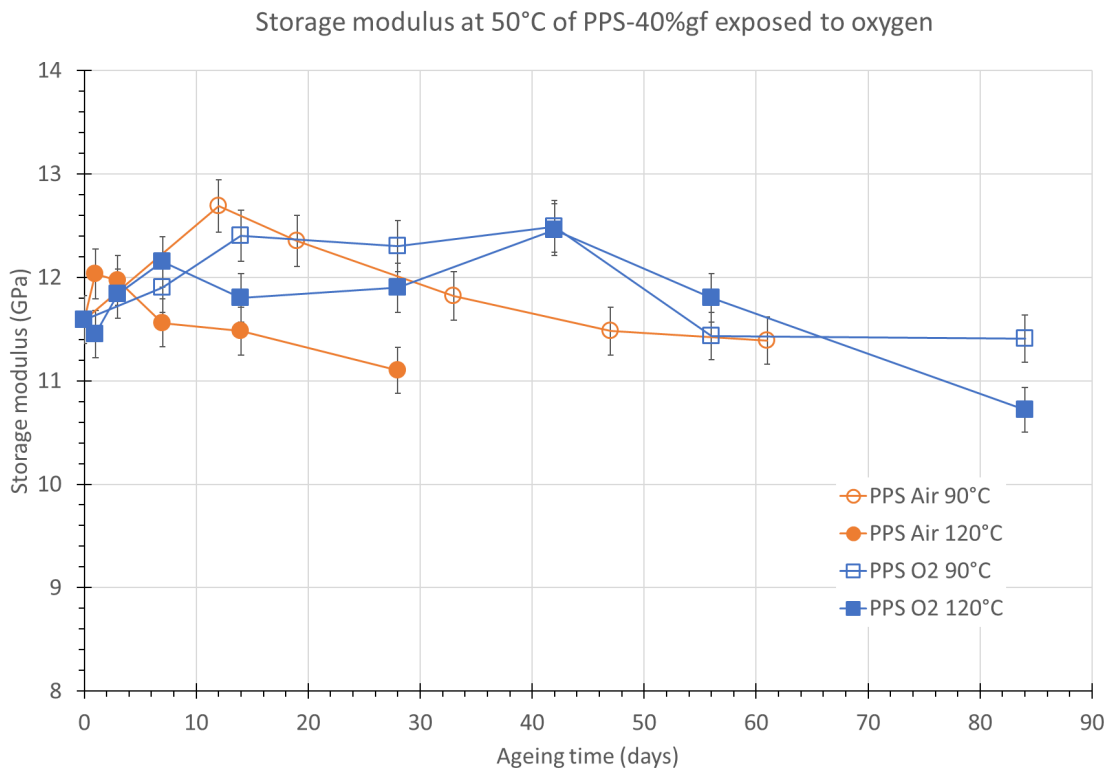
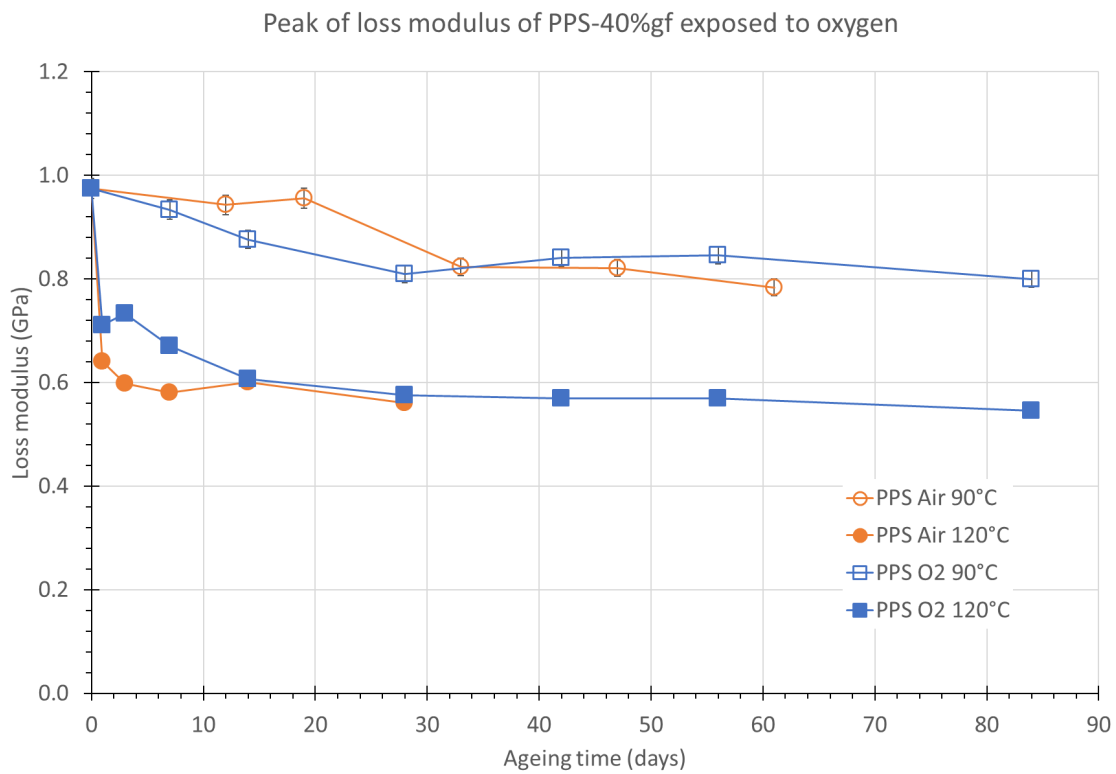
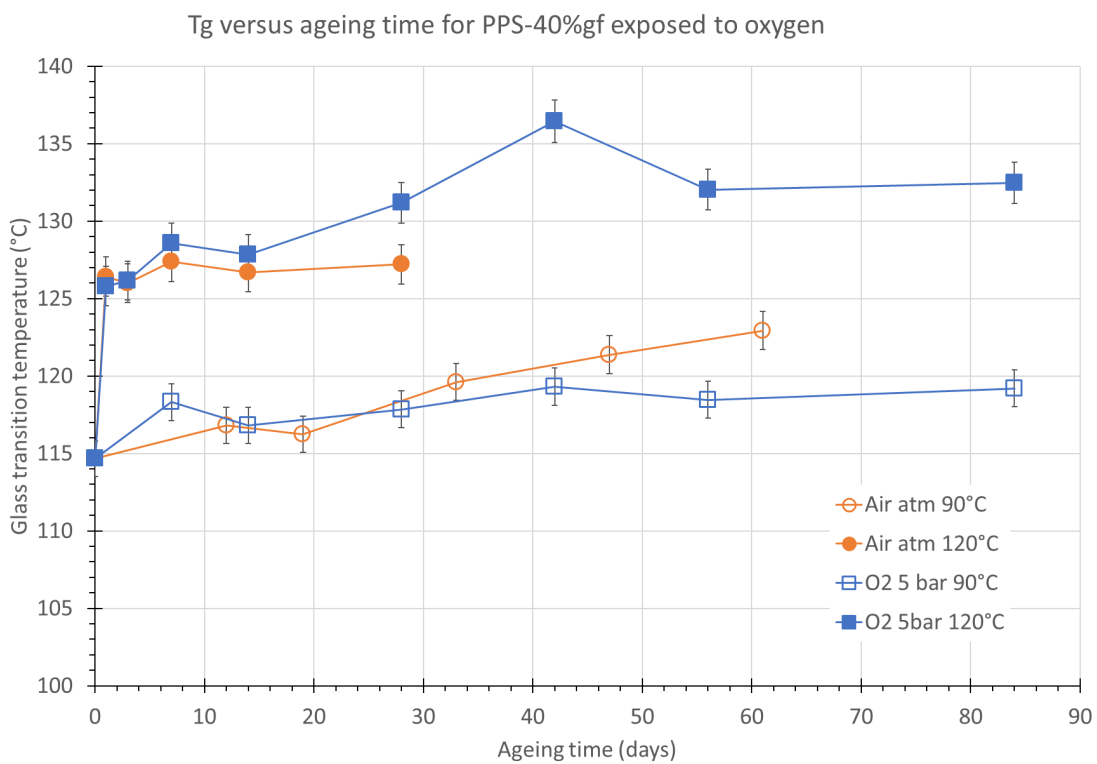


Figure 5.7: The storage modulus at (a) 50 °C and (b) 200 °C over time for PPS-40%gf exposed to oxygen.



(a)



(b)

Figure 5.8: The (a) peak of the loss modulus and (b) T_g over time for PPS-40%gf exposed to oxygen.

5.1.3 FTIR (PPS-40%gf; oxygen)

It is expected that if oxidation took place in the polymer, the formation of oxidised chemical structures would be visible in the FTIR spectra. For example, for polyolefins it is expected that oxidative degradation leads to the formation of carbonyl groups, which show peaks in the region from 1790 - 1684 cm^{-1} [38].

Figure 5.9 shows an FTIR spectrum for unaged PPS-40%gf. The absorbance peaks represent certain molecular structures, which have been identified using IRPal 2.0 and different publications of ATR-FTIR analysis of PPS-40%gf [15, 22, 89] (see Table 5.2).

Figure 5.10 shows the FTIR spectra of unaged PPS-40%gf, after 4 weeks of ageing in pure oxygen at 5 bar and 120 °C and after 8 weeks of ageing. The noise in region 2250 - 1900 cm^{-1} is due to the presence of CO_2 . From a first glance the spectra seem to be exactly the same, no new peaks have formed and no changes in relative peak intensities have been observed. This is confirmed when stacking the spectra on top of each other, shown in Figure 5.11. However, it is possible that very small changes occurred below the detection limit of the ATR-FTIR.

Table 5.2: ATR-FTIR peaks expected for PPS-40%gf.

Peak	Chemical Structure
3600 - 3000, 1680 - 1550	O-H stretching
1572, 1469, 1385	C-C stretching in aromatic ring [89]
2960, 807, 740	C-H in aromatic ring
1178	O=S=O stretching [89]
1091	C-S
1075	S=O [89]
1005	C=CH ₂ [15]

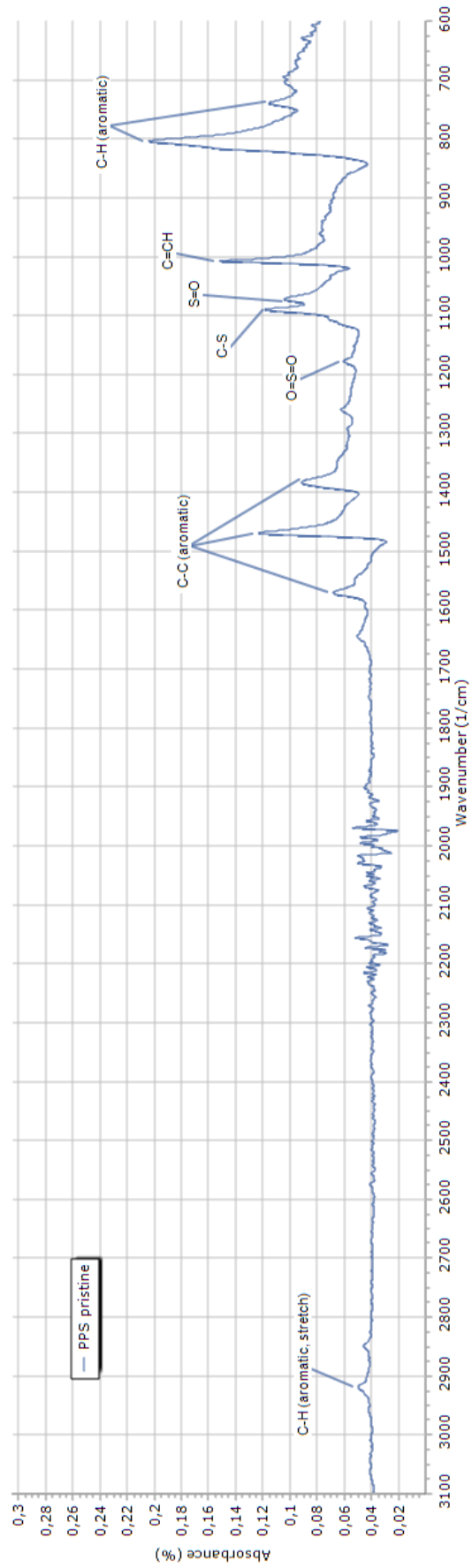


Figure 5.9: Labelled FTIR spectrum of unaged PPS-40wt%gf.

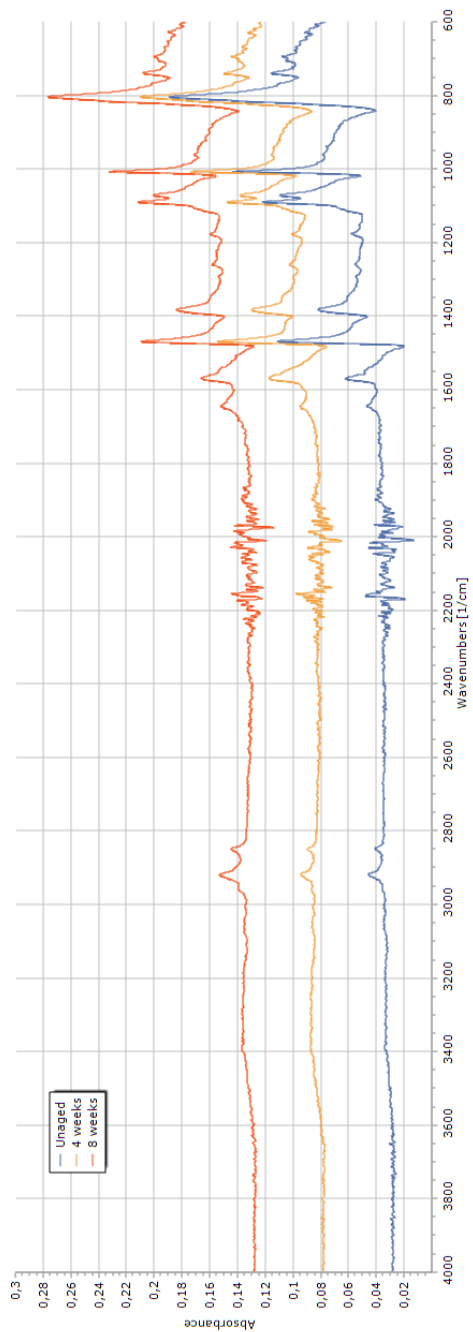


Figure 5.10: FTIR spectra of PPS-40wt%gf aged in O₂ at 5 bar and 120 °C.

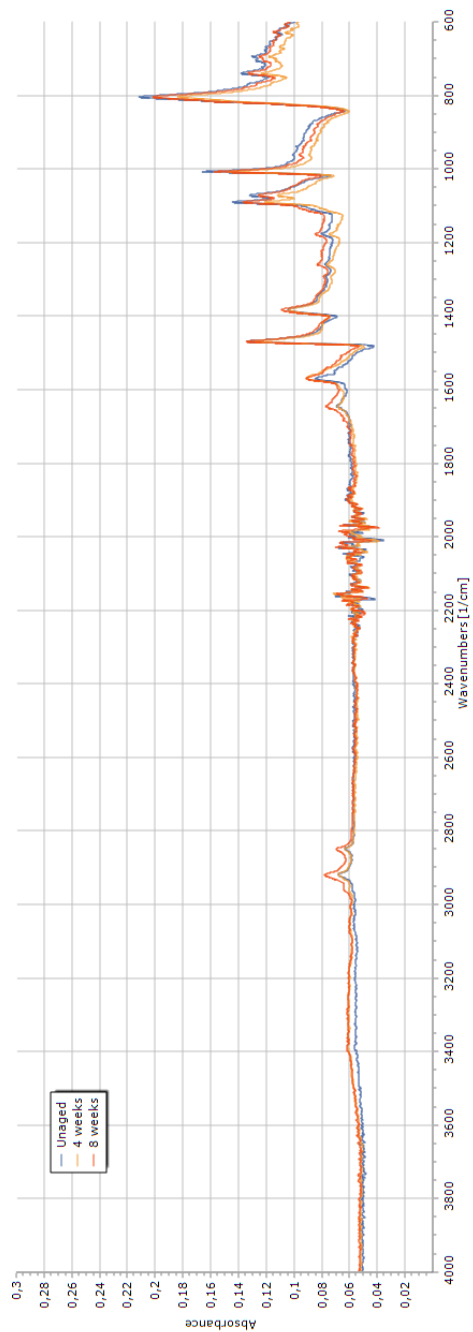


Figure 5.11: Stacked FTIR spectra of PPS-40wt%gf aged in O₂ at 5 bar and 120 °C.

5.1.4 Other measurement techniques (PPS-40%gf; oxygen)

XRD has also been used to characterise the semi-crystalline nature of PPS-40%gf. Even though, it is expected that (oxidative) degradation will mainly attack the amorphous parts of the polymer, it is interesting to see whether the XRD spectra change over ageing time. Since the samples are exposed to relatively high temperatures (up to 120 °C), it is possible for re-crystallisation to occur. However, after 8 weeks at 120 °C no significant change in XRD spectrum has been observed as shown in Figure 5.12, except for the most left peak, which seems to have increased after 8 weeks.

Weight measurements have also been performed. These did not show any change at all. The graphs are also plotted in Appendix C.1. Furthermore, SEM images have been taken of the fracture surfaces of unaged and aged PPS-40%gf and are also shown in Appendix C.1. No significant differences have been observed.

Finally, a couple of DSC measurements have been performed in order to see whether the large change in T_g has also been observed in the DSC measurements (see Figure 5.13). The large peak around 280 °C is the melt peak of PPS. The red curve is unaged PPS-40%gf, brown is after 2 weeks of oxygen at 5 bar and 120 °C and black after 4 weeks. The glass transition temperature is not very visible in these graphs, but is determined from the unaged curve to be around 90 °C. Both the 2 weeks and 4 weeks aged curves do not show a visible T_g but instead show an endothermic peak. The position of the melt peak does not seem to have changed.

The green DSC curve is that of KOH, which has a different baseline because of the presence of water in the sample. However, this curve also shows an endothermic peak around T_g .

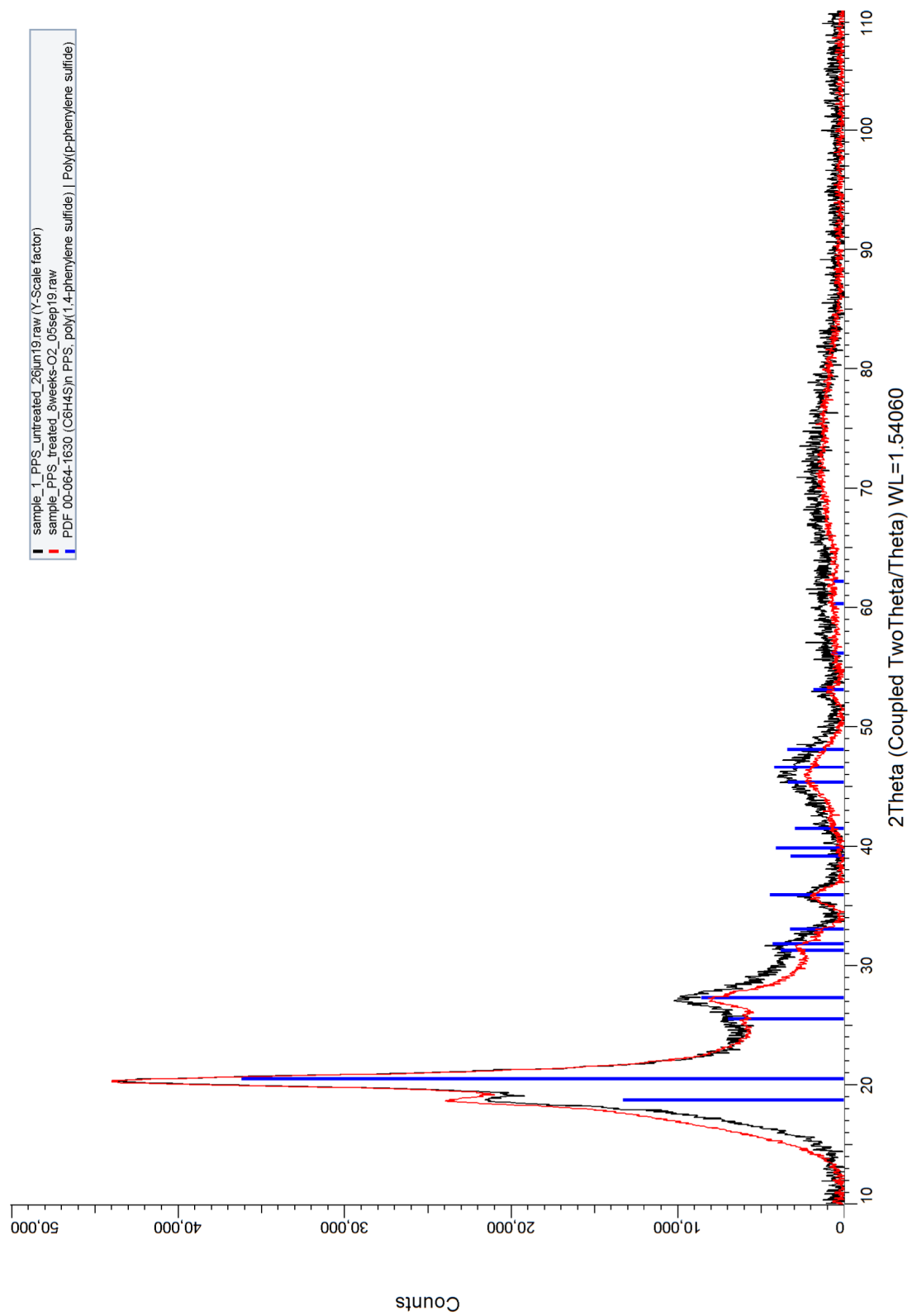


Figure 5.12: XRD pattern of PPS-40%gf exposed to O₂ 5 bar 120 °C for 8 weeks (red) compared to unaged PPS-40%gf (black).

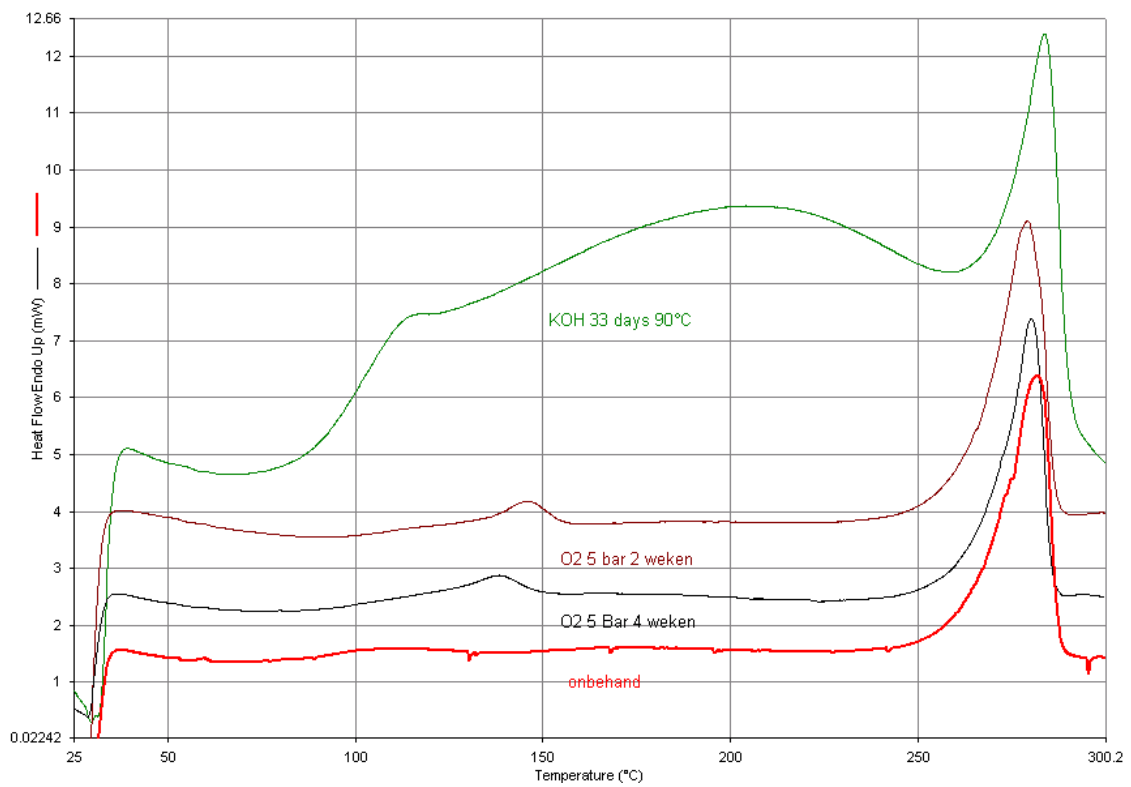


Figure 5.13: DSC analysis of different PPS-40%gf curves.

5.2 Discussion: what happens to PPS-40%gf when aged in an oxygen environment?

As shown in the results, which are summarised in Table 5.3, very subtle changes are observed for PPS-40%gf when exposed to oxygen. The largest changes are observed for the samples exposed to 120 °C. From the results it can be concluded that the UTS has increased, strain at UTS has decreased and the T_g has increased to higher temperatures.

Table 5.3: Results of PPS-40%gf exposed to oxygen.

Characterisation technique	Results
Tensile tests	increase in UTS, decrease in strain at UTS and no significant change in Young's modulus and toughness
DMA	no significant change in storage modulus of both glass and rubbery plateau and an increase in T_g
SEM	no significant differences observed
Weight	no change in weight
FTIR	no signs of formation of new chemical bonds or further incorporation of oxygen into the polymer
XRD	no big differences in spectra
DSC	endothermic peak around T_g observed

These changes in properties can be caused by a couple of different mechanisms. These are due to formation of cross-links, due to physical ageing of the polymer, due to a stronger fibre-matrix interface, due to further curing of unreacted molecules, due to further crystallisation of the polymer or due to evaporation of volatile molecules.

As discussed in Chapter 3, exposing PPS-40%gf to oxygen at elevated temperatures can lead to cross-linking [86, 90]. Cross-linking leads to a reduction in free volume and restricted molecular motion. This means more energy is needed for the same chain movement to be able to take place. The macroscopic consequences are a higher glass transition temperature and an increase in modulus, which is accompanied by an increase in UTS and a decrease in maximum elongation. At higher degrees of cross-linking it is expected that the T_g becomes broader and less well defined [31]. Moreover, the value of the storage modulus of the rubbery plateau is related to the number of cross-links, degree of crystallinity and the presence of entanglements, because these physical structures give a polymer 'rubbery' properties [10, 31]. From the DMA results of PPS-40%gf no increase in the storage modulus

of the rubbery plateau has been observed. Furthermore, the FTIR results show no sign of oxidation of the PPS molecular chain.

As shown in Chapter 5, the increase in UTS and T_g occurred very rapidly and then plateaued at a higher value. Furthermore, the change in material behaviour is independent of the oxygen partial pressure, but only dependent on temperature. This is unexpected for cross-linking reactions, since oxygen is involved in the cross-linking reaction. The independence of oxygen partial pressure can be explained by the oxidation reaction not being limited by oxygen diffusion. This would mean that the rate of oxidation is reaction limited. However, if that would be the case, the rapid change in properties, followed by nearly no change in properties, is hard to explain.

Thus, it seems that even though the mechanical properties have changed toward what is expected to happen when more cross-links are introduced into the material, no other lines of evidence are present to prove that cross-linking has indeed occurred in the material.

Physical ageing is the change of polymer behaviour due to isothermal relaxation of the glassy state towards equilibrium [26]. This occurs in the amorphous parts of the polymer, where the molecular chains are disordered and contain a large amount of free volume, or enthalpy. In order to reduce the enthalpy, the polymer chains start to better align themselves, leading to a reduction of free volume. Physical ageing is very slow at temperatures far away from T_g when the molecular chains have very low mobility, but occurs faster at temperatures higher to T_g when it is called 'annealing'.

This process is also shown in Figure 5.14, in which the volume of unaged and aged glass is shown with respect to temperature [48]. In this graph the liquid line (melt) is represented by AB, line BC gives the super-cooled melt line (*i.e.* solidification without crystallisation), and line BL represents the isothermal crystallisation process at T_m . The change in enthalpy versus temperature of the crystals is given by line ML. The cooling process is represented by path ABCDE, whereas path EDFCBA represents the reheating process. As explained before, when a glassy polymer is isothermally aged, the volume and enthalpy decrease as shown in Figure 5.14, where ΔH represents the released enthalpy through relaxation. When this aged polymer is reheated again, it follows path HGJKBA, through which an endothermic overshoot is observed, which is due to the rapid recovery of the lost enthalpy (ΔH) [48]. This is shown by the dotted line in Figure 5.14.

This endothermic overshoot is also called the relaxation enthalpy of the polymer and is visualised by the peak close to T_g which is observed in the DSC results of the aged PPS-40%gf samples. Figure 5.15 shows a schematic of the relaxation enthalpy. The area under the DSC relaxation peak, is equal to the relaxation enthalpy. Unfortunately, this has not been calculated.

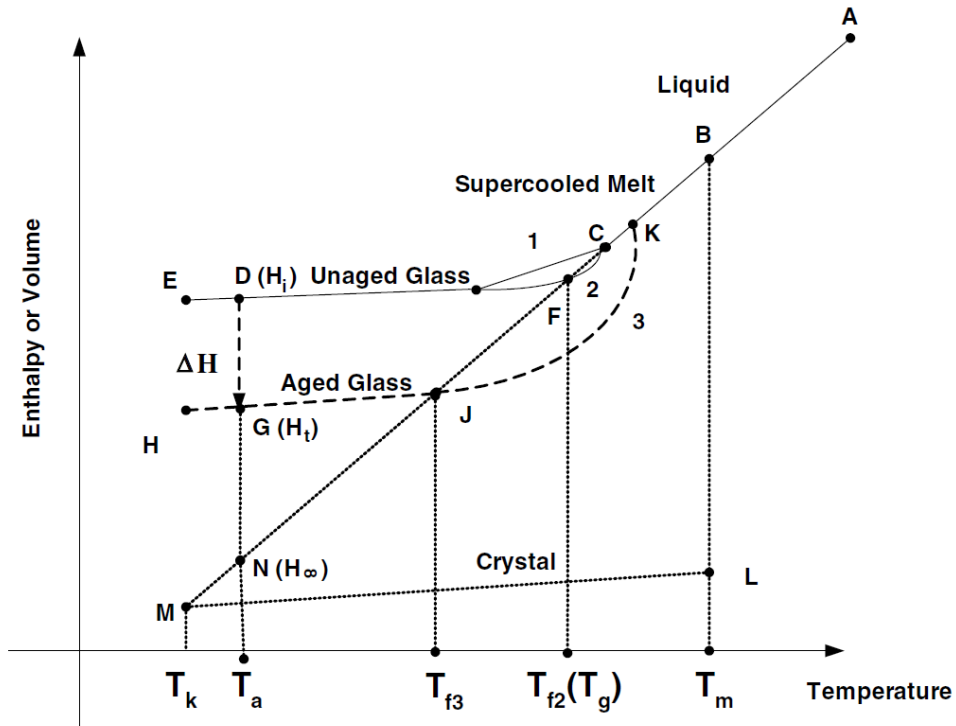


Figure 5.14: Schematic of the change in enthalpy of a polymer glass with isothermal ageing and without ageing [48].

As shown in Figure 5.13, for longer ageing times the endothermic peak of relaxation enthalpy shifts slightly to lower temperatures. This is expected as longer ageing times lead to a larger decrease in free volume and enthalpy leading to the overshoot to occur at lower temperatures.

The effects of physical ageing and chain relaxation for the mechanical properties of the polymer are as follows. The tighter arrangement of the chains and the reduction in free volume lead to a faster stretching of the polymer backbone and thus a lower strain and higher stiffness. Furthermore, the reduction in free volume and closer alignment of the polymer chains lead to larger Van der Waals forces between the chains and therefore to a higher UTS. This has been observed in the tensile test results. Similar results have been observed in studies with different polymers [79]. A larger T_g is also expected, since it is expected that more energy is required for the molecules to regain their mobility.

It, therefore, seems plausible that physical ageing due to the high ageing temperatures relative to the glass transition temperature is causing the changes in polymer behaviour. However, there is one complication: the samples aged at 120 °C show the greatest change in mechanical properties and T_g . This cannot be completely explained by physical ageing, because 120 °C is within the glass transition region of PPS-40%gf, meaning the polymer is already close to its equilibrium state, as shown in Figure 5.14.

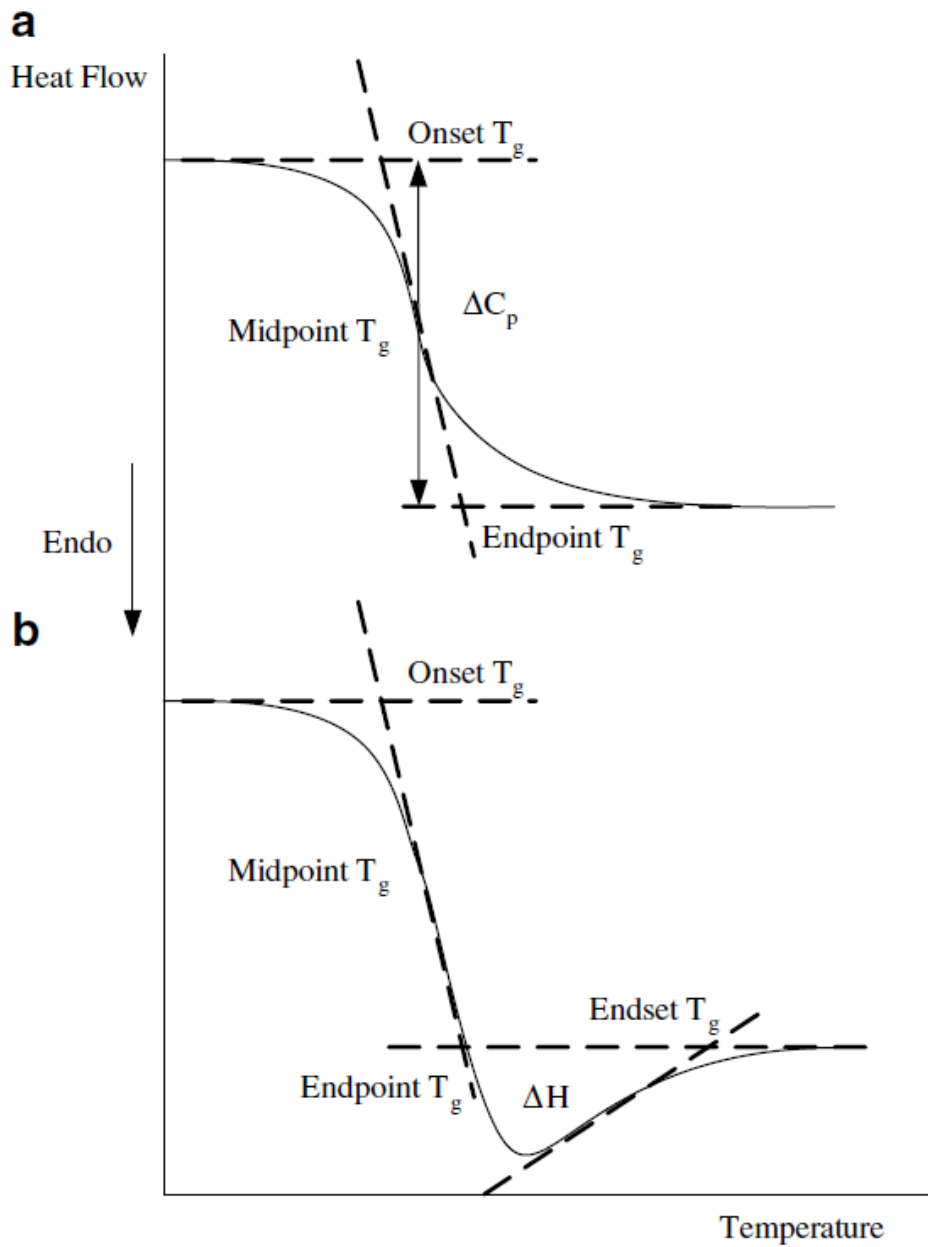


Figure 5.15: The glass transition using DSC for (a) an unaged sample and (b) an aged sample. The aged sample shows an endothermic peak associated with T_g which represents the enthalpy recovery, ΔH [48].

Other mechanisms, such as further crystallisation of the polymer, a stronger fibre-matrix interphase, further curing of unreacted molecules, or the loss of volatile additives, can all have attributed to changes in the observed properties. However, there is no direct proof that any of these mechanisms are taking place. Another, mechanism which could explain the larger changes in properties observed for the 120 °C case than for the 90 °C case is the fact that residual water may have evaporated out of the polymer when exposed to 120 °C. Water molecules act as plasticisers and when removed can lead to similar changes in behaviour as expected for physical ageing. It can be concluded, that the results can for a large part be explained by a combination physical ageing and water evaporation.

5.3 PPS-40%gf aged in KOH

5.3.1 Tensile tests (PPS-40%gf; KOH)

Figure 5.16 shows the stress-strain curves obtained from PPS-40%gf samples aged in a 30wt% KOH solution at 90 °C. For these curves the same procedure has been applied as described in Section 5.1.1 in order to obtain the desired mechanical parameters. The graph shows a large decrease in UTS from 153.5 to 79.6 (± 3.5) MPa. Furthermore, the strain at UTS drops significantly from 2.7 to 1.9 (± 0.1) %. The same is seen in the Young's modulus and toughness which decrease from 7.5 to 5.9 (± 0.3) and from 2.6 to 1.3 (± 0.2), respectively.

The results of the PPS-40%gf exposed to KOH-15wt% and KOH-45wt% compared to that of KOH-30wt% are shown in Figure 5.17 to 5.20. These show the same trends as described above. However, it seems that the higher KOH concentration of 45wt% has less effect on the reduction of mechanical properties than the lower 15 and 30wt% KOH concentrations. The extent of change in property between the 15 and 30wt% samples coincide with each other.

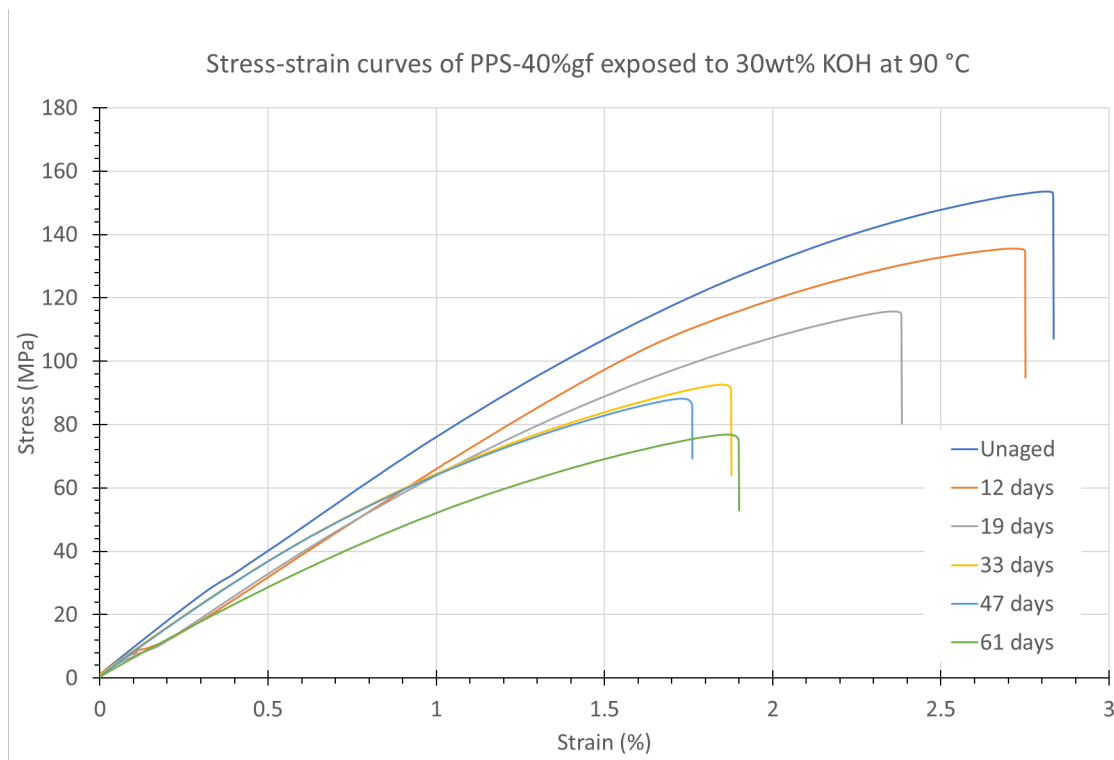


Figure 5.16: Stress-strain curves of PPS-40%gf exposed to 30wt% KOH at 90 °C.

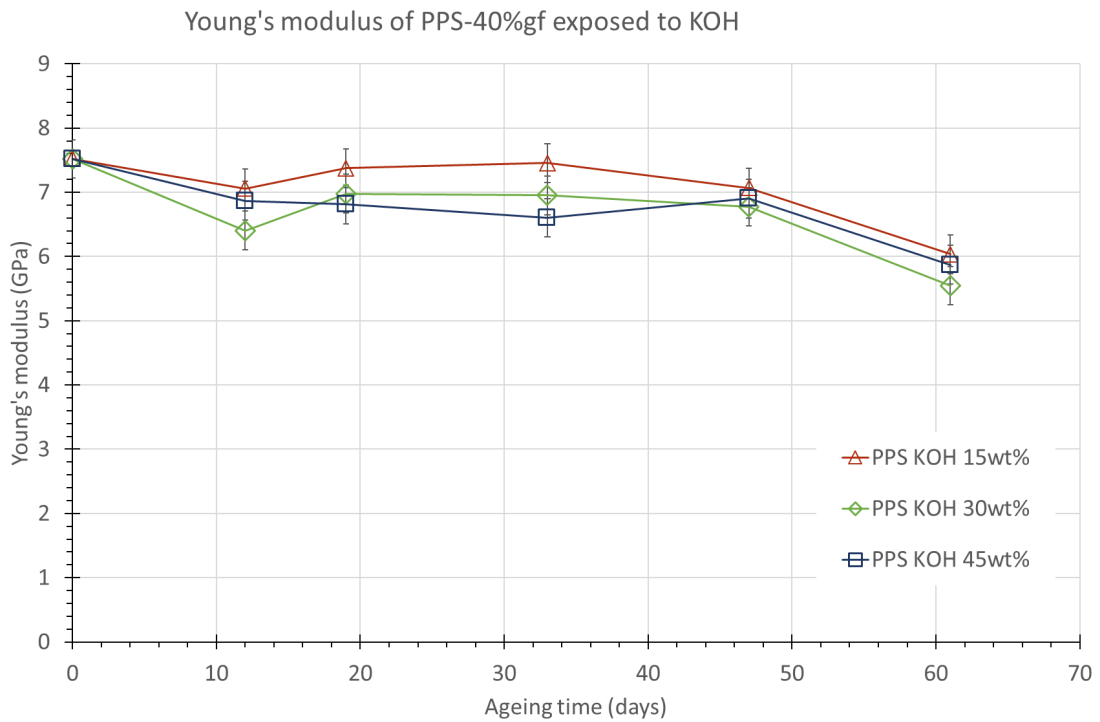


Figure 5.17: The Young's modulus over time for PPS-40%gf exposed 15wt% KOH (red line), 30wt% (green line) and 45wt% (blue line) at 90 °C.

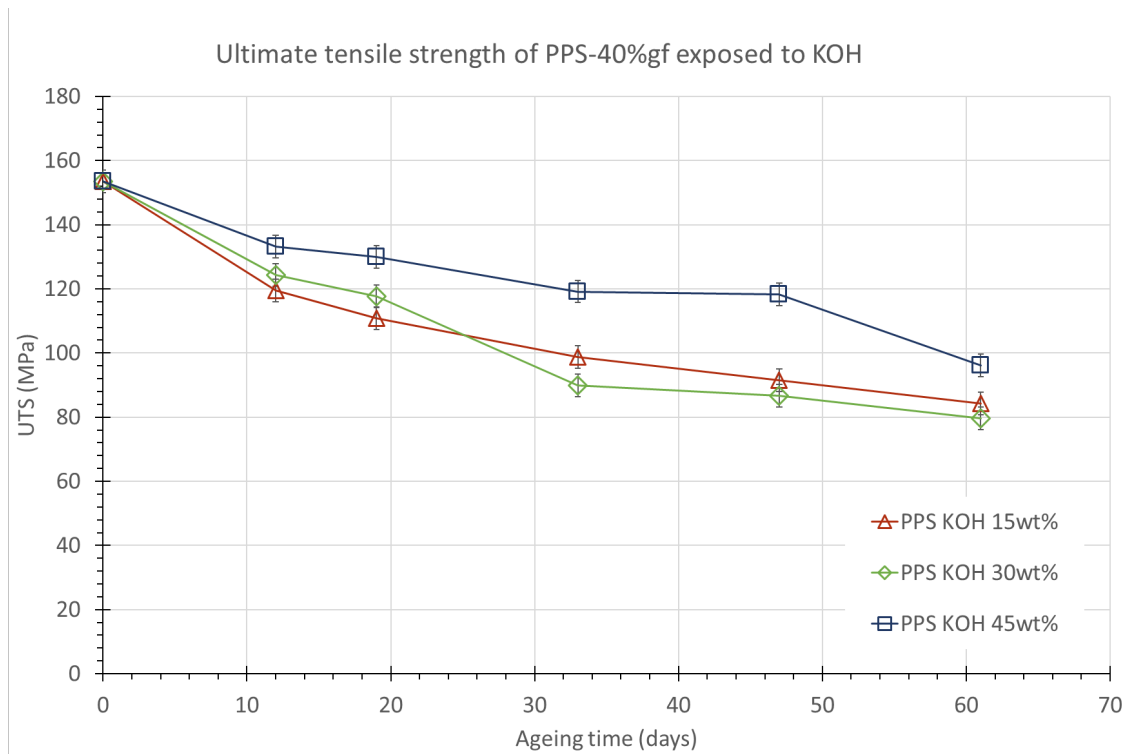


Figure 5.18: The ultimate tensile strength over time for PPS-40%gf exposed 15wt% KOH (red line), 30wt% (green line) and 45wt% (blue line) at 90 °C.

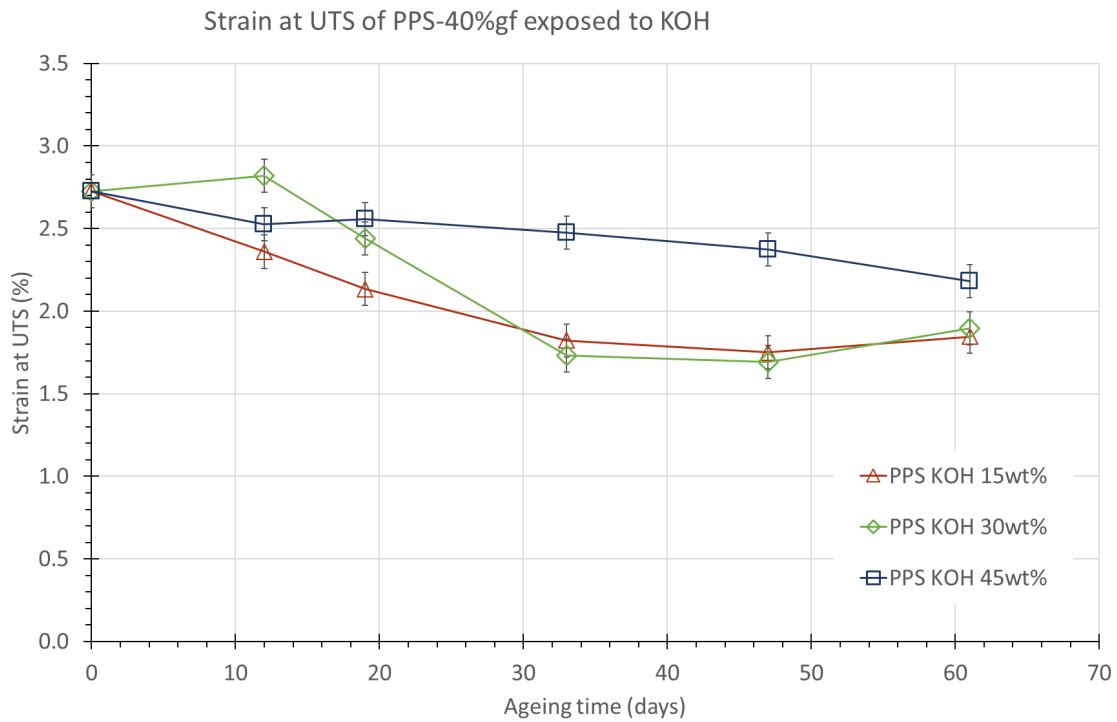


Figure 5.19: The strain at UTS over time for PPS-40%gf exposed 15wt% KOH (red line), 30wt% (green line) and 45wt% (blue line) at 90 °C.

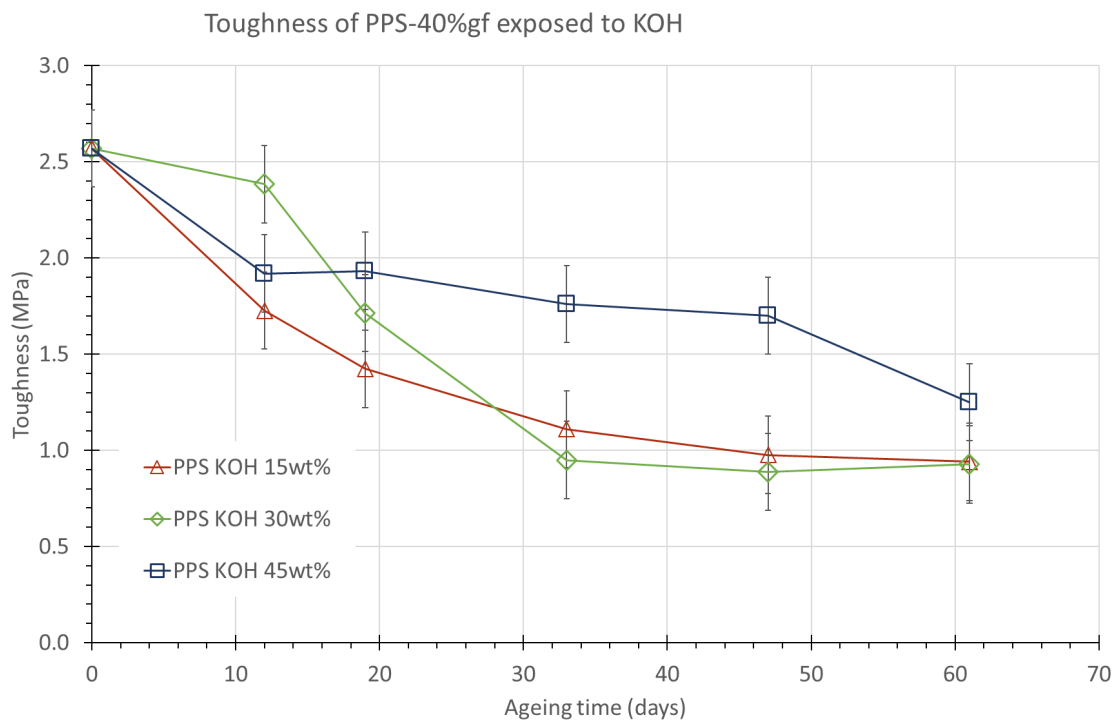


Figure 5.20: The material toughness over time for PPS-40%gf exposed 15wt% KOH (red line), 30wt% (green line) and 45wt% (blue line) at 90 °C.

5.3.2 DMA tests (PPS-40%gf; KOH)

Figure 5.21 shows the storage modulus and loss modulus of the PPS-40%gf samples which have been aged in 30wt% KOH solution at 90 °C. As shown, the initial storage modulus decreases, which has also been shown for the Young's modulus for the tensile curves. The storage modulus before and after the glass transition at 50 and 200 °C are plotted in Figure 5.22. Both the storage modulus of the glass plateau and the rubbery region decrease by about a third, similar to the decrease in Young's modulus.

However, the position of the peaks of the loss modulus, which indicate the glass transition temperature, do not change much as shown in Figure 5.23 and Table 5.4. If anything, the T_g of the composite increases from 115 to 121 ± 1 °C.

Table 5.4: Results of T_g for PPS-40%gf for different KOH concentrations. The T_g is defined as the peak of the 1 Hz loss modulus curve.

Ageing condition	T_g (°C)				
Unaged	114.66				
KOH 15wt% 90 °C	119.55	117.09	123.68		
	(12d)	(19d)	(61d)		
KOH 30wt% 90 °C	118.99	117.33	119.45	121.64	121.90
	(12d)	(19d)	(33d)	(47d)	(61d)
KOH 45wt% 90 °C	117.47	115.96	123.03		
	(12d)	(19d)	(61d)		

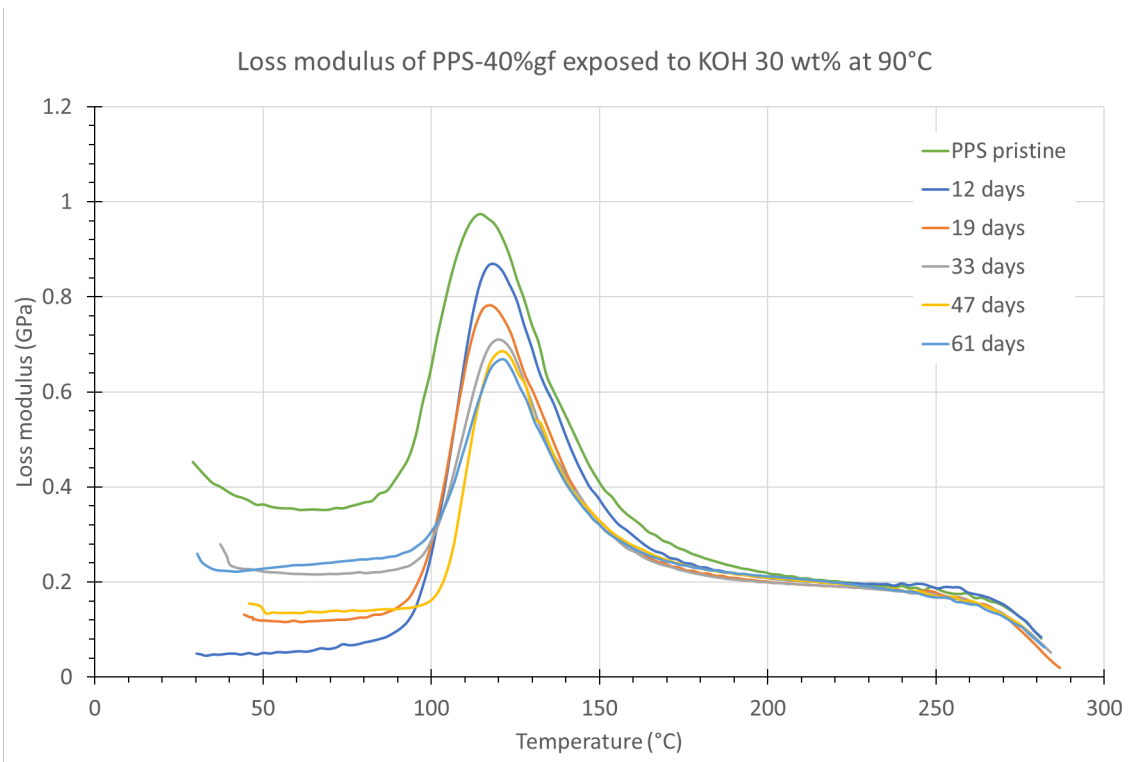
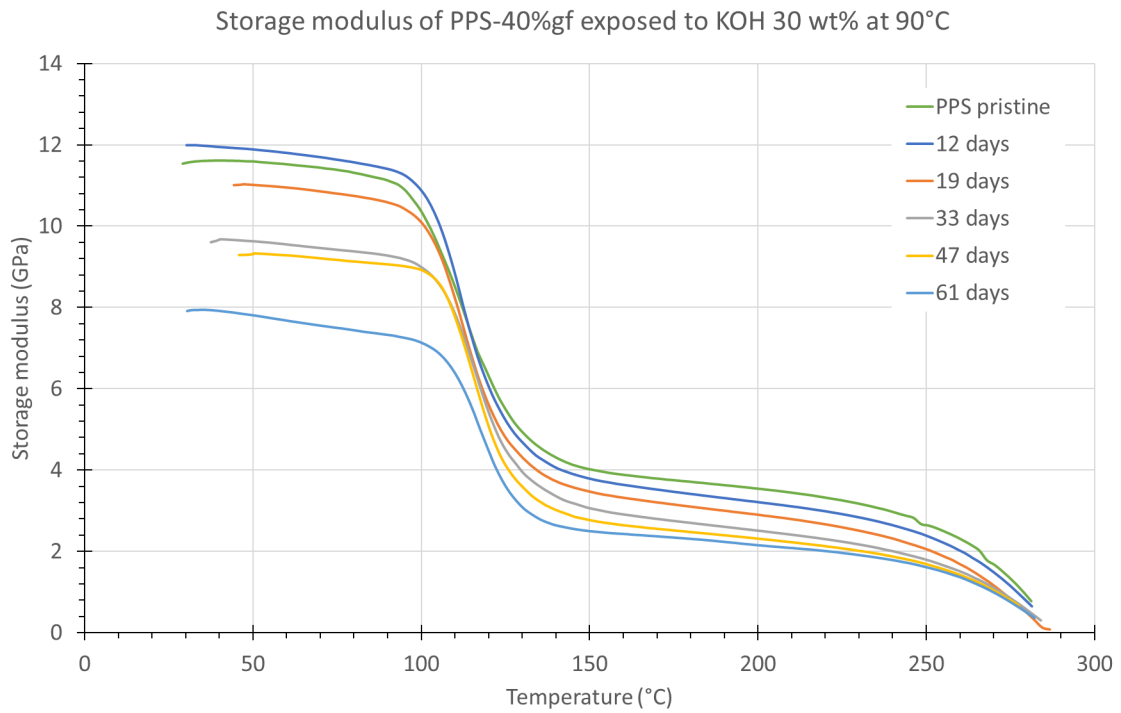


Figure 5.21: DMA curves of PPS-40%gf aged in 30wt% KOH at 90 °C showing (a) the storage modulus and (b) the loss modulus.

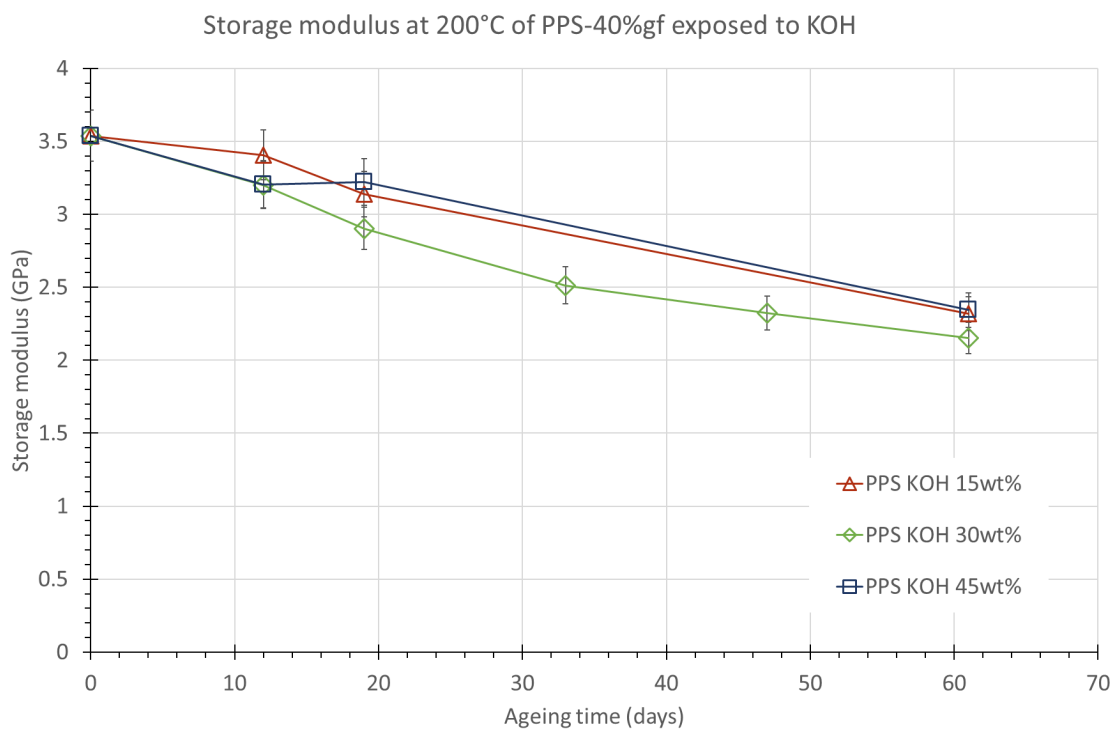
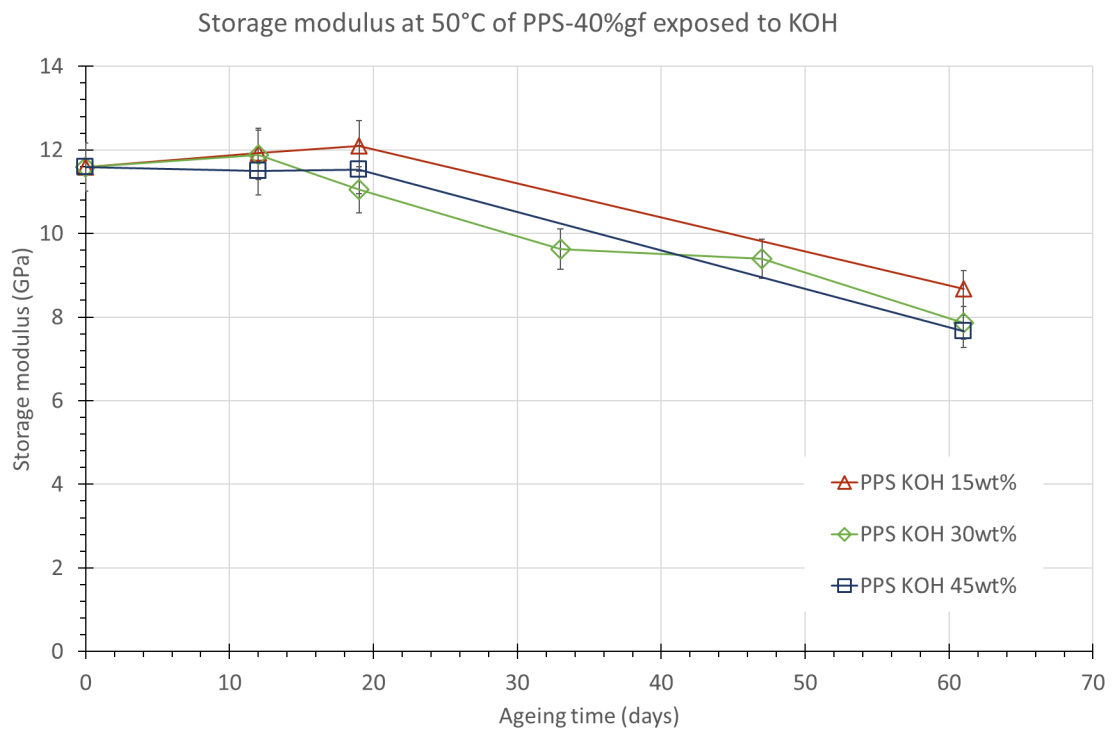
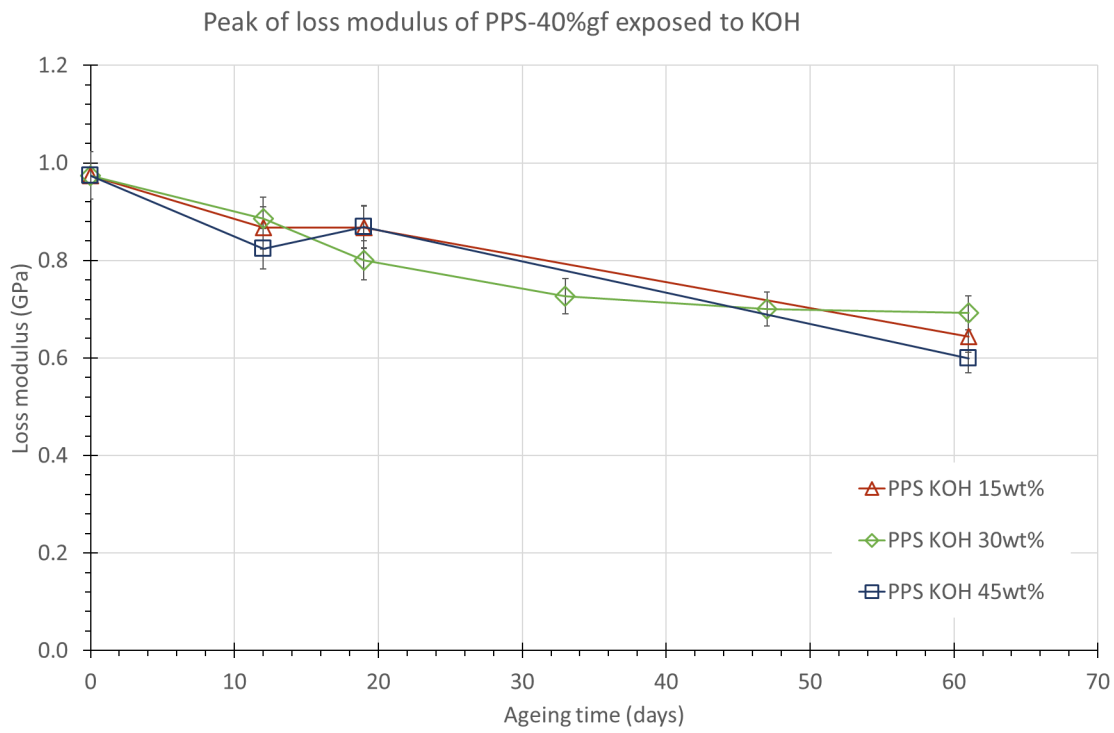
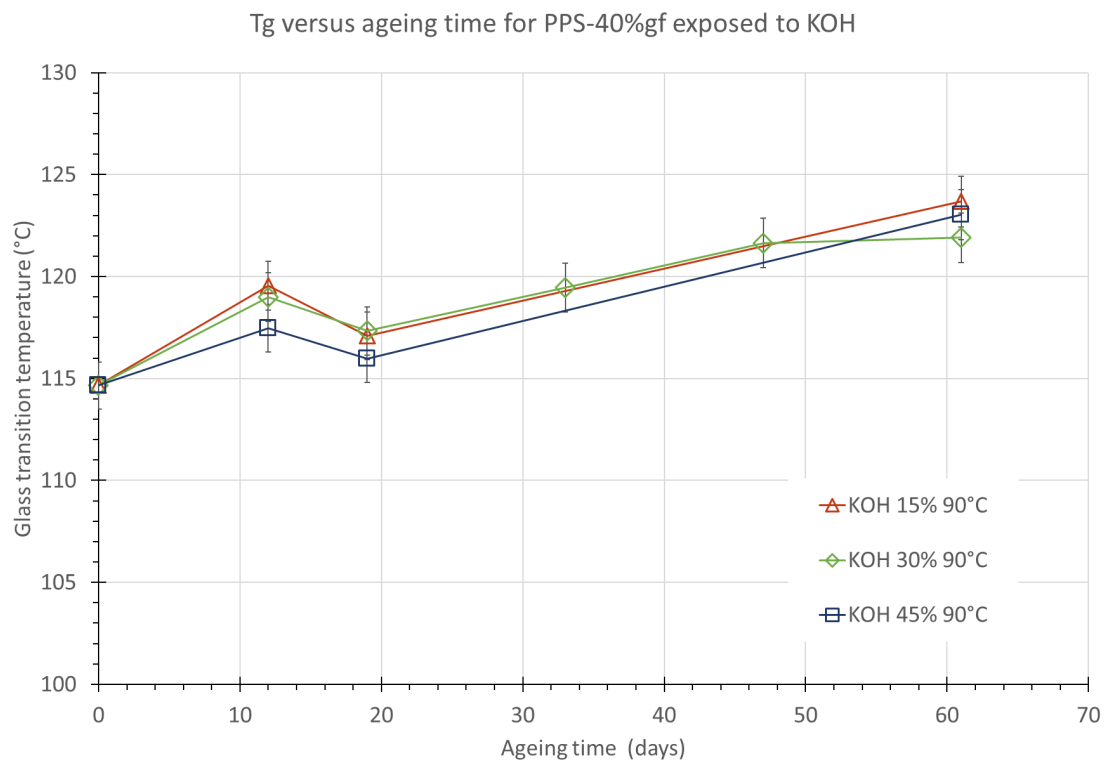


Figure 5.22: The storage modulus at (a) 50 °C and (b) 200 °C over time for PPS-40%gf exposed to different concentrations of KOH.



(a)



(b)

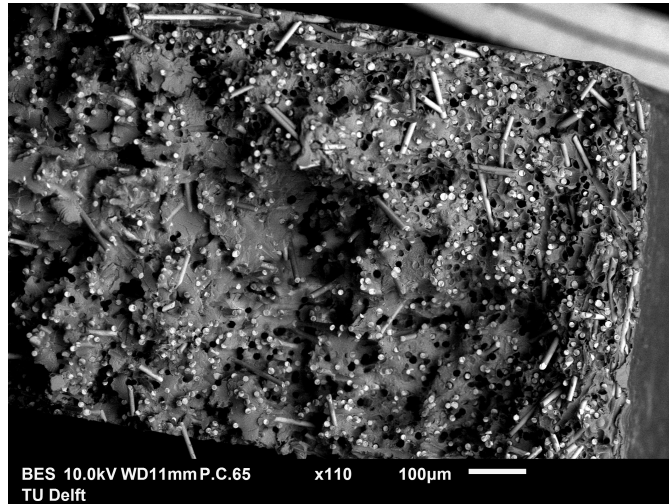
Figure 5.23: The (a) peak of the loss modulus and (b) T_g versus time for PPS-40%gf exposed to different concentrations of KOH at 90 °C.

5.3.3 SEM (PPS-40%gf; KOH)

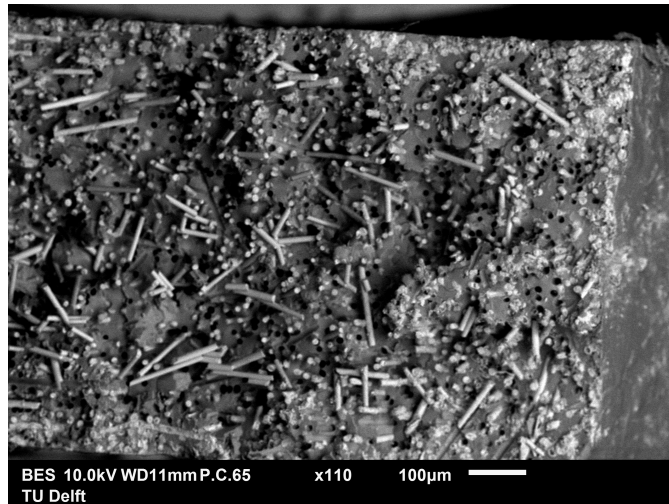
Scanning electron microscopy images have been taken of the fracture surfaces induced by tensile testing, as shown in Figure 5.24. The top image is the unaged sample, the middle image after 33 days of ageing and the bottom image after 61 days of ageing in a 30wt% KOH solution at 90 °C. The images clearly show an increase of damage over time, which starts at the surface and penetrates towards the core. A more detailed image at 300x magnification (see Figure 5.25) shows that the fibres have been attacked by the KOH solution. After 61 days, most of the fibres near the surface have been dissolved and replaced by some sort of precipitate containing potassium, as is confirmed by an energy-dispersive X-ray (EDS) analysis, as shown in Appendix C.2.

The dissolution does not occur uniformly throughout the sample, but starts from the surface and moves inwards. Since this dissolution front is very distinct, it can be argued that the reaction is limited by the diffusion of water and KOH into the polymer. However, it can be noted that the degraded samples show many more pulled out fibres and empty holes throughout the bulk than the unaged sample. This indicates that the fibre-matrix interface has been damaged throughout the whole sample. Apparently small amounts of KOH solution are enough to break the fibre-matrix interface.

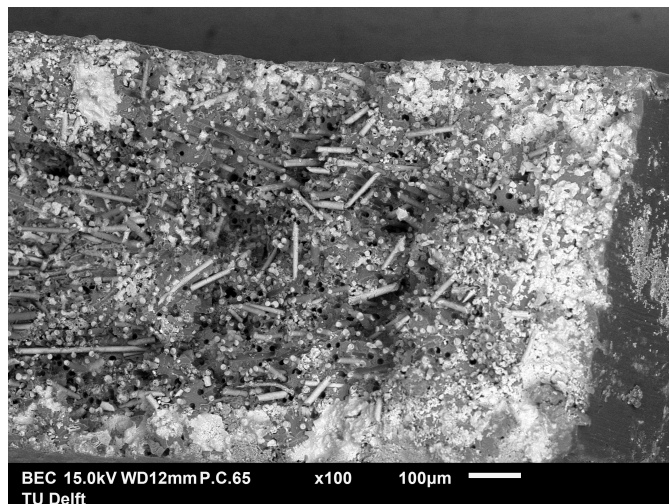
Finally, Figure 5.25 shows that swelling has taken place in the PPS-40%gf samples, due to water diffusion into the samples. This is enhanced by the swelling of the glass fibres and the space between fibre and matrix, where water can collect.



(a)

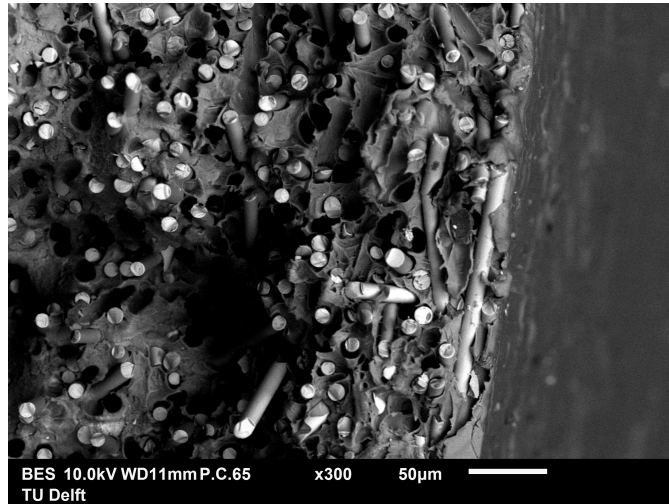


(b)

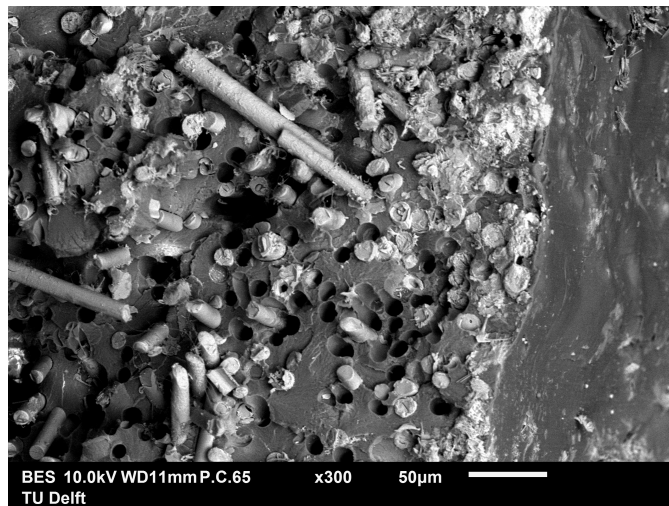


(c)

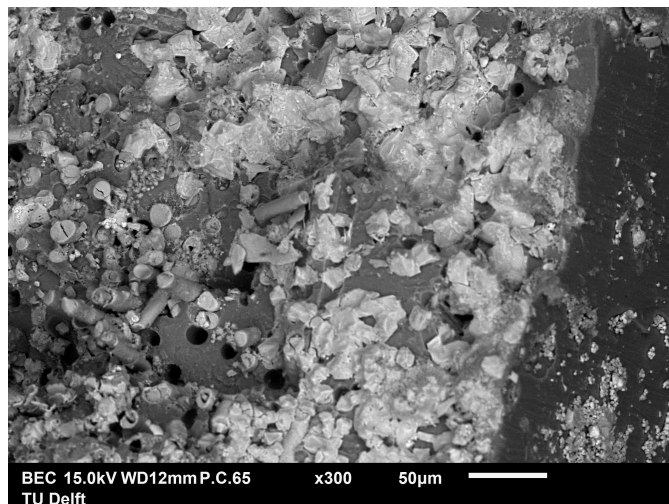
Figure 5.24: SEM images of the fracture surface of (a) unaged PPS-40%gf, and PPS-40%gf exposed to 30wt% KOH at 90 °C for (b) 33 days and (c) 61 days.



(a)



(b)



(c)

Figure 5.25: SEM images 300x magnification of the fracture surface of (a) unaged PPS-40%gf, and PPS-40%gf exposed to 30wt% KOH at 90 °C for (b) 33 days and (c) 61 days.

5.3.4 Other measurement techniques (PPS-40%gf; KOH)

The swelling of PPS-40%gf due to water absorption is also shown in the weight measurements (Figure 5.26) and the FTIR measurements (Figure 5.27). It is important to note here that the KOH 15wt% and KOH 45wt% samples have been weighed after a couple weeks, whereas the KOH 30wt% samples were weighed straight away. It is expected that most of the weight increase is due to the dissolution of the glass fibres and the precipitation of a new phase, since water diffusion into PPS matrix is low because the polymer is *not* hygroscopic. Figure 6.22 shows that the 15wt% and 45wt% samples have a lower weight increase over time, which is due to the release of water out of the samples during storage before the weight was measured. The 30wt% samples show a steady weight increase with no signs of an equilibrium being reached. This is expected since the reactions involving the dissolution of the glass fibres and the precipitation of a new phase are still ongoing.

Regarding FTIR results, peaks at 3600 - 3000 and 1680 - 1550 indicate the presence of water molecules. This is shown in Figure 5.27 and is especially clear for the 61 day sample. This is again due to the fact that the 61 day sample was FTIR measured almost immediately, whereas the 33 day sample was measured after several weeks of extraction, meaning it lost a part of its water already. Apart from these peaks, no other changes have been observed in the FTIR spectra.

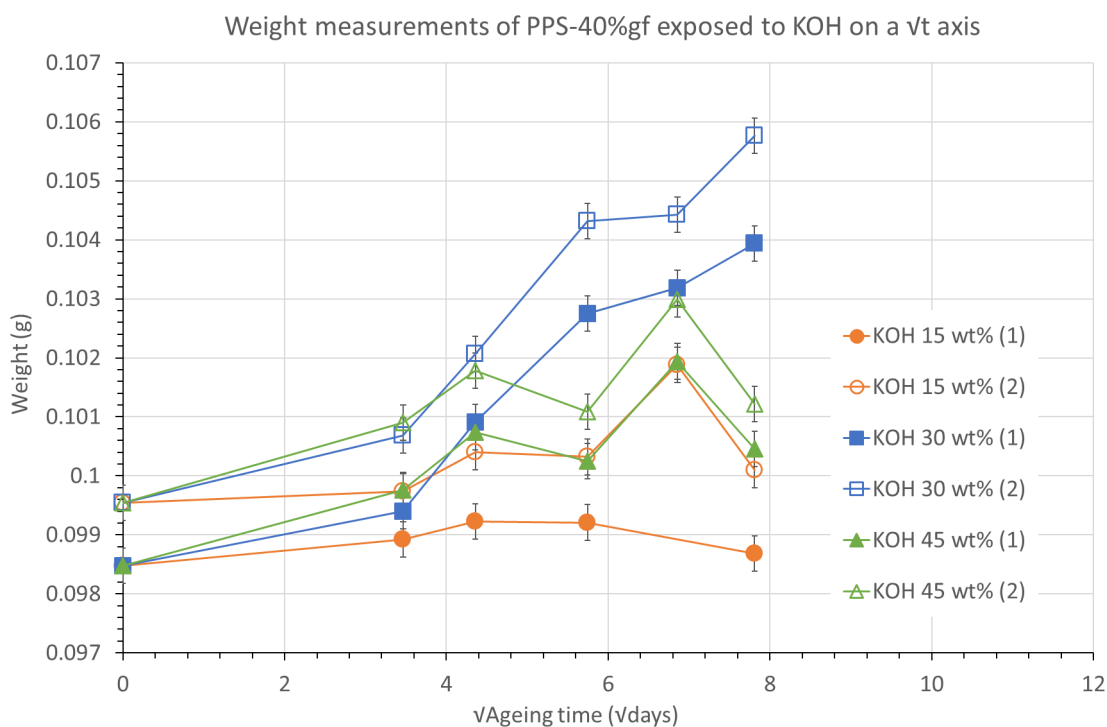


Figure 5.26: Graphs showing the weight change of PPS-40%gf exposed to KOH at 90 °C plotted against the square-root of ageing time.

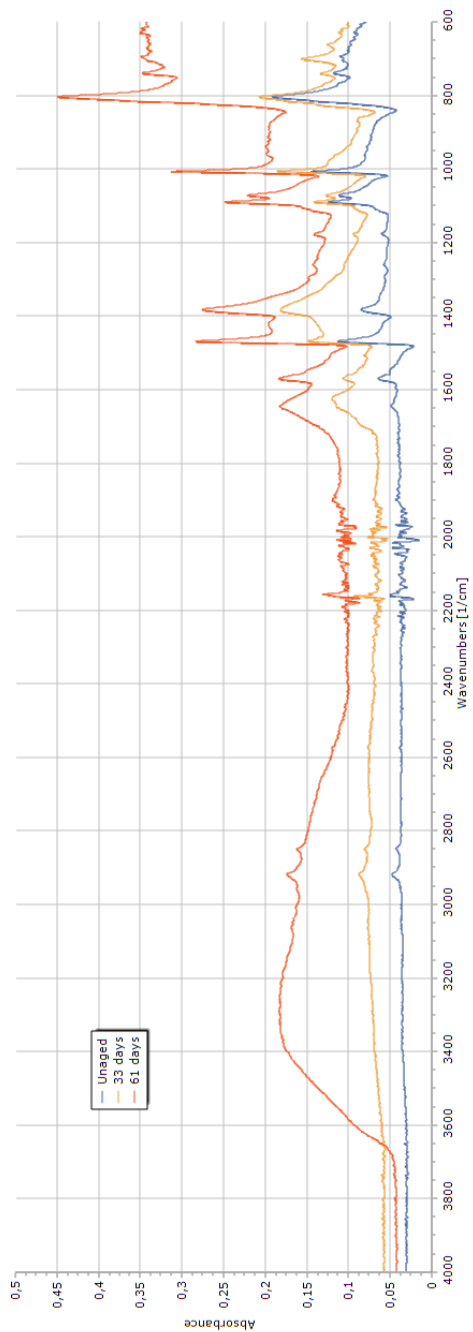


Figure 5.27: FTIR spectra of PPS-40wt% aged in KOH 30wt% at 90 °C.

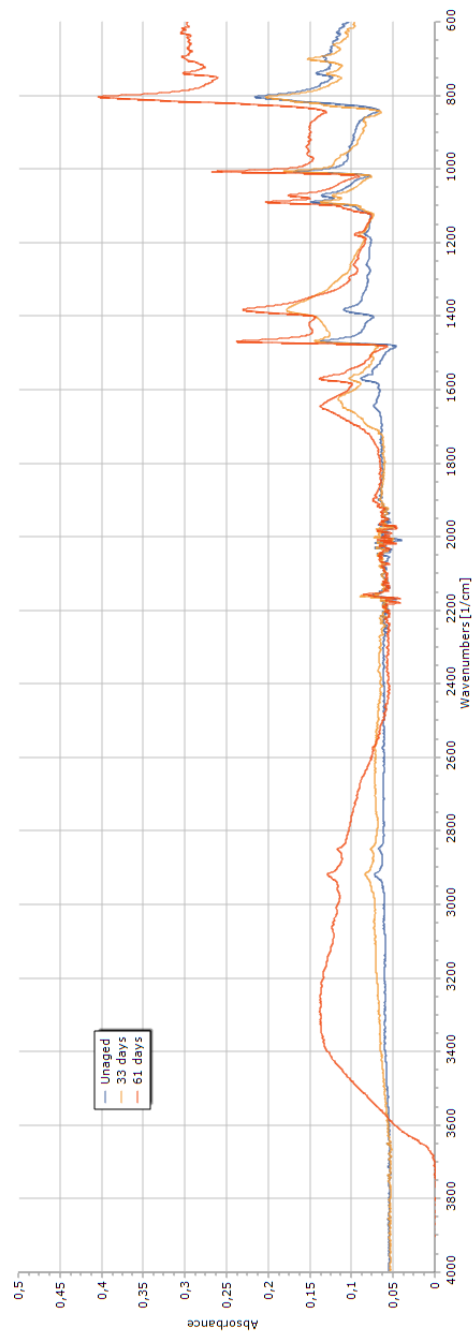


Figure 5.28: Stacked FTIR spectra of PPS-40wt% aged in KOH 30wt% at 90 °C.

One DSC measurements has been taken and is shown in Figure 5.1.4 in Section 5.1.4. Finally, XRD measurements have been taken and are shown in Figure 5.29. The KOH treated samples show a distinct change by the appearance of many more crystalline peaks. One possible explanation of these extra peaks is the presence of KOH crystals on the surface of the sample, which can give rise to the extra peaks shown. However, Figure C.18 in Appendix C.2 shows that this is not the case, since the relevant peaks of the KOH precipitates do not overlap with the PPS-40%gf aged in KOH spectrum. It is expected that these peaks arise from the precipitation products which interacted with the dissolved glass fibres. Two phases which could be distinguished are Portlandite and Katoite, which are shown in Figure 5.29 with blue and red bars, respectively.

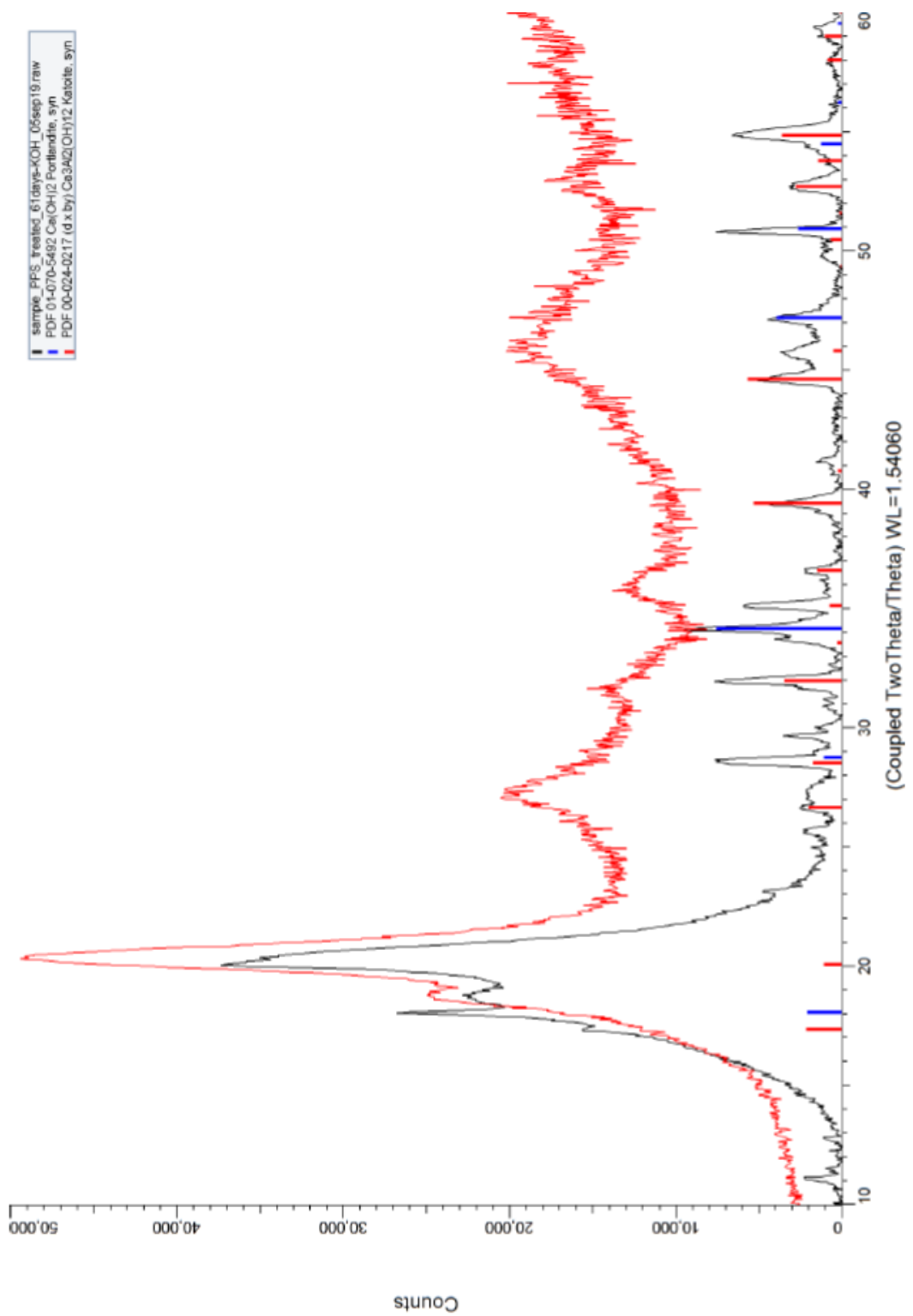


Figure 5.29: XRD pattern of PPS-40%gf exposed to KOH 30wt% 90 °C for 61 days in black compared to untreated PPS-40%gf in red. The blue peaks represent the peaks of Portlandite and the red peaks represent Katoite.

5.4 Discussion: what happens to PPS-40%gf when aged in KOH?

Exposing PPS-40%gf to different concentrations of KOH solution at 90 °C, leads to a series of interesting results as summarised in Table 5.5. For example, the SEM results clearly show that both the fibres and the fibre-matrix interface have degraded. If a composite loses its reinforcements, it is expected that the mechanical properties reduce to the properties of that of the unfilled polymer. According to CES EduPack, unfilled PPS has a Young's modulus of 5.9 - 8.3 GPa, a UTS of 48 - 86 MPa and a toughness of 0.5 - 0.9 MPa. The experimental values of the Young's modulus of 5.9 ± 0.3 GPa, the UTS of 79.6 ± 3.5 MPa and toughness of 1.3 ± 0.2 MPa of PPS-40%gf exposed to 30wt% KOH for 61 days lay within the range of values for unfilled PPS.

The question now is whether the reduction in properties can solely be explained by the dissolution of the fibres and the deterioration of fibre-matrix interface, or has the polymer matrix itself degraded?

Table 5.5: Results of PPS-40%gf exposed to KOH.

Characterisation technique	Results
Tensile tests	decrease in UTS, Young's modulus, strain at UTS and toughness
DMA	decrease in storage modulus of both glass and rubbery plateau and an increase in T_g
SEM	dissolution of glass fibres and deterioration of fibre-matrix interface
Weight	increase in weight
FTIR	presence of peaks indicating water absorption, but no other signs of reaction
XRD	more crystalline peaks visible
DSC	different baseline due to water present in sample, endothermic peak around T_g observed

In order to answer this question, the DMA results should be considered. The glass transition temperature is a polymer property, which is, in theory, not influenced by the presence of glass fibres. In practice, the interface between the glass and the polymer matrix is often not a perfect two-dimensional surface, but is better described by an *interphase*. An interphase is a three-dimensional region, which is affected by the interactions taking place at the interface [17]. These adhesion interactions can be in the form of chemical

coupling, such as adsorption of chemical groups and the formation of covalent bonds; physical interactions, such as dispersive (London forces); and mechanical interlocking or arising from residual stresses formed upon cooling. The surface of the fibre can also act as a nucleation site in semi-crystalline polymers called the trans-crystalline phenomena. In general, the level of adhesion between thermoplastic polymers and fibres is lower than that for thermosetting polymers, such as epoxies. This is due to the lack of the formation of strong covalent bonds, insufficient wetting and interlocking [17].

The presence of this interphase region leads to a non-uniform compliance in the matrix. The interphase becomes stiffer than the bulk matrix, due to the different adhesion mechanisms. These gradients in the elastic modulus of the matrix can yield a broader glass transition, which for PPS-40%gf spans a region of about 50 °C [4]. The same effect can be due to the presence of crystals, since interactions between the crystal and the bulk matrix around it also lead to gradients in the elastic modulus.

A slight increase in T_g , is observed in the DMA results. This can be explained by the relaxation of the chains, as explained in the previous section, which is further confirmed by the DSC results of PPS-40%gf exposed to KOH (Figure 5.1.4), which shows a small relaxation enthalpy peak.

Thus, since this glass transition region does not change to lower temperatures over time for PPS-40%gf exposed to KOH, it can be concluded that the polymer matrix retains its intrinsic structure. It is therefore expected that the degradation of mechanical properties is solely due to the degradation of the glass-reinforcement and the fibre-matrix interface.

5.5 Concluding remarks

From the above results, especially the results of PPS-40%gf exposed to KOH, it can be concluded that *glass-reinforced* PPS is **unsuitable** for the purpose of the encapsulation of the ZEF AEC. Since, the PPS matrix, itself does not seem to have degraded this conclusion can be extended to *all* glass filled polymers will be **unsuitable** for application in strong alkaline environments. PPS on its own is very brittle, which is undesirable for the ZEF AEC. However, PPS reinforced with other reinforcements, such as aramid fibres, could potentially be resistant to the ZEF AEC conditions.

Chapter 6

Results and discussion PSU

This chapter is concerned with the results and discussion of ageing of PSU in oxygen and KOH.

6.1 PSU aged in oxygen

6.1.1 Tensile tests (PSU; oxygen)

The same procedure and correction as described in Section 5.1.1 and Appendix C.3 has been applied to the stress-strain curves of the PSU samples. Figure 5.1 shows the stress-strain curves of PSU exposed to O₂ at 5 bar and 90 °C. The Young's modulus, UTS, strain at UTS and toughness are plotted in Figure 6.2 to 6.5. The major differences in mechanical behaviour between PPS-40%gf and PSU are that PSU has a much lower unaged UTS of 62 ± 1 MPa compared to that of unaged PPS-40%gf (153.5 ± 2.5 MPa). It is also less stiff with a much lower Young's modulus (2.07 ± 0.05 GPa compared to 7.5 ± 0.3 GPa for PPS-40%gf). These differences can be attributed to the fact that PSU is not a composite as PPS-40%gf is.

PSU is much more ductile than PPS-40%gf. It has a higher strain at UTS (5.5 ± 0.1 % compared to 2.7 ± 0.1 for PPS-40%gf) and it does not break in a brittle way such as PPS-40%gf does. Instead PSU deforms plastically and necking occurs. The tensile test has been stopped just when necking starts to occur, because necking causes the cross-sectional dimensions of the sample to change which corrupts the results and because for this research the onset of necking means the material has failed.

As shown in Figure 6.2, the Young's modulus of the samples aged in 90 or 120 °C do not show a significant change within the error margins. The samples aged in air at 170 °C on the other hand show an immediate increase of the Young's modulus which plateaus at a higher value of about 2.22 ± 0.05 GPa.

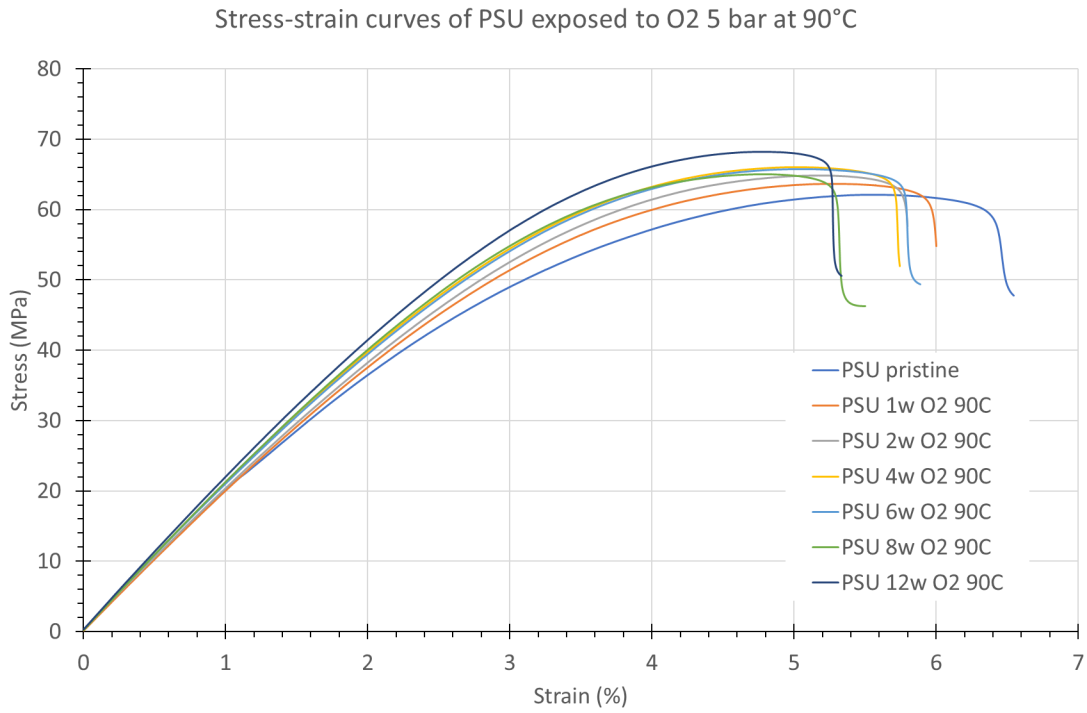


Figure 6.1: Stress-strain curves of PSU exposed to O₂ at 5 bar and 90 °C.

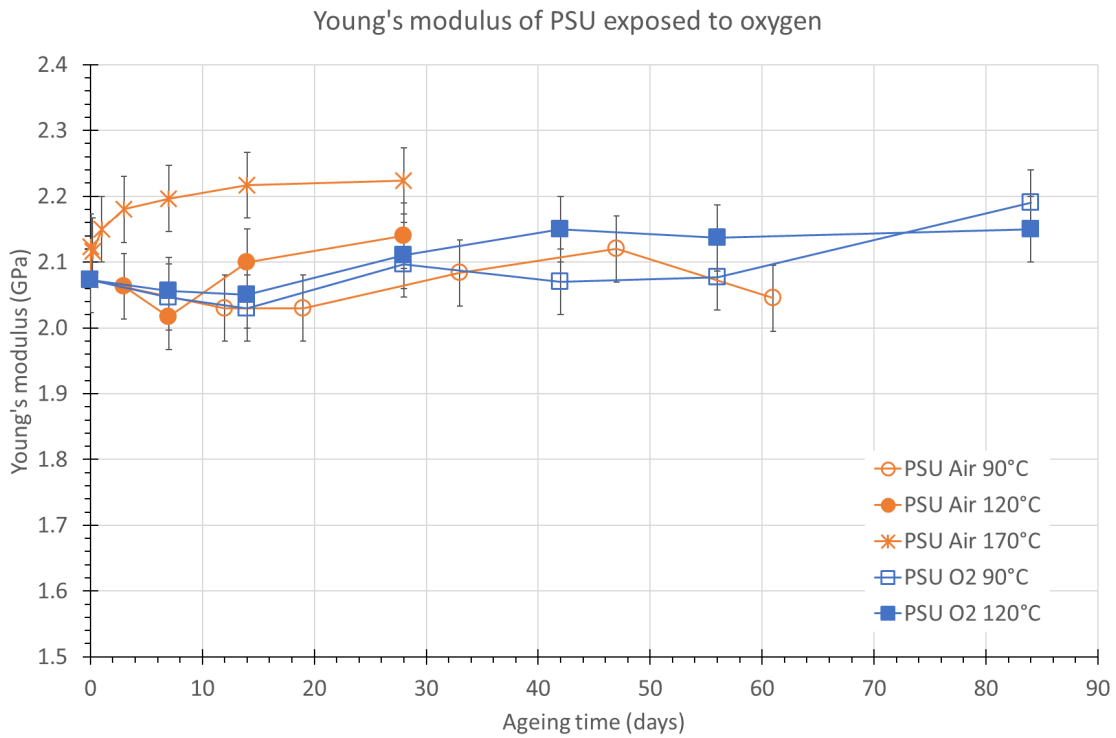


Figure 6.2: The Young's modulus over time for PSU exposed air (orange lines) at 90, 120 and 170 °C and oxygen at 5 bar (blue lines) at 90 and 120 °C.

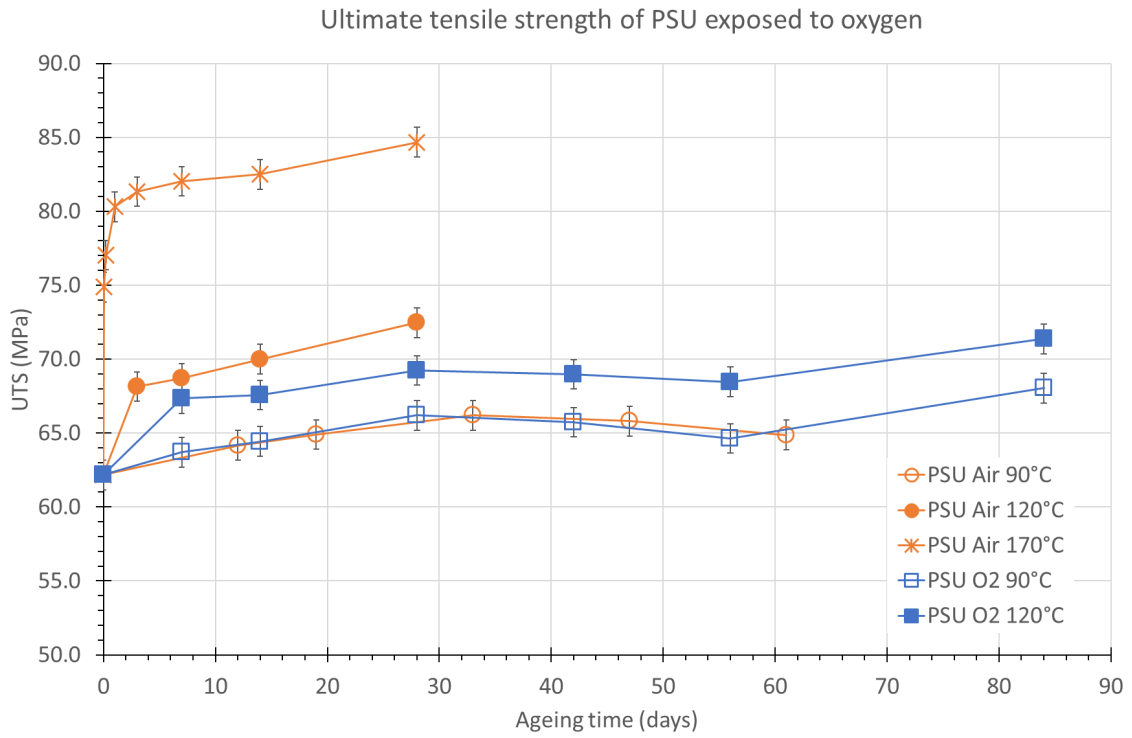


Figure 6.3: The ultimate tensile strength over time for PSU exposed air (orange lines) at 90, 120 and 170 °C and oxygen at 5 bar (blue lines) at 90 and 120 °C.

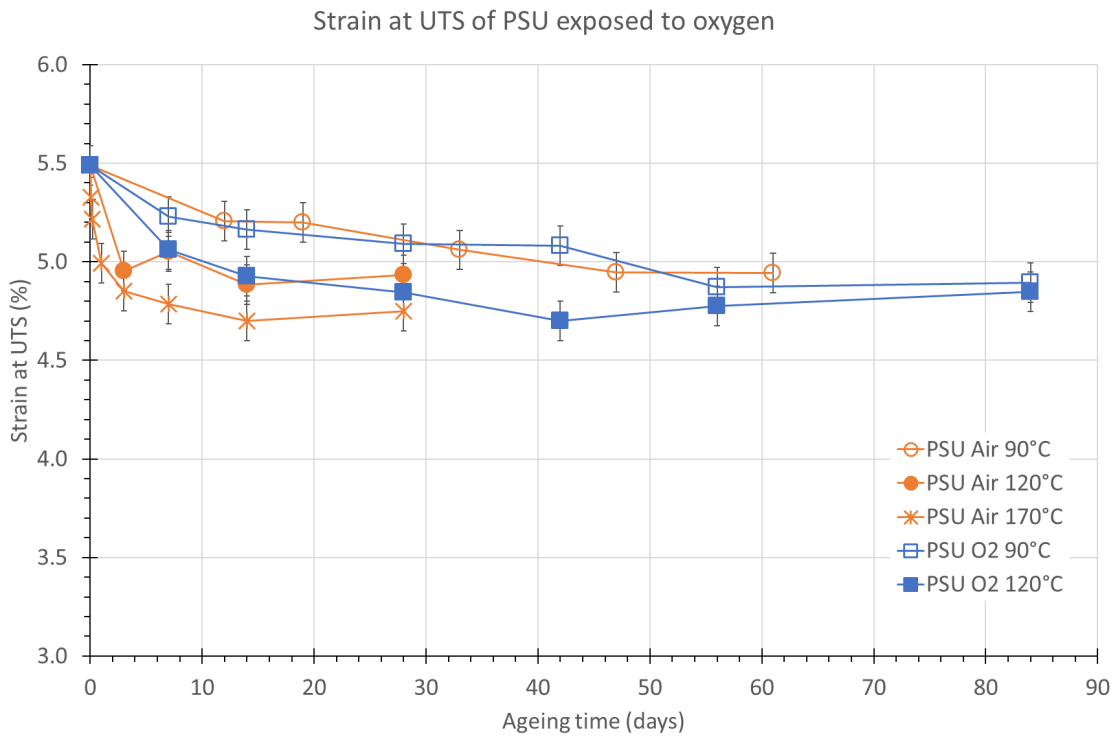


Figure 6.4: The strain at UTS over time for PSU exposed air (orange lines) at 90, 120 and 170 °C and oxygen at 5 bar (blue lines) at 90 and 120 °C.

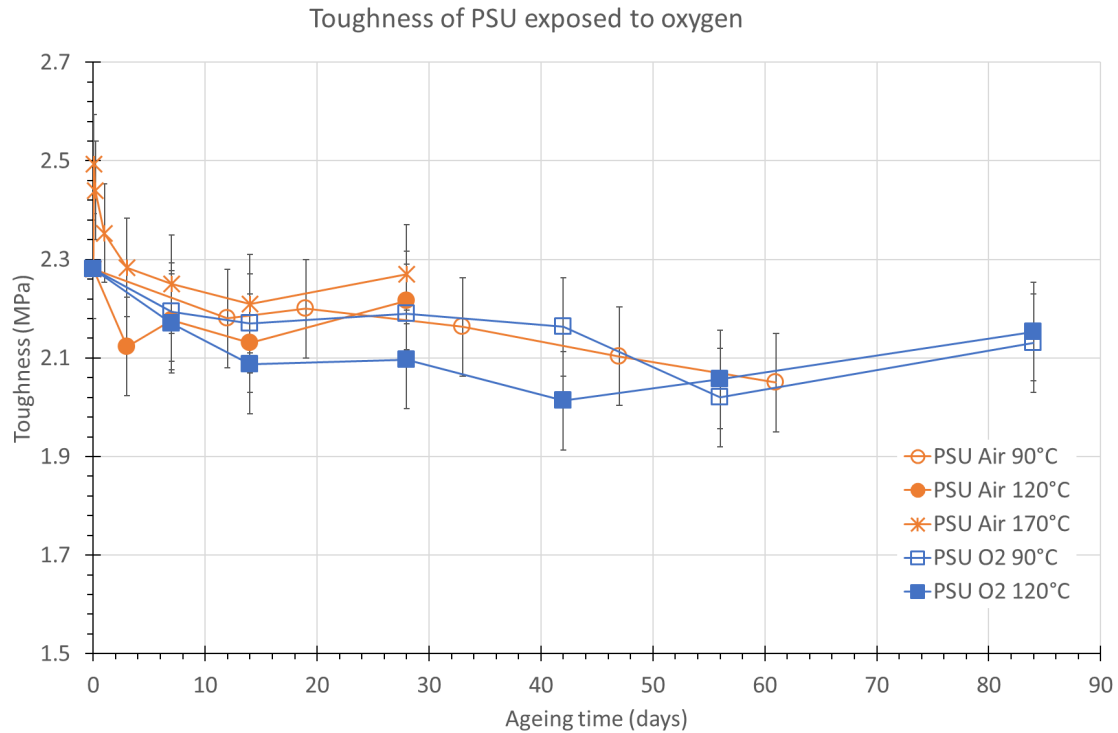


Figure 6.5: The material toughness over time for PSU exposed air (orange lines) at 90, 120 and 170 °C and oxygen at 5 bar (blue lines) at 90 and 120 °C.

When looking at the UTS of the aged samples, larger differences between the samples are observed. The samples aged in oxygen or air at 90 °C show the least increase in UTS up to 68 ± 1 after 12 weeks and 65 ± 1 MPa after 61 days, respectively. The samples aged in either oxygen or air at 120 °C show a more significant increase in UTS. After as short as a couple days the UTS has increased to values between 65 and 70 MPa, where it seems to plateau. This initial increase in UTS is even more remarkable for the samples aged at 170 °C. After 1 hour at 170 °C the UTS has increased to 75 ± 1 MPa, after 5 hours to 77 ± 1 MPa, then after 1 day to 80 ± 1 MPa, where the increase starts to slow down over time. This shows that the reaction which leads to these changes in mechanical properties is very fast, especially at 170 °C and independent of the oxygen partial pressure, since no differences between ageing in air or oxygen at the same temperature are observed.

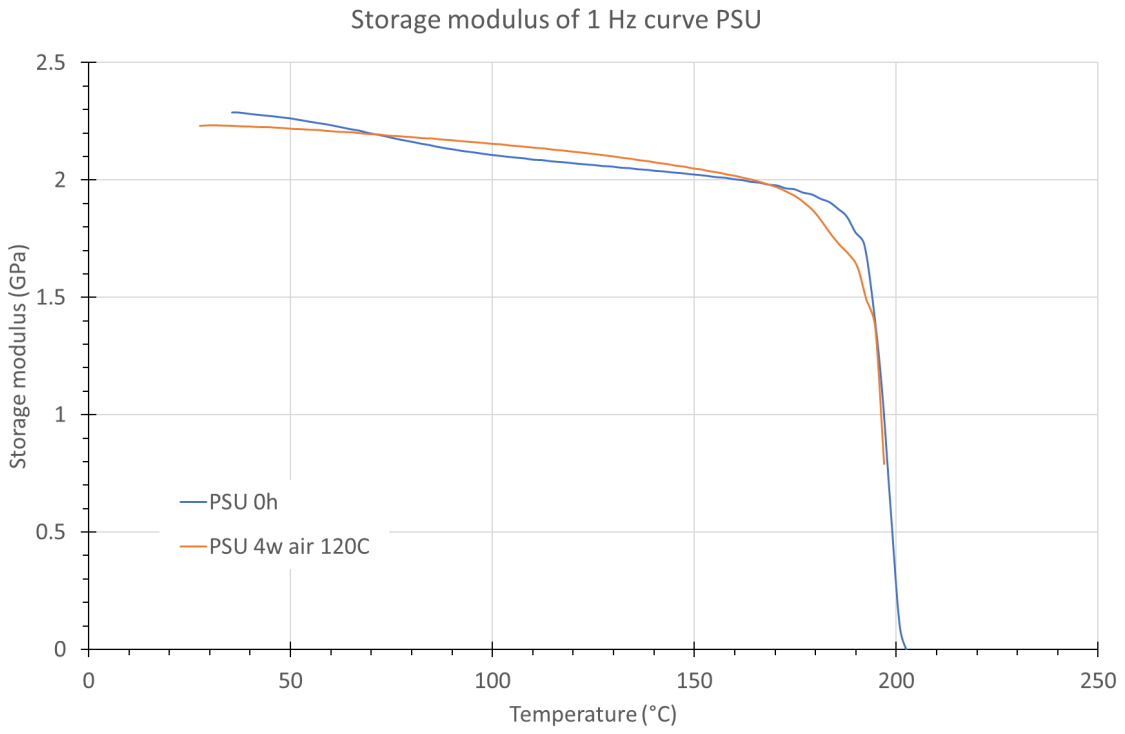
The strain at UTS and toughness both show a very similar trend, a decrease over time, which is faster in the beginning, but plateaus after a few days. A larger decrease in the strain at UTS is observed for the samples aged at higher temperatures. For the toughness, the curves of the different ageing conditions overlap a lot. This is expected, since the toughness depends on both the UTS and the strain at UTS, and we have seen that the samples with a higher UTS display a lower strain at UTS, which balance each other.

6.1.2 DMA tests (PSU; oxygen)

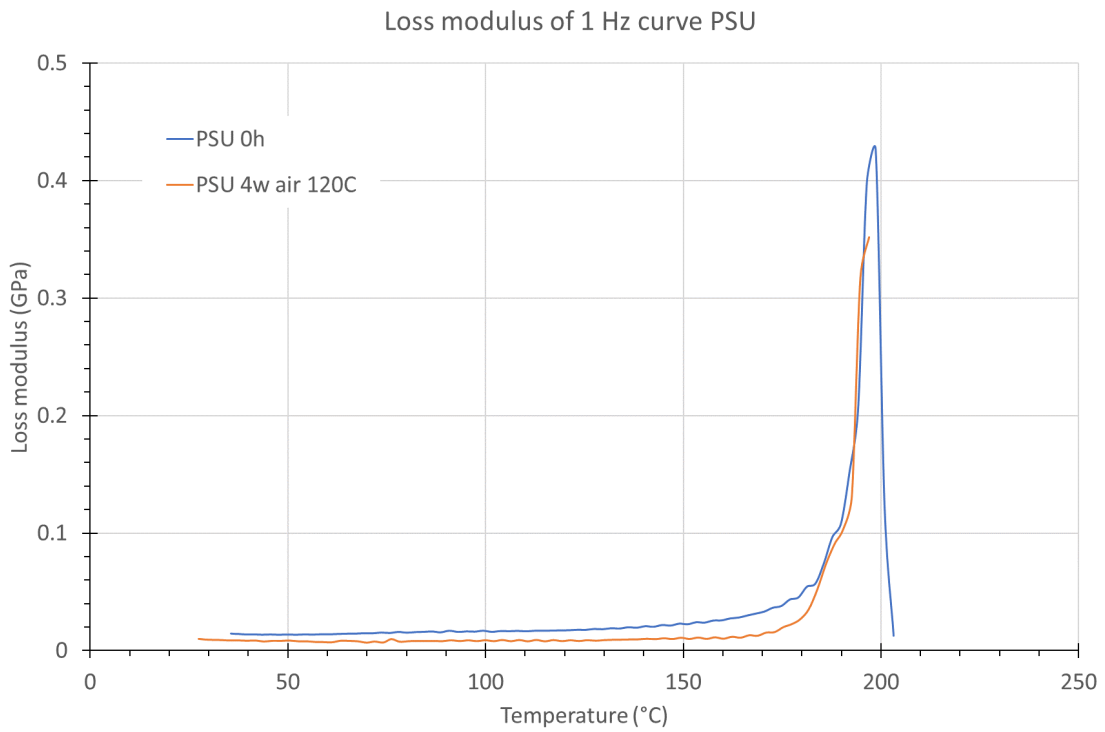
Unfortunately, DMA tests with PSU did not provide much information about the glass transition of PSU. This is due to the amorphous nature of PSU. From literature, the glass transition temperature of PSU is around 190 °C, at which point the amorphous part of the polymer starts to flow and does not behave visco-elastically any more. Since PSU is completely amorphous and does not seem to display 'rubbery' behaviour, the sample starts to deform plastically around its T_g . Figure 6.8 shows this very clearly. The top specimen is an undeformed, original samples, whereas the bottom specimen is a PSU sample which has undergone a DMA test. It is very clear the sample has deformed plastically. This is also visible in Figure 6.6 where the storage and loss modulus of PSU rapidly go to zero around 190-200 °C, at which point there is no elastic behaviour left in the polymer. Around 200 °C a huge increase in tan delta is observed (Figure 6.7) up to 1.4, which also indicates that at that temperature the behaviour of PSU is more as a viscous fluid than an elastic solid.

In order to test whether oxidative ageing has a significant effect on the behaviour of PSU another DMA test after 4 weeks of ageing in air at 120 °C has been performed. These results are plotted in orange in Figure 6.6 and 6.7. The results are very similar to that of unaged PSU, meaning PSU is still completely amorphous and the T_g has not changed significantly.

In order to be able to say more about the T_g and visco-elastic behaviour of PSU other characterisation techniques such as differential scanning calorimetry and creep-recovery testing have been applied.



(a)



(b)

Figure 6.6: Results of DMA tests on PSU (a) storage modulus (b) loss modulus.

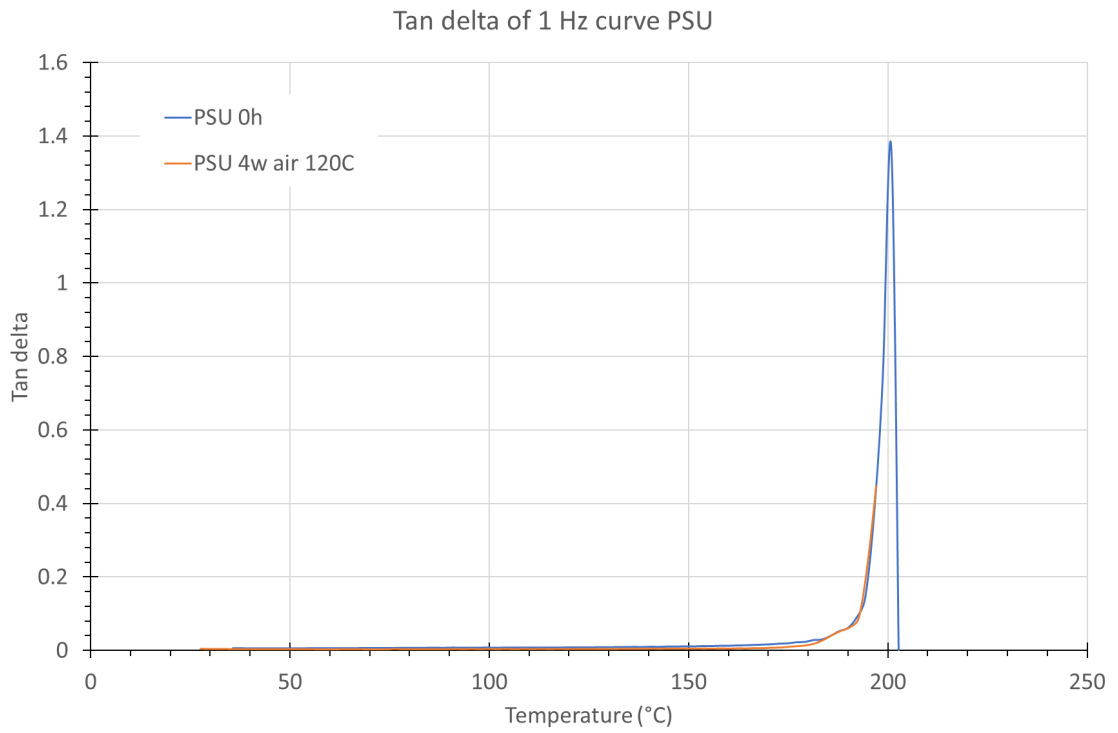


Figure 6.7: Tan delta curve of PSU.



Figure 6.8: Image of a PSU sample after performing a DMA test.

6.1.3 DSC tests (PSU; oxygen)

The DSC results confirm what the DMA had shown already: oxidative ageing in PSU does not show a significant change in the glass transition temperature (see Figure 6.9). It should be noted that in the DSC analysis a less conventional way of taking the glass transition temperature has been applied, *i.e.* the onset, instead of the middle, has been taken as the T_g . This method has been adopted because some of the curves show a small (endothermic) peak right after T_g , which makes it easier to take the onset, rather than the middle due to differing slopes. The small peak is a result of relaxation of the chains at T_g as explained in Chapter 5.

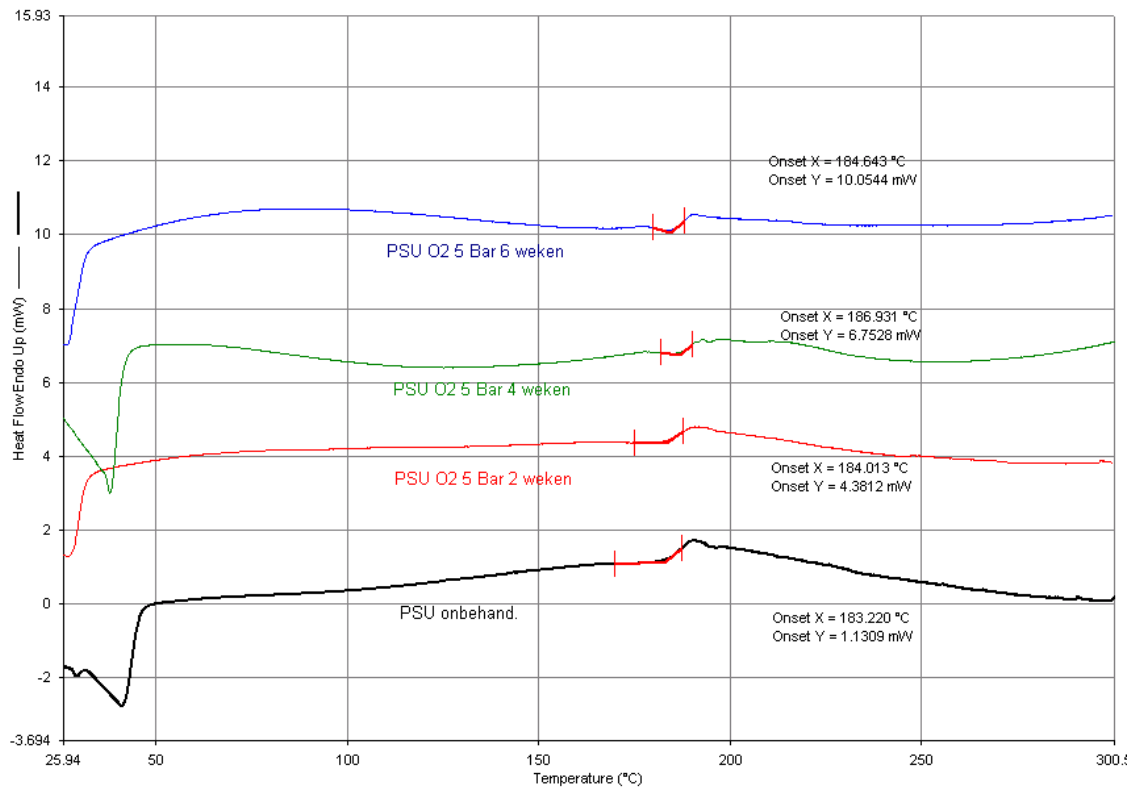


Figure 6.9: DSC analysis of different PSU curves exposed to oxygen.

6.1.4 Creep-recovery testing (PSU; oxygen)

Apart from changes in mechanical and thermal behaviour, oxidative ageing induces changes in the visco-elastic behaviour of the polymer. Figure 6.10 shows the creep compliance of an unaged PSU sample compared to PSU aged in pure oxygen at 5 bar and 120 °C for 2 weeks and for 12 weeks. The creep measurement was taken at 150 °C at a stress of 5 MPa for 1 hour. As shown the compliance reduces as a function of ageing time, meaning the polymer has become stiffer.

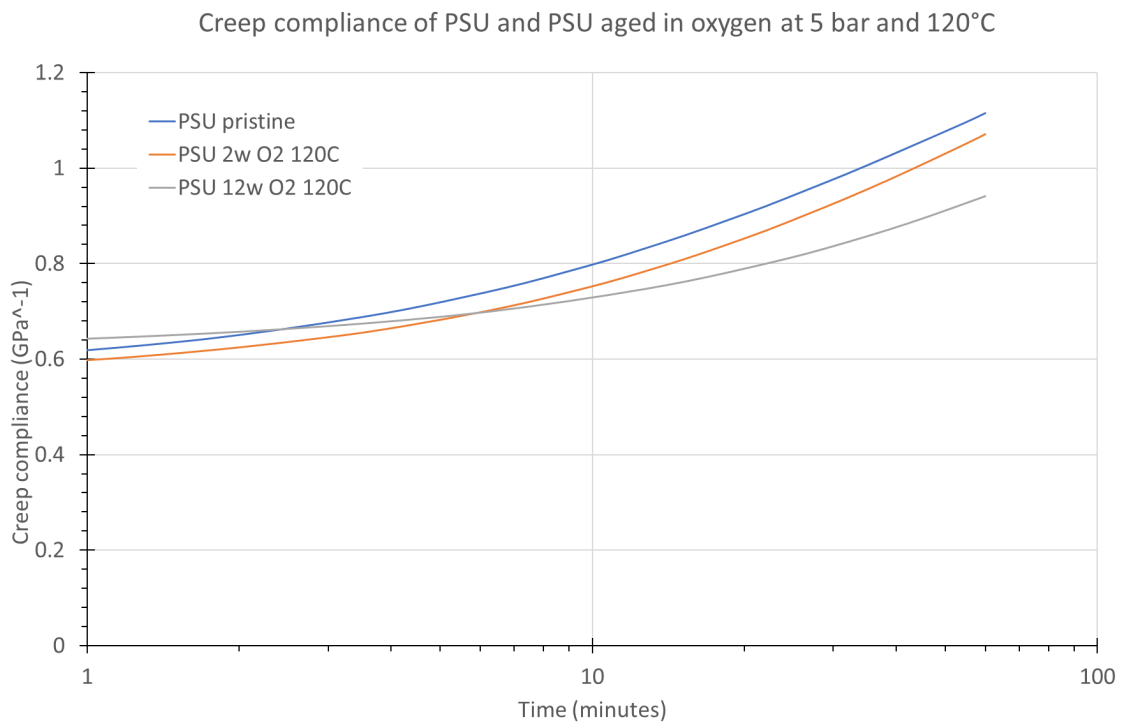


Figure 6.10: Creep compliance of PSU and PSU aged in oxygen at 5 bar and 120 °C for 2 weeks and 12 weeks. The curve is given for a creep-recovery measurement at 150 °C at a stress of 5 MPa for 1 hour.

6.1.5 FTIR (PSU; oxygen)

A labelled FTIR spectrum of unaged PSU is shown in Figure 6.11. The correspondence of the peaks with the correct molecular structure is given in Table 6.1 [32, 55].

The FTIR spectra of PSU unaged and aged in oxygen at 5 bar and 120 °C for 4 and 8 weeks are shown in Figure 6.12. It seems that the peak intensity becomes lower for the 4 and 8 weeks samples. However, since there are no differences between the relative heights of the peaks for each spectrum, no change is observed and neither have there been new peaks observed. Furthermore, since PSU already contains oxidised sulphur atoms, it is unclear to which chemical structure the oxygen may react with.

Table 6.1: ATR-FTIR peaks expected for PSU.

Peak	Chemical Structure
1584, 1504, 1486, 1411	C-C stretching in aromatic ring
2960, 874, 851, 830, 717, 735, 687	C-H in aromatic ring
1152, 1325	O=S=O symmetric and asymmetric stretching [55]
1385	-CH ₃ [32]
1240	C-O-C [55]
1170	C=S
1100	C-S
1080	S=O
1011	C=CH

6.1.6 Other measurement techniques (PSU; oxygen)

PSU has also been subjected to other characterisation techniques, such as weight measurements, XRD and SEM. The results of these measurements are shown in Appendix D.1. The weight measurements do not show any change during the ageing period. The XRD measurements confirm that PSU is an amorphous polymer, since no crystalline peaks have been detected. However, no significant changes in spectrum are observed between the aged and unaged samples. The SEM measurement clearly show the flow lines during processing, but apart from that, no other differences have been observed.

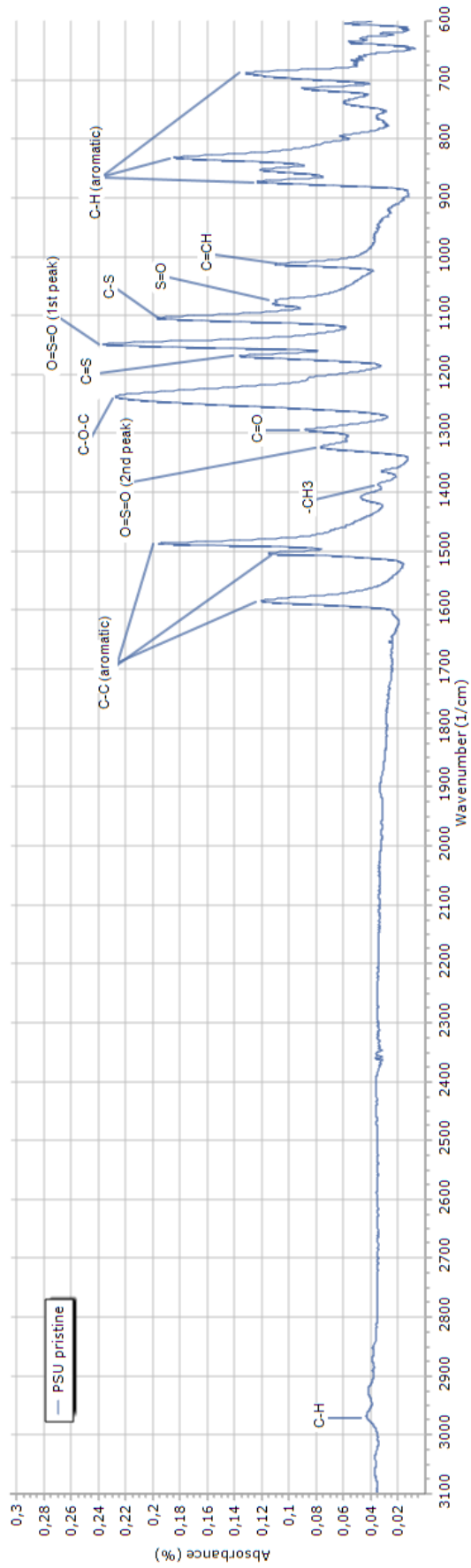


Figure 6.11: Labelled FTIR spectrum of unaged PSU.

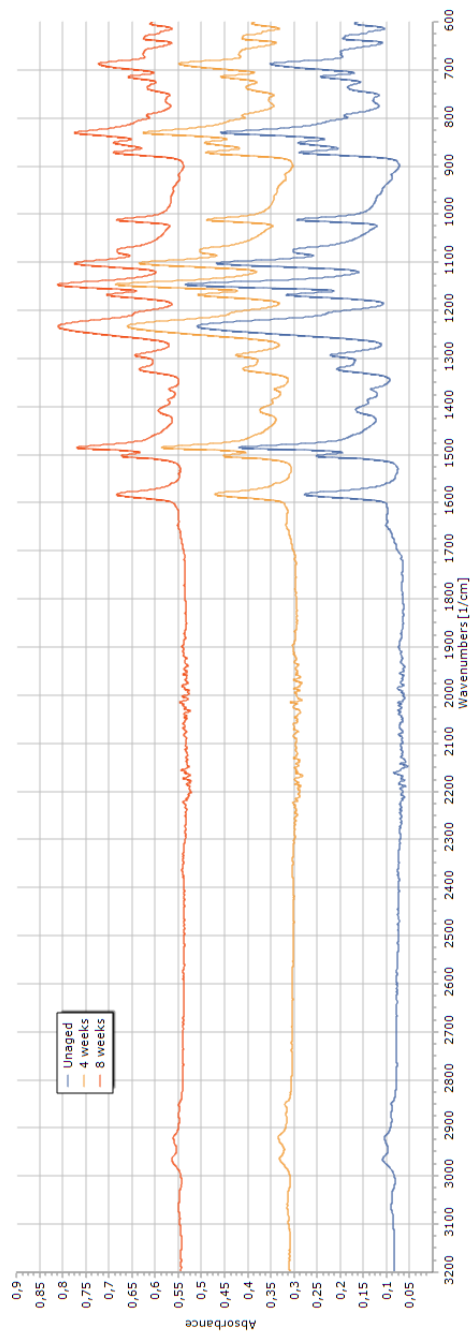


Figure 6.12: FTIR spectra of PSU aged in O₂ at 5 bar and 120 °C.

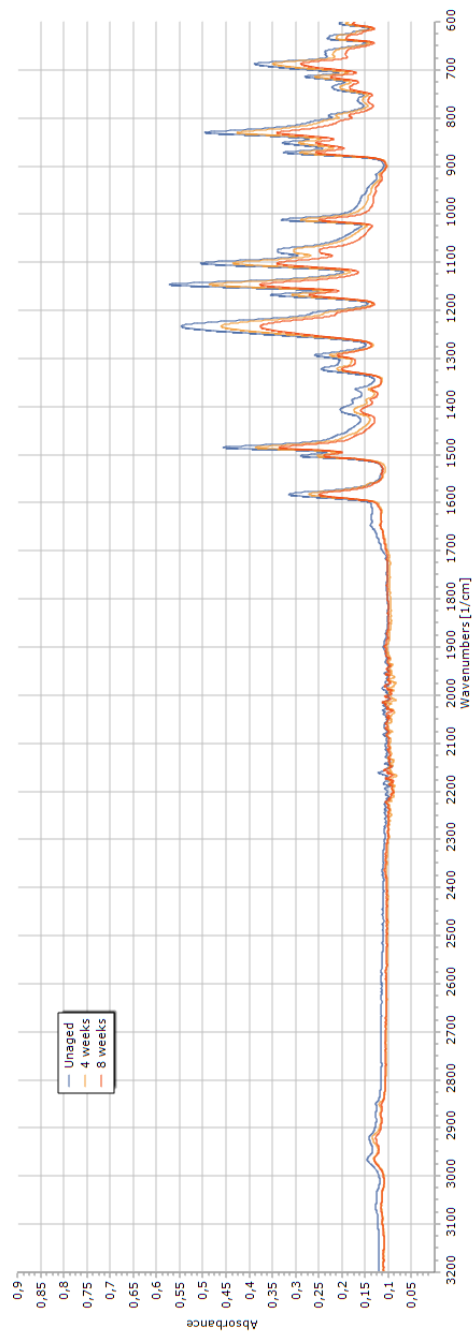


Figure 6.13: Stacked FTIR spectra of PSU aged in O₂ at 5 bar and 120 °C.

6.2 Discussion: what happens to PSU when aged in an oxygen environment?

The results for PSU aged in oxygen are summarised in Table 6.2. The results obtained are very similar to the results of PPS-40%gf exposed to oxygen. Therefore, a similar flow of arguments is followed as used for PPS-40%gf in Section 6.2. Some highlights, are summarised as follows:

- The UTS and Young's modulus increase independently of oxygen partial pressure, but only seem to depend on the ageing temperature. This complies with the effects expected for physical ageing. Furthermore, the increase abruptly levels off after some time, which is unexpected for a cross-linking reaction.
- The FTIR results show no difference between untreated and treated samples, meaning it is unlikely that oxygen has reacted with the PSU chains, since this would be visible in changes in the relative height or appearance of new peaks in the FTIR spectra.
- The 4 weeks aged in air at 120 °C sample tested in DMA shows the exact same visco-elastic behaviour as the unaged sample. If oxidative cross-linking would have occurred, it is expected that a rubbery plateau would have appeared in the DMA measurements, but since this is completely absent it can be concluded that no cross-links have formed. Unfortunately, no DMA test has been conducted for PSU at 170 °C. Since reactions are more likely to occur at the high temperature of 170 °C, perhaps a rubbery plateau may have formed.
- In the DSC results, no large enthalpy relaxation peak are observed, such as for PPS-40%gf. However, there are signs of a broader, lower peak. This could be explained by the fact that perhaps not a lot of relaxation occurred in PSU, since its molecular structure is bulkier and more complex than that of PPS.

Table 6.2: Results of PSU exposed to oxygen.

Characterisation technique	Results
Tensile tests	increase in UTS and Young's modulus, decrease in strain at UTS and toughness
DMA	no significant change in storage modulus of glass plateau and an absence of rubbery plateau
Creep	decreasing creep compliance for longer ageing times
SEM	no significant differences observed
Weight	no change in weight observed
FTIR	no signs of formation of new chemical bonds or further incorporation of oxygen into the polymer
XRD	no big differences in spectra
DSC	no significant changes in T_g observed

6.3 PSU aged in KOH

6.3.1 Tensile tests (PSU; KOH)

Figure 6.14 shows the stress-strain curve of PSU exposed to 30wt% KOH at 90 °C. As shown, the stress-strain curves look very different from the PPS-40%gf curves. Instead of lowered mechanical properties, the PSU samples seem to have obtained a higher ultimate tensile strength over time (from 62 to 67 ± 1 MPa), along with a decrease in strain at UTS (from 5.5 to 4.7 ± 0.2 %) and a decrease in toughness (from 2.3 to 2.0 ± 0.1 MPa). Within the measurement variation, no distinct change in the Young's modulus has been observed. However, the initial drop in Young's modulus around 12 days can be explained by the fact that the unaged sample was a *dry* sample, whereas all the aged samples are wet samples. Water diffused into the polymer can act as a plasticiser, making the polymer softer and less stiff.

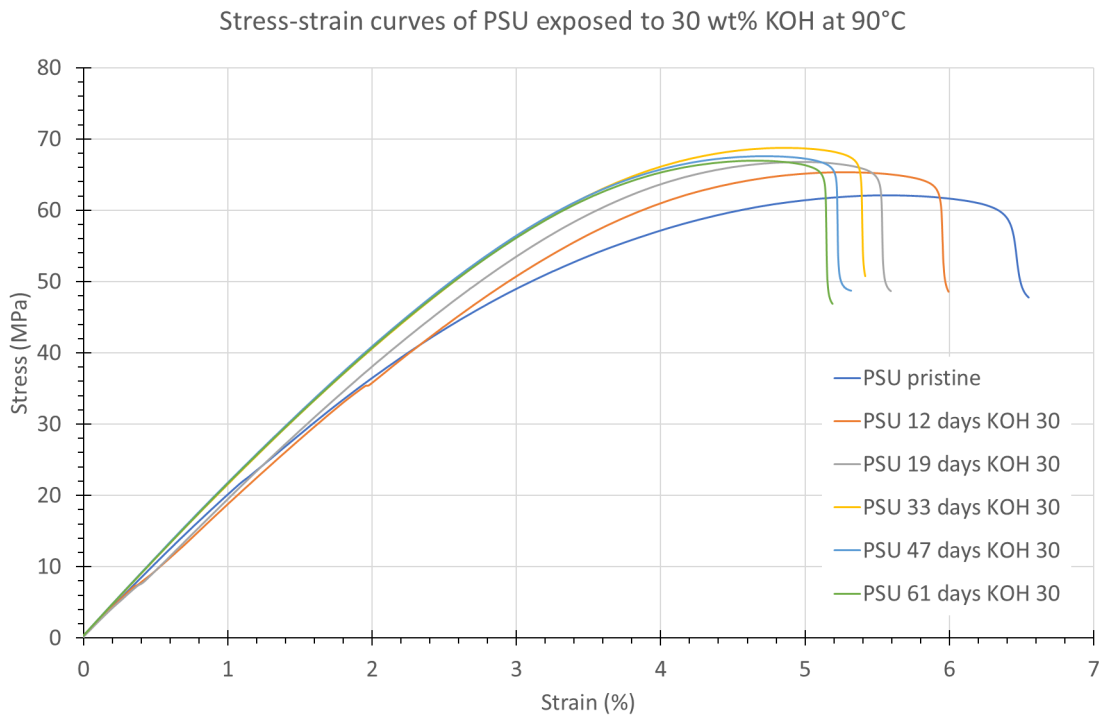


Figure 6.14: Stress-strain curves of PSU exposed to 30wt% KOH at 90 °C.

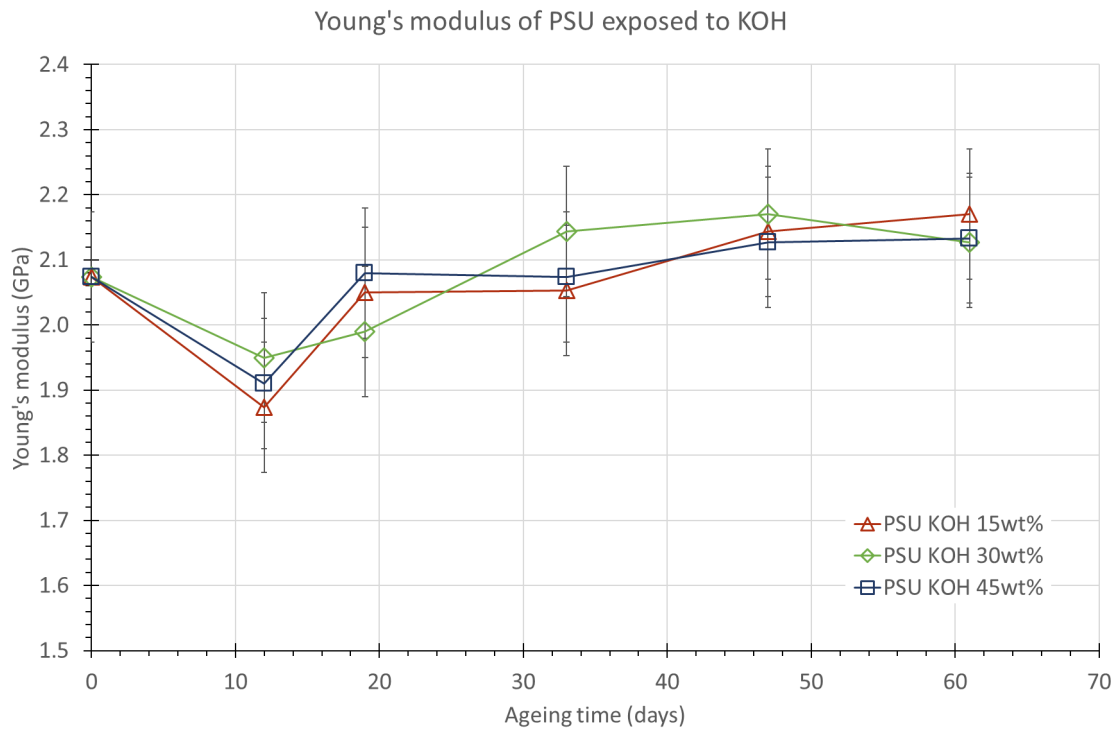


Figure 6.15: The Young's modulus over time for PSU exposed 15wt% KOH solution (red line), 30wt% KOH solution (green line) and 45wt% KOH (dark blue line), all at 90 °C.

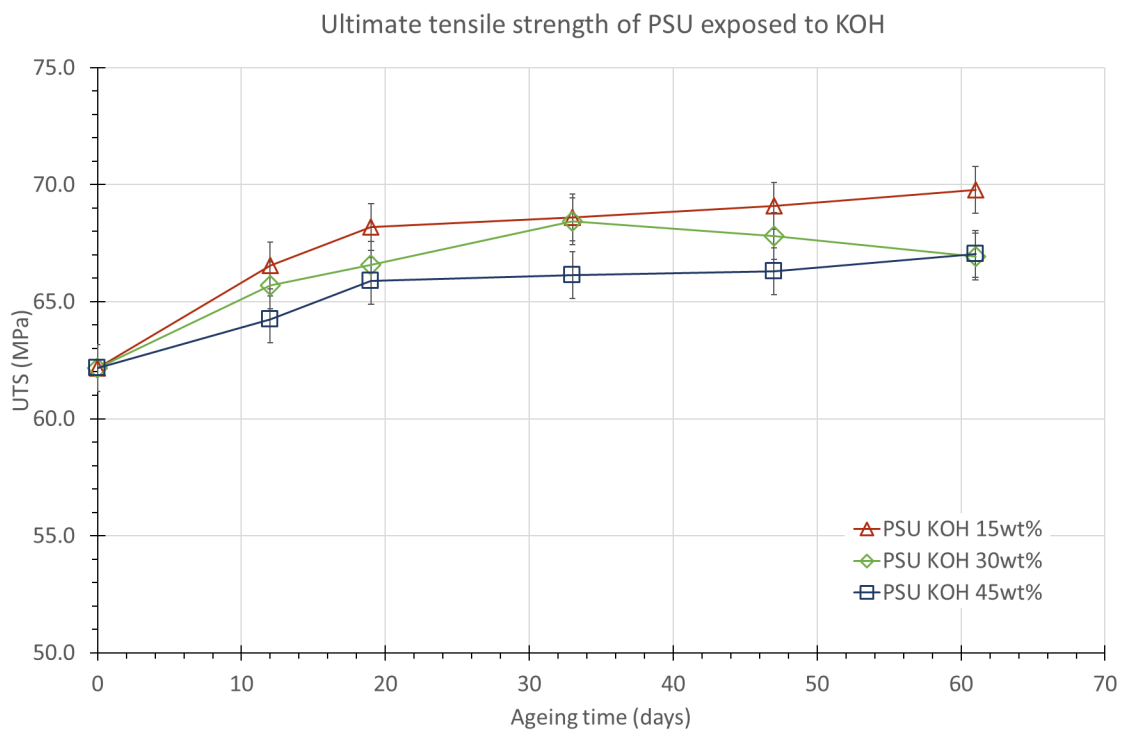


Figure 6.16: The UTS over time for PSU exposed 15wt% KOH solution (red line), 30wt% KOH solution (green line) and 45wt% KOH (dark blue line), all at 90 °C.

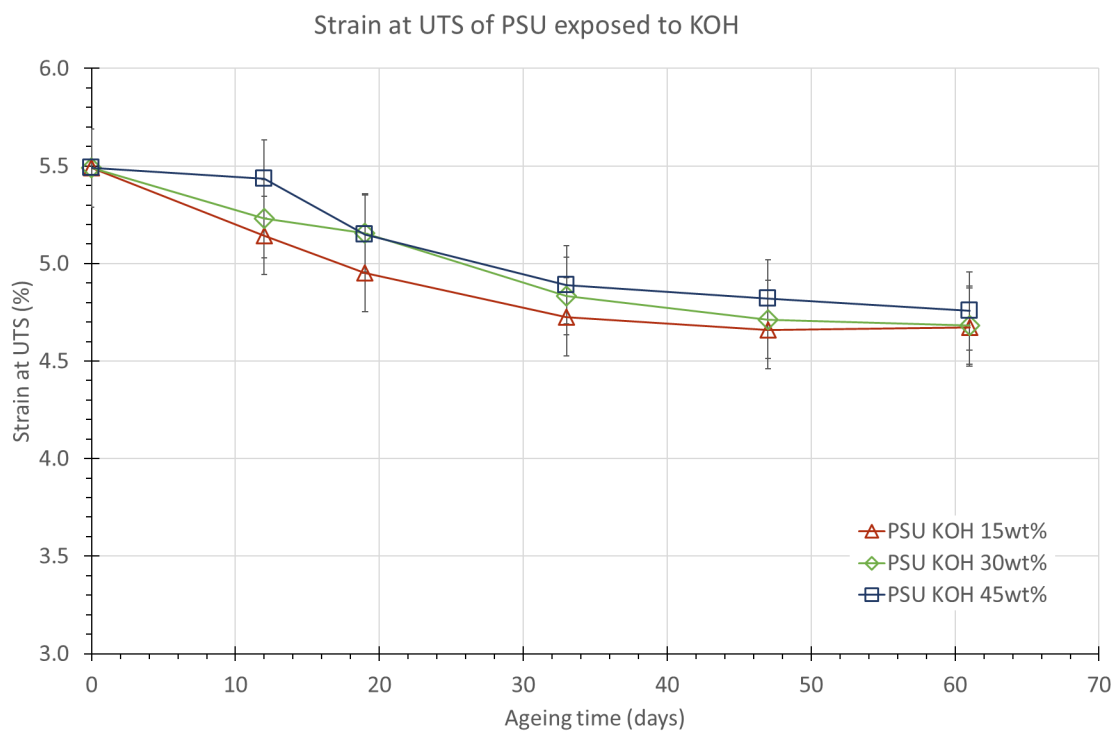


Figure 6.17: The strain at UTS over time for PSU exposed 15wt% KOH solution (red line), 30wt% KOH solution (green line) and 45wt% KOH (dark blue line), all at 90 °C.

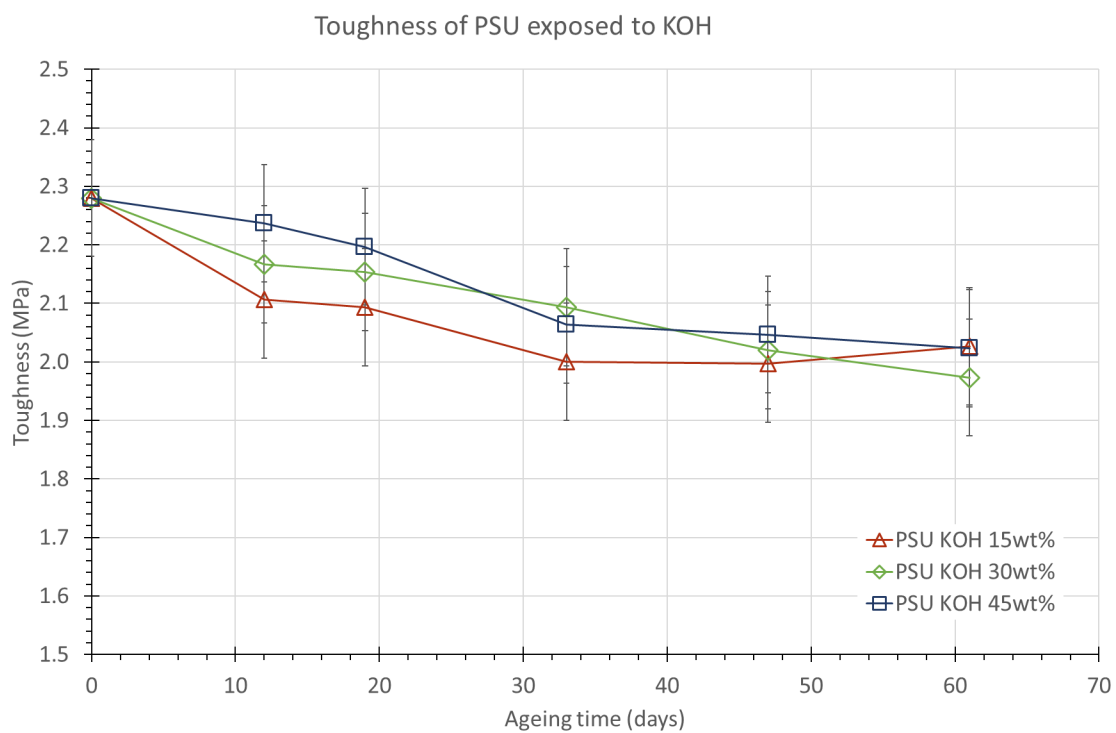


Figure 6.18: The material toughness over time for PSU exposed 15wt% KOH solution (red line), 30wt% KOH solution (green line) and 45wt% KOH (dark blue line), all at 90 °C.

6.3.2 Creep-recovery testing (PSU; KOH)

The creep-recovery tests, as shown in Figure 6.19, show no change in creep behaviour after 19 days, but after 61 days the creep compliance decreases slightly, meaning the polymer has become stiffer.

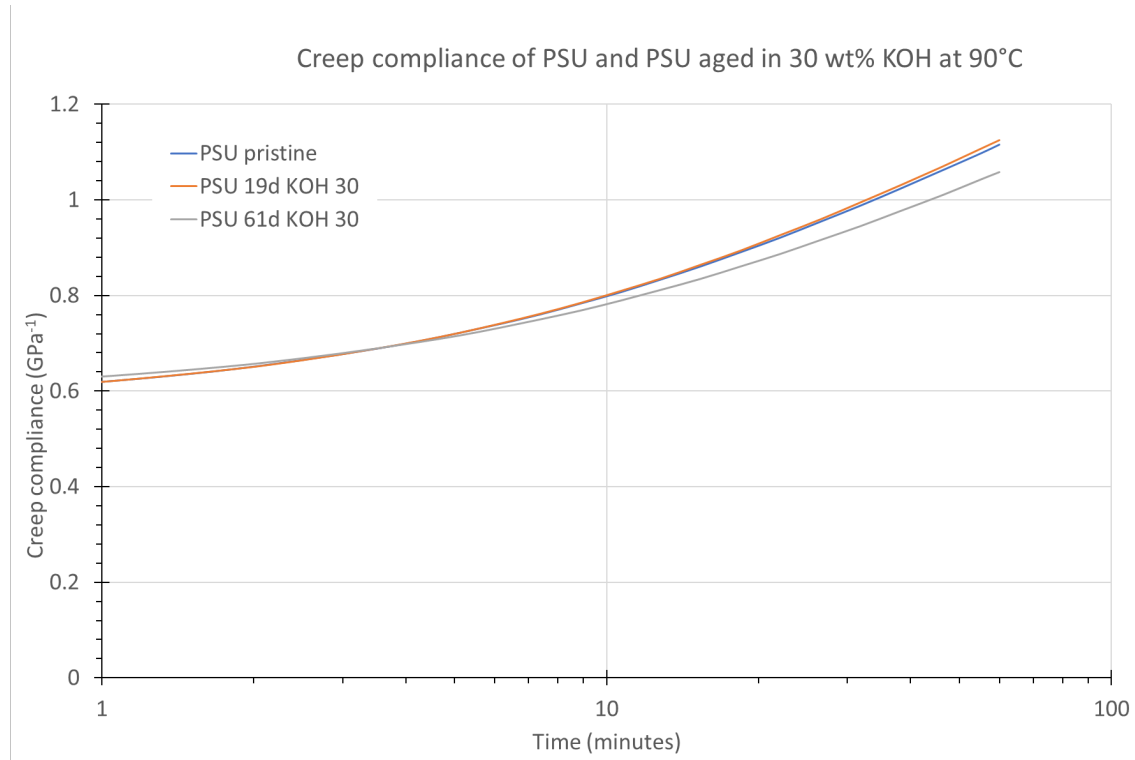


Figure 6.19: Creep compliance of PSU and PSU aged in a 30wt% KOH solution at 90 °C for 19 days and 61 days. The curve is given for a creep-recovery measurement at 150 °C at a stress of 5 MPa for 1 hour.

6.3.3 FTIR (PSU; KOH)

The FTIR results also show no change in *relative* peak height or the appearance/disappearance of (new) peaks.

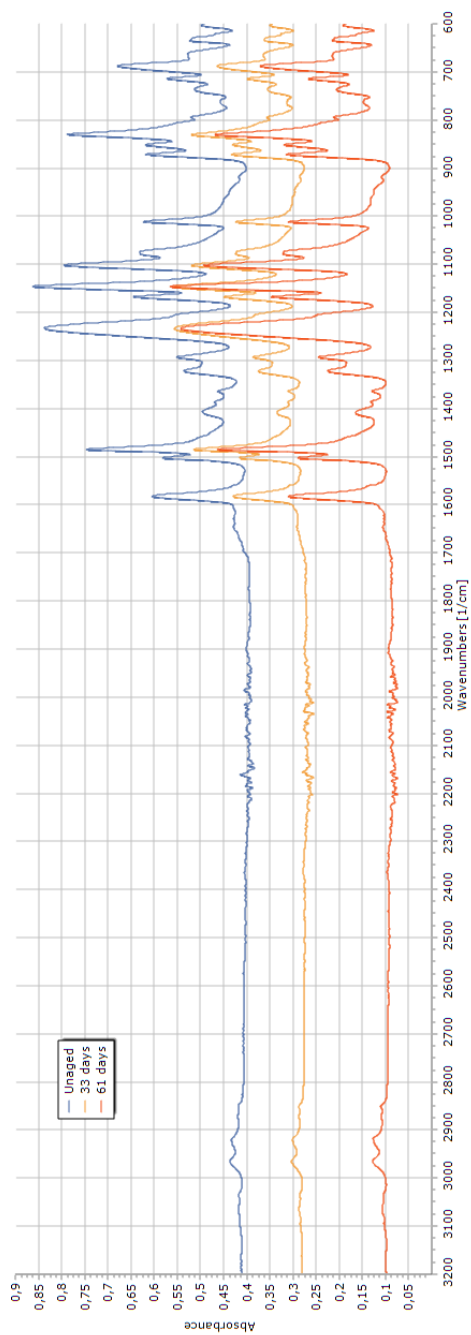


Figure 6.20: FTIR spectra of PSU aged in KOH 30wt% at 90 °C.

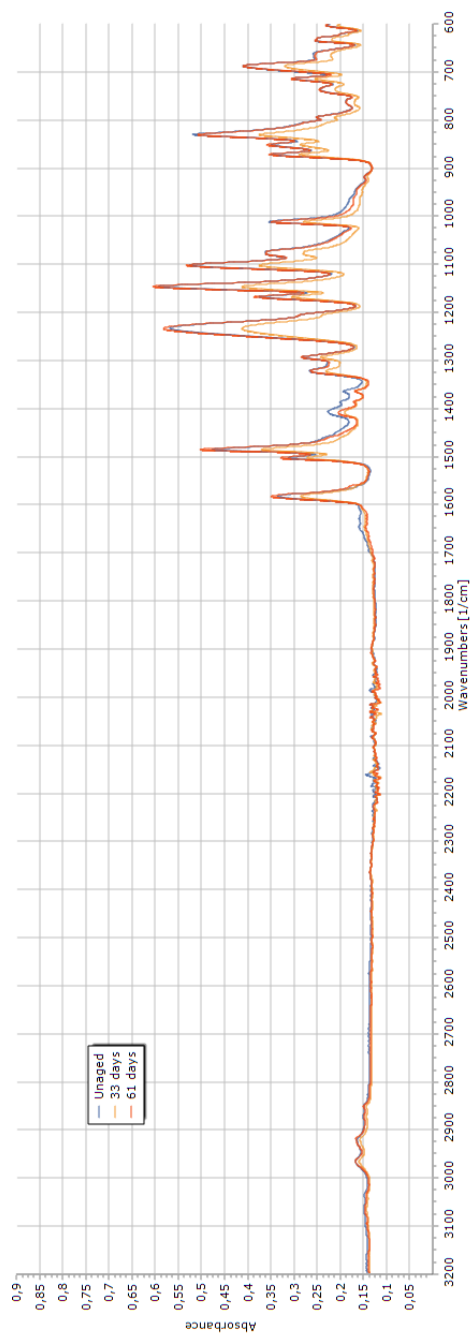


Figure 6.21: Stacked FTIR spectra of PSU aged in KOH 30wt% at 90 °C.

6.3.4 Other measurement techniques (PSU; KOH)

PSU has also been subjected to other characterisation techniques, such as weight measurements, XRD and SEM. The results of these measurements are shown in Appendix D.2. Surprisingly, the weight measurements (Figure 6.22) do not show much change during the ageing period, perhaps a very slight increase due to water diffusion into the sample. The XRD and SEM measurements do not show any changes.

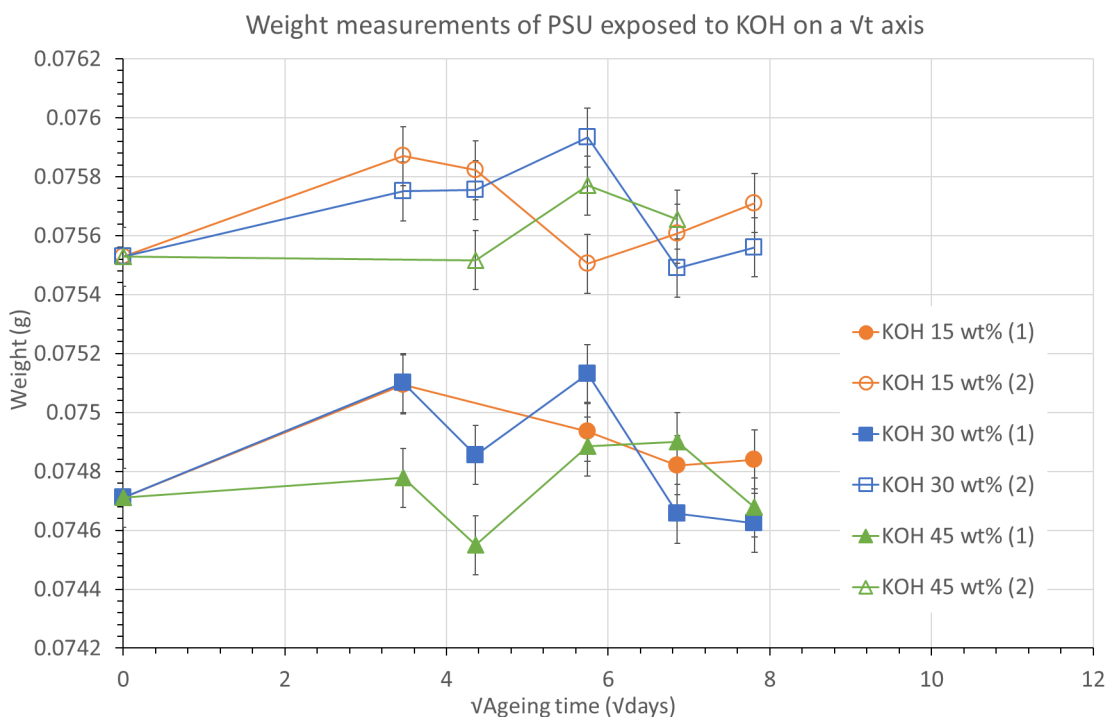


Figure 6.22: Graphs showing the weight change of PSU exposed to oxygen plotted against the square-root of ageing time.

6.4 Discussion: what happens to PSU when aged in KOH?

The results discussed above are summarised in Table 6.3. From these results it can be concluded that PSU has **not** undergone any degradation or hydrolysis due to the presence of water and KOH. The different KOH concentrations did not result in different mechanical and thermal properties. The change in properties observed are very subtle. The polymer seems to have become slightly stronger and stiffer. These property changes can all be attributed to physical ageing as discussed before. Since the samples have been exposed to a modest 90 °C, only small relaxation behaviour is observed, similar to that of PSU exposed to air or oxygen at 90 °C.

Table 6.3: Results of PSU exposed to KOH.

Characterisation technique	Results
Tensile tests	increase in UTS, decrease in strain at UTS and toughness, no significant change in Young's modulus
Creep	decreasing creep compliance for longer ageing times
SEM	no significant differences observed
Weight	no change in weight observed
FTIR	no signs of formation of new chemical bonds or further incorporation of oxygen into the polymer
XRD	no big differences in spectra
DSC	no significant changes in T_g observed

6.5 Concluding remarks

The ageing experiments confirm that PSU is a very stable polymer. This is for a large part due to its very high T_g of around 190 °C. This means that the polymer chains show very low mobility for the operation temperature of 90 °C. Therefore, aggressive and reactive substances such as KOH and O₂ cannot penetrate the material very easily, making the material resistant to these conditions. PSU should therefore be further considered as a material for encapsulation of the ZEF AEC.

Chapter 7

Extrapolation of the results

The previous two chapters were concerned with the results obtained from the ageing experiments and with discussing these results. This chapter, will look into some extrapolations, which can be done to predict the properties of the material after the operation time of 20 years.

7.1 Predicting the creep compliance in 20 years (PSU)

The creep-recovery tests have been performed at multiple temperatures, which make it possible to use time-temperature superposition to create a master curve for a specific reference temperature and the associated shift curve, as described in Chapter 2. This procedure of horizontally shifting the higher temperature curves to longer times has been performed for unaged PSU and resulted in the master curve and shift curve in Figure 7.1. The reference temperature of the master curve is 90 °C, since this is equal to the operation temperature of the ZEF AEC. Using the shift-factor curve it is possible to shift the curve to a different reference temperature.

The shift-factor is a property which can be used to calculate the activation energy of the mechanical relaxation. Since the reference temperature is below the T_g of PSU, the Arrhenius model can be used (Equation 2.1). From this model it is clear that the activation energy of relaxation can be derived from the slope of $\ln(a_T)$ versus $1/T$ as shown in Figure 7.1b, multiplied by the universal gas constant ($R = 8.314 \text{ J/K/mole}$). For unaged PSU this gives a value of 187 kJ/mol. This value is in the same order of magnitude as values for other thermoplastics as found by Williams, Landel and Ferry in their 1955 paper [87].

In order to extrapolate the compliance to larger timescales, the creep master curve data can be fitted to the empirical Kohlrausch-Williams-Watts (KWW) function. The KWW function, also called the empirical stretched exponential law, is widely used to describe *relaxation* phenomena. *Relaxation* is the change of a system from one physical state to

another, involving the dissipation of energy [49]. For long-term tensile creep results, the following KWW model can be used (Prof. dr. ir. J. Van Turnhout, pers. comm.):

$$D(t, T) = D_0 + (D_\infty - D_0)(1 - e^{-[t/\tau(T)]^b}), \quad (7.1)$$

where D is the *tensile* creep compliance at $t = 0$ and $t = \infty$, τ is the relaxation time and is dependent on the temperature, and b is the exponent, which is often a value between 0 and 1, which makes the function a stretched exponential. Equation 7.1 is used for the long-term creep prediction.

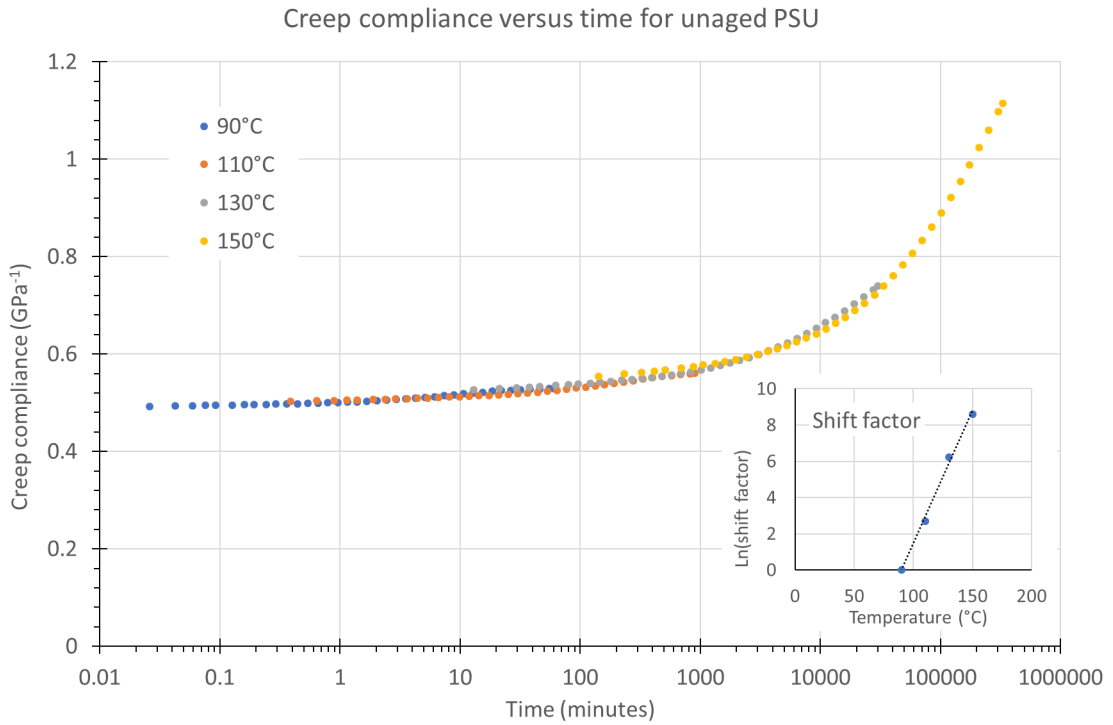
When fitting the master curve to the KWW function with four variables (D_0 , D_∞ , τ and b), the following fit is obtained as shown in Figure 7.2. The values found for the four parameters are:

- $D_0 = 501.4$ MPa,
- $D_\infty = 8056$ MPa,
- $\tau = 1.541 \times 10^8$ minutes ≈ 293 years,
- and $b = 0.4013$.

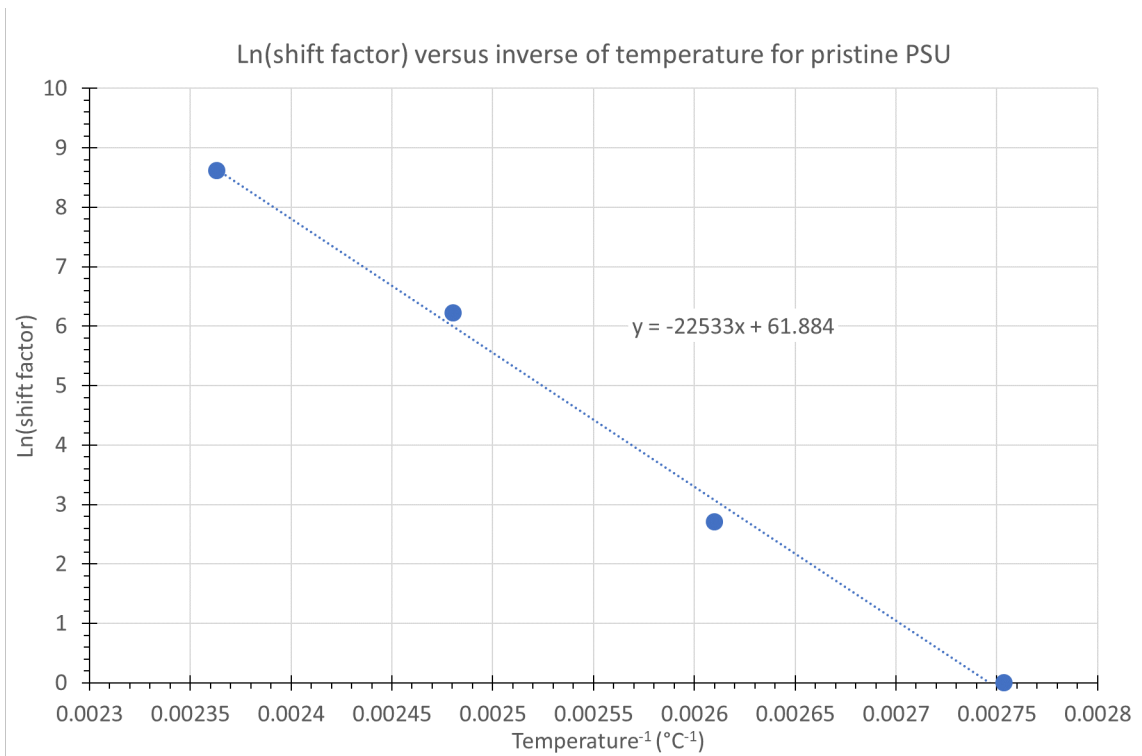
The extrapolated master curve with the KWW fit can be used to predict the creep compliance after a certain time period given that the material is being held at a constant pressure and temperature of 90 °C. If the ZEF AEC would continuously operate at a pressure of 50 bar and 90 °C for 20 years, the creep compliance would be equal to about 2.7 GPa⁻¹, which is equal to a strain of about 1.4%.

Figure 7.3 shows the three stages of creep. The primary stage is characterised by the decreasing creep rate over time, which is attributed to strain hardening. The secondary stage, also called the steady-state region, is when the creep rate remains almost constant. The tertiary or acceleration state is most critical and is when necking occurs. The creep rate increases rapidly, until the material ruptures [40]. As shown in Figure 7.3, after 20 years the shape of the creep curve is expected to be still in the secondary, steady-state region. However, this is also attributed to Equation 7.1, in which the compliance approaches D_∞ .

In the above analysis, only the creep compliance curves of unaged PSU has been discussed. However, time-temperature superposition can also be applied to the aged samples. Figure 7.4 shows the master curves of the aged samples when the same shift curve as for the unaged PSU is used. As shown, the obtained curves do not show good overlap between the different isothermal curves. This means that the shift curve itself changes during ageing, meaning the apparent activation energy of creep changes during ageing.



(a)



(b)

Figure 7.1: Time-temperature superposition of creep curves of unaged PSU: (a) master curve creep compliance versus time and (b) the shift curve versus inverse temperature.

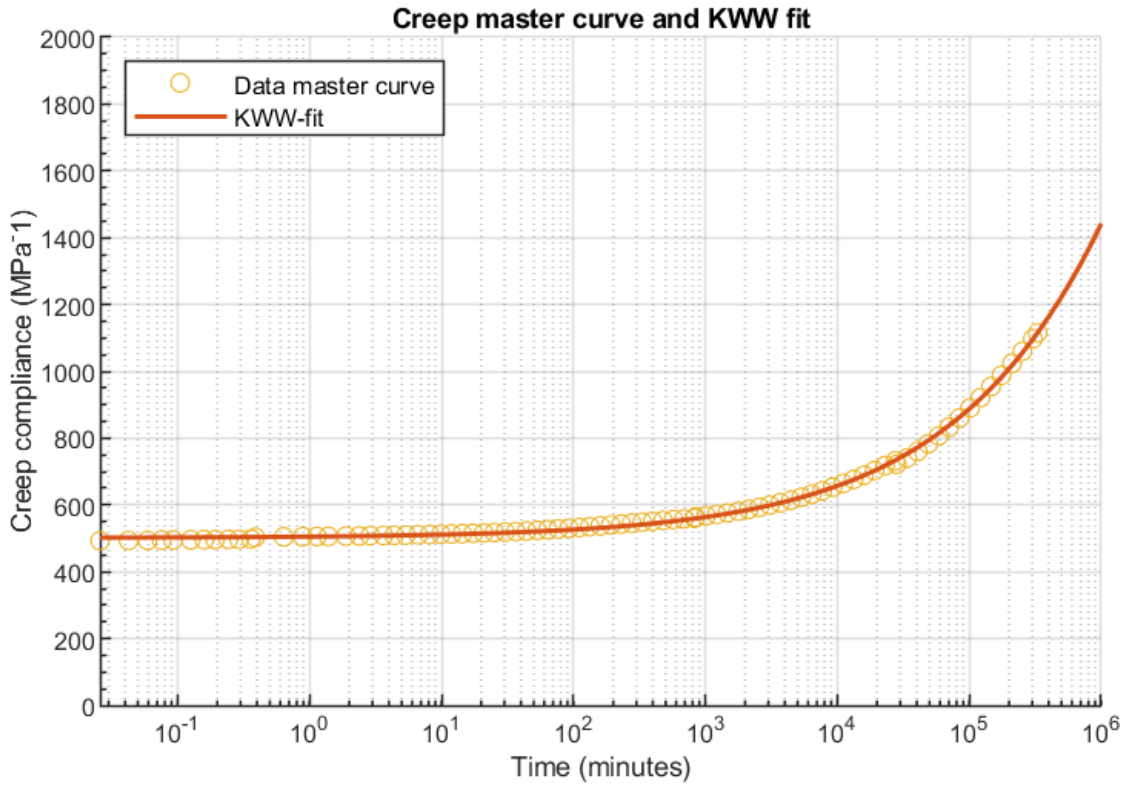
What is even more striking is that vertical shifts are observed in the 12 weeks and 61 days samples (Figure 7.4b and 7.4d, respectively). For the 12 weeks O₂ 120 °C the compliance suddenly increases by about 60 MPa⁻¹ for the 130 and 150 °C curves. For the 61 days KOH 30wt% at 90 °C the compliance drops for the 110 °C curve and increases again for the 130 and 150 °C creep curves.

Vertical shift-factors are sometimes needed to account for changes in material density, hygrological effects and thermal expansion and contraction [6]. An explanation of the drop in compliance for 110 °C curve of the samples aged in KOH 30wt% for 61 days, could be due to the evaporation of water out of the sample. As shown in Figure 7.4d, the blue 90 °C curve is at a higher compliance than the unaged (dry) and 19 days sample, meaning the material has become less stiff. This can be explained by the absorption of water, which acts as a plasticiser, making the polymer softer. At 110 °C, this water could have evaporated leading to the drop in compliance, *i.e.* an increase in stiffness to a value comparable to those of the unaged (dry) and 19 days PSU.

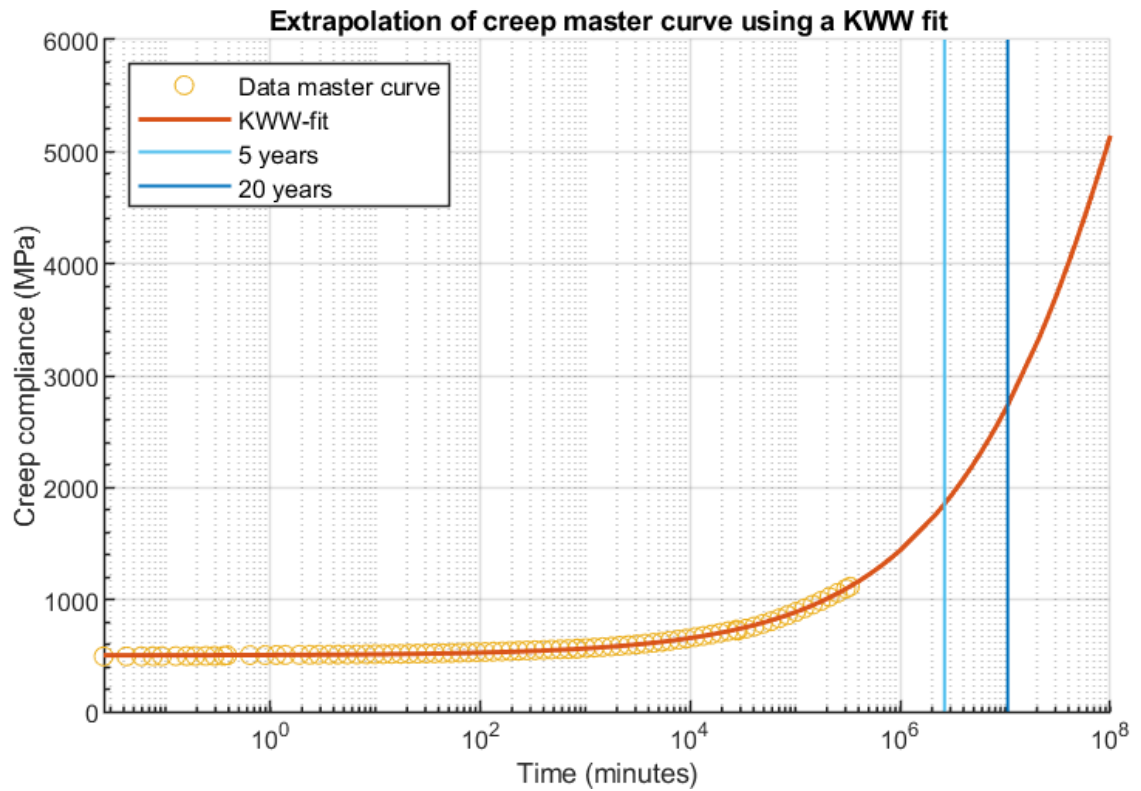
For the increase in compliance between the 110 and 130 °C curves, something else occurs. This increase in compliance is seen for both the 12 weeks oxygen 120 °C as the 61 days KOH 30wt% samples. One of the options could be a secondary transition in the polymer, such as the beta transition, which is due to the movement of side chains. PSU does not have any side chains, apart from the very small methyl groups. However, it is known that the benzene rings in PSU have local conformational mobility in the form of rotations. The freezing temperature of these rotations is, however, around -30 to -20 °C [42]. This could, thus, not be the cause of the increase in compliance at 130 °C.

One hypothesis is that the increase of compliance is an effect of the physical ageing and the accompanied decrease in free volume. Since, when the sample is heated again, it reaches the equilibrium free volume earlier, leading to an earlier increase in free volume as shown in Figure 5.14. This increase in free volume could explain the higher creep compliance. However, this is speculative.

When both horizontal and vertical shift-factors have been used for each individual curve in order to correct for the changes in volume and density, the master and shift curves as displayed in Figure 7.5 are obtained. As shown for aged in oxygen, the more the material is aged, the more the creep compliance curve shifts to the right and therefore the stiffer the material. For ageing in KOH an initial shift to the left is shown, which is probably due to water diffusion into the material, making it slightly softer. For longer ageing times, however, the material does become stiffer.

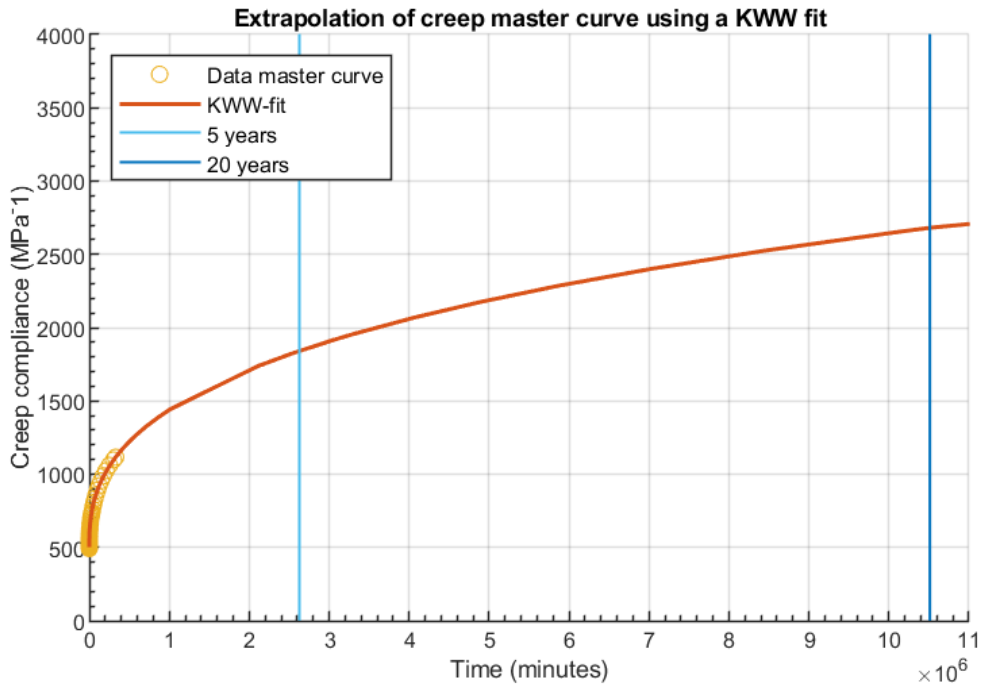


(a)

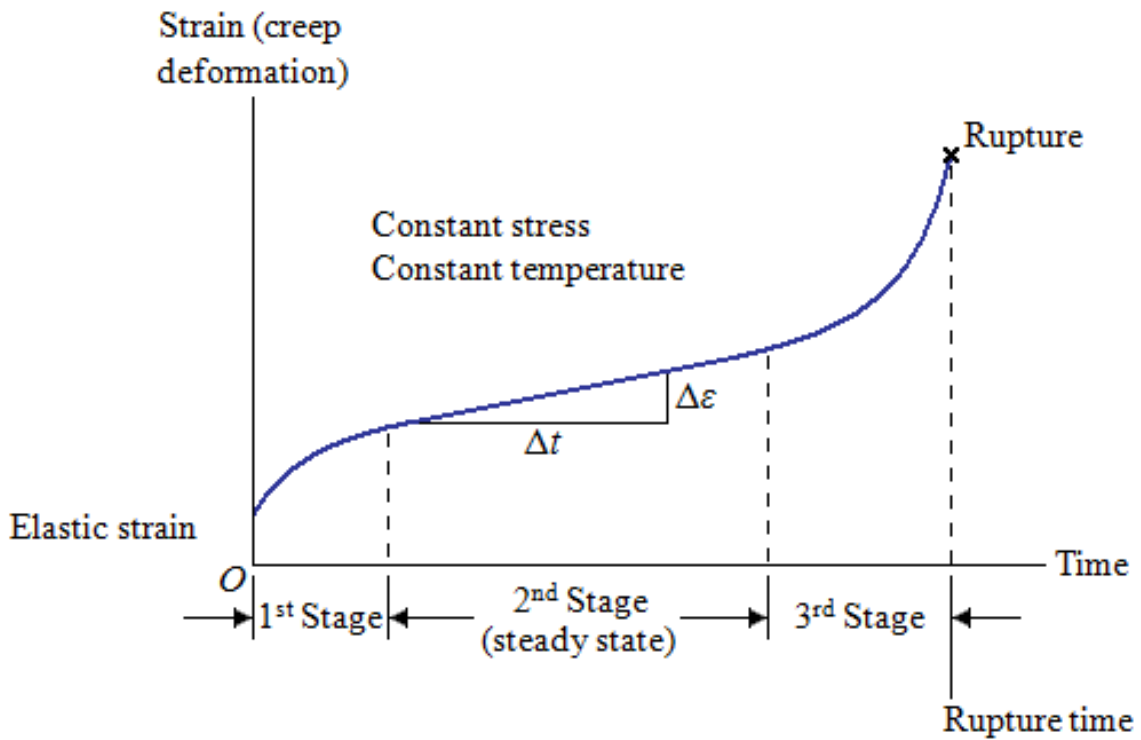


(b)

Figure 7.2: Creep compliance master curve of unaged PSU with a KWW fit on (a) a log scale and (b) a linear scale. The blue lines represent the time after 5 and 20 years.



(a)



(b)

Figure 7.3: Creep compliance master curve on (a) a linear scale compared to (b) the stages of creep.

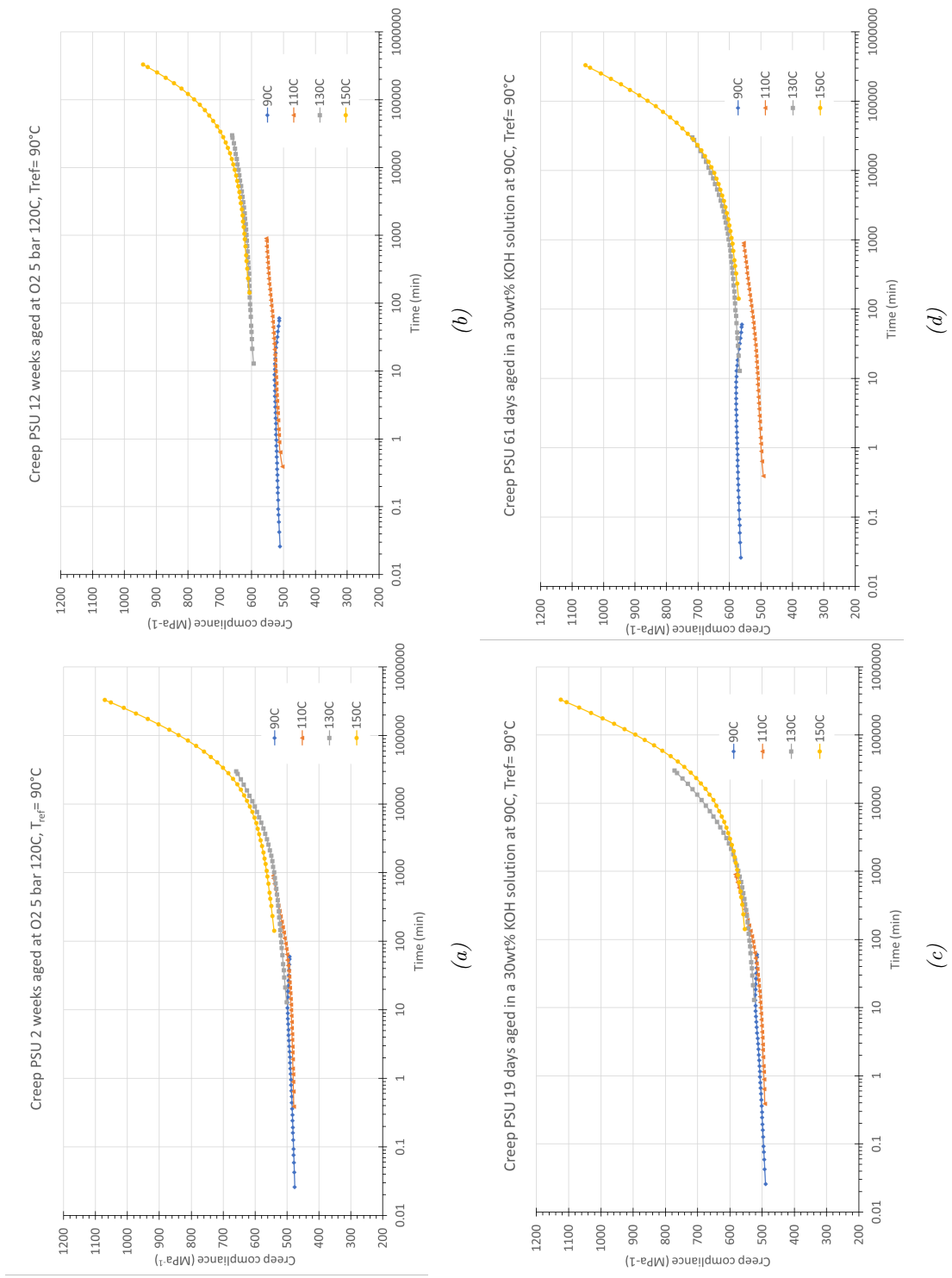


Figure 7.4: Time-temperature superposition of creep curves of aged PSU samples for (a) 2 weeks aged in oxygen at 5 bar and 120 °C, (b) 12 weeks aged in oxygen at 5 bar and 120 °C, (c) 19 days in 30wt% KOH at 90 °C and (d) 33 days in 30wt% KOH at 90 °C, using the same shift-factor curve as unaged PSU.

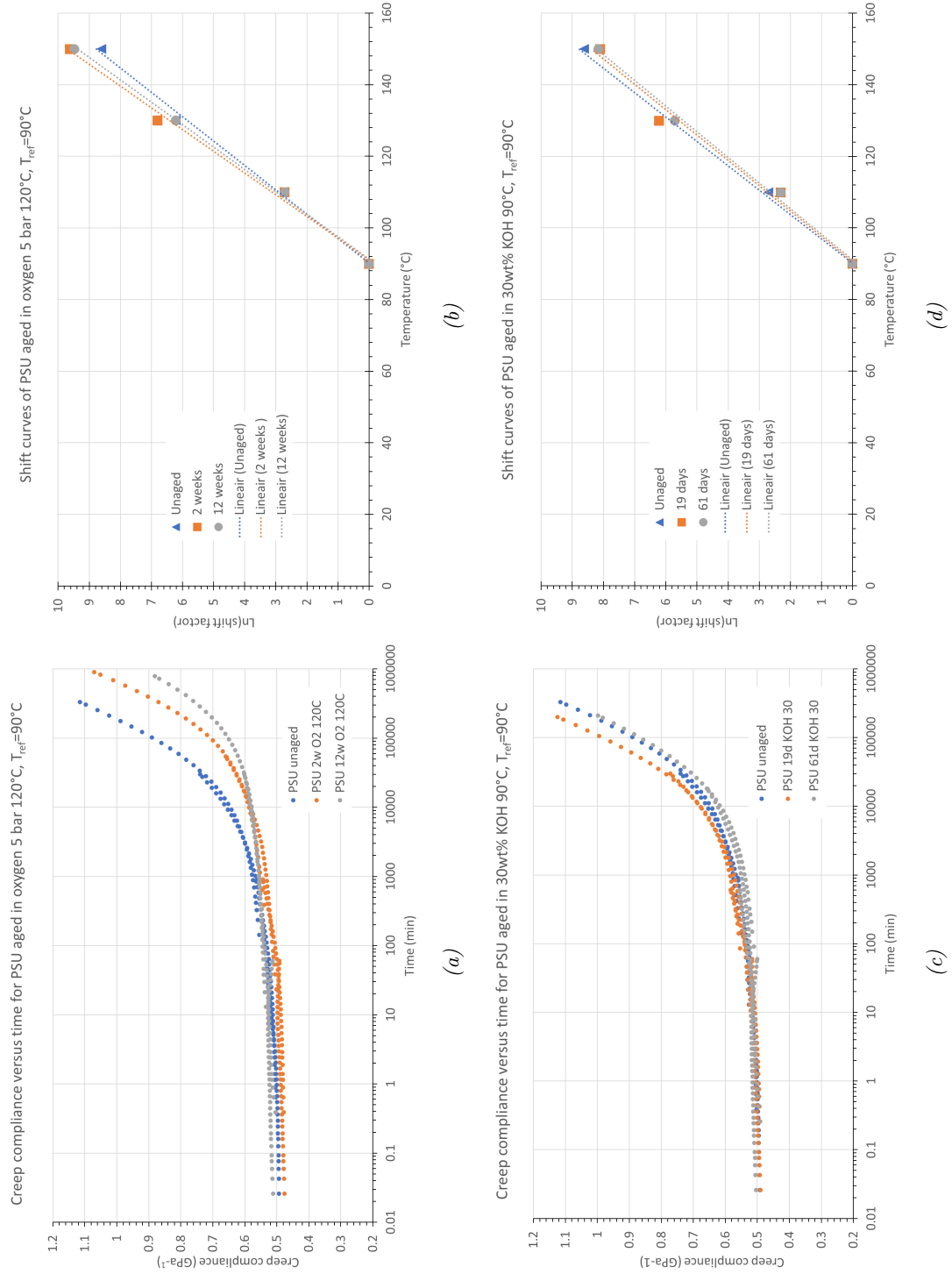
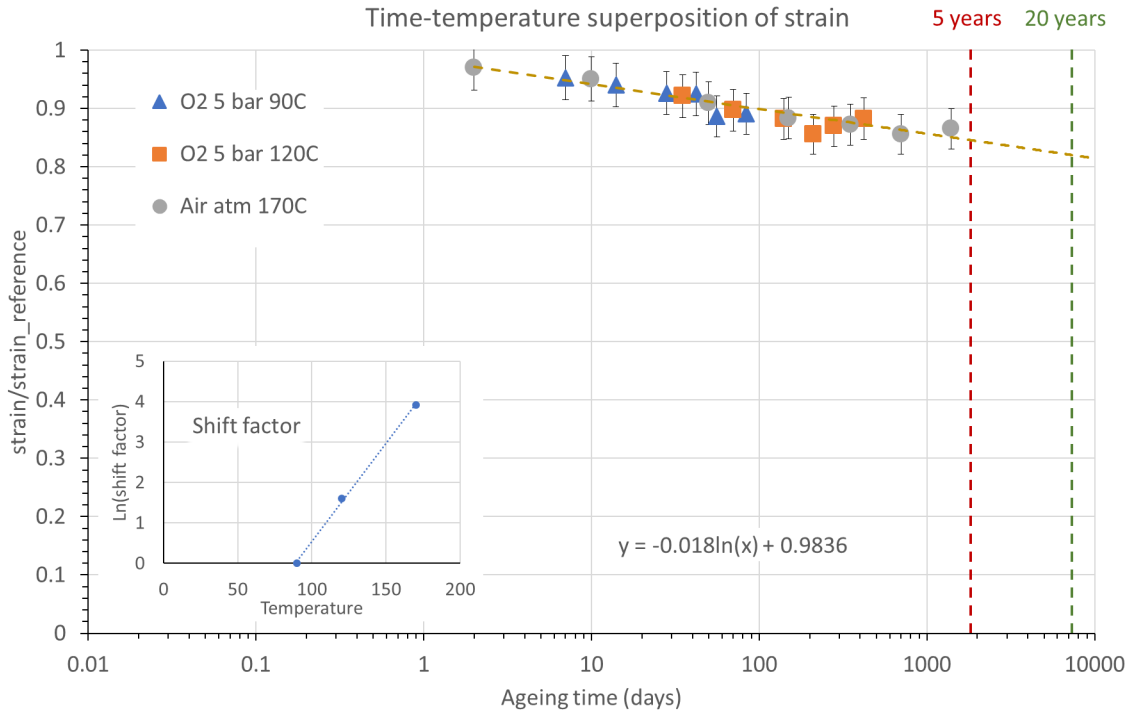


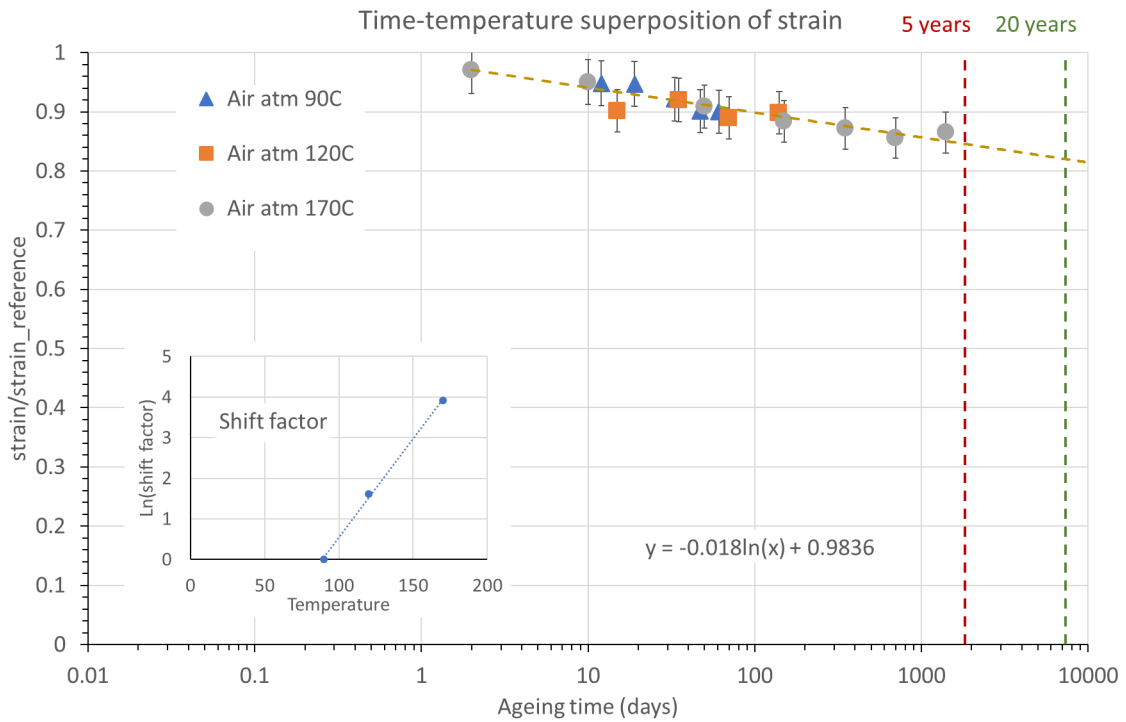
Figure 7.5: Comparison of the master curves of (a) PSU aged in oxygen, (b) the corresponding shift curves and (c) the master curves of PSU aged in KOH and (d) the corresponding shift curves.

7.2 Extrapolation of the mechanical results (PSU)

Time-temperature superposition can also be applied to other properties than the creep compliance curves. It is assumed that higher exposure temperatures accelerate the change in property which is being monitored in a uniform way, such that a constant multiplicative shift-factor (a_T) can be obtained in order to shift the data along the time axis [33]. This has been applied to the strain data from PSU aged in oxygen and air at 90, 120 and 170 °C. The results are shown in Figure 7.6. After 20 years, it is expected that the strain at break is about 80% the initial value. This can be translated to a 4.5% strain before necking starts to occur. From the creep extrapolation, 20 years at 50 bar will lead to a strain of 1.4%. This is still below the 4.5% strain before necking, meaning the polymer will probably not fail because of creep after 20 years at 90 °C.



(a)



(b)

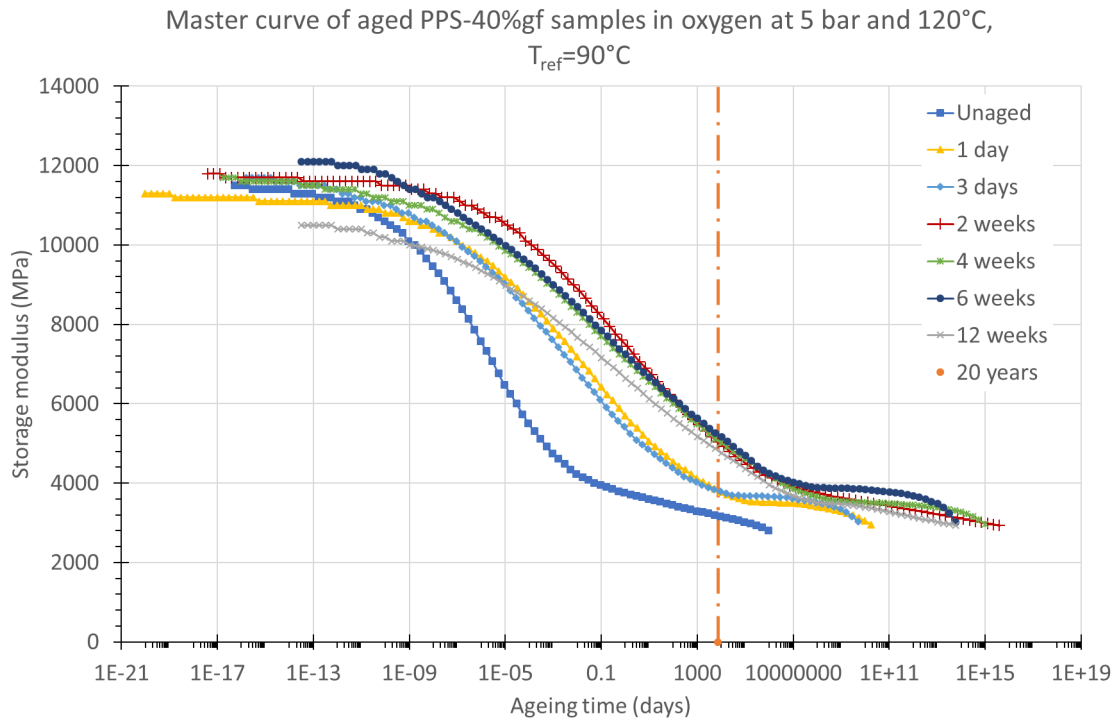
Figure 7.6: Time-temperature superposition of strain at UTS results of PSU for (a) samples aged in air and (b) samples aged in oxygen. The red and green lines represent the time after 5 and 20 years, respectively.

7.3 Predicting the storage modulus in 20 years (PPS-40%gf)

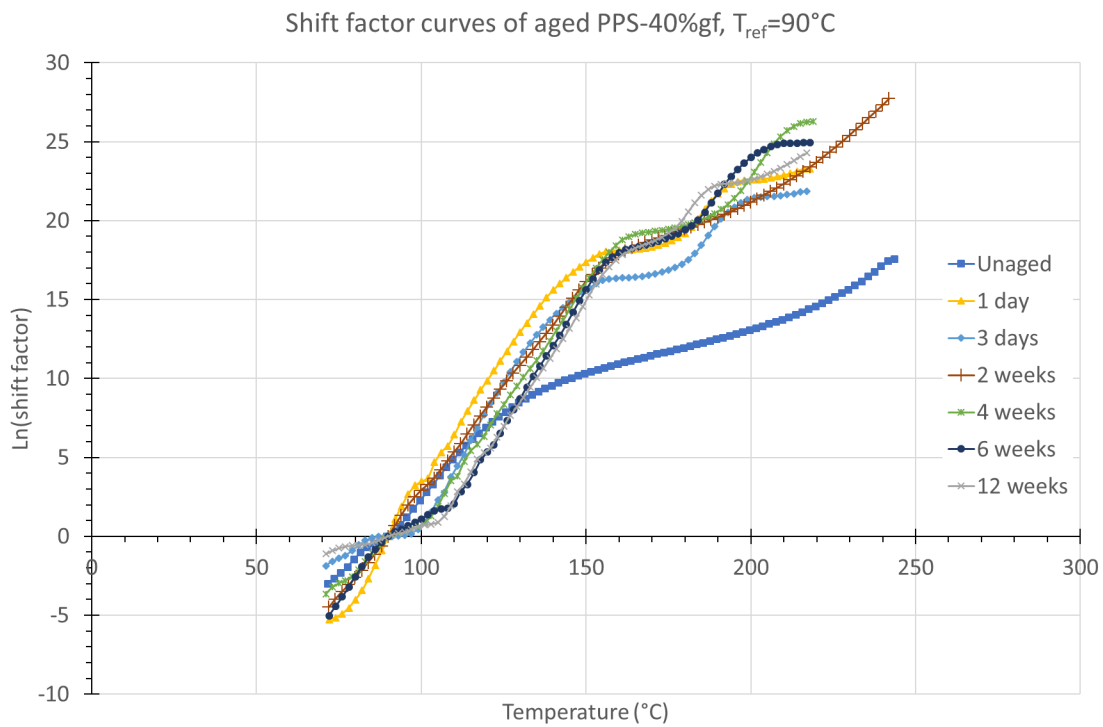
Since the DMA measurements were taken for 5 different frequencies (60, 31.6, 10, 3.2 and 1 Hz), it is possible to apply frequency-temperature superposition in order to obtain a master curve and associated shift curve by shifting along the frequency axis. This procedure has been applied to different PPS-40%gf samples, which were exposed to oxygen at 5 bar and 120 °C for different time periods, using a Matlab code written by Prof. dr. ir. K. Jansen. This resulted in Figure 7.7, in which the master curves and shift curves are compared of different ageing times. The reference temperature is 90 °C.

In order to be able to do a prediction of the storage modulus after 20 years, it is necessary to apply the frequency-temperature superposition to the samples aged at 90 °C and preferably to one or two other ageing temperatures. It is then possible to again perform time-temperature superposition of the master curves of the different ageing conditions themselves. However, this is a tedious and perhaps not very reliable method of comparing and predicting material properties. This is partly because the shift curve accompanying each master curve is different from the others. Especially the unaged shift curve is very different from the others, which explains why the unaged master curve is different from the other curves. However, since the Matlab program finds the best possible shift curve for creating each master curve, a different shift curve can have a physical basis, as explained in Section 7.1. Perhaps, due to the ageing the internal structure of the polymer changed and therefore the apparent activation energy and shift curve. It is remarkable that all the shift curves of the aged samples look much more similar.

The conclusion of looking at the master curves is that for PPS-40%gf the storage modulus is expected to drop by a factor of 3 after 20 years, which means the material is likely to lose its dimensional stability. Over time, however, ageing in the sample results in a stiffer material. This means a higher storage modulus is expected in 20 years.



(a)



(b)

Figure 7.7: (a) Master curves and (b) shift curves of PPS-40%gf aged in oxygen at 5 bar and 120 $^{\circ}\text{C}$.

7.4 Sources of errors

The uncertainty of a measurement is especially important for durability testing, since any variability in the results is magnified by an extrapolation procedure. The uncertainty arises from the measurement instruments, the procedure, the material variability and the variability in environmental exposure.

The uncertainty from the measurement instruments and material variability has been minimised in this study by repeating the measurement for multiple samples in order to gain information regarding the variability within the same group of samples and in order to determine a more accurate average property. Therefore, sets of three samples were used for tensile testing and sets of four samples were used for the weight measurements.

In this study, the ageing procedure itself has not been tested for repeatability or reproducibility, since the environmental exposure of the samples have only been conducted once.

At the end of the ageing procedure, control samples, *i.e.* samples which have not been exposed to any ageing, have been characterised using tensile testing and DMA, in order to assess if ambient conditions led to any changes in properties.

It is important to highlight that the ageing conditions applied in this study are not exactly the same as the operation conditions, due to practical reasons. To summarise, the ageing was **not** performed at 50 bar; the oxygen and KOH have not been tested together under pressure, so any synergies have not been studied; and the presence of other chemicals and metals from the electrodes and membrane have not been included.

Apart from the uncertainty arising from the ageing experiment itself, there is an amount of uncertainty regarding the usefulness of the extrapolation procedure and the predicted lifetime, when in reality there is a variation in operation conditions. For the ZEF AEC, the operation conditions vary between 0 °C to 90 °C, 30 bar to 50 bar, and the KOH concentration may change over time. It is common practice to consider the worst case conditions (*i.e.* 90 °C and 50 bar) for durability testing. Thus, even if the ageing conditions would be equivalent to this worst case scenario, the variability in operation conditions adds an extra layer of uncertainty to the lifetime prediction.

Furthermore, degradation in polymers is often a two step process: an induction period followed by rapid degradation [88]. The induction period is a time period during which very little degradation occurs. This is due to the presence of protective additives (stabilisers and antioxidants) in the material. Unfortunately, standard PPS-40%gf and PSU also contain certain stabilisers and anti-oxidants, which interfere with the reaction kinetics. Since the onset of the rapid degradation step by thermo-oxidation has not been observed in the

experiments, more uncertainty is added to the value of the extrapolation.

Finally, something to stress is that the mechanical tests performed in this thesis: tensile tests, creep-recovery tests and DMA, are all performed *parallel* to the flow direction in the mould during processing. Considerable variation has been reported in the creep of unreinforced semi-crystalline polymers cut nominally parallel and perpendicular to the direction of flow in the mould. This difference becomes even more marked with short fibre-reinforcement [14]. PPS is a fibre-reinforced semi-crystalline polymer. As shown in the SEM images of PPS-40%gf in Appendix C.2, most of the fibres seem to have aligned parallel to the flow direction of the mould. It is therefore expected that the mechanical properties are much worse perpendicular to the flow direction. This could be a difference in the order of a factor two [14].

Chapter 8

Conclusions and recommendations

8.1 Conclusions

The key conclusions from this thesis are as follows:

1. Even though the material database CES EduPack rates HDPE as a polymer with a high enough maximum operation temperature and resistant to a strong alkaline solution, HDPE is found **not** suitable for operation in the ZEF AEC conditions for a lifetime of 20 years. HDPE rapidly deteriorates in the presence of oxygen and KOH at elevated temperatures.
2. PPS-40%gf is **unsuitable** for the use as encapsulation of the ZEF AEC due to the dissolution of the glass fibres in the KOH solution. This leads to a vast reduction of mechanical and barrier properties. This conclusion can be extended to any glass-reinforced polymer to be unsuitable for operation in alkaline conditions.
3. The PPS matrix itself and PSU are found to be resistant to oxygen and KOH solution at elevated temperatures. Only subtle changes in mechanical, visco-elastic and thermal behaviour are observed, which can be assigned to the effects of physical ageing. PPS and PSU do not seem to be sensitive to irreversible degradation processes such as thermo-oxidative cross-linking and hydrolysis in the tested ageing conditions.
4. When extrapolating the experimental data it is found that if PSU is subjected to a 5 MPa pressure for 20 years, the creep compliance increases from 0.5 GPa^{-1} to 2.7 GPa^{-1} , which is equal to a strain of 1.4%. From extrapolating the mechanical results, it is found that PSU will remain 80% of its strain at UTS after 20 years in an oxygen environment at $90 \text{ }^\circ\text{C}$, which is equal to 4.5% elongation. It, therefore, seems that PSU will remain most of its integrity and internal structure after 20 years of static exposure to air at $90 \text{ }^\circ\text{C}$.

5. PPS, especially without reinforcement, is a very brittle material, which is undesirable for the encapsulation of the AEC. Therefore, it can be concluded that PSU, which has a higher toughness is a promising candidate for the long-term application in alkaline electrolysis.

8.2 Recommendations

Performing a full durability and lifetime assessment is an enormous task, and this thesis has only grasped the tip of the iceberg. Therefore, there are plenty of recommendations to be made.

8.2.1 Regarding the experiments

Data supporting physical ageing occurring in the polymer has been found and is qualitatively described in this thesis. This can be further confirmed by performing ageing experiments in a vacuum oven or in an inert gas.

Furthermore, in order to obtain a better understanding of the underlying processes, it is interesting to conduct further experiments. Ageing accompanied with dilatometry could perhaps quantify the free volume change expected for physical ageing. If done for multiple temperatures and time-periods, a quantitative analysis of the kinetics of physical ageing can be performed.

The change in visco-elastic behaviour of the polymers over time can be characterised with creep and DMA measurements. However, due to time constraints, only qualitative statements regarding the changes in visco-elastic behaviour have been made. By performing more creep-recovery measurements for the aged specimens, a more quantitative analysis can be conducted on the change of the apparent activation energy, the change in relaxation time constant (τ) and how this relates to the free volume.

8.2.2 Other polymers

As described in Chapter 3 some other polymers are found to be promising candidates according to the CES EduPack material database. These include the cheap CPVC, relatively cheap FEP, LCP, PMP, and more expensive options, such as PFA, ETFE and PEEK. These polymers can also be subjected to the ageing tests as described in this thesis, to judge their suitability for the application in the ZEF AEC.

8.2.3 Other reinforcements

Apart from using other polymers, other reinforcements can be considered. In this study, glass-reinforcement has been used, since glass fibres are the most commonly used reinforce-

ment for PPS. However, as shown in the results in Chapter 5, the dissolution of the glass fibres of the PPS-40%gf is the main source of degradation.

Since PPS is a brittle material by itself, it is recommended to use it reinforced. Fortunately, there are many other reinforcement materials which can be used. These include carbon fibres, aramid fibres, wood fibres or inorganic particulates. According to CES Edu-Pack carbon has a limited resistance to strong alkaline solutions, whereas aramid fibres have an acceptable resistance [35]. Furthermore, it is possible to reinforce PSU, in order to improve its mechanical properties.

8.2.4 Further improvement of the material

Something which has not been further considered in this thesis is the use of additives and stabilisers such as antioxidants to improve the material properties of the polymer. This improvement can be very significant and is something which should be looked into to further extend the lifetime.

8.2.5 Other degradation mechanisms

This thesis was mainly focused on the effect of thermo-oxidative degradation and chemical degradation due to the strong alkaline solution. However, since the operation conditions can not be fully simulated and material testing has been performed instead of product testing, other degradation mechanisms may have been overlooked. The two, which are believed most important are failure due to environmental stress cracking and the role of metal induced degradation.

Environmental stress cracking is stress cracking which is accelerated by contact with a fluid. Fluid, load and temperature are the three ingredients required for environmental stress cracking to occur. All three of these are present in the ZEF AEC and should therefore not be overlooked. Fluids are present in the form of the alkaline solution, the system operates at elevated temperatures, and loading is induced by the system working at 50 bar and by the day/night cyclicality of conditions. Durability against environmental stress cracking can be studied using fatigue tests under different conditions.

As mentioned before in Chapter 2, metal ions can catalyse the oxidation reaction, which can be very significant. The role of metal induced degradation has been overlooked in this thesis, but is deemed important when it is clear which metals will be present in the electrodes.

8.2.6 Testing the product/prototype

This thesis has been concerned with testing the material on its own. However, it is generally desirable to test the whole product or prototype at some point. Especially, at the operation pressure and at elevated temperatures.

Bibliography

- [1] Thermal oxidative degradation of polymers. <https://polymerdatabase.com/polymer%20chemistry/Thermal%20Degradation.html>. [Online; accessed 11-03-2019].
- [2] Abbas, H. F. and Daud, W. W. (2010). Hydrogen production by methane decomposition: a review. *International journal of hydrogen energy*, 35(3):1160–1190.
- [3] Agfa-Gevaert N.V. (2016). Zirfon perl utp 500: Separator membrane for alkaline water electrolysis.
- [4] Akay, M. (1993). Aspects of dynamic mechanical analysis in polymeric composites. *Composites science and technology*, 47(4):419–423.
- [5] Allebrod, F., Chatzichristodoulou, C., and Mogensen, M. B. (2013). Alkaline electrolysis cell at high temperature and pressure of 250°C and 42 bar. *Journal of Power Sources*, 229:22–31.
- [6] Alwis, K. and Burgoyne, C. (2006). Time-temperature superposition to determine the stress-rupture of aramid fibres. *Applied Composite Materials*, 13(4):249–264.
- [7] Ashby, M. F., Shercliff, H., and Cebon, D. (2018). *Materials: engineering, science, processing and design*. Butterworth-Heinemann.
- [8] AZO Materials (2001). E-glass fibre. [Online; accessed 11-07-2019].
- [9] Badwal, S. P., Giddey, S., and Munnings, C. (2013). Hydrogen production via solid electrolytic routes. *Wiley Interdisciplinary Reviews: Energy and Environment*, 2(5):473–487.
- [10] Barszczewska-Rybarek, I. M., Korytkowska-Wałach, A., Kurcok, M., Chladek, G., and Kasperski, J. (2017). DMA analysis of the structure of crosslinked poly (methyl methacrylate) s. *Acta of bioengineering and biomechanics*, 19(1).
- [11] Barth, R. R., Simmons, K. L., and San Marchi, C. (2013). Polymers for hydrogen infrastructure and vehicle fuel systems. *This report is available at <http://prod.sandia.gov/techlib/access-control.cgi/2013/138904.pdf>*.

- [12] Bashir, S., Yang, L., Liggat, J., and Thomason, J. (2018). Kinetics of dissolution of glass fibre in hot alkaline solution. *Journal of materials science*, 53(3):1710–1722.
- [13] Bowen, C., Davis, H., Henshaw, B., Lachance, R., LeRoy, R., and Renaud, R. (1984). Developments in advanced alkaline water electrolysis. *International journal of hydrogen energy*, 9(1-2):59–66.
- [14] Brown, R. P. and Greenwood, J. H. (2002). *Practical guide to the assessment of the useful life of plastics*. Smithers Rapra Publishing.
- [15] Cai, W. and Hu, G. (2015). Oxidation degradation of polyphenylene sulfide needle felt at different sulfuric acid dew point temperatures. *High Performance Polymers*, 27(1):94–99.
- [16] Cam, D., Hyon, S.-h., and Ikada, Y. (1995). Degradation of high molecular weight poly (L-lactide) in alkaline medium. *Biomaterials*, 16(11):833–843.
- [17] Carnevale, P. (2014). *Fibre-matrix interfaces in thermoplastic composites: A meso-level approach*. PhD thesis, Delft University of Technology.
- [18] Celanese (2016). Fortron PPS: Short term properties guide.
- [19] Celina, M. C. (2013). Review of polymer oxidation and its relationship with materials performance and lifetime prediction. *Polymer Degradation and Stability*, 98(12):2419–2429.
- [20] Chirinos-Padrón, A. J., Hernández, P. H., Chávez, E., Allen, N. S., Vasiliou, C., and DePoortere, M. (1987). Influences of unsaturation and metal impurities on the oxidative degradation of high density polyethylene. *European polymer journal*, 23(12):935–940.
- [21] Chong, K., Lai, S., Thiam, H., Teoh, H., and Heng, S. (2016). Recent progress of oxygen/nitrogen separation using membrane technology. *J. Eng. Sci. Technol*, 11:1016–1030.
- [22] Coates, J. (2006). Interpretation of infrared spectra, a practical approach. *Encyclopedia of analytical chemistry: applications, theory and instrumentation*.
- [23] D 3045-18, A. (2018). Standard practice for heat aging of plastics without load. Technical report, ASTM international.
- [24] D 794-93, A. (1993). Standard practice for determining permanent effect of heat on plastics. Technical report, ASTM international.
- [25] Das, P. and Tiwari, P. (2017). Thermal degradation kinetics of plastics and model selection. *Thermochimica Acta*, 654:191–202.

- [26] De Vreugd, J. (2011). *The effect of aging on molding compound properties*. PhD thesis, Delft University of Technology.
- [27] Dobkowski, Z. (2005). Lifetime prediction for polymer materials using OIT measurements by the DSC method. *Polimery*, 50(3):213–215.
- [28] Faulkner, D. L. (1982). Effects of high oxygen pressure and temperature on the aging of polypropylene. *Polymer Engineering & Science*, 22(8):466–471.
- [29] Fischer, E., Sterzel, H. J., and Wegner, G. (1973). Investigation of the structure of solution grown crystals of lactide copolymers by means of chemical reactions. *Kolloid-Zeitschrift und Zeitschrift für Polymere*, 251(11):980–990.
- [30] Ganley, J. C. (2009). High temperature and pressure alkaline electrolysis. *International journal of hydrogen energy*, 34(9):3604–3611.
- [31] Geiger, M. (2017). Introduction to Dynamic Mechanical Testing for Rubbers and Elastomers. http://www.tainstruments.com/wp-content/uploads/Introduction-to-Dynamic-Mechanical-Analysis_Akron-Workshop.pdf. [Online; accessed 29-10-2019].
- [32] Gesner, B. and Kelleher, P. (1968). Thermal and photo-oxidation of polysulfone. *Journal of Applied Polymer Science*, 12(5):1199–1208.
- [33] Gillen, K. T. and Clough, R. L. (1989). Time-temperature-dose rate superposition: a methodology for extrapolating accelerated radiation aging data to low dose rate conditions. *Polymer Degradation and Stability*, 24(2):137–168.
- [34] Grabmayer, K., Wallner, G. M., Beißmann, S., Braun, U., Steffen, R., Nitsche, D., Röder, B., Buchberger, W., and Lang, R. W. (2014). Accelerated aging of polyethylene materials at high oxygen pressure characterized by photoluminescence spectroscopy and established aging characterization methods. *Polymer degradation and stability*, 109:40–49.
- [35] Granta Design (2018). CES materials selector (version 18.1.1) [Software].
- [36] Hamid, S. H. (2000). *Handbook of polymer degradation*. CRC Press.
- [37] Hecen, W., Dehou, J., and Ying, L. (2011). Life problem analysis on pps filter application of bag dedusters in coal-fired power plants.
- [38] Hinsken, H., Moss, S., Pauquet, J.-R., and Zweifel, H. (1991). Degradation of polyolefins during melt processing. *Polymer degradation and stability*, 34(1-3):279–293.

- [39] Hsuan, Y. and Li, M. (2005). Temperature and pressure effects on the oxidation of high-density polyethylene geogrids. *Geotextiles and Geomembranes*, 23(1):55–75.
- [40] Jansen, K. (2007). Thermomechanical modeling and characterization of polymers. *course book, TU Delft*.
- [41] Ju, W., Heinz, M. V., Pusterla, L., Hofer, M., Fumey, B., Castiglioni, R., Pagani, M., Battaglia, C., and Vogt, U. F. (2018). Lab-scale alkaline water electrolyzer for bridging material fundamentals with realistic operation. *ACS Sustainable Chemistry & Engineering*, 6(4):4829–4837.
- [42] Kamalova, D. and Shaimukhametova, E. (2011). Study of secondary relaxation transitions in polysulfone and polycarbonate by a method of conformational probes. *Journal of Applied Spectroscopy*, 78(4):506–511.
- [43] Kimmish, D. J. (2011). *Practical guide to high performance engineering plastics*. Smithers Rapra.
- [44] Kreuter, W. and Hofmann, H. (1998). Electrolysis: the important energy transformer in a world of sustainable energy. *International Journal of Hydrogen Energy*, 23(8):661–666.
- [45] Lampman, S. et al. (2003). *Characterization and failure analysis of plastics*. Asm International.
- [46] Lee, S., Kim, D.-H., Park, J.-H., Park, M., Joh, H.-I., and Ku, B.-C. (2013). Effect of curing poly (p-phenylene sulfide) on thermal properties and crystalline morphologies. *Advances in Chemical Engineering and Science*, 3(02):145.
- [47] Li, J. and Stoliarov, S. I. (2014). Measurement of kinetics and thermodynamics of the thermal degradation for charring polymers. *Polymer degradation and stability*, 106:2–15.
- [48] Liu, Y., Bhandari, B., and Zhou, W. (2007). Study of glass transition and enthalpy relaxation of mixtures of amorphous sucrose and amorphous tapioca starch syrup solid by differential scanning calorimetry (DSC). *Journal of food engineering*, 81(3):599–610.
- [49] Lukichev, A. (2019). Physical meaning of the stretched exponential Kohlrausch function. *Physics Letters A*, 383(24):2983–2987.
- [50] Marini, S., Salvi, P., Nelli, P., Pesenti, R., Villa, M., Berrettoni, M., Zangari, G., and Kiros, Y. (2012). Advanced alkaline water electrolysis. *Electrochimica Acta*, 82:384–391.
- [51] McKeen, L. W. (2016). *Permeability properties of plastics and elastomers*. William Andrew.

- [52] Menard, K. P. (1999). *Dynamic mechanical analysis: A practical introduction*. CRC Press LLC.
- [53] Meng, F., Geng, J., Besser, M., Kramer, M., and Ott, R. (2014). Glass transition in a marginal glass-forming alloy studied by dynamic mechanical analysis. *Journal of Applied Physics*, 116(22):223505.
- [54] Mueller, W. and Jakob, I. (2003). Oxidative resistance of high-density polyethylene geomembranes. *Polymer Degradation and Stability*, 79(1):161–172.
- [55] Nayak, L., Pradhan, R. R., Khastgir, D., and Chaki, T. K. (2015). Thermally stable electromagnetic interference shielding material from polysulfone nanocomposites: Comparison on carbon nanotube and nanofiber reinforcement. *Polymer Composites*, 36(3):566–575.
- [56] Okada, F. and Naya, K. (2012). Electrolysis for ozone water production. In *Electrolysis*. IntechOpen.
- [57] Oluwoye, I., Altarawneh, M., Gore, J., and Dlugogorski, B. Z. (2015). Oxidation of crystalline polyethylene. *Combustion and Flame*, 162(10):3681–3690.
- [58] Osswald, T. A. and Menges, G. (2012). *Materials science of polymers for engineers*. Carl Hanser Verlag GmbH Co KG.
- [59] Park, J. W., Oh, S. C., Lee, H. P., Kim, H. T., and Yoo, K. O. (2000). A kinetic analysis of thermal degradation of polymers using a dynamic method. *Polymer degradation and Stability*, 67(3):535–540.
- [60] Pascuzzi, S., Blanco, I., Anifantis, A. S., and Scarascia-Mugnozza, G. (2016). Hazards assessment and technical actions due to the production of pressured hydrogen within a pilot photovoltaic-electrolyser-fuel cell power system for agricultural equipment. *Journal of Agricultural Engineering*, 47(2):88–93.
- [61] Peterson, J. D., Vyazovkin, S., and Wight, C. A. (2001). Kinetics of the thermal and thermo-oxidative degradation of polystyrene, polyethylene and polypropylene. *Macromolecular Chemistry and Physics*, 202(6):775–784.
- [62] Quintana, A. and Celina, M. C. (2018). Overview of dlo modeling and approaches to predict heterogeneous oxidative polymer degradation. *Polymer degradation and stability*, 149:173–191.
- [63] Reich, L. and Stivala, S. (1971). *Elements of Polymer Degradation*. McGraw-Hill.

- [64] Reshetnikov, S. M. and Reshetnikov, I. S. (1999). Oxidation kinetic of volatile polymer degradation products. *Polymer degradation and stability*, 64(3):379–385.
- [65] Richaud, E., Farcas, F., Bartolomé, P., Fayolle, B., Audouin, L., and Verdu, J. (2006). Effect of oxygen pressure on the oxidation kinetics of unstabilised polypropylene. *Polymer Degradation and Stability*, 91(2):398–405.
- [66] Richaud, E., Farcas, F., Divet, L., and Benneton, J. P. (2008). Accelerated ageing of polypropylene geotextiles, the effect of temperature, oxygen pressure and aqueous media on fibers—methodological aspects. *Geotextiles and Geomembranes*, 26(1):71–81.
- [67] Romanzini, D., Lavoratti, A., Ornaghi Jr, H. L., Amico, S. C., and Zattera, A. J. (2013). Influence of fiber content on the mechanical and dynamic mechanical properties of glass/ramie polymer composites. *Materials & Design*, 47:9–15.
- [68] Rubinstein, M., Colby, R. H., et al. (2003). *Polymer physics*, volume 23. Oxford university press New York.
- [69] Saeidi, S., Amin, N. A. S., and Rahimpour, M. R. (2014). Hydrogenation of CO₂ to value-added products — a review and potential future developments. *Journal of CO₂ utilization*, 5:66–81.
- [70] Sánchez-Jiménez, P. E., Pérez-Maqueda, L. A., Perejón, A., and Criado, J. (2009). Combined kinetic analysis of thermal degradation of polymeric materials under any thermal pathway. *Polymer degradation and stability*, 94(11):2079–2085.
- [71] Sánchez-Jiménez, P. E., Pérez-Maqueda, L. A., Perejón, A., and Criado, J. M. (2010). A new model for the kinetic analysis of thermal degradation of polymers driven by random scission. *Polymer Degradation and Stability*, 95(5):733–739.
- [72] Santos, D. M., Sequeira, C. A., and Figueiredo, J. L. (2013). Hydrogen production by alkaline water electrolysis. *Química Nova*, 36(8):1176–1193.
- [73] Smolinka, T. (2014). Water electrolysis: status and potential for development. *Fraunhofer Institute for Solar Energy Systems ISE, Freiburg*.
- [74] Smolinka, T., Günther, M., and Garcke, J. (2011). Now-studie “stand und entwicklungspotenzial der wasserelektrolyse zur herstellung von wasserstoff aus regenerativen energien” kurzfassung des abschlussberichts. *Fraunhofer ISE, FCBAT*.
- [75] Solvay (2017). Ryton PPS processing guide. http://catalogservice.solvay.com/downloadDocument?fileId=MDkwMTY20WM4MDE4ZmRjNQ==&fileName=Ryton-PPS-Processing-Guide_EN.pdf&base=FAST. [Online; accessed 12-10-2019].

- [76] Soustelle, M. (2013). *An introduction to chemical kinetics*. John Wiley & Sons.
- [77] Steele, B. C. and Heinzl, A. (2011). Materials for fuel-cell technologies. In *Materials For Sustainable Energy: A Collection of Peer-Reviewed Research and Review Articles from Nature Publishing Group*, pages 224–231. World Scientific.
- [78] Strobl, G. R. and Strobl, G. R. (1997). *The physics of polymers*, volume 2. Springer.
- [79] Susa, A., Bijleveld, J., Hernandez Santana, M., and Garcia, S. J. (2017). Understanding the effect of the dianhydride structure on the properties of semiaromatic polyimides containing a biobased fatty diamine. *ACS sustainable chemistry & engineering*, 6(1):668–678.
- [80] Tanaka, E. and van Eijden, T. (2003). Biomechanical behavior of the temporomandibular joint disc. *Critical Reviews in Oral Biology & Medicine*, 14(2):138–150.
- [81] Ticona (1999). Designing with Fortron Polyphenylene Sulfide. <http://www.hipolymers.com.ar/pdfs/fortron/diseno/Designing%20with%20Fortron%20PPS.PDF>. [Online; accessed 12-07-2019].
- [82] Tsuji, H. and Ikada, Y. (1998). Properties and morphology of poly (l-lactide). ii. hydrolysis in alkaline solution. *Journal of Polymer Science Part A: Polymer Chemistry*, 36(1):59–66.
- [83] Verdu, J. (2012). *Oxidative ageing of polymers*. John Wiley & Sons.
- [84] Vink, P. and Fontijn, H. (2000). Testing the resistance to oxidation of polypropylene geotextiles at enhanced oxygen pressures. *Geotextiles and geomembranes*, 18(5):333–343.
- [85] Wang, H. C., Jiang, D. H., and Liu, Y. (2011). Life problem analysis on pps filter application of bag dedusters in coal-fired power plants. In *Application of Chemical Engineering*, volume 236 of *Advanced Materials Research*, pages 2464–2470. Trans Tech Publications Ltd.
- [86] Wejchan-Judek, M. and Perkowska, B. (1992). Curing of poly (p-phenylene sulfide). *Polymer degradation and stability*, 38(3):261–264.
- [87] Williams, M. L., Landel, R. F., and Ferry, J. D. (1955). The temperature dependence of relaxation mechanisms in amorphous polymers and other glass-forming liquids. *Journal of the American Chemical society*, 77(14):3701–3707.
- [88] Wright, D. (2001). *Failure of plastics and rubber products: causes, effects and case studies involving degradation*. Smithers Rapra Publishing.

- [89] Xing, J., Xu, Z., and Deng, B. (2018). Enhanced oxidation resistance of polyphenylene sulfide composites based on montmorillonite modified by benzimidazolium salt. *Polymers*, 10(1):83.
- [90] Yamashita, T., Kudo, T., Horie, K., Maeda, S., and Nagata, K. (1993a). Degradation of sulfur-containing aromatic polymers (II): Change in fluorescence spectra of polyphenylenesulfide (PPS) during annealing. *Polymer degradation and stability*, 39(3):279–284.
- [91] Yamashita, T., Tomitaka, H., Kudo, T., Horie, K., and Mita, I. (1993b). Degradation of sulfur-containing aromatic polymers: Photodegradation of polyethersulfone and polysulfone. *Polymer degradation and stability*, 39(1):47–54.
- [92] Zanzinger, H. and Hausmann, S. (2015). Determination of the Thermal Oxidation Resistance of HDPE Geomembranes and PP Geotextiles by using High Pressure Autoclave Tests (HPAT). Conference Geosynthetics 2015.

Appendices

Appendix A

Datasheets PPS-40%gf and PSU

The dog-bone shaped samples have been produced by Promolding B.V. For the PPS samples Fortron 1140L4 is used, which is a 40% glass-reinforced grade. This is the most commonly used form of PPS. PPS is almost always used with reinforcements, in order to overcome its inherent brittleness.

For PSU the opaque black Udel P-1700 BK 937 is used, which contains <1% carbon black. The choice of black PSU over the pure, transparent PSU, is purely based on availability. The presence of carbon black is not expected to have an effect on the mechanical, chemical, and thermal properties of the polymer.

FORTRON 1140L4 | PPS | Glass Reinforced
Physical properties

	Value Unit	Test Standard
Density	1650 kg/m ³	ISO 1183
Mold shrinkage - parallel	0.2 - 0.6 %	ISO 294-4
Mold shrinkage - normal	0.4 - 0.6 %	ISO 294-4
Water absorption (23°C-sat)	0.02 %	ISO 62

Mechanical properties

	Value Unit	Test Standard
Tensile modulus (1mm/min)	14700 MPa	ISO 527-2/1A
Tensile stress at break (5mm/min)	195 MPa	ISO 527-2/1A
Tensile strain at break (5mm/min)	1.9 %	ISO 527-2/1A
Flexural modulus (23°C)	14500 MPa	ISO 178
Flexural stress @ break	285 MPa	ISO 178
Charpy impact strength @ 23°C	53 kJ/m ²	ISO 179/1eU
Charpy impact strength @ -30°C	53 kJ/m ²	ISO 179/1eU
Charpy notched impact strength @ 23°C	10 kJ/m ²	ISO 179/1eA
Charpy notched impact strength @ -30°C	10 kJ/m ²	ISO 179/1eA
Unnotched impact str (Izod) @ 23°C	34 kJ/m ²	ISO 180/1U
Notched impact strength (Izod) @ 23°C	10 kJ/m ²	ISO 180/1A
Notched impact strength (Izod) @ -30°C	10 kJ/m ²	ISO 180/1A
Rockwell hardness	100 M-Scale	ISO 2039-2

Thermal properties

	Value Unit	Test Standard
Melting temperature (10°C/min)	280 °C	ISO 11357-1,-2,-3
Glass transition temperature (10°C/min)	90 °C	ISO 11357-1,-2,-3
DTUL @ 1.8 MPa	270 °C	ISO 75-1/2
DTUL @ 8.0 MPa	215 °C	ISO 75-1/2
Coeff.of linear therm. expansion (parallel)	0.26 E-4/°C	ISO 11359-2
Coeff.of linear therm. expansion (normal)	0.62 E-4/°C	ISO 11359-2
Limiting oxygen index (LOI)	47 %	ISO 4589
Flammability @1.6mm nom. thickn. thickness tested (1.6)	V-0 class 1.5 mm	UL94 UL94
Flammability at thickness h thickness tested (h)	V-0 class 0.38 mm	UL94 UL94
Flammability 5V at thickness h thickness tested (5V)	5VA class 3 mm	UL94 UL94

Electrical properties

	Value Unit	Test Standard
Relative permittivity - 10kHz	4 -	IEC 60250
Relative permittivity - 1 MHz	4.6 -	IEC 60250
Dissipation factor - 10kHz	2 E-4	IEC 60250
Dissipation factor - 1 MHz	62 E-4	IEC 60250
Volume resistivity	>1E13 Ohm*m	IEC 60093
Surface resistivity	>1E15 Ohm	IEC 60093
Electric strength	28 kV/mm	IEC 60243-1
Comparative tracking index CTI	125 -	IEC 60112

Test specimen production

	Value Unit	Test Standard
Injection molding melt temperature	310 - 340 °C	ISO 294
Injection molding mold temperature	135 - 160 °C	ISO 294

Rheological Calculation properties

	Value Unit	Test Standard
Specific heat capacity of melt	1500 J/(kg K)	Internal

Disclaimer

NOTICE TO USERS: Values shown are based on testing of laboratory test specimens and represent data that fall within the standard range of properties for natural material. These values alone do not represent a sufficient basis for any part design and are not intended for use in establishing maximum, minimum, or ranges of values for specification purposes. Colorants or other additives may cause significant variations in data values.

Properties of molded parts can be influenced by a wide variety of factors including, but not limited to, material selection, additives, part design, processing conditions and environmental exposure. Any determination of the suitability of a particular material and part design for any use contemplated by the users and the manner of such use is the sole responsibility of the users, who must assure themselves that the material as subsequently processed meets the needs of their particular product or use.

To the best of our knowledge, the information contained in this publication is accurate; however, we do not assume any liability whatsoever for the accuracy and completeness of such information. The information contained in this publication should not be construed as a promise or guarantee of specific properties of our products. It is the sole responsibility of the users to investigate whether any existing patents are infringed by the use of the materials mentioned in this publication.

Moreover, there is a need to reduce human exposure to many materials to the lowest practical limits in view of possible adverse effects. To the extent that any hazards may have been mentioned in this publication, we neither suggest nor guarantee that such hazards are the only ones that exist. We recommend that persons intending to rely on any recommendation or to use any equipment, processing technique or material mentioned in this publication should satisfy themselves that they can meet all applicable safety and health standards.

We strongly recommend that users seek and adhere to the manufacturer's current instructions for handling each material they use, and entrust the handling of such material to adequately trained personnel only. Please call the telephone numbers listed (+49 (0) 69 30516299 for Europe and +1 908 598-4169 for the Americas) for additional technical information. Call Customer Services for the appropriate Materials Safety Data Sheets (MSDS) before attempting to process our products.

The products mentioned herein are not intended for use in medical or dental implants.

© Copyright 2005, Ticona LLC, all rights reserved. (Pub. 12-19-2005)

Udel® P-1700

Polysulfone

Solvay Specialty Polymers



Prospector

Product Description

Udel P-1700 polysulfone (PSU) is a tough, rigid, high-strength thermoplastics suitable for continuous use up to 300°F (149°C). It is resistant to oxidation and hydrolysis and withstand prolonged exposure to high temperatures and repeated sterilization. Udel P-1700 polysulfone is highly resistant to mineral acids, alkali and salt solutions. Resistance to detergents and hydrocarbon oils is good, but the resin may be attacked by polar solvents such as ketones, chlorinated hydrocarbons and aromatic hydrocarbons.

These resins are also highly resistant to degradation by gamma or electron beam radiation. Electrical properties of Udel P-1700 polysulfones are stable over a wide temperature range and after immersion in water or exposure to high humidity.

The resins comply with FAR 21 CFR 177.1655 and may be used in articles intended for repeated use in contact with foods. Additionally, they are approved by the NSF, by the Department of Agriculture for contact with meat and poultry and by the 3-A Sanitary Standards of the Dairy Association.

- Transparent: Udel P-1700 CL 2611
- Transparent: Udel P-1700 NT 06
- Transparent: Udel P-1700 NT 11
- Opaque Black : Udel P-1700 BK 937
- Opaque White: Udel P-1700 WH 6417

General

Material Status	• Commercial: Active		
Availability	• Asia Pacific • Europe	• North America • South America	
Features	• Acid Resistant • Alcohol Resistant • Alkali Resistant • Autoclave Sterilizable • Biocompatible • Detergent Resistant • E-beam Sterilizable • Ethylene Oxide Sterilizable	• Food Contact Acceptable • Good Chemical Resistance • Good Dimensional Stability • Good Sterilizability • Good Surface Finish • Good Toughness • Heat Sterilizable • High Heat Resistance	• Hydrocarbon Resistant • Hydrolytically Stable • Radiation (Gamma) Resistant • Radiation Sterilizable • Radiotranslucent • Steam Resistant • Steam Sterilizable
Uses	• Appliance Components • Appliances • Automotive Electronics • Dental Applications • Electrical Parts • Electrical/Electronic Applications	• Food Service Applications • Hospital Goods • Industrial Parts • Medical Appliances • Medical/Healthcare Applications • Microwave Cookware	• Piping • Plumbing Parts • Surgical Instruments • Valves/Valve Parts
Agency Ratings	• FDA 21 CFR 177.1655 • ISO 10993	• ISO 10993-Part 1 • NSF 51 ¹	• NSF 61 ²
RoHS Compliance	• RoHS Compliant		
Appearance	• Colors Available	• Transparent - Slight Yellow	
Forms	• Pellets		
Processing Method	• Extrusion • Extrusion Blow Molding • Film Extrusion • Injection Blow Molding	• Injection Molding • Machining • Pipe Extrusion • Profile Extrusion	• Sheet Extrusion • Thermoforming

Physical	Nominal Value Unit	Test Method
Specific Gravity	1.24 g/cm ³	ASTM D792
Melt Mass-Flow Rate (MFR) (343°C/2.06 kg)	6.5 g/10 min	ASTM D1238
Molding Shrinkage - Flow	0.70 %	ASTM D955
Water Absorption (24 hr)	0.30 %	ASTM D570

Mechanical	Nominal Value Unit	Test Method
Tensile Modulus	2480 MPa	ASTM D638
Tensile Strength	70.3 MPa	ASTM D638
Tensile Elongation (Break)	50 to 100 %	ASTM D638
Flexural Modulus	2690 MPa	ASTM D790
Flexural Strength	106 MPa	ASTM D790

Impact	Nominal Value Unit	Test Method
Notched Izod Impact	69 J/m	ASTM D256
Tensile Impact Strength	420 kJ/m ²	ASTM D1822

Revision History

Document Created: Tuesday, August 30, 2011
 Added to Prospector: March, 1997
 Last Updated: 12/15/2010

Udel® P-1700
Polysulfone
Solvay Specialty Polymers

Tuesday, August 30, 2011

Thermal	Nominal Value Unit	Test Method
Deflection Temperature Under Load 1.8 MPa, Unannealed	174 °C	ASTM D648
CLTE - Flow	0.000056 cm/cm/°C	ASTM D696
Electrical	Nominal Value Unit	Test Method
Volume Resistivity	3.0E+16 ohm·cm	ASTM D257
Dielectric Strength	17 kV/mm	ASTM D149
Dielectric Constant		ASTM D150
60 Hz	3.03	
1 kHz	3.04	
1 MHz	3.02	
Dissipation Factor		ASTM D150
60 Hz	0.00070	
1 kHz	0.0010	
1 MHz	0.0060	
Injection	Nominal Value Unit	
Drying Temperature	135 to 163 °C	
Drying Time	3.5 hr	
Suggested Shot Size	50 to 75 %	
Processing (Melt) Temp	329 to 385 °C	
Mold Temperature	121 to 163 °C	

Notes

- ¹ Maximum Temperature of Use: 149°C (300°F)
² Tested at 82 °C (180 °F) (Commercial Hot)
³ Typical properties: these are not to be construed as specifications.

Revision History

Document Created: Tuesday, August 30, 2011
 Added to Prospector: March, 1997
 Last Updated: 12/15/2010

Appendix B

Safety assessment: ageing in pure oxygen and KOH

Working with pure oxygen, whilst under pressure and heated up to temperatures up to 120 °C brings certain hazards for which precautions have to be made. Pure oxygen leads to the risk of fire hazard due to combustion, which is caused by particle impact, heat of compression, or external heat. This is a very serious hazard. This appendix is concerned with the safety assessment which has been carried out prior to designing and building the ageing set up. In this safety assessment calculations have been carried out in order to determine the amount of pressure release after potential combustion of the samples and whether the Swagelok construction is able to hold this sudden increase in pressure. To further guarantee the safety of the setup, the set up is placed in a fume-hood with a polycarbonate glass window.

In order to perform an oxygen compatibility assessment process, the following components have been considered:

- determining the worst case scenario,
- assessing the setup,
- and evaluating the ignition mechanisms.

B.1 Determining the worst case scenario

The energy release and the pressure change after a potential combustion reaction has been calculated on the next page. In these simple calculations the volume of the container, the oxygen pressure and the temperature are the variable parameters. The energy release and pressure have been calculated with respect to the volume of the stainless steel container. Several assumptions have been made for this calculation.

- The calculations have been performed for a case where the fuel and oxygen are very well mixed and deflagration, instead of detonation occurs, which produces subsonic shock waves and a pressure build-up. Since the fuel is a solid, *i.e.* the PPS/PSU samples or the stainless steel container, the oxygen and fuel are not very well mixed. This means detonation will most likely not occur, which could have been critical for the system.
- The heat capacity has been taken for the case at 300 K, however at 6000 K the heat capacity is almost double. This assumption increases the safety margin of the calculation.
- In the calculation it is assumed that the plastic samples do not take any volume in the tube. In reality a significant part of the volume is sample and not oxygen.
- Another assumption is that the oxygen reacts with hydrogen. A reaction with carbon would release less energy and create less molecules, and therefore a smaller pressure change.

Safety Calculations

Constants	COMMENTS
Molar mass O2 Molar Volume O2 Molar mass H2 Molar mass H2O HHV H2 Universal Gas constant Molar increase from reaction Heat Capacity of Steam	Assuming Ideal Gas Law: $V/n = RT/P$ -> the molar volume depends on the temperature Source: https://www.engineeringtoolbox.com/fuels-higher-calorific-values-d_169.html Source: https://www.engineeringtoolbox.com/water-vapor-d_979.html Worse case scenario: at 300K the heat capacity is 1.864 J/kg. However, at higher temperatures the heat capacity becomes higher up to 3.35 J/kg at 6000 K
Variables Container Volumer Pressure in container Container Temperature	Volume from needle valve to needle valve 0.02 L 5 bar 393.15 K
Calculation for the system Equivalent volume of O2 Max mol O2 present Weight of O2 present Max mol H2 in reaction Weight H2 reacted Max mol H2O (Steam) produced Weight H2O (Steam) produced Energy Released Temperature increase of steam Calculation of Pressure increase: Assuming ideal gas law $PV = nRT$	container volume*pressure volume/molar volume mol*molar mass Assuming all oxygen will react with hydrogen: $2H_2 + O_2 \rightarrow 2H_2O$ mol*molar mass mol*molar mass mol H2 reacted* higher heating value of H2 Assuming steam absorbs all energy released, energy released/steam mass/heat capacity of steam
P1 V1 T1 n1 n2 V2 T2 P2 Pressure in container after reaction	0.1 normal L 3.06E-03 mol O2 9.79E-02 g 6.12E-03 mol H2 1.23E-02 g 6.12E-03 mol H2O 1.10E-01 g 1747.82 J 8506.60 K
P1 V1 T1 n1 n2 V2 T2 P2 Pressure in container after reaction	https://www.swagelok.com/downloads/webcatalogs/EN/MS-01-107.PDF https://www.swagelok.com/downloads/webcatalogs/en/MS-01-181.pdf https://northern.swagelok.com/when-will-it-burst Burst pressure check valves: 12 000 psig (826 bar) at 20°C. Burst pressure tube: Estimated burst pressure is 4 x working pressure. So, it depends on which tube you take, but typically 10 000 psig = 690 bar.
Calculation heating of container itself Diameter tube Thickness tube Length of tube Volume of steel Volume in cc Weight tube Weight in grams Cp Temperature increase	To calculate whether burst pressure will decrease because of increasing temperature of the steel tube. Temperature increase is too small to have a significant effect on the burst pressure of the tube. Source: https://www.engineeringtoolbox.com/specific-heat-capacity-d_391.html

In Table B.1 an overview of the energy release for different container volumes and oxygen pressures and for two temperatures (100 and 150 °C) is given. As shown, the pressure after the reaction is independent of the container volume and decreases with increasing system temperature. The energy release in joules depends on the volume of the container and also decreases with increasing system temperature.

Table B.1: Energy release and pressure after deflagration reaction.

Container Volume	Pressure (bar)	Energy Released (J)	Pressure after reaction (bar)
For T = 100 °C			
1cc	1	18.4	47.59
	5	92.08	237.97
	10	184.15	475.93
	15	276.23	713.9
3cc	1	55.25	47.59
	5	276.23	237.97
	10	552.45	475.93
	15	828.68	713.9
For T = 150 °C			
1cc	1	16.24	42.21
	5	82.2	211.03
	10	162.39	422.06
	15	243.59	633.09
3cc	1	48.72	42.21
	5	243.59	211.03
	10	487.17	422.06
	15	730.76	633.09

B.2 Assessing the setup

It is important that when deflagration would occur, the experimental set up can withstand the pressure and temperature change. The pressure change in case of deflagration is dependent on the oxygen pressure in the container. The burst pressure of the Swagelok tubes depends on which tube you take, but a typical tube has a burst pressure of about 10,000

psig, which is equivalent to 690 bar. Thus, as long as the pressure change due to deflagration stays below the burst pressure of the tubes, the tube will not explode. According to the calculations in Table B.1 the pressure change will not exceed 600 bar, if the initial oxygen pressure stays below 10 bar.

The increase in temperature due to deflagration influences the burst pressure of the tube. The last section of the safety calculations deals with how much the stainless steel tube is heated up after deflagration. It has been calculated that the temperature increase of the stainless steel tube is about 70 K, which is too small to have a significant effect on the burst pressure of the tube.

B.3 Evaluating the ignition mechanisms

In order for any type of combustion to occur, three things are needed: oxygen, a fuel and ignition energy. The first two (oxygen and fuel) are present in the setup. The latter, ignition energy, can be sourced from different ignition mechanisms. These include particle impact, flow friction, mechanical impact, static discharge, or external heat exceeding the auto-ignition temperature of the materials involved.

It is therefore important to prevent combustion by working at temperatures lower than the auto-ignition temperatures of the materials in the set up. The flammability of the oxygen-wetted materials involved has been assessed. The auto-ignition temperature of stainless steel 300 series is between 1500 and 1600 K at 50 bar. The auto-ignition temperature of polyphenylene sulfide (PPS) is 533 °C at 1 bar pure oxygen pressure. These temperatures are well above the operating temperatures of the accelerated ageing set up.

Thus, according to the performed safety calculations and the auto-ignition temperatures, it is deemed to be safe to operate the setup with pure oxygen in very small closed containers at 1, 5 and 10 bar oxygen pressure, for a range of temperatures between 90 and 170 °C.

B.4 Safety assessment: KOH

Potassium hydroxide, especially when heated, is very hazardous in case of skin contact (corrosive, irritant), eye contact (irritant, corrosive), ingestion, or inhalation. The amount of tissue damage depends on the length of contact. Eye contact can result in corneal damage or blindness. Skin contact can produce inflammation and blistering. Inhalation of dust will produce irritation to gastro-intestinal or respiratory tract, characterised by burning, sneezing and coughing. Severe over-exposure can produce lung damage, choking, uncon-

sciousness or death. Inflammation of the eye is characterised by redness, watering, and itching. Skin inflammation is characterised by itching, scaling, reddening, or, occasionally, blistering. Therefore, working with KOH should be well handled to minimise the risks.

The major risk of using potassium hydroxide is the risk of accidental spills. This can be prevented by properly containing the chemicals that will be used and make sure that the person doing the experiments wears protective clothing and safety glasses at all times. Furthermore, the experimental setup is put in a drip tray in order to prevent leaking of the KOH solution.

Appendix C

Additional results PPS-40%gf

C.1 Additional Results PPS-40% exposed to oxygen

Weight measurements

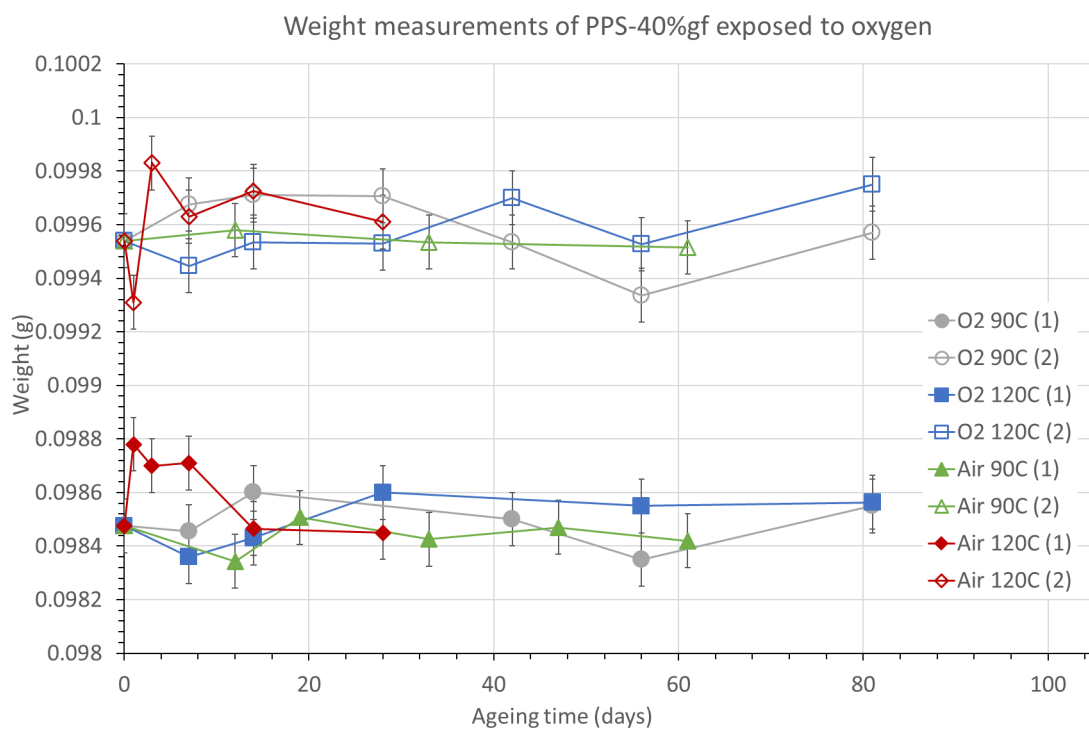
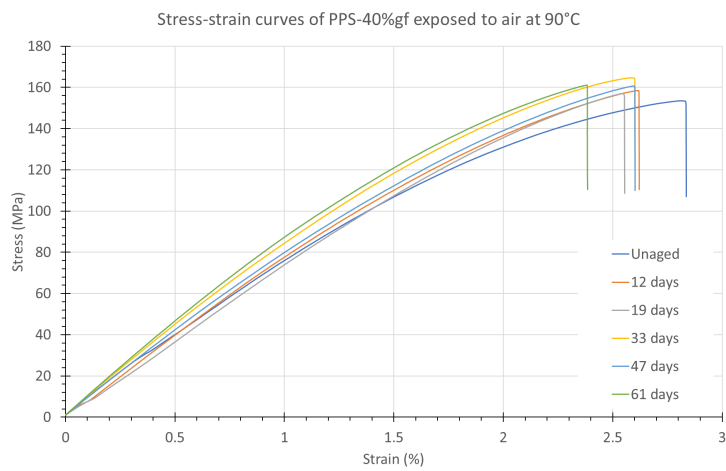
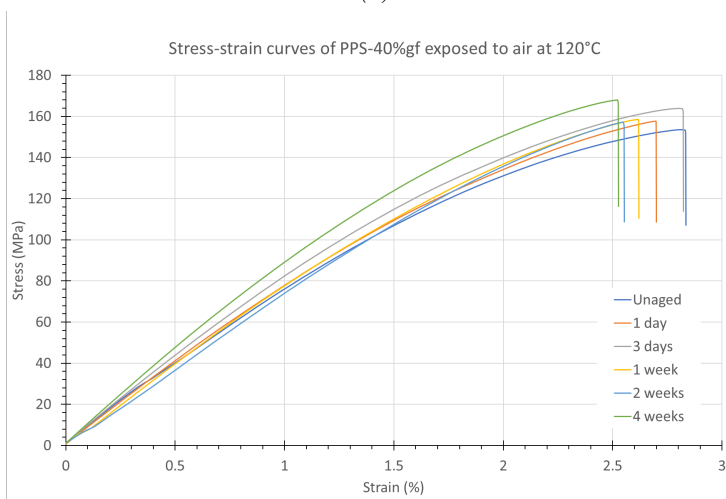


Figure C.1: Graphs showing the weight change of PPS-40%gf exposed to oxygen over time.

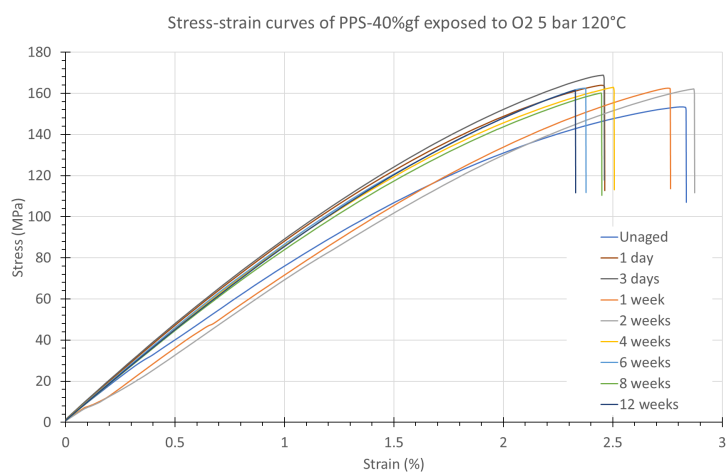
Tensile tests



(a)



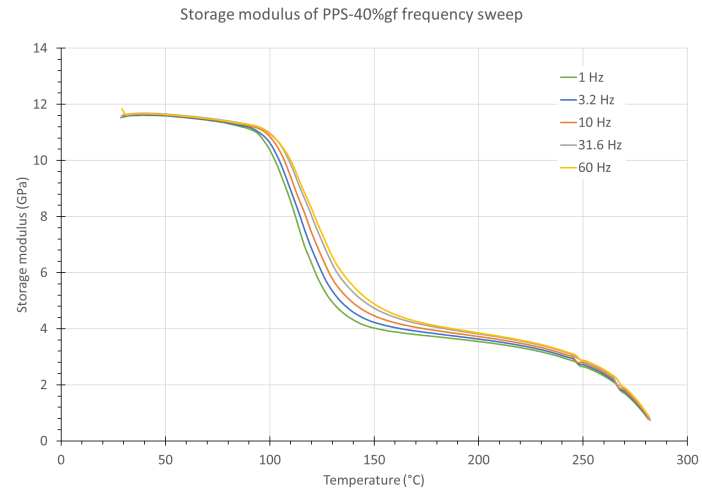
(b)



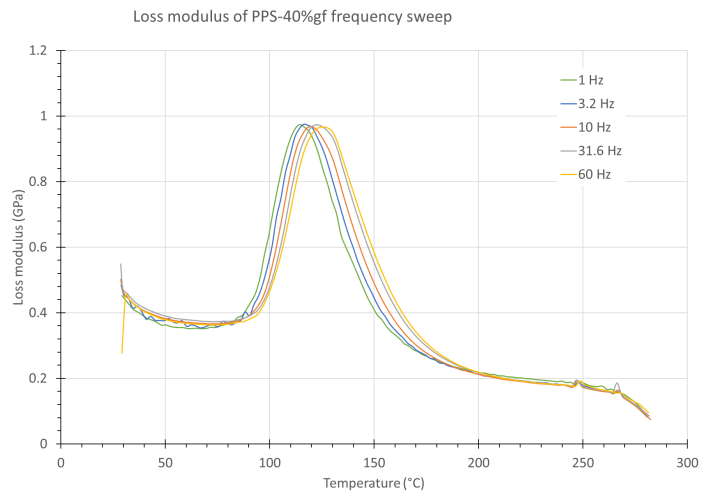
(c)

Figure C.2: Stress-strain curves of PPS-40%gf exposed to air and oxygen at 90 and 120 °C.

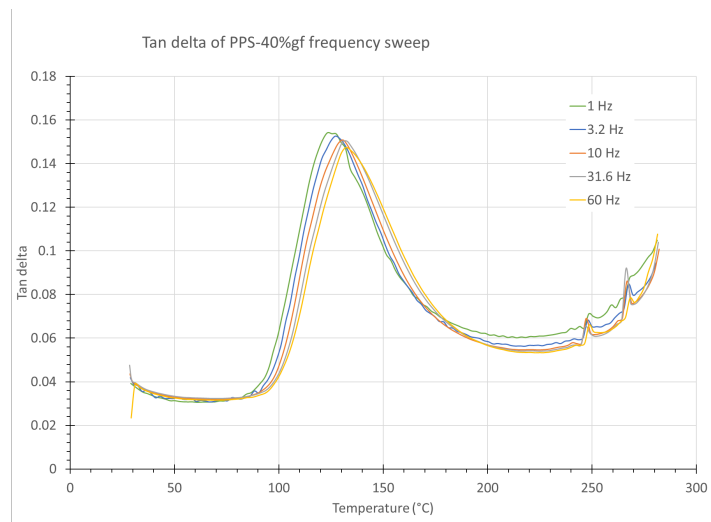
DMA



(a)

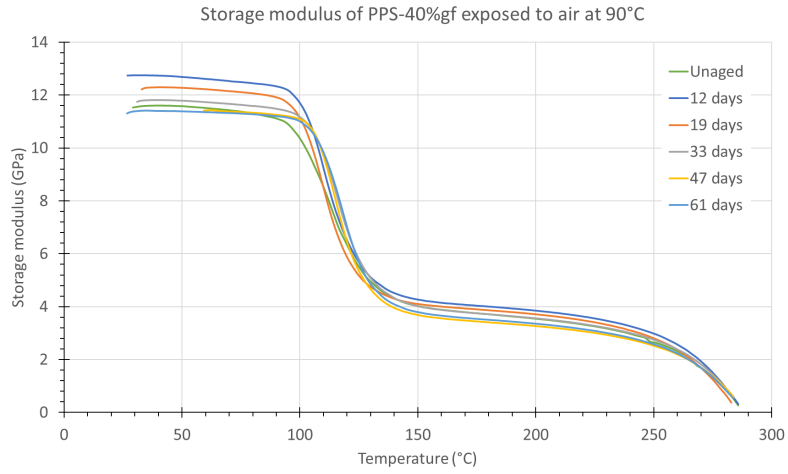


(b)

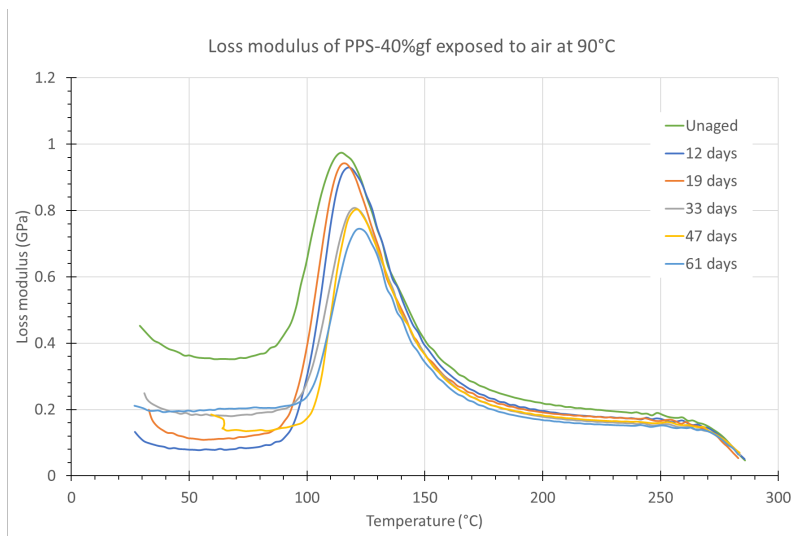


(c)

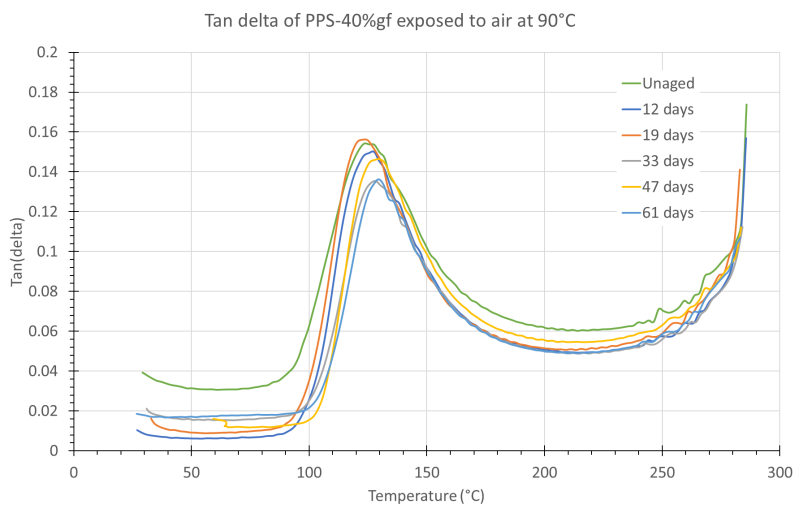
Figure C.3: DMA frequency sweep of unaged PPS-40%gf showing (a) the storage modulus, (b) the loss modulus and (c) tan delta.



(a)

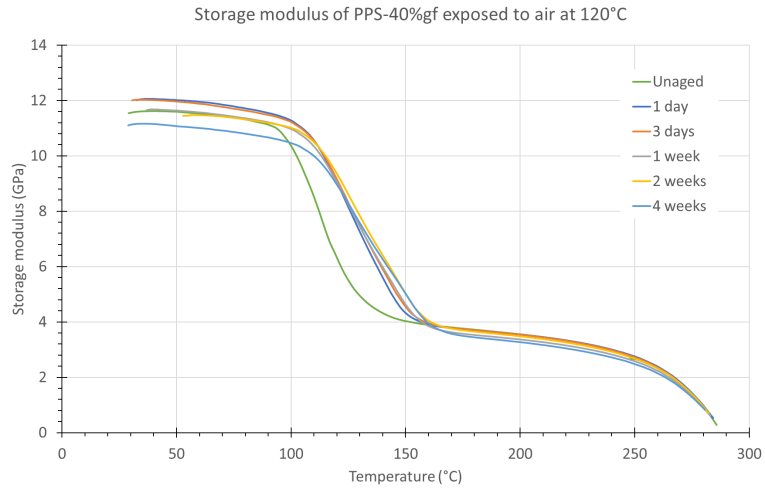


(b)

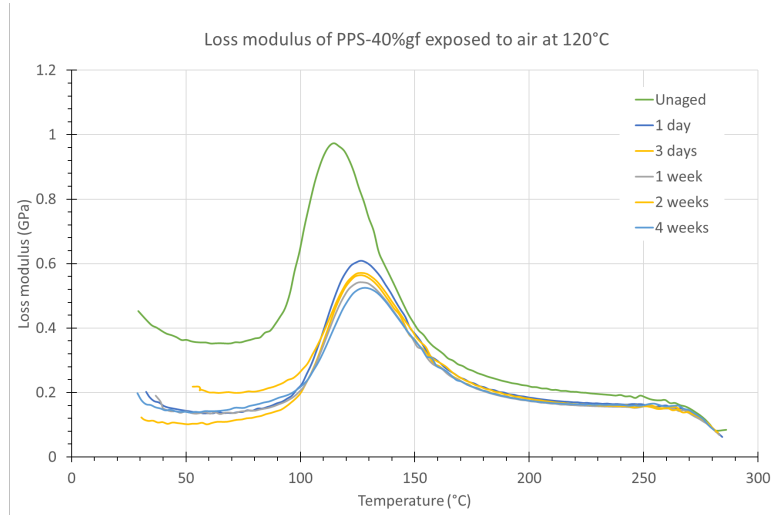


(c)

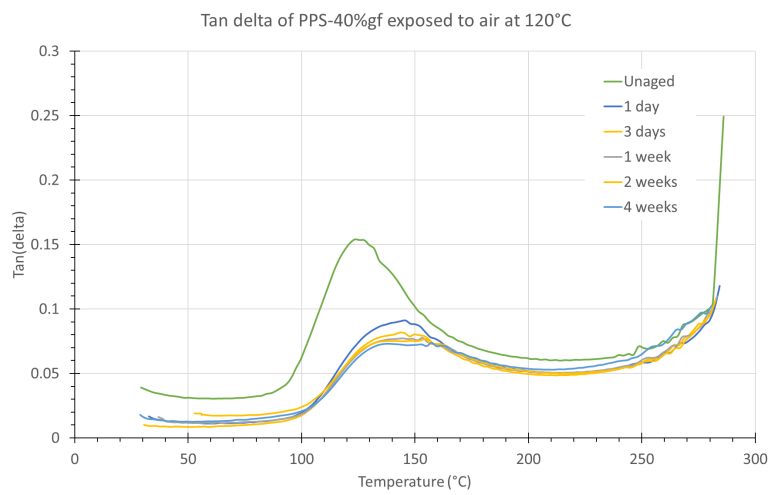
Figure C.4: DMA curves for PPS-40%gf aged in air at 90 °C showing (a) the storage modulus, (b) the loss modulus and (c) tan delta.



(a)

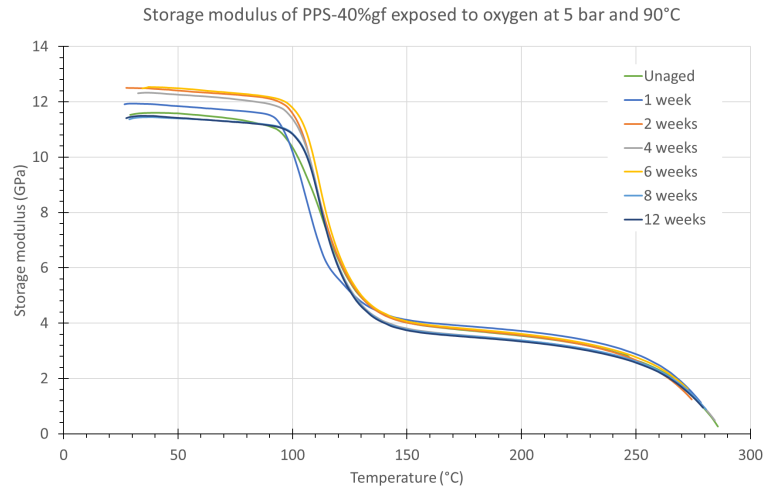


(b)

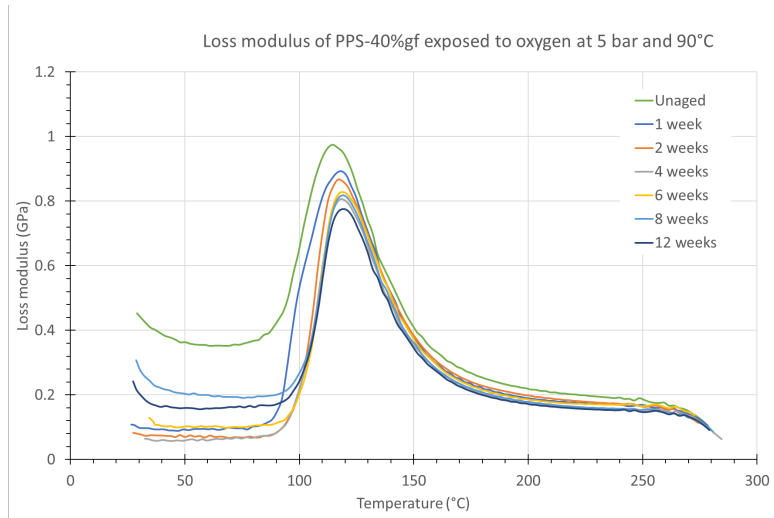


(c)

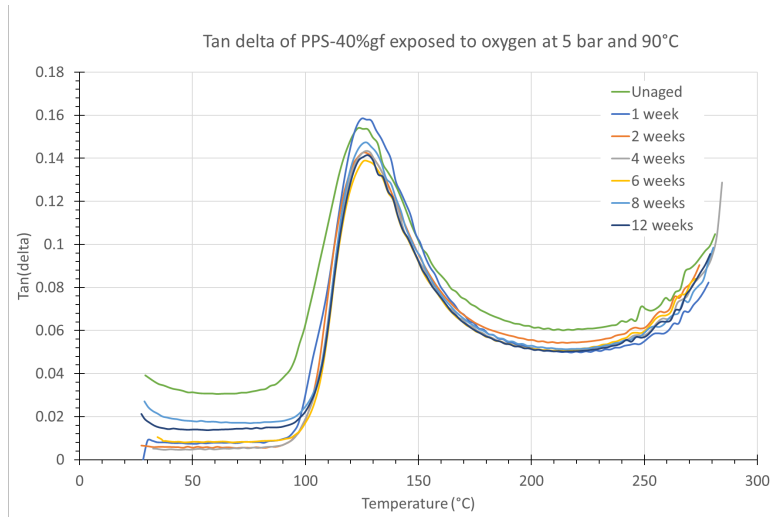
Figure C.5: DMA curves of PPS-40%gf aged in air at 120 °C showing (a) the storage modulus, (b) the loss modulus and (c) tan delta.



(a)

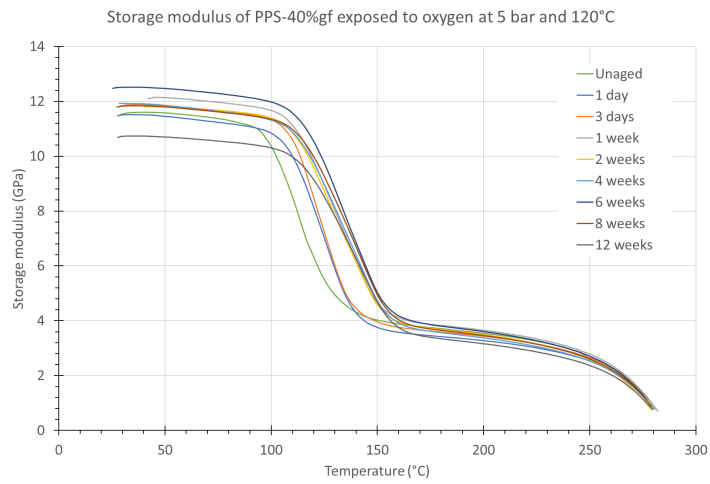


(b)

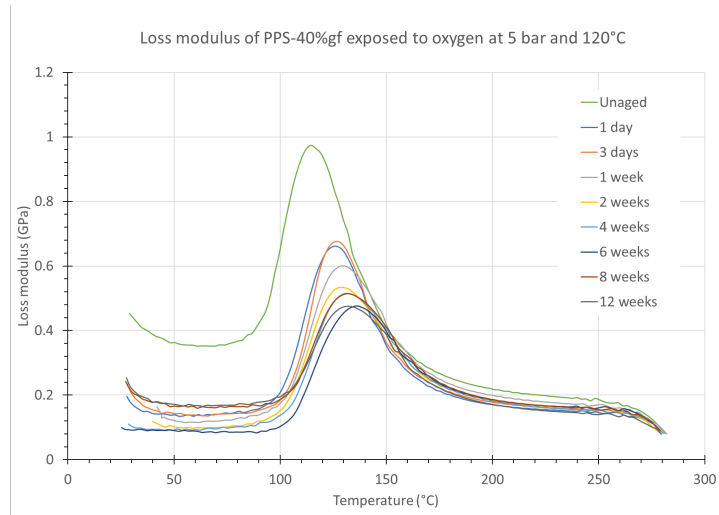


(c)

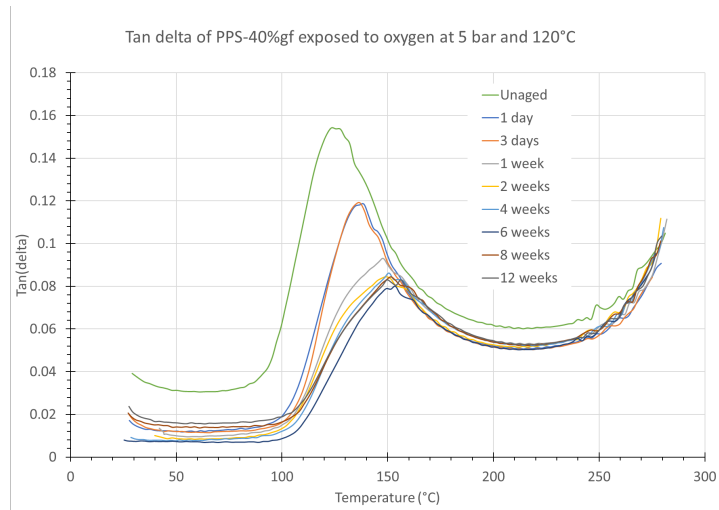
Figure C.6: DMA curves of PPS-40%gf aged in oxygen at 5 bar and 90 °C showing (a) the storage modulus, (b) the loss modulus and (c) tan delta.



(a)



(b)



(c)

Figure C.7: DMA curves for PPS-40%gf aged in oxygen at 5 bar and 120 °C showing (a) the storage modulus, (b) the loss modulus and (c) tan delta.

XRD

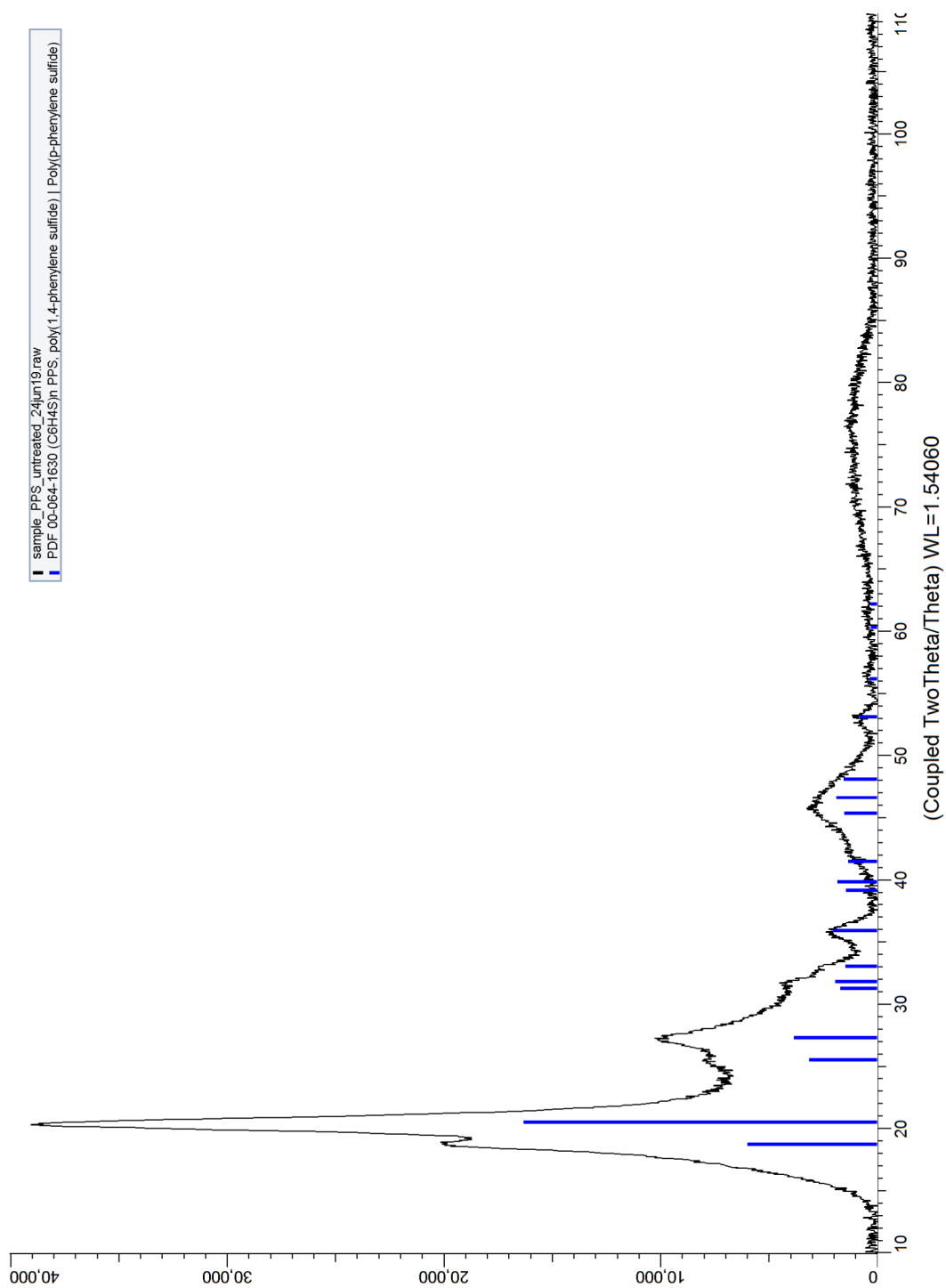


Figure C.8: XRD Pattern of unaged PPS-40%gf. The y-axis represents the number of counts.

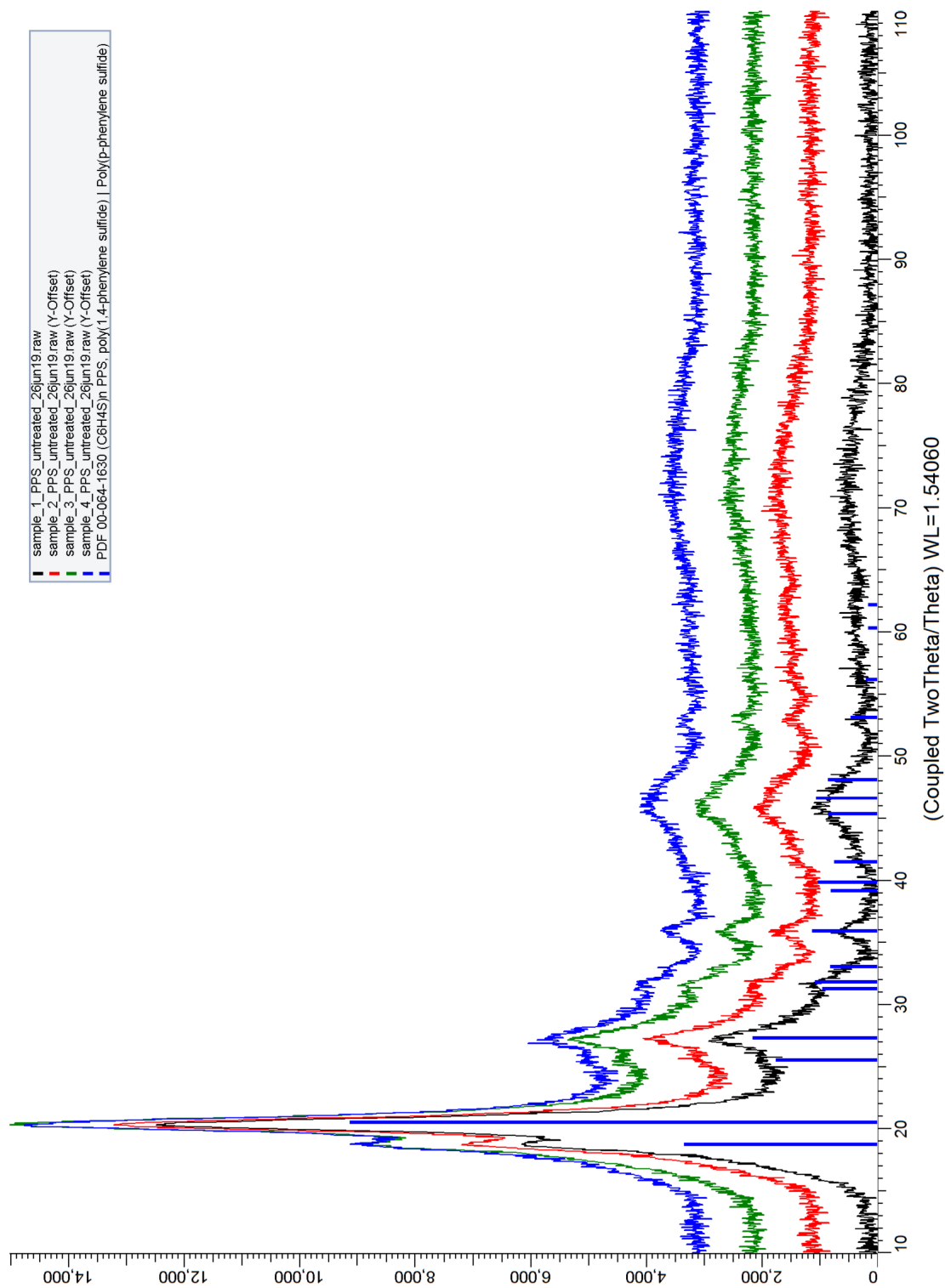
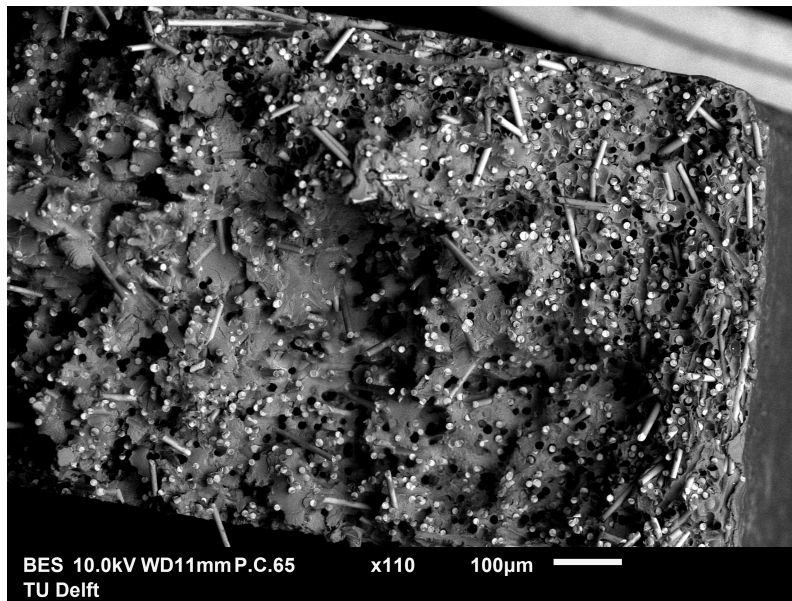
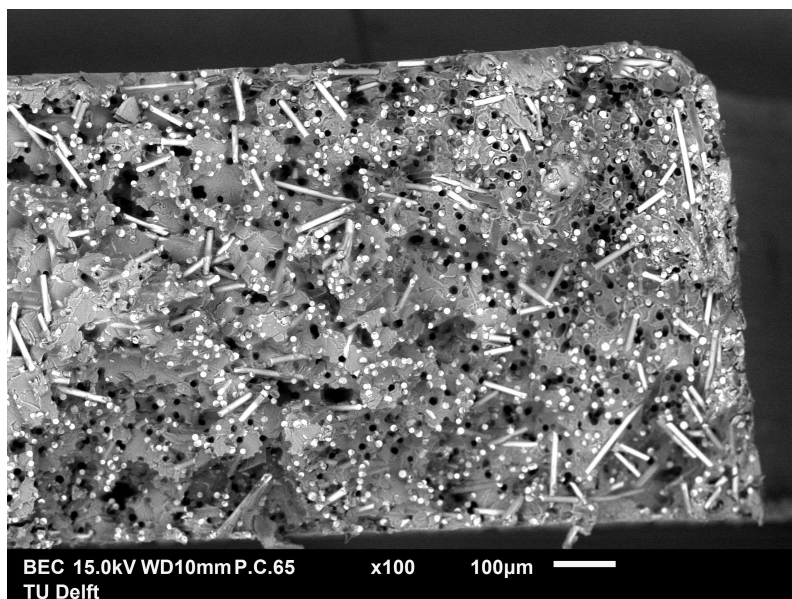


Figure C.9: XRD pattern of 4 different samples of unaged PPS-40%gf. As shown the four curves are nearly identical, meaning the XRD measurements are reproducible. The y-axis represents the number of counts.

SEM

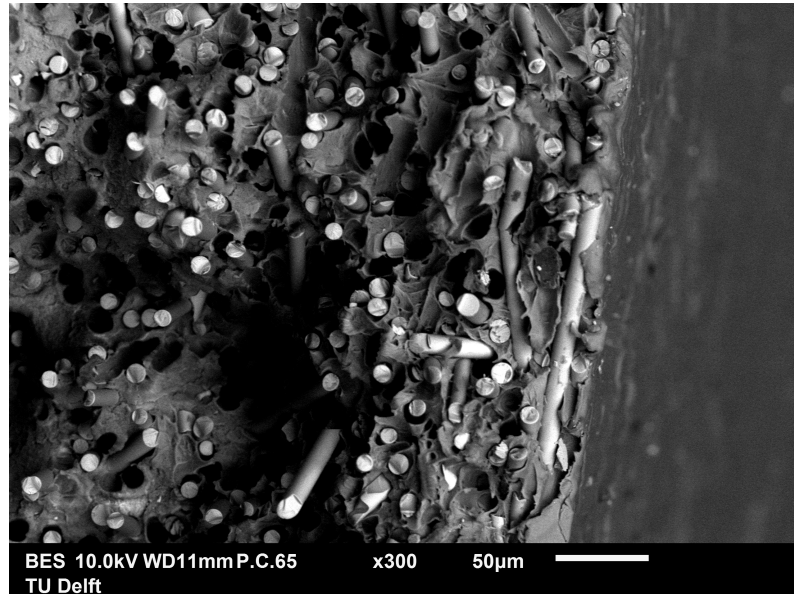


(a)

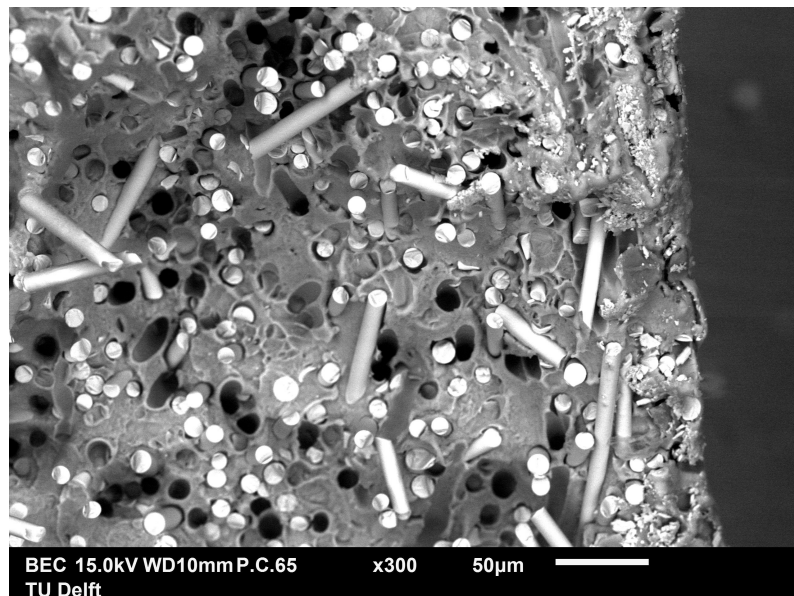


(b)

Figure C.10: SEM images of the fracture surface of (a) unaged PPS-40%gf and (b) aged PPS-40%gf in O₂ at 5 bar and 120 °C for 8 weeks.



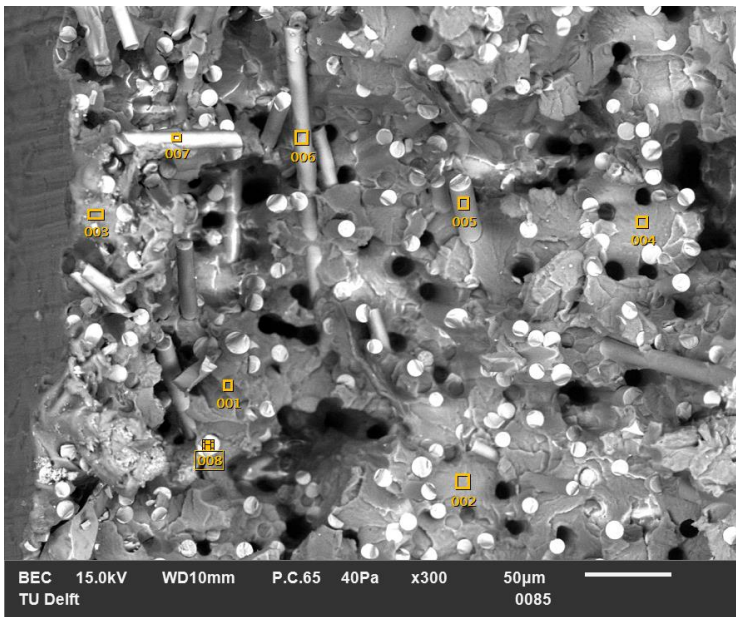
(a)



(b)

Figure C.11: SEM 300x magnification of the fracture surface of (a) unaged PPS-40%gf and (b) aged PPS-40%gf in O₂ at 5 bar and 120 °C for 8 weeks.

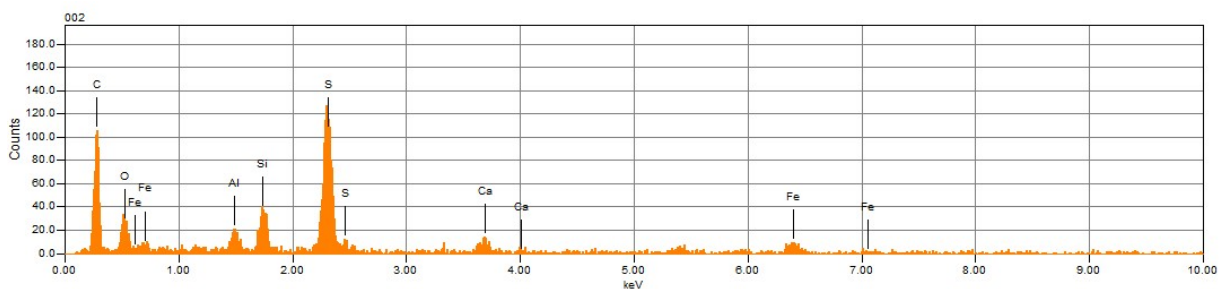
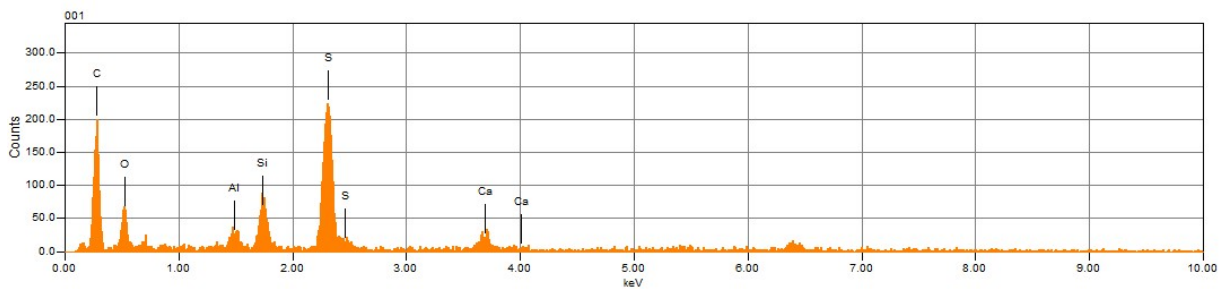
EDS analysis PPS 8 weeks O2 5 bar 120°C

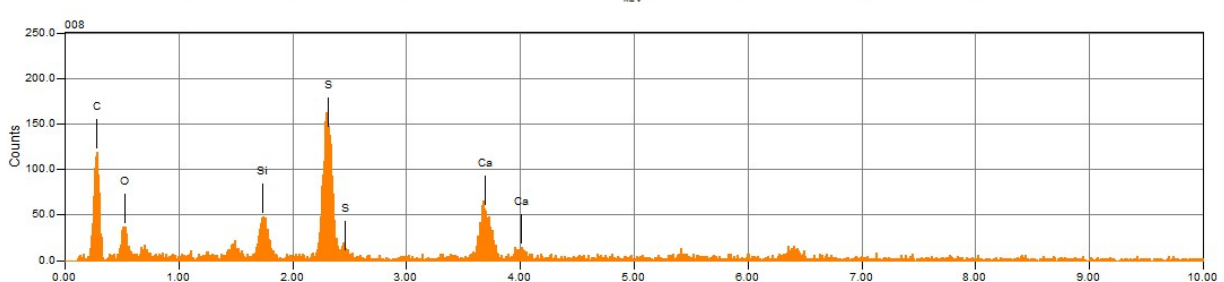
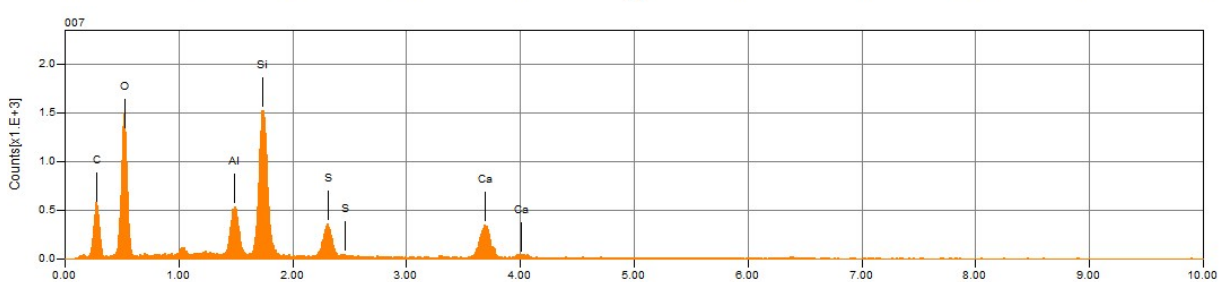
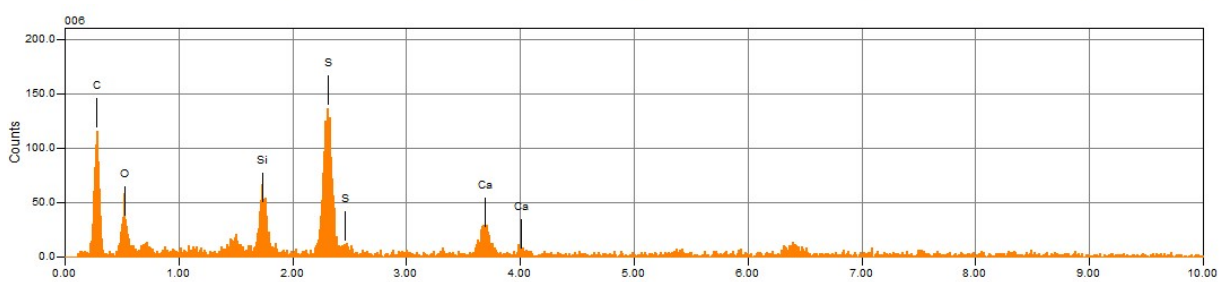
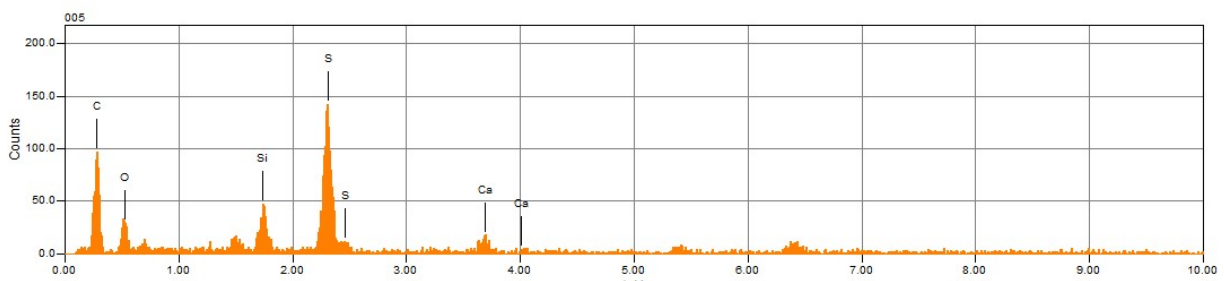
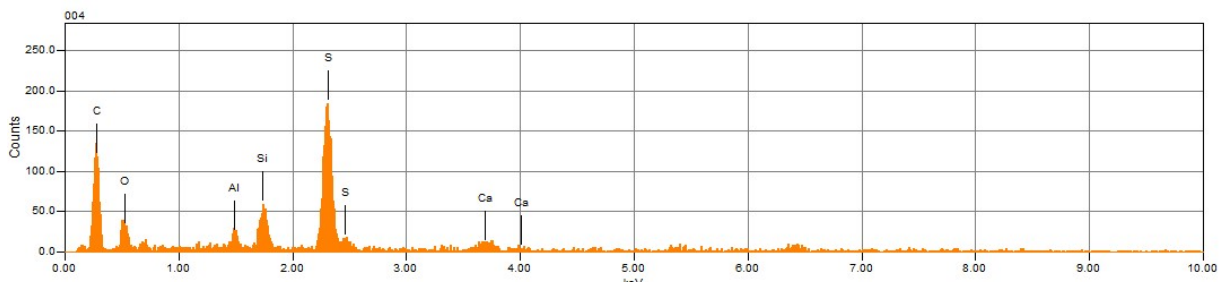
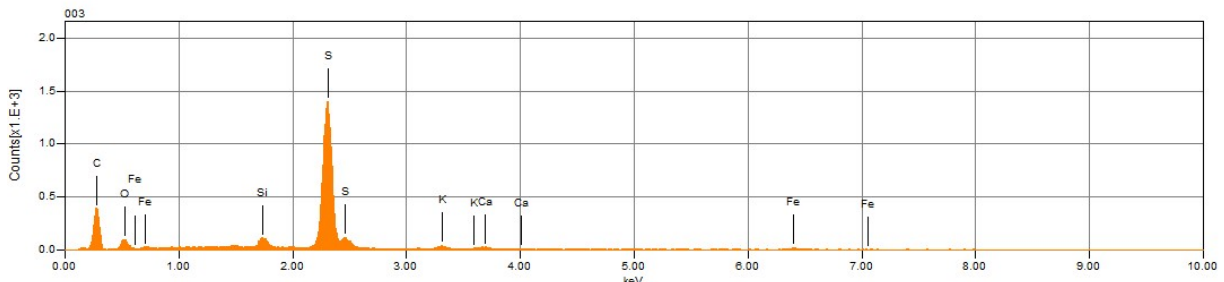


Volt : 15.00 kV
 Mag. : x 300
 Date : 2019/09/17
 Pixel : 1280 x 960

Acquisition Condition
 Instrument : IT100LA
 Volt : 15.00 kV
 Current : ---
 Process Time : T4
 Live time : 30.00 sec.
 Real Time : 30.48 sec.
 DeadTime : 2.00 %
 Count Rate : 279.00 CPS

	Fe	K	O	C	Al	Si	S	Ca
001			17.17	60.13	1.09	3.39	15.37	2.84
002	6.89		15.47	56.32	1.20	3.09	14.85	2.19
003	1.72	1.00	8.57	58.80		1.24	28.06	0.61
004			15.10	61.97	1.21	3.13	17.22	1.37
005			18.10	59.08		3.35	16.59	2.88
006			19.03	56.52		4.18	14.76	5.51
007			43.11	29.37	3.87	12.54	4.31	6.80
008			15.55	55.70		2.86	15.70	10.19





C.2 Additional Results PPS-40% exposed to KOH

Weight measurements

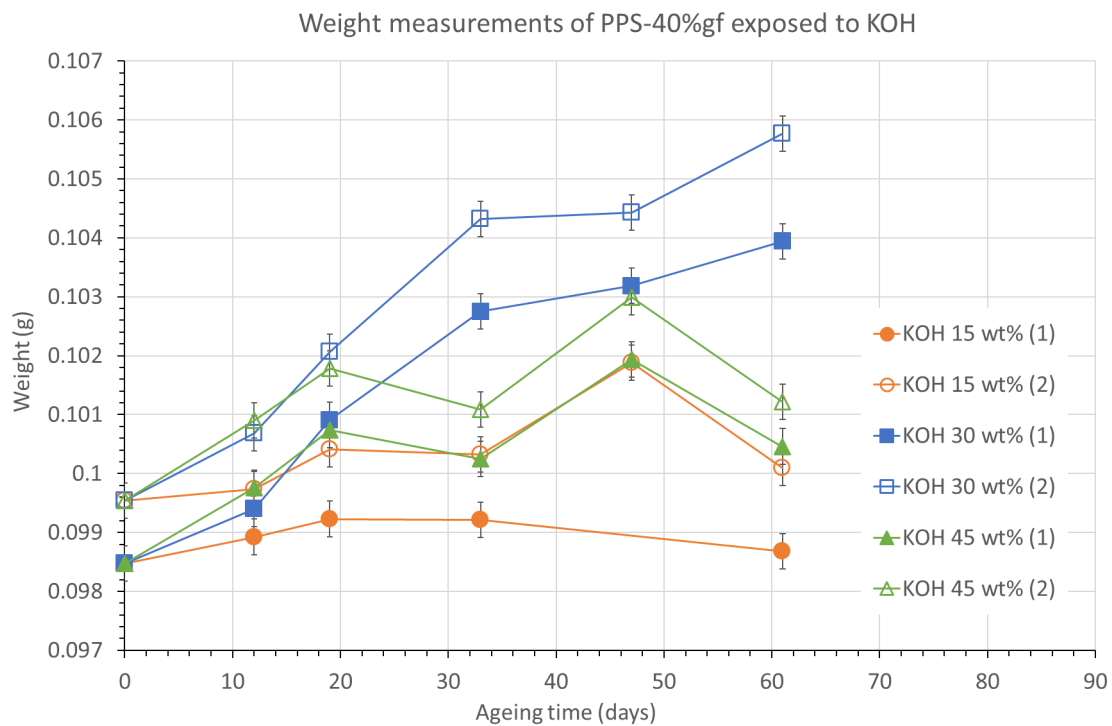


Figure C.12: Graphs showing the weight change over time of PPS-40%gf exposed to KOH at 90 °C.

Tensile tests

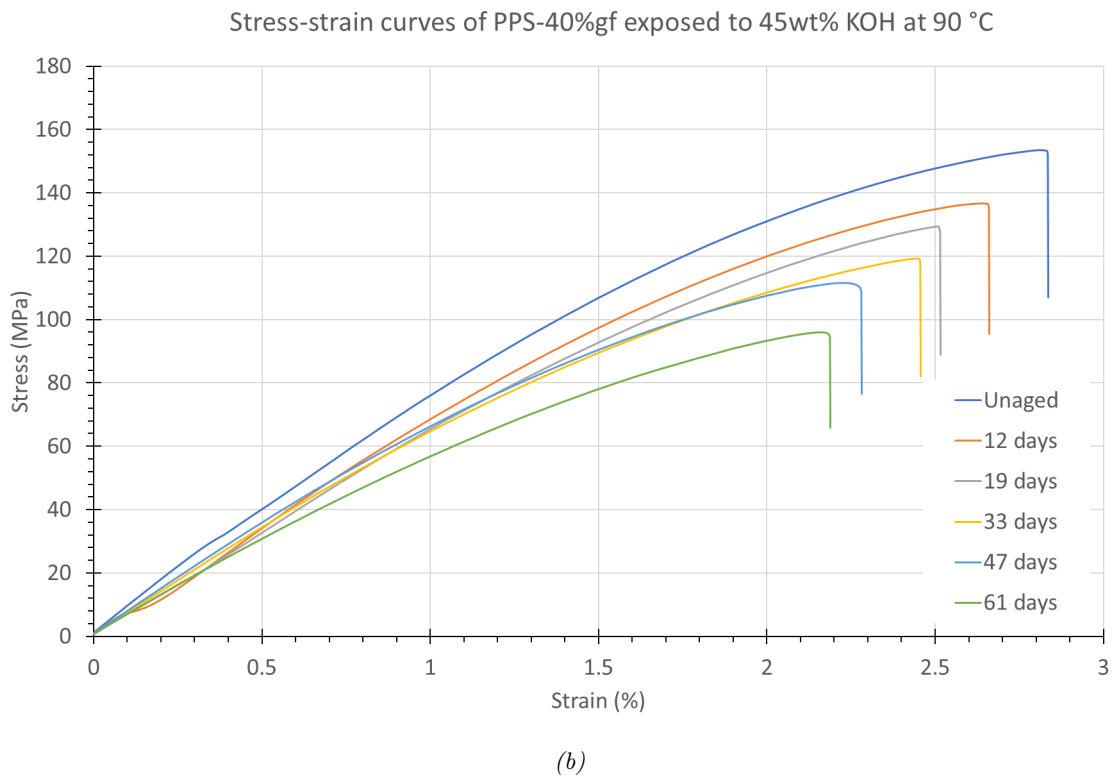
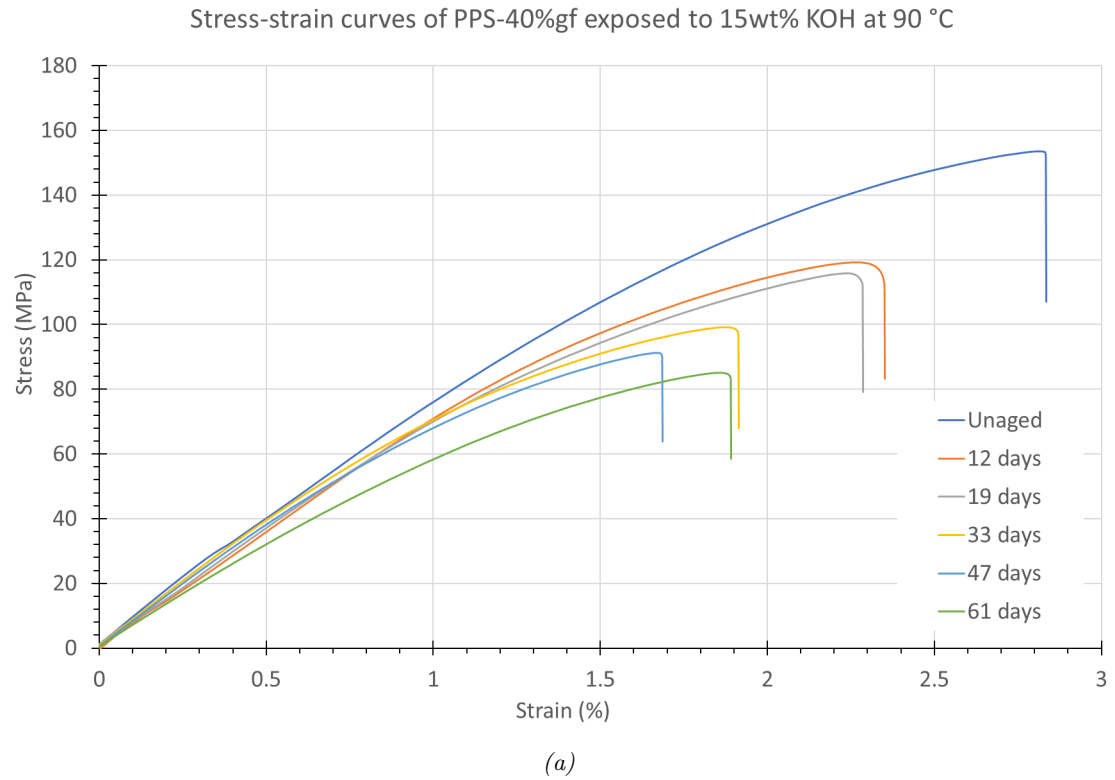
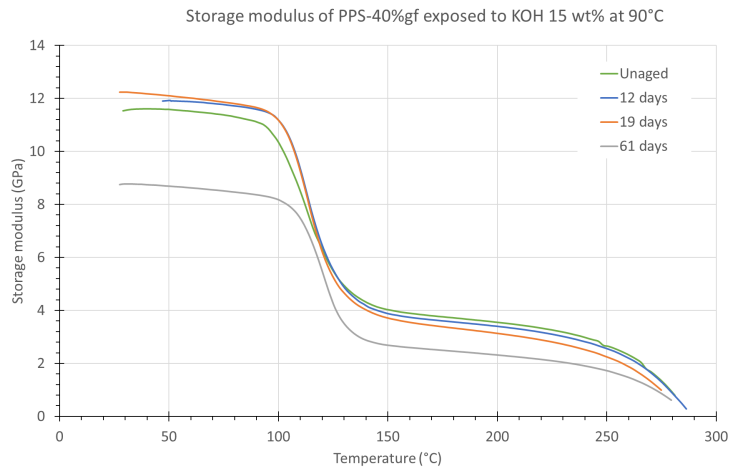
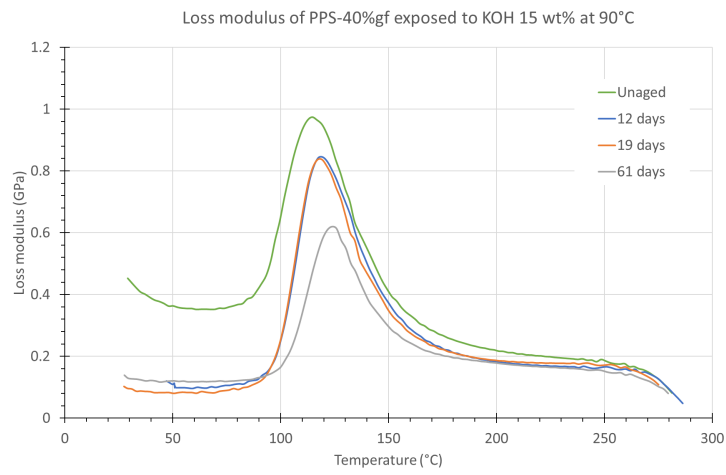


Figure C.13: Stress-strain curves of PPS-40%gf exposed to (a) 15wt% and (b) 45wt% KOH at 90 °C.

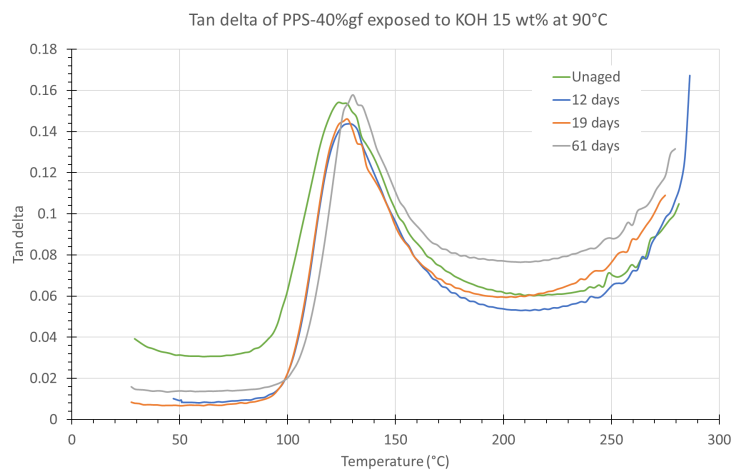
DMA



(a)

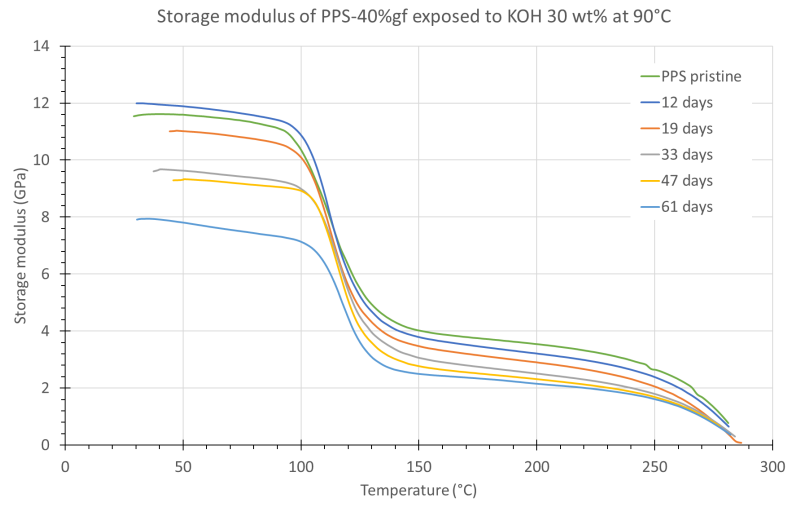


(b)

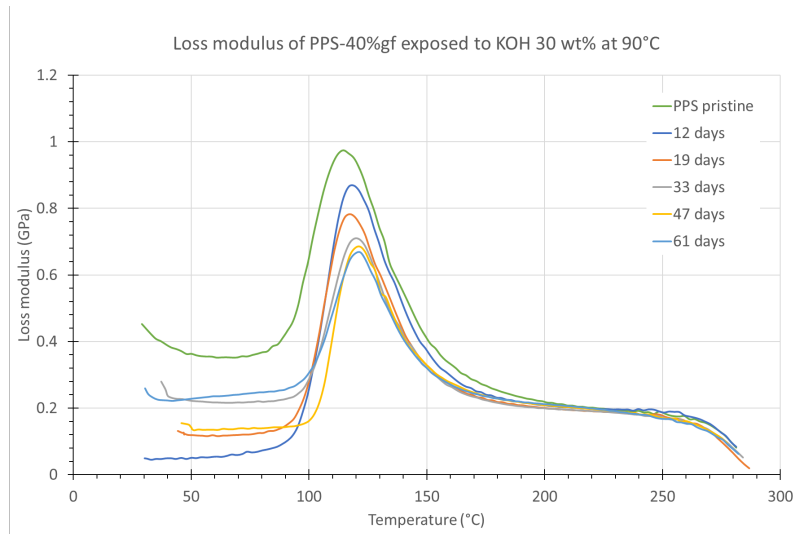


(c)

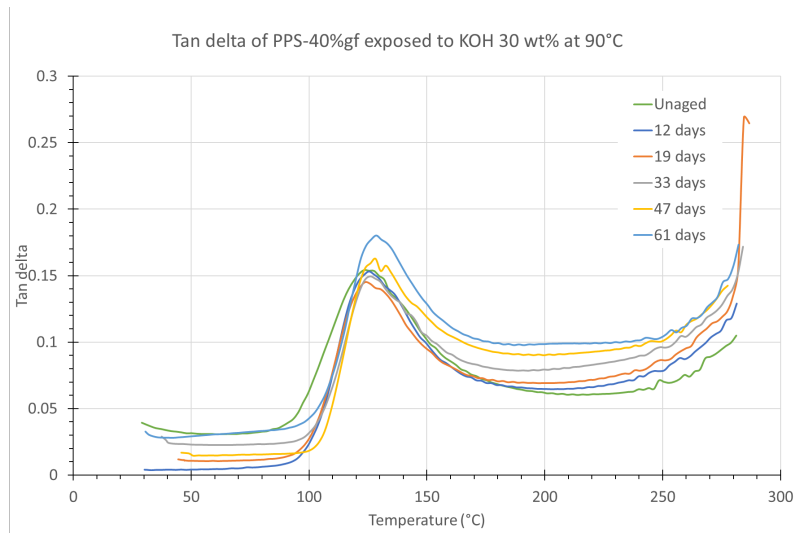
Figure C.14: DMA curves of PPS-40%gf aged in KOH 15wt% at 90 °C showing (a) the storage modulus, (b) the loss modulus and (c) tan delta.



(a)

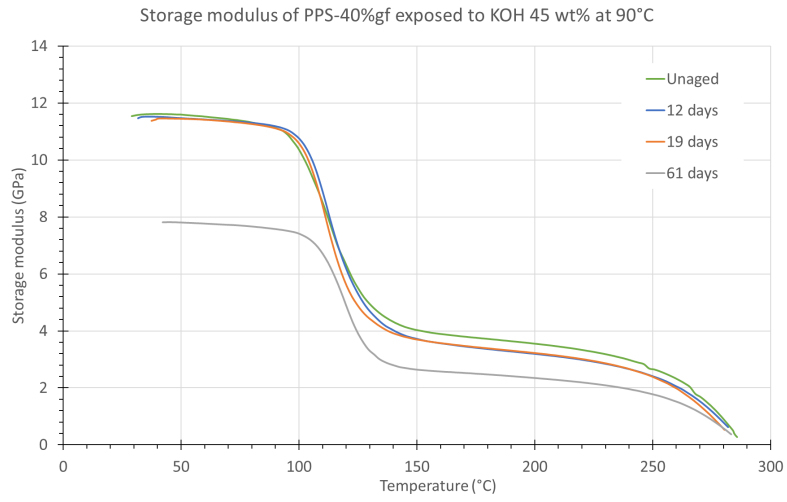


(b)

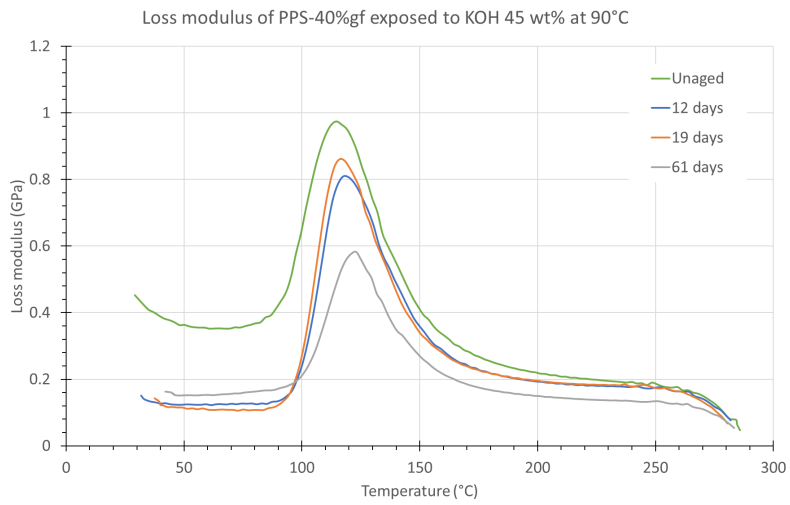


(c)

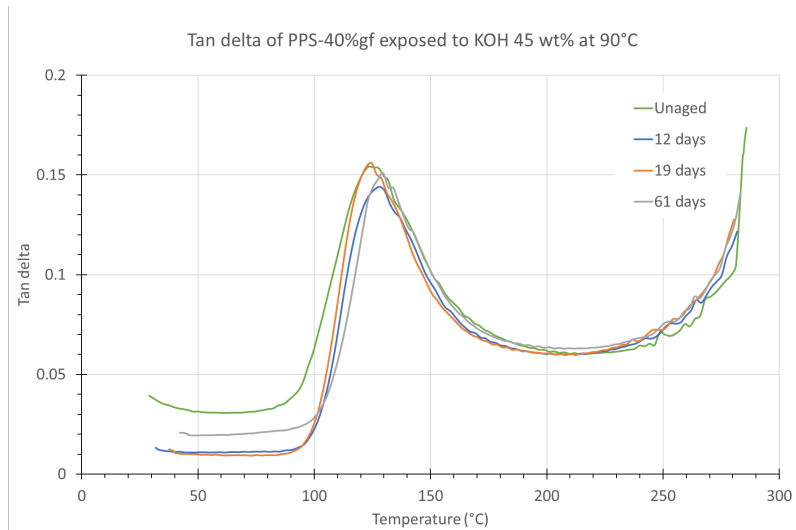
Figure C.15: DMA curves of PPS-40%gf aged in KOH 30wt% at 90 °C showing (a) the storage modulus, (b) the loss modulus and (c) tan delta.



(a)



(b)



(c)

Figure C.16: DMA curves of PPS-40%gf aged in KOH 45wt% at 90 °C showing (a) the storage modulus, (b) the loss modulus and (c) tan delta.

XRD

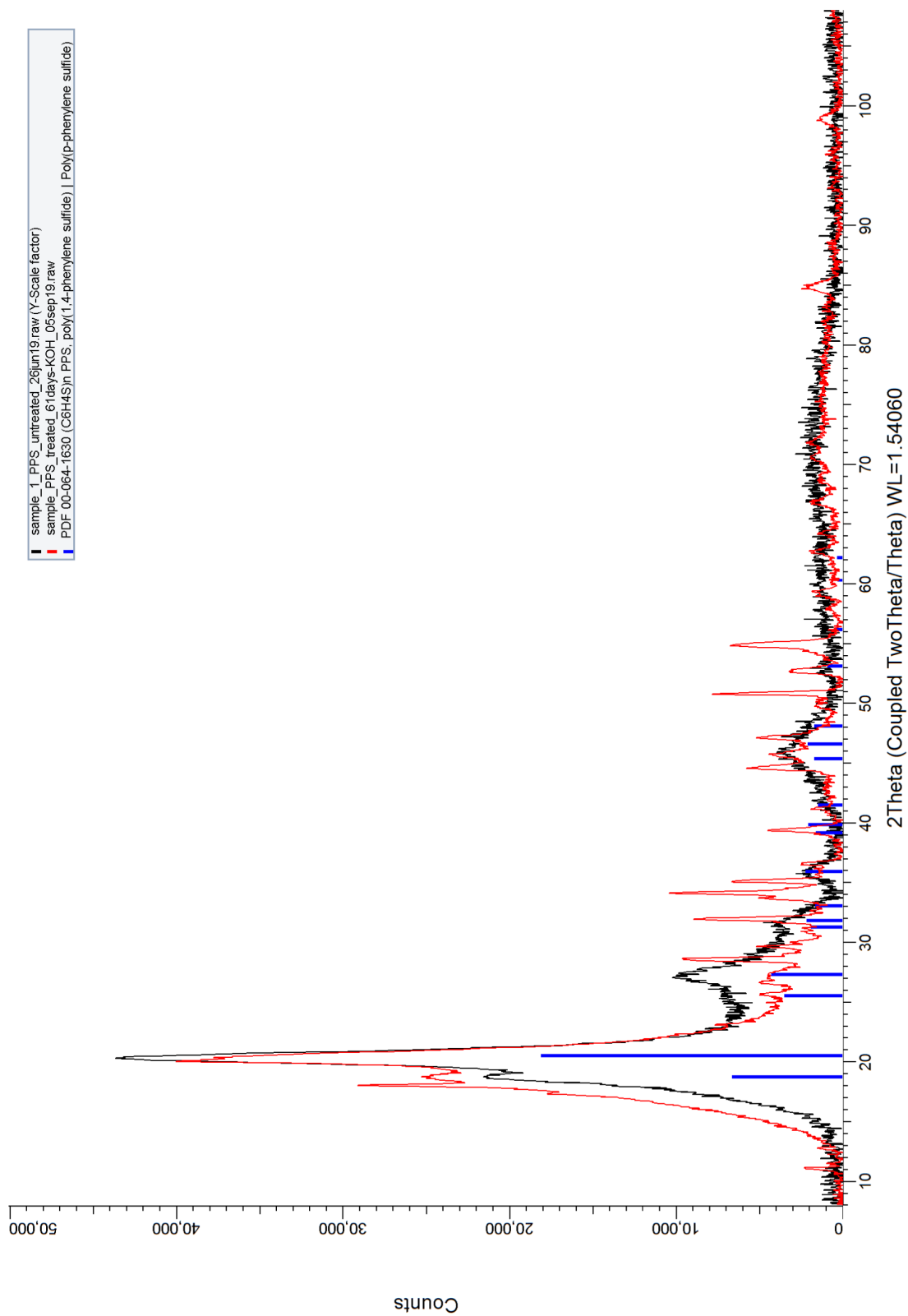


Figure C.17: XRD pattern of PPS-40%gf exposed to KOH 30wt% 90 °C for 61 days compared to unaged PPS-40%gf

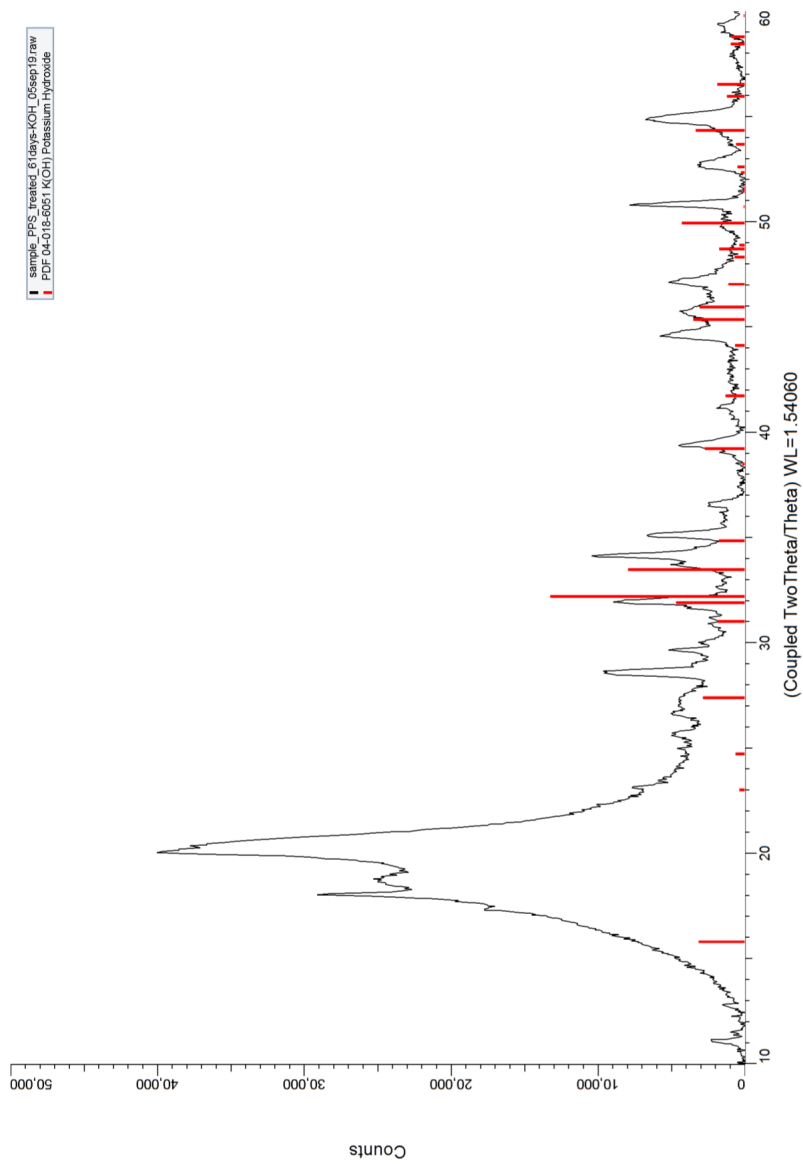


Figure C.18: XRD pattern of PPS-40%gf exposed to KOH 30wt% 90 °C for 61 days compared to a KOH spectrum. The red peaks indicate the peak positions and relative intensities for KOH precipitates.

SEM

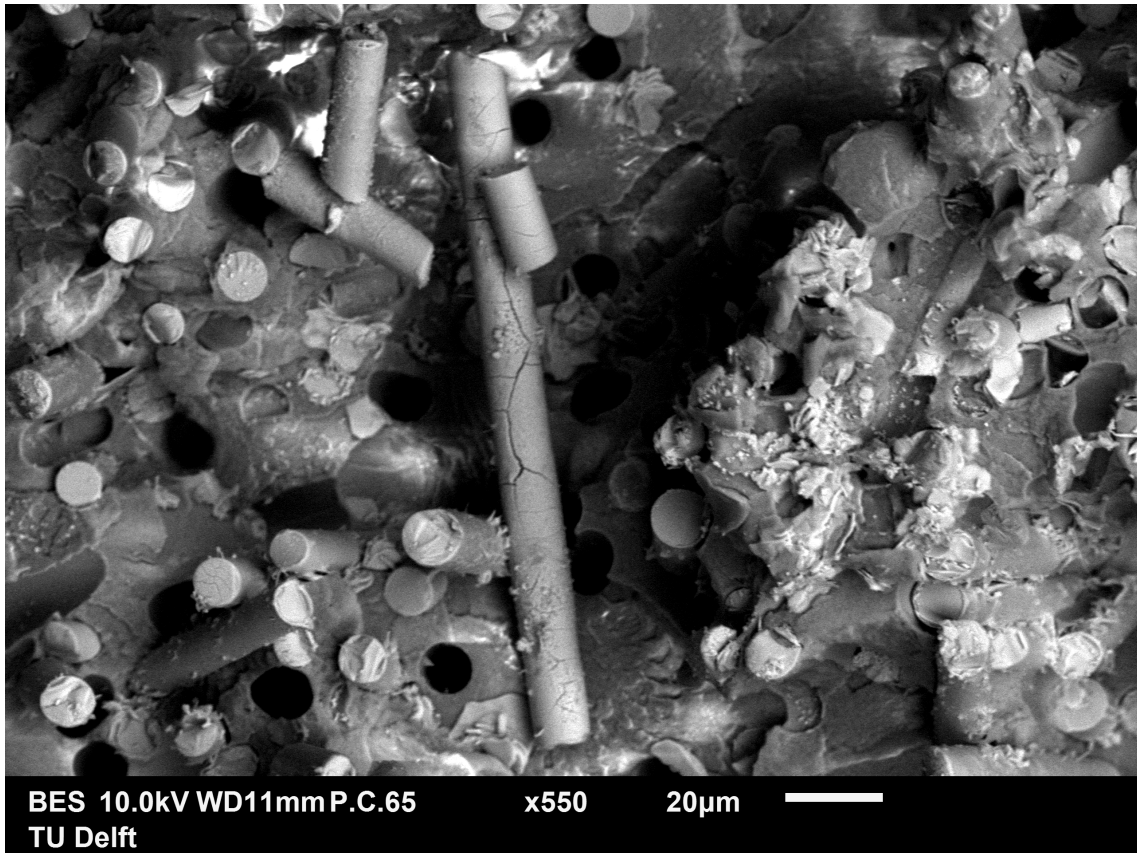
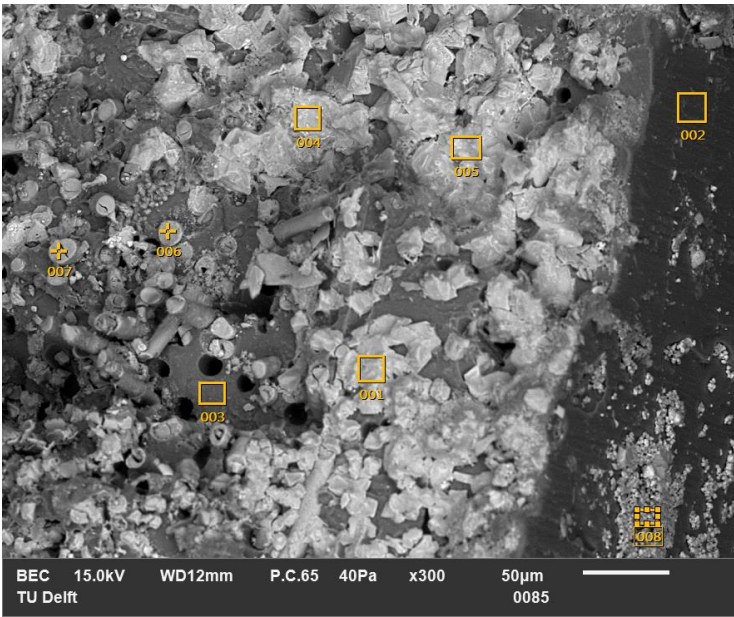


Figure C.19: SEM image of a single broken fibre on fracture surface of PPS-40%gf exposed to KOH 30wt% for 33 days.

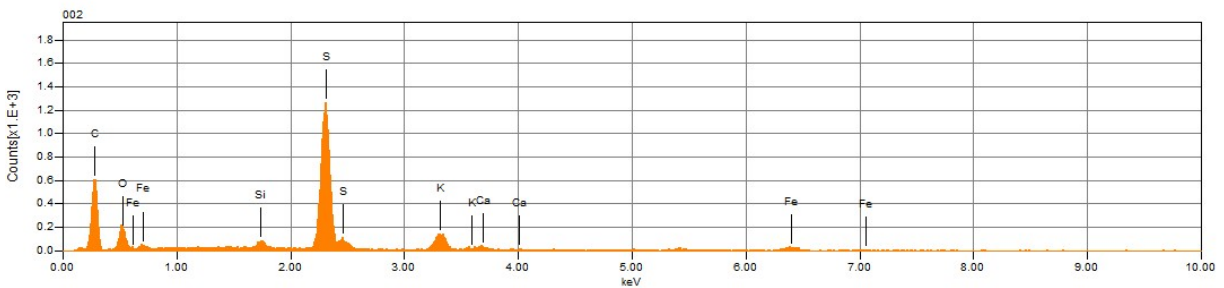
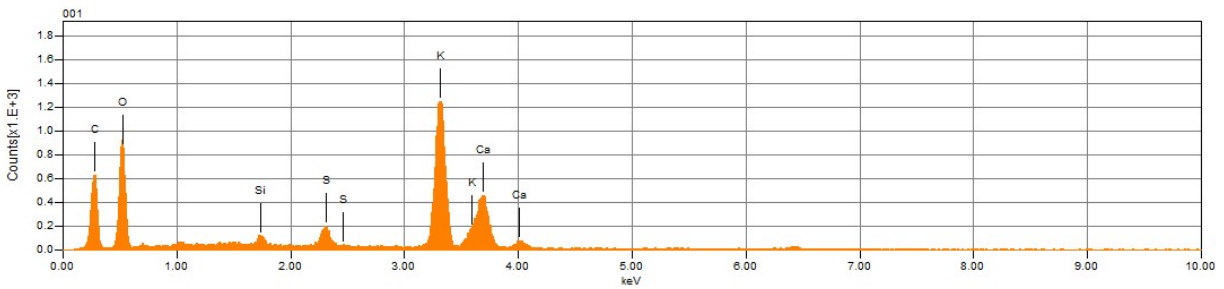
EDS analysis PPS 61 days KOH 30wt% 90°C

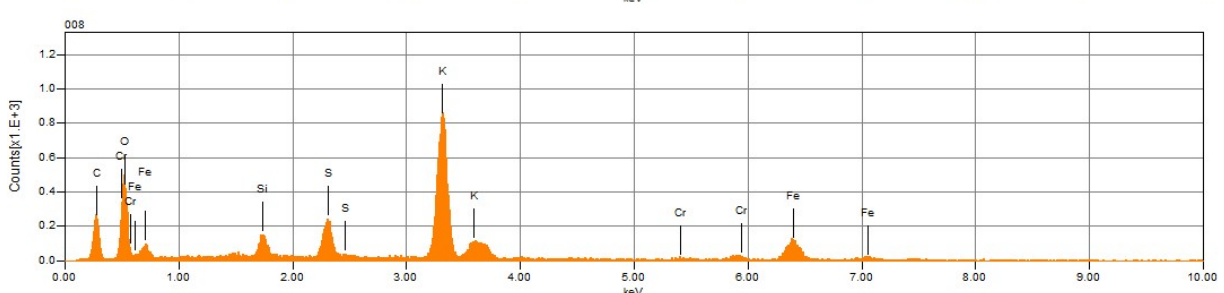
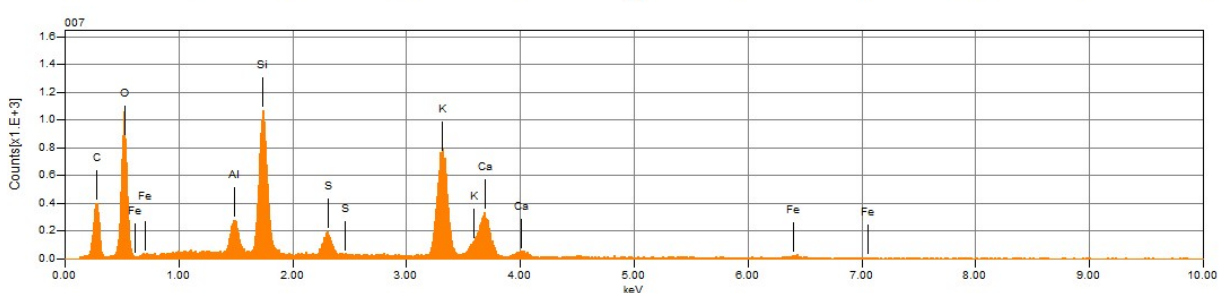
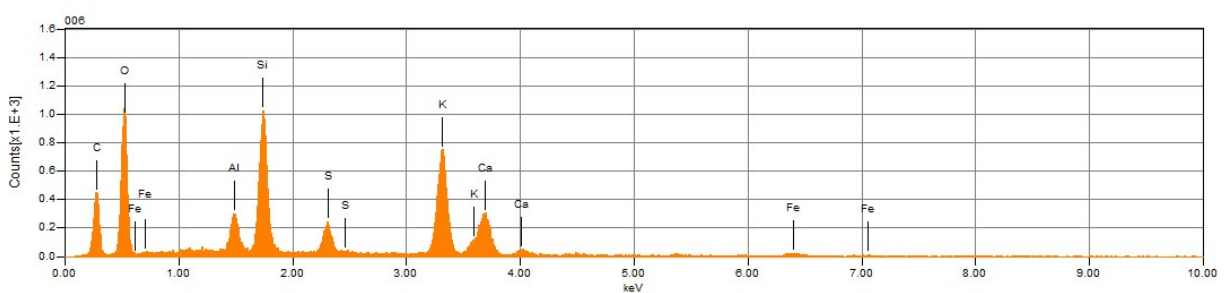
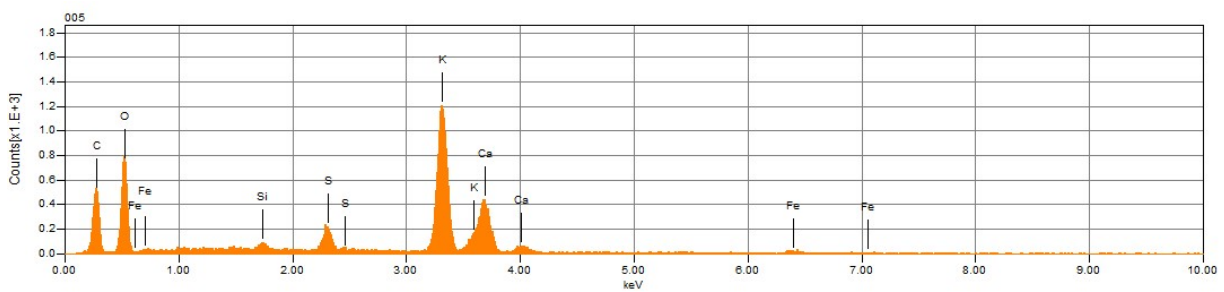
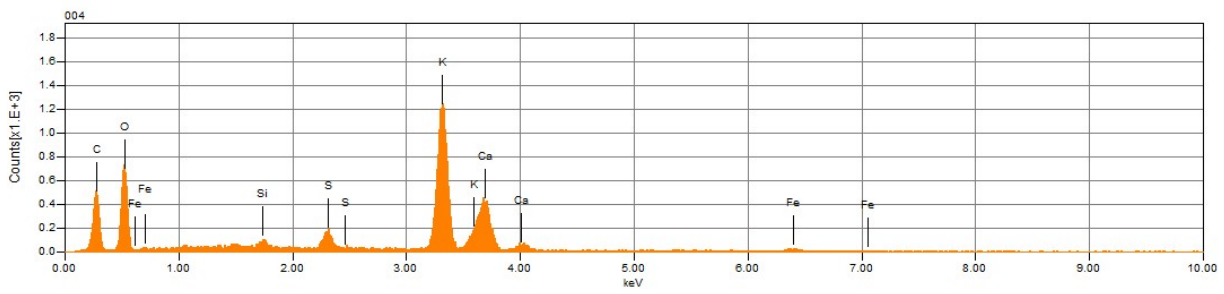
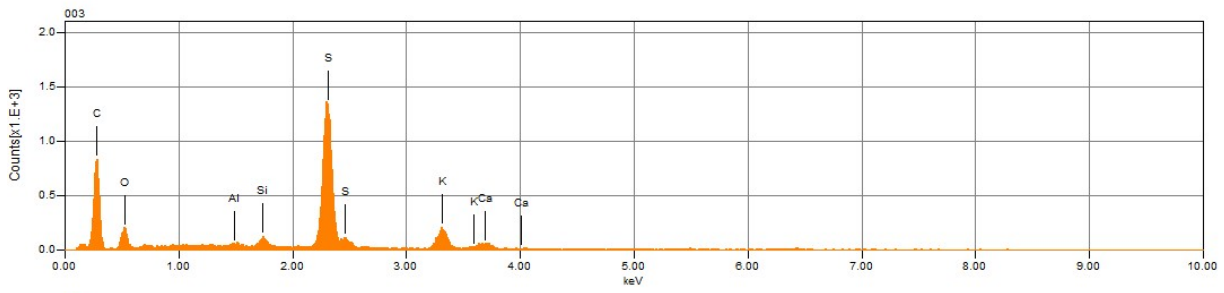


Volt : 15.00 kV
 Mag. : x 300
 Date : 2019/09/17
 Pixel : 1280 x 960

Acquisition Condition
 Instrument : IT100LA
 Volt : 15.00 kV
 Current : ---
 Process Time : T4
 Live time : 30.00 sec.
 Real Time : 30.94 sec.
 DeadTime : 3.00 %
 Count Rate : 1030.00 CPS

	Fe	K	O	C	Al	Si	S	Ca	Cr
001		27.08	42.35	17.53		0.80	2.13	10.11	
002	3.17	4.02	14.82	55.79		0.74	20.60	0.87	
003		4.39	12.83	61.30	0.23	0.77	19.26	1.23	
004	1.86	29.61	39.27	15.52		0.71	2.26	10.78	
005	2.34	27.68	39.75	16.52		0.56	2.80	10.35	
006	1.89	15.79	40.31	20.66	2.26	9.27	2.94	6.88	
007	1.69	17.71	39.91	19.00	2.15	9.82	2.36	7.38	
008	17.47	28.98	29.99	15.49		2.01	4.94		1.11





C.3 Correction of stress-strain curves

The tensile test results of the first two weeks for both PPS-40%gf and PSU all show the same shift in the curve, due to the grip element not being tightly attached to the bottom of the tensile test machine. This meant that at the beginning of the curve the bottom grip element was lifted up at a certain stress level, meaning a large displacement is shown for the same stress. Luckily, since the shift was the same for all curves, this could be easily corrected for, as shown in Figure C.20.

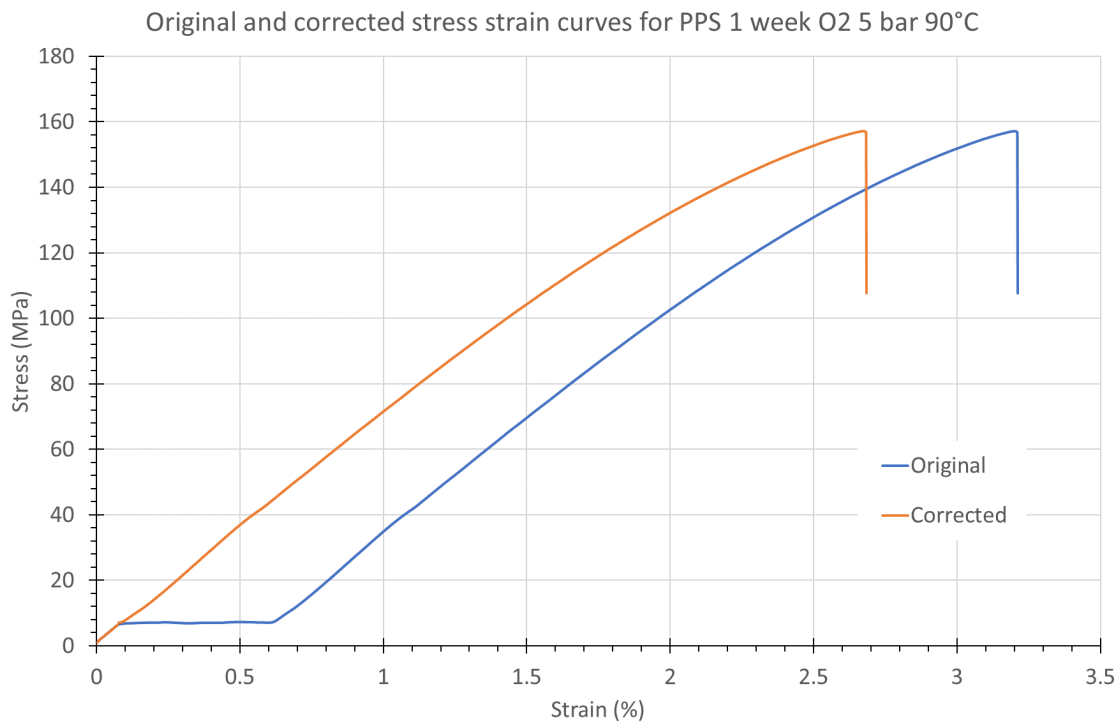


Figure C.20: Corrected stress-strain curve of PPS-40%gf exposed to oxygen at 5 bar and 90 °C for 1 week.

C.4 Control samples

Unaged PPS-40%gf has been characterised at the start of the ageing experiment and after 12 weeks. During those 12 weeks the samples have been stored in plastic bags in ambient conditions. Figure C.21 gives the stress-strain curves. It seems that after 12 weeks the curve shifts to the left to shorter elongations. However, it should be noted that the blue PPS-40%gf unaged curve shows a small slip at the beginning of the curve, meaning it shifted slightly to the right.

The Young's modulus changed from 7.5 ± 0.3 to 8.7 ± 0.2 , the UTS changed from 154 ± 2.5 to 155 ± 1 , the strain at UTS from 2.7 ± 0.1 to 2.4 ± 0.1 and the toughness from 2.6 ± 0.2 to 2.3 ± 0.1 .

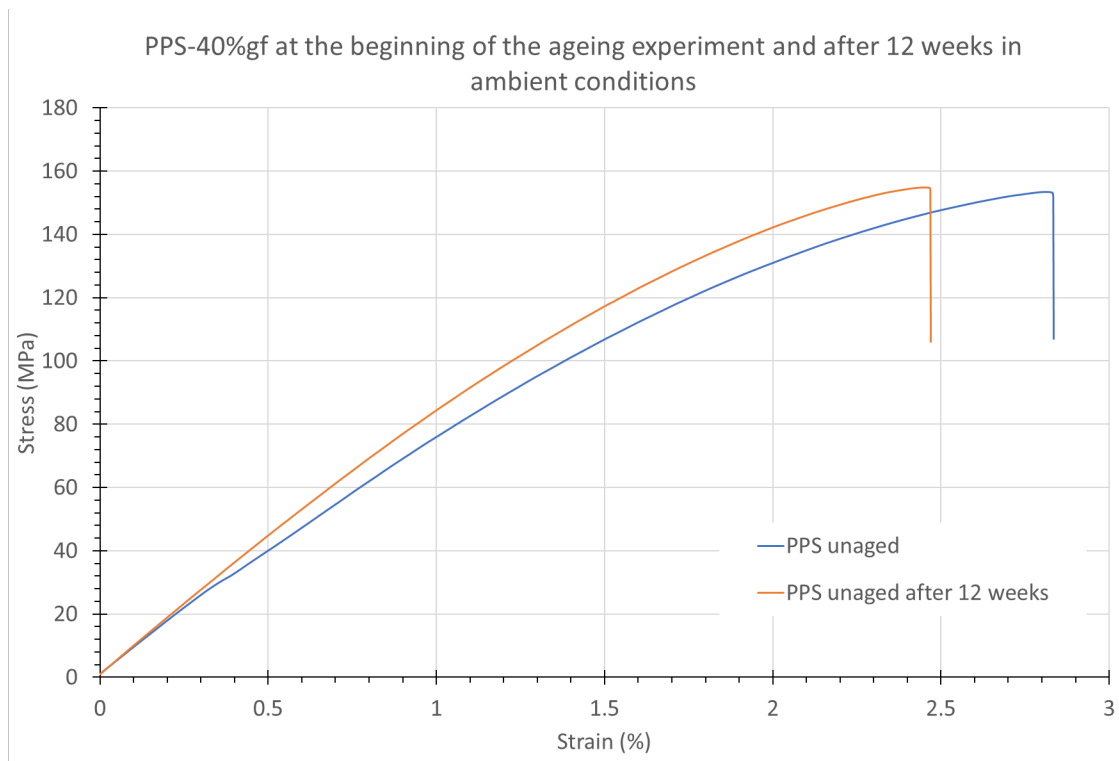
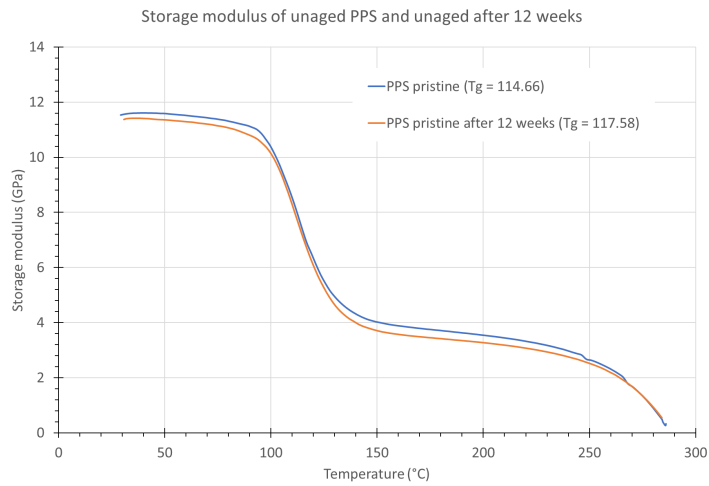
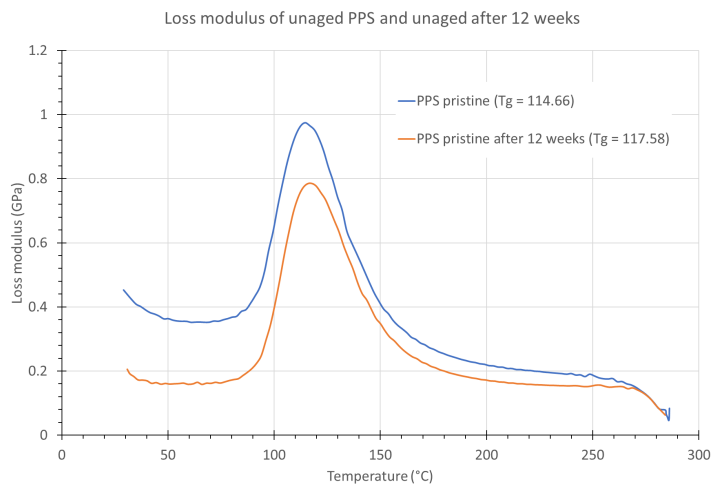


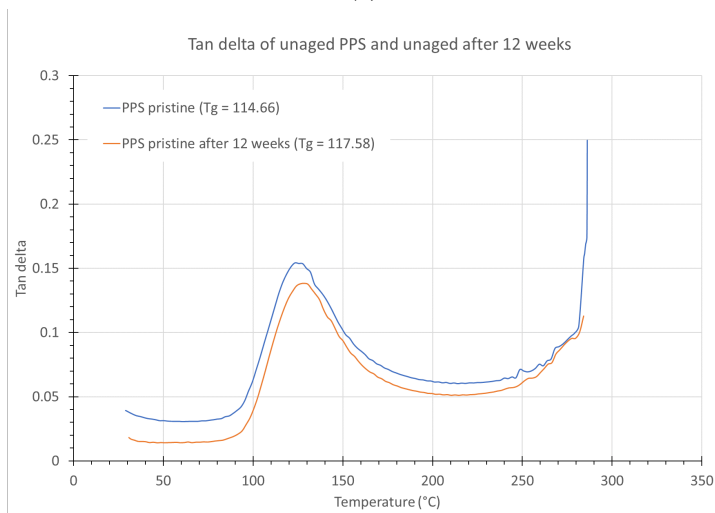
Figure C.21: Stress-strain curves of PPS-40%gf unaged and after 12 weeks of ambient conditions



(a)



(b)



(c)

Figure C.22: DMA curves for unaged PPS-40%gf and after 12 weeks of ambient conditions showing (a) the storage modulus, (b) the loss modulus and (c) tan delta.

Appendix D

Additional results PSU

D.1 Additional Results PSU exposed to oxygen

Weight measurements

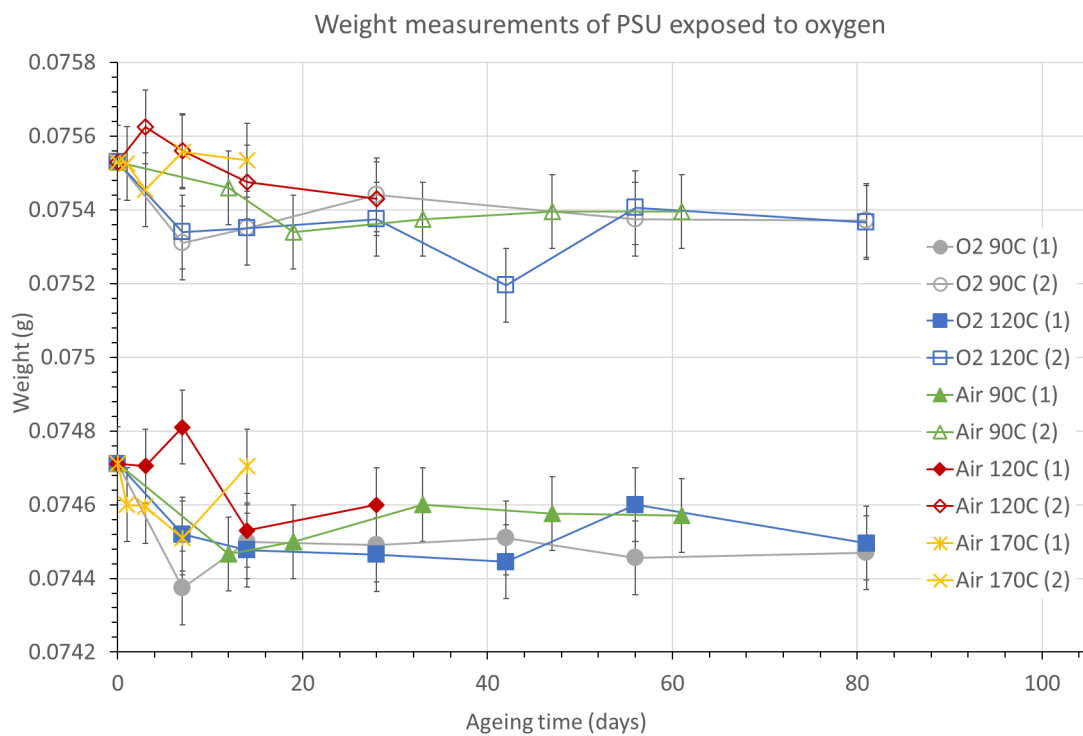
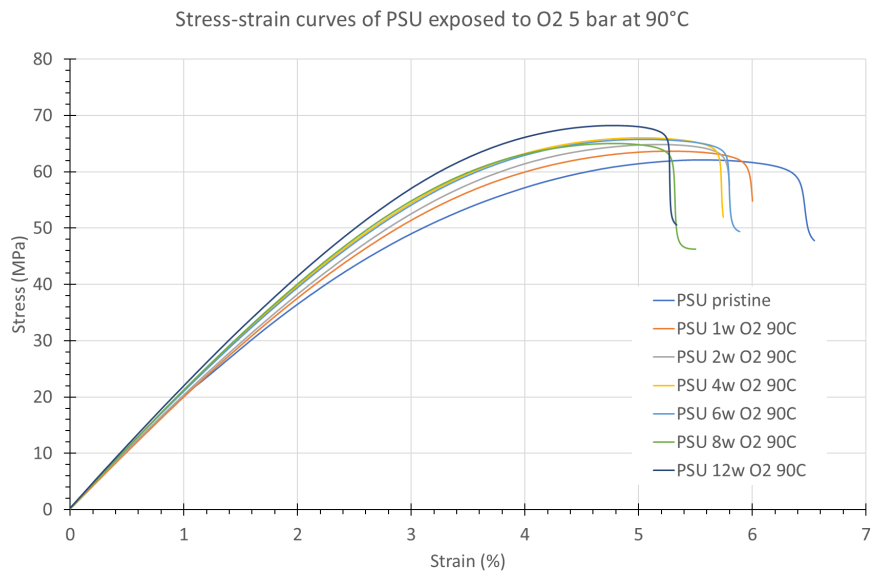
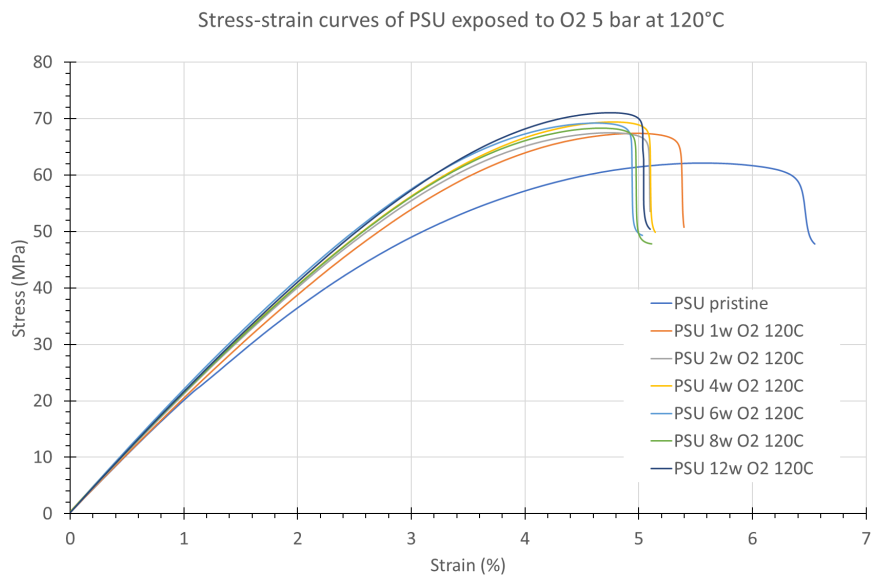


Figure D.1: Graphs showing the weight change of PSU exposed to oxygen over time.

Tensile tests



(a)



(b)

Figure D.2: Stress-strain curves of PSU exposed to oxygen at bar and (a) 90 °C and (b) 120 °C.

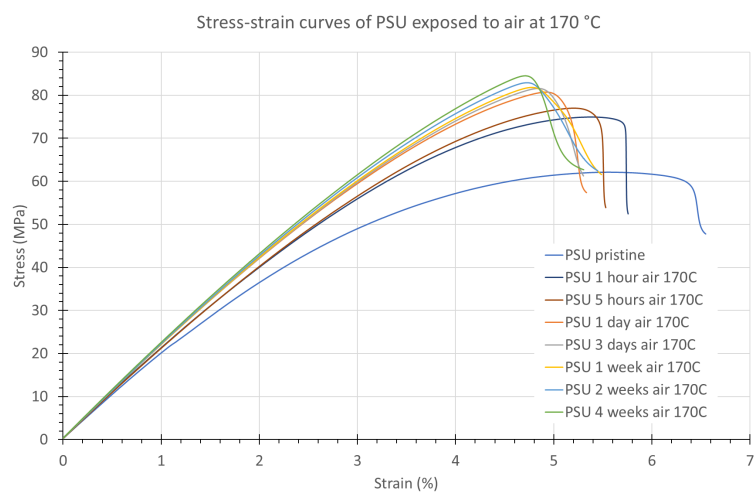
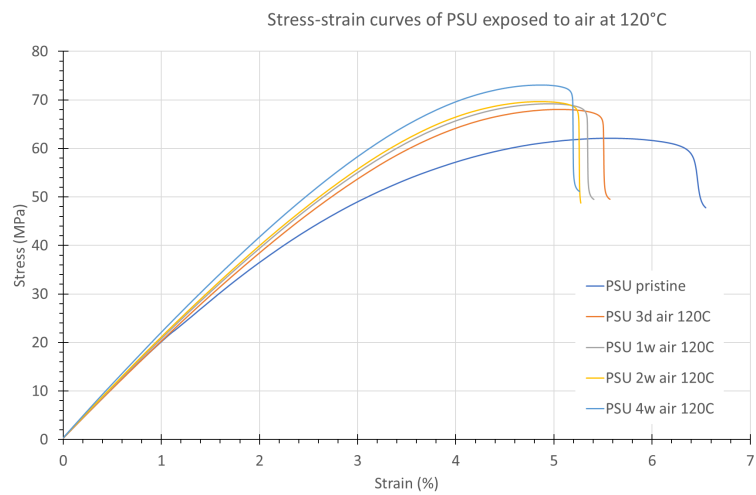
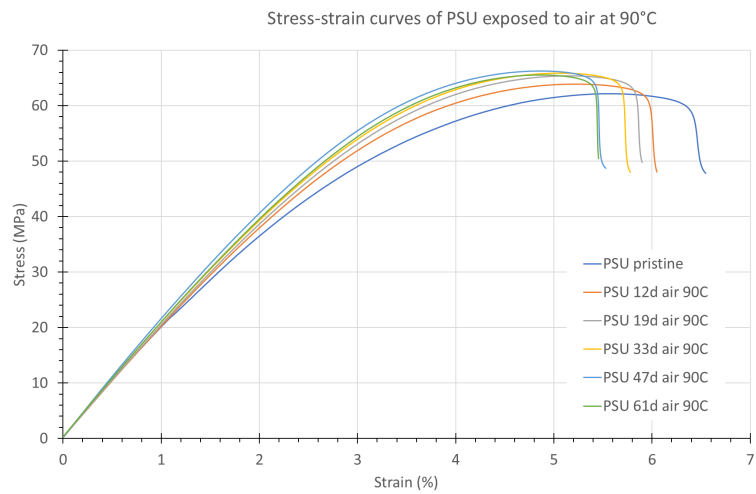


Figure D.3: Stress-strain curves of PSU exposed to air at (a) 90 °C, (b) 120 °C and (c) 170 °C.

DSC

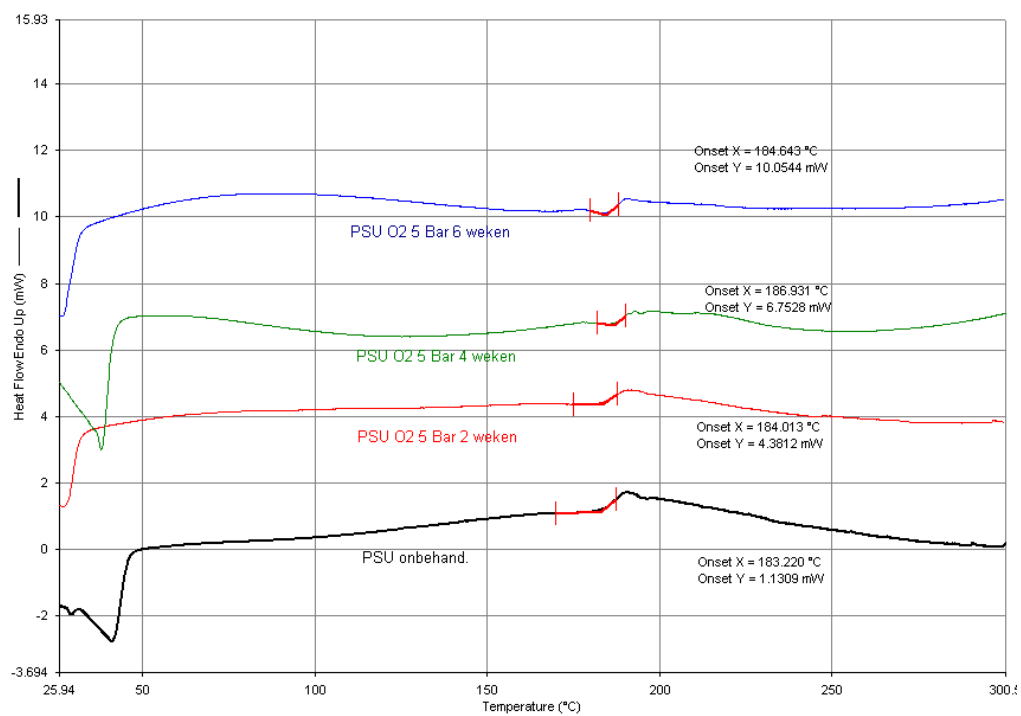


Figure D.4: DSC analysis of different PSU curves exposed to oxygen.

XRD

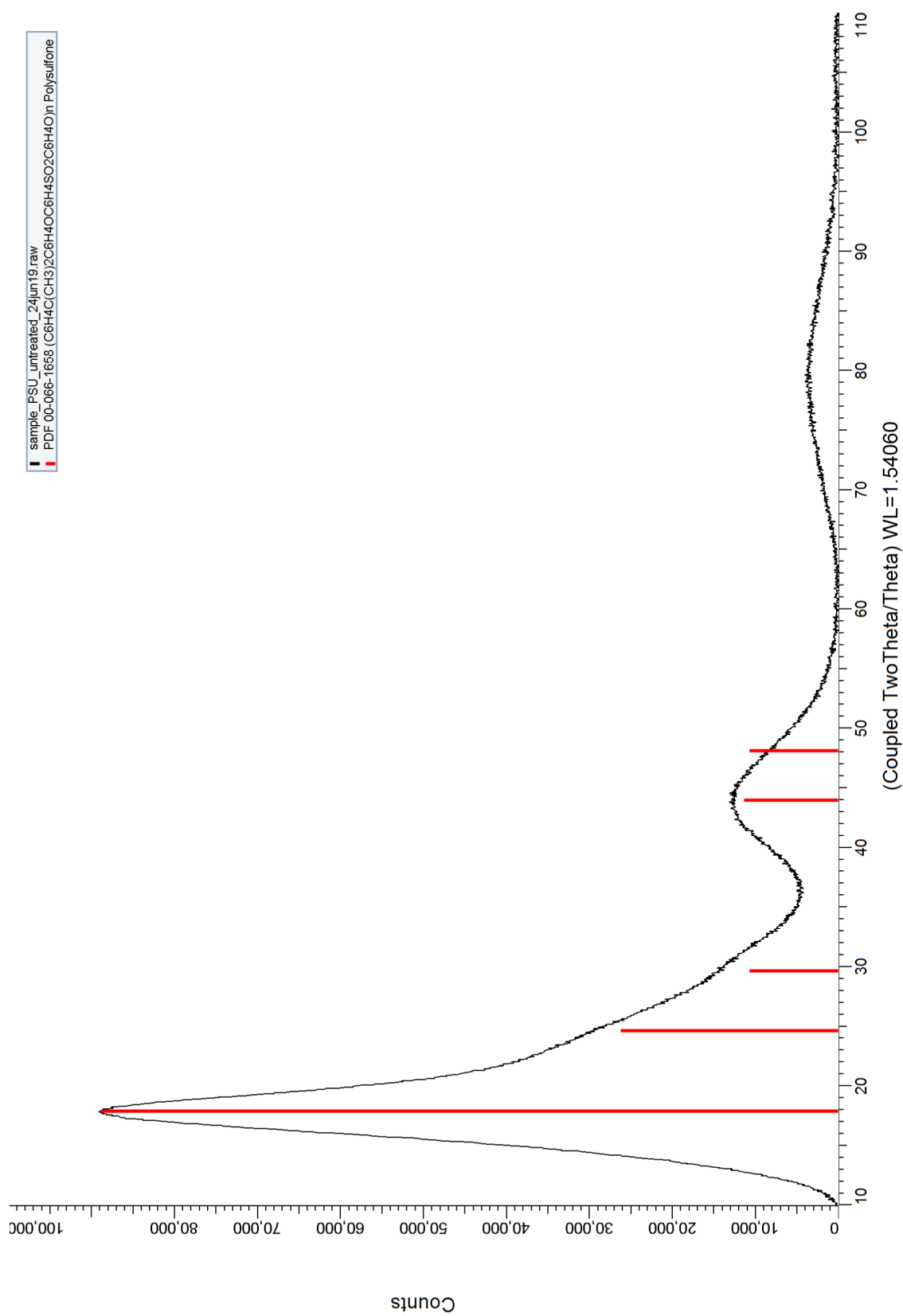


Figure D.5: XRD pattern of unaged PSU.

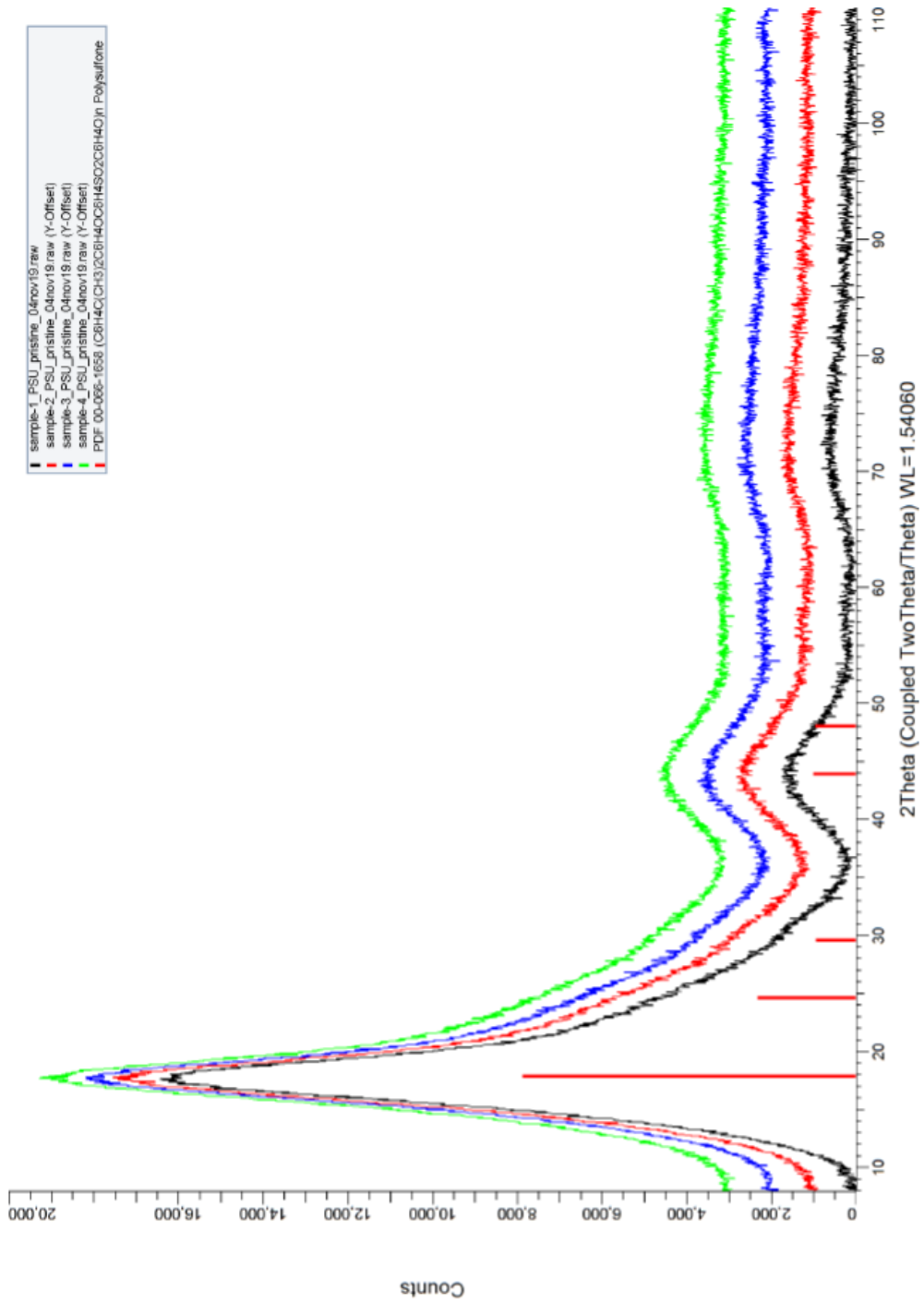


Figure D.6: XRD pattern of 4 different unaged PSU samples. As shown the four curves are nearly identical, meaning the XRD measurements are reproducible.

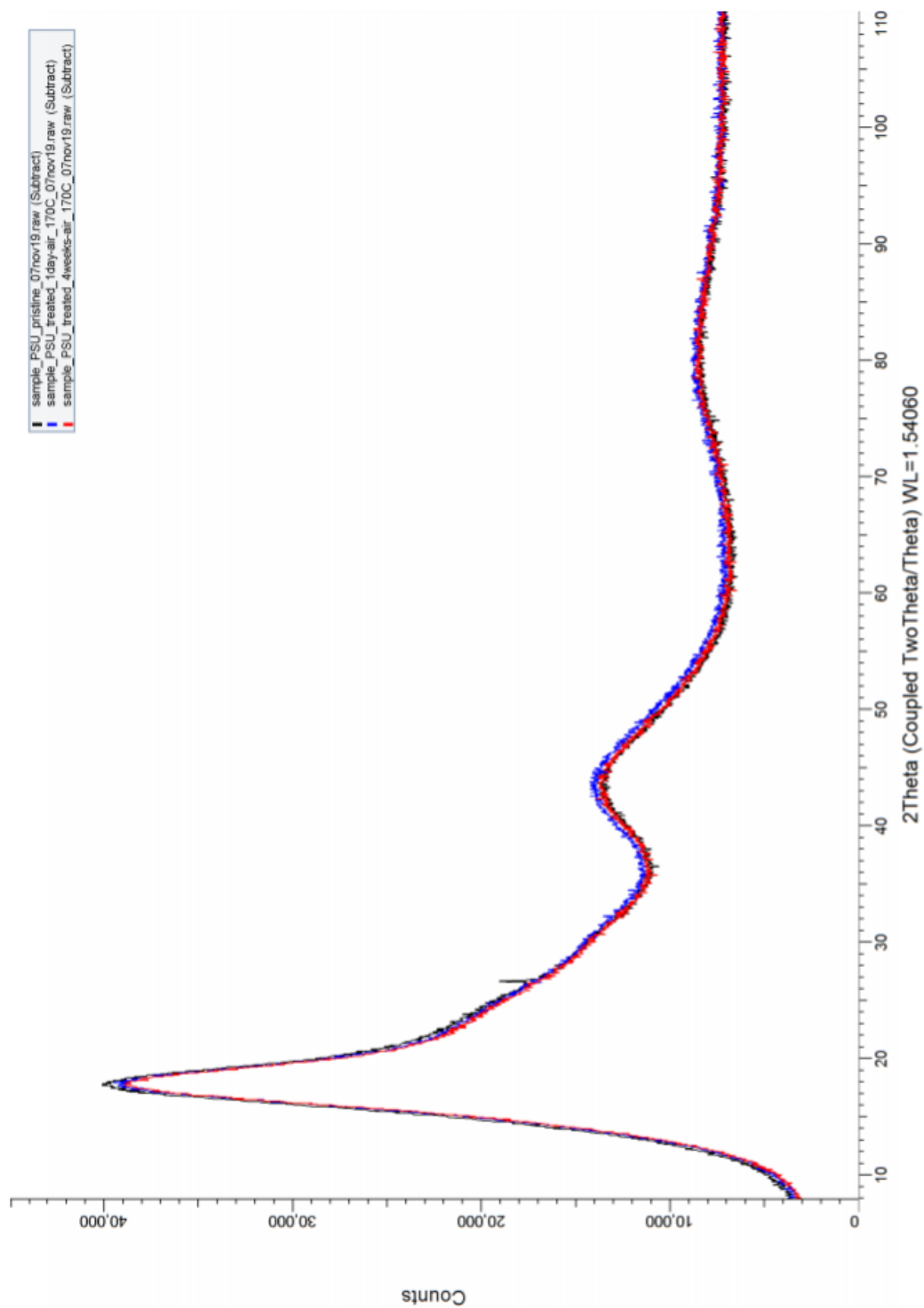
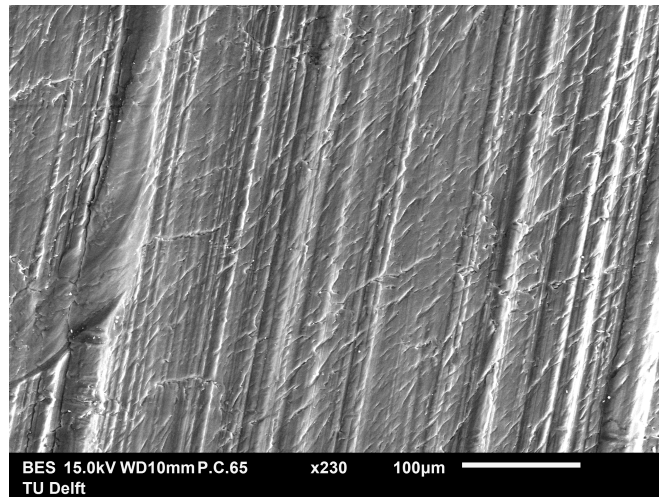
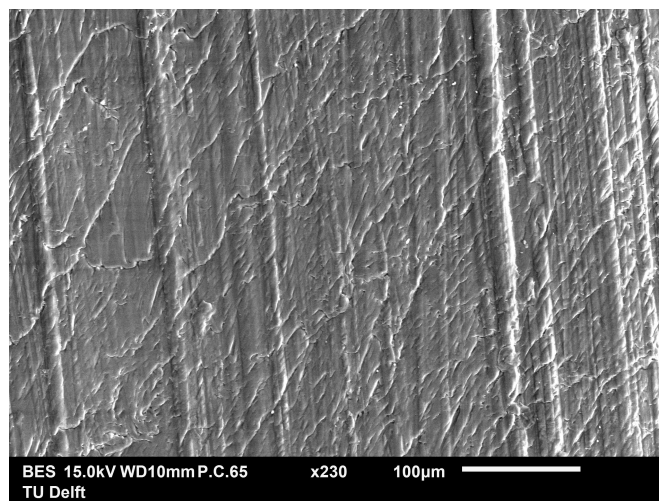


Figure D.7: XRD pattern of unaged PSU in black, PSU exposed to air at 170 °C for 1 day in blue and for 4 weeks in red.

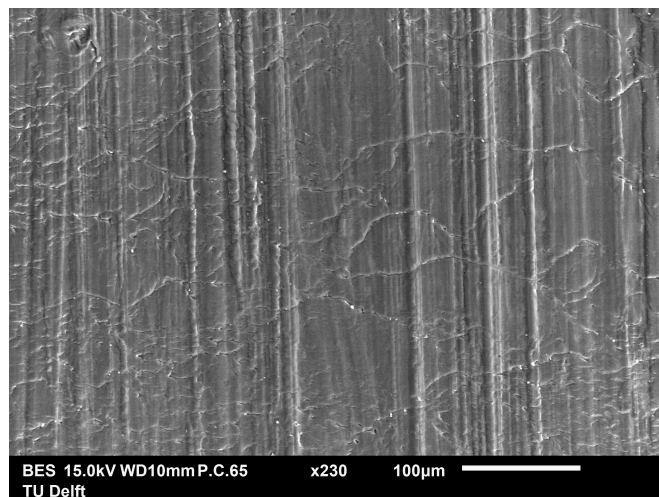
SEM



(a)



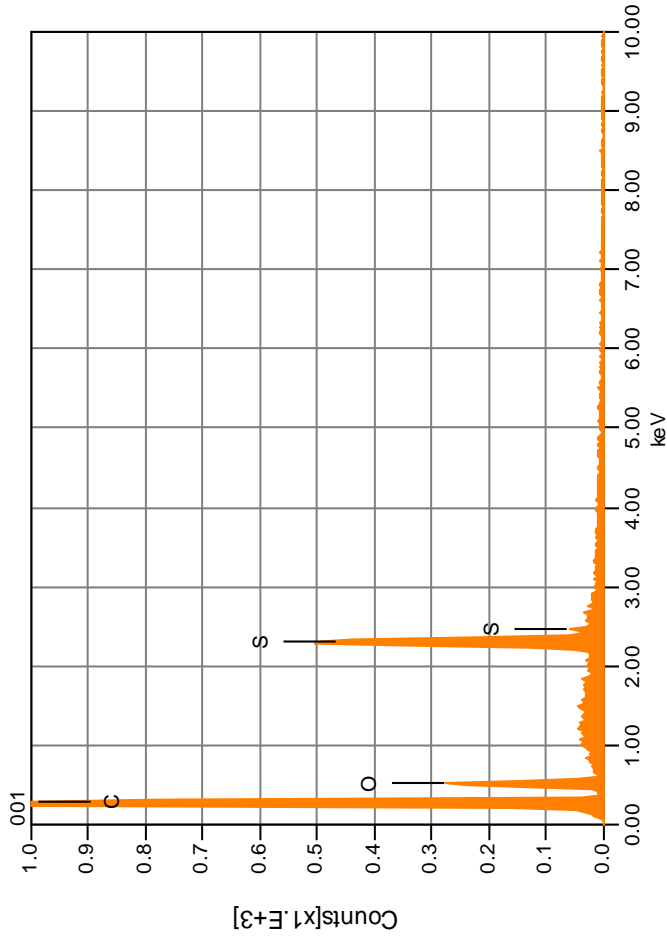
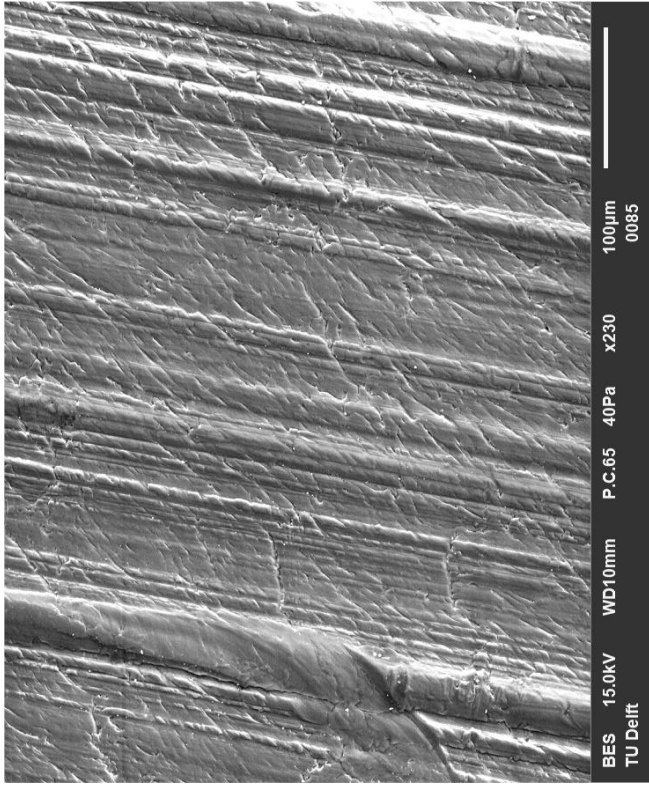
(b)



(c)

Figure D.8: SEM images of the surface of (a) unaged PSU sample (b) PSU exposed to O₂ 5 bar 120 °C for 8 weeks and (c) PSU exposed to a 30wt% KOH solution at 90 °C for 61 days.

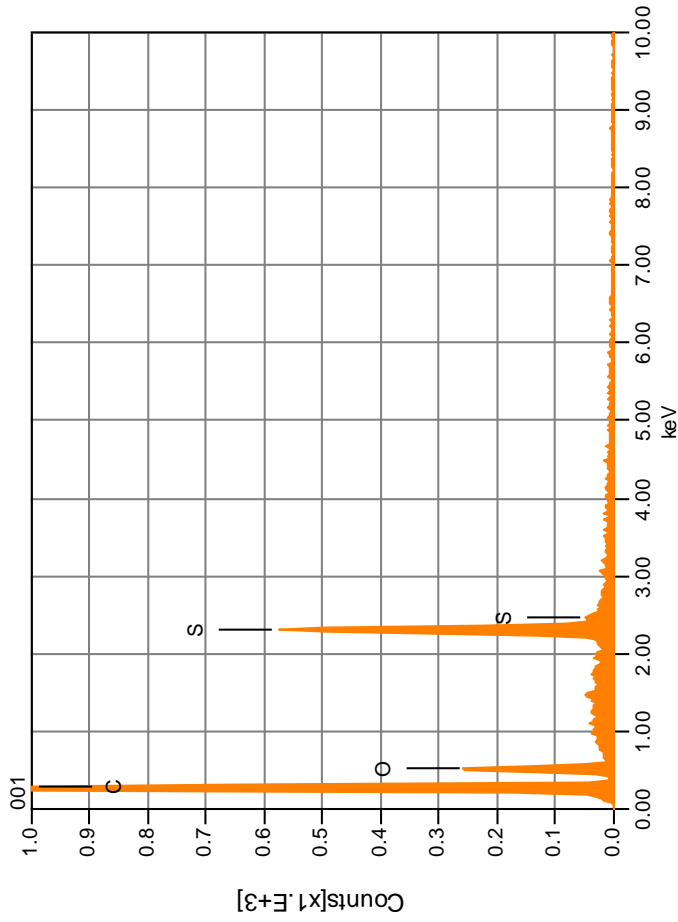
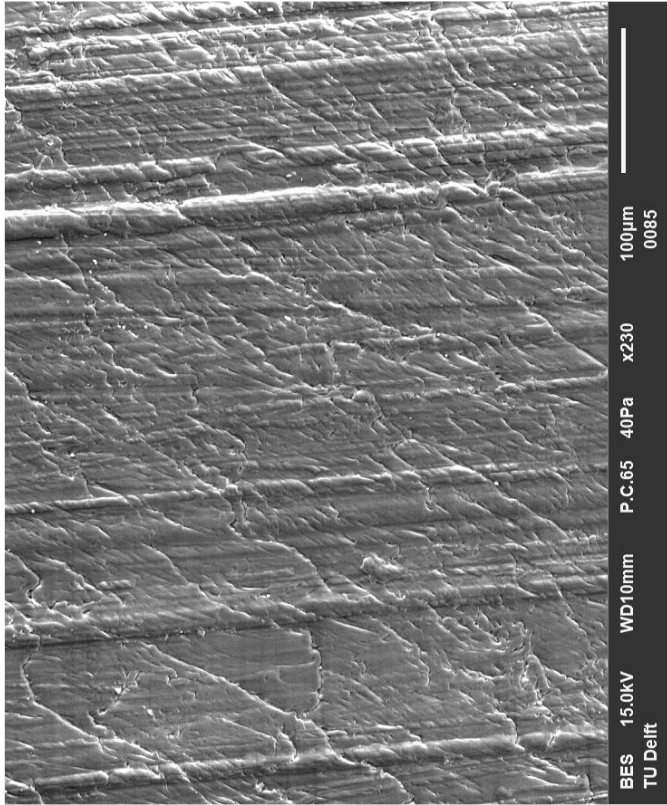
PSU Pristine



Element	mass%	Atom%	Sigma	Net	K ratio	Line
C	74.88	82.14	0.07	53415	0.0157096	K
O	18.25	15.03	0.16	7175	0.0073416	K
S	6.88	2.83	0.06	22098	0.0145225	K
Total	100.00	100.00				

Parameter	Value
Volt	: 15.00 kV
Mag.	: x 230
Date	: 2019/09/10
Pixel	: 960
Instrument	: IT100LA
Volt	: 15.00 kV
Current	: ---
Process Time	: T4
Live time	: 30.00 sec.
Real Time	: 30.79 sec.
Formula	: C O S Total

PSU 8 weeks O2 5 bar 120°C



		Acquisition Condition		Formula		mass%		Atom%		Sigma		Net		K ratio		Line	
Volt	: 15.00 kV	Instrument	: IT100LA	C		74.83	82.26	0.07	51827			0.0152426					K
Mag.	: x 230	Volt	: 15.00 kV	O		17.84	14.73	0.16	6994			0.0071568					K
Date	: 2019/09/10	Current	: ---	S		7.33	3.02	0.06	23594			0.0155058					K
Pixel	: 960	Process Time	: T4	Total		100.00	100.00										
		Live time	: 30.00														
		Real Time	: 30.77														
			sec.														
			sec.														

D.2 Additional Results PSU exposed to KOH

Weight measurements

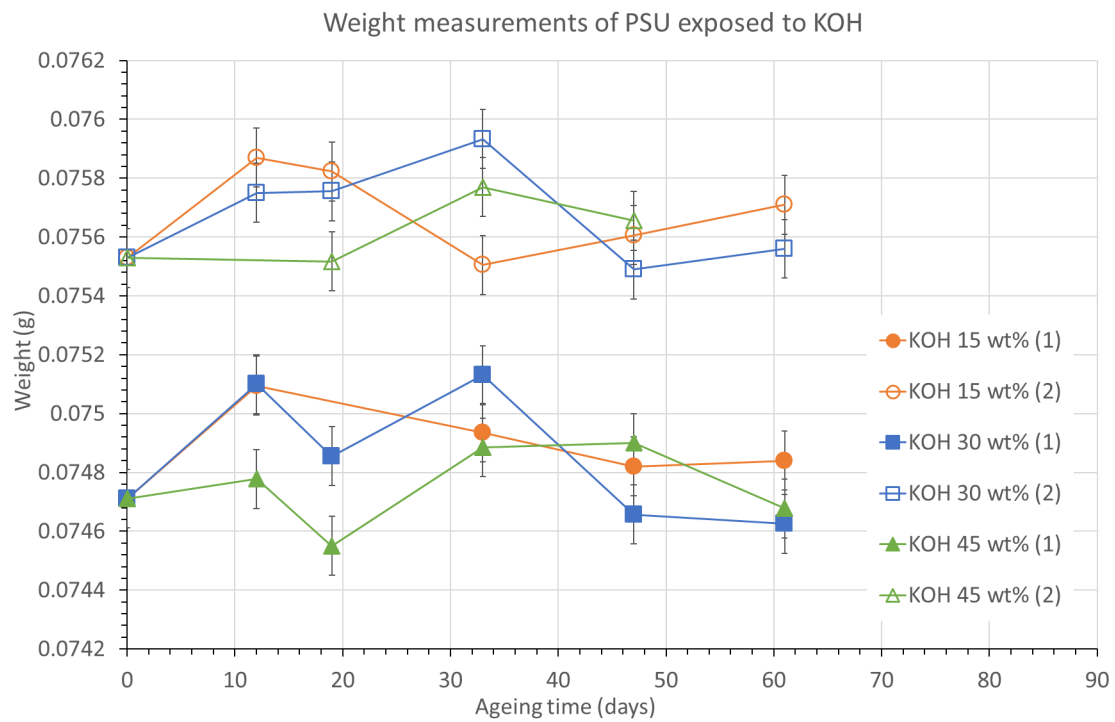
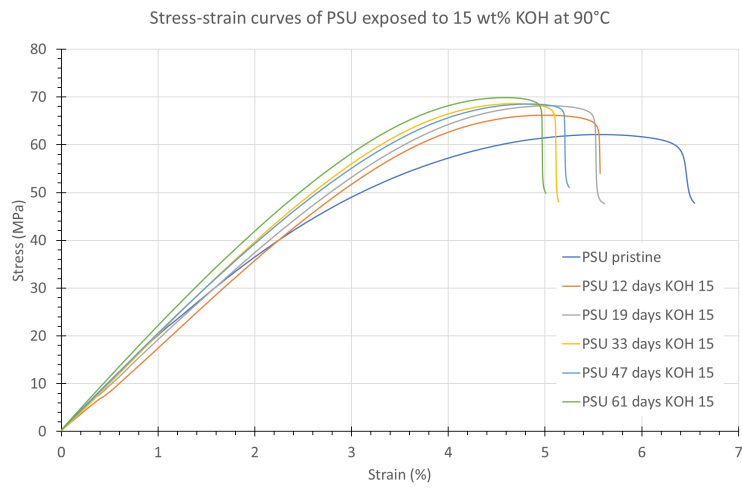
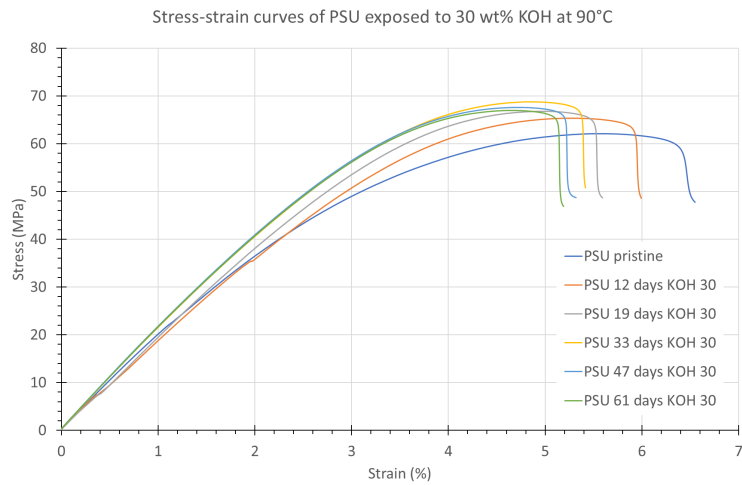


Figure D.9: Graphs showing the weight change of PSU exposed to KOH at 90 °C over time.

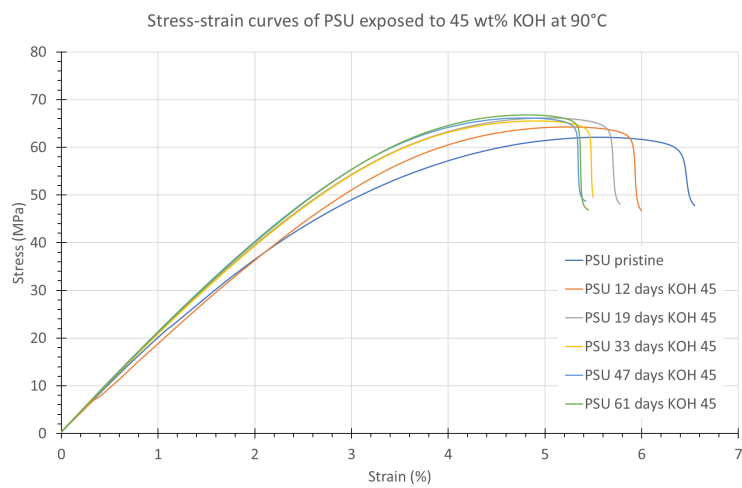
Tensile tests



(a)



(b)



(c)

Figure D.10: Stress-strain curves of PSU exposed to (a) 15, (b) 30 and (c) 45wt% KOH at 90 °C.

DSC

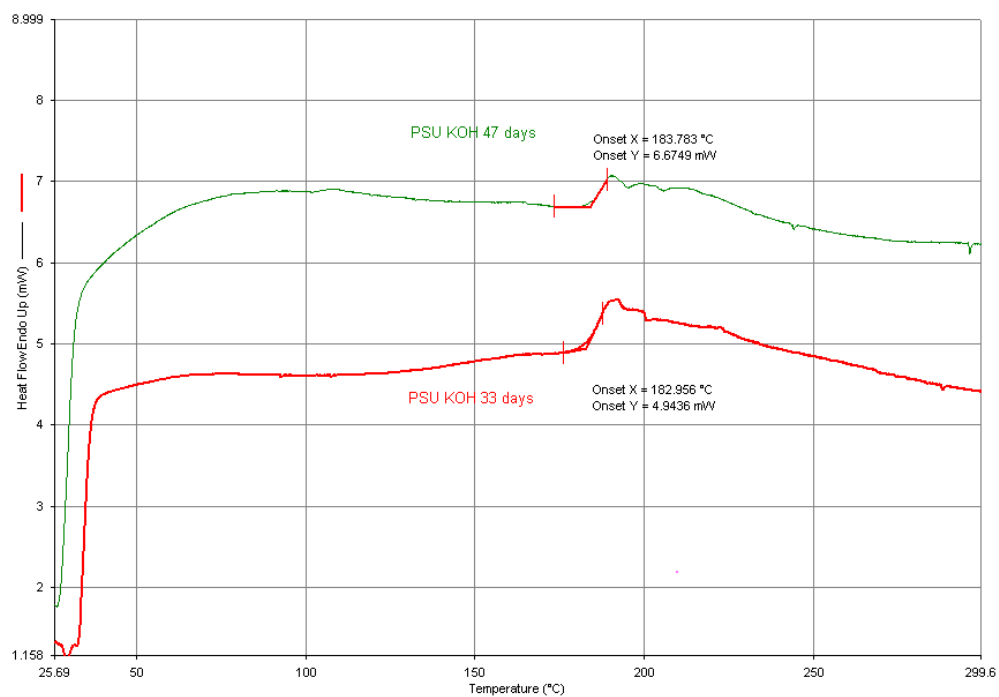


Figure D.11: DSC analysis of different PSU curves exposed to KOH.

SEM

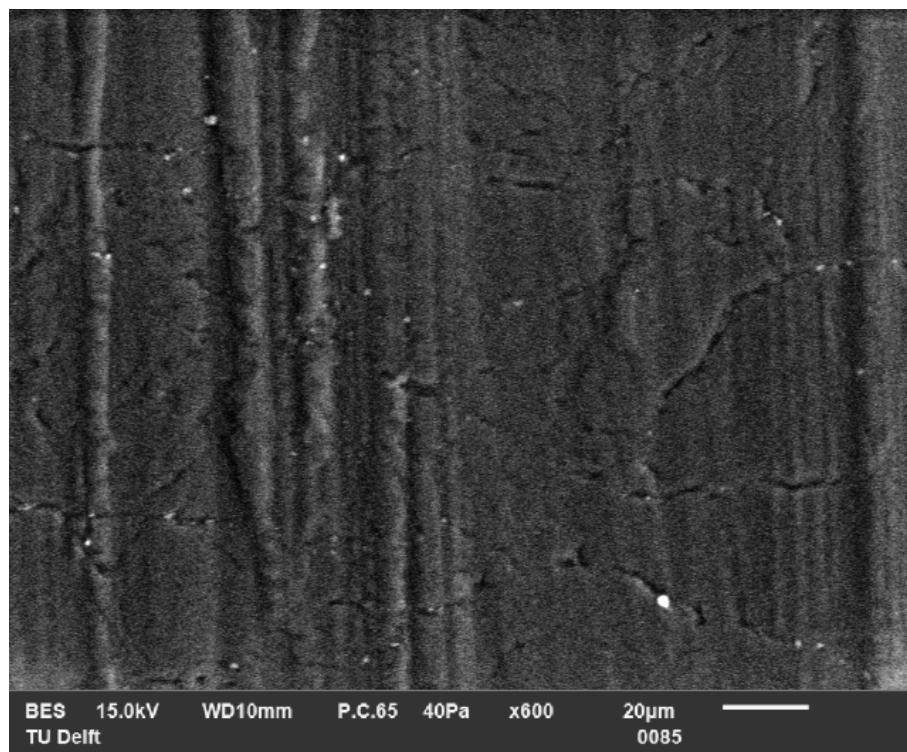
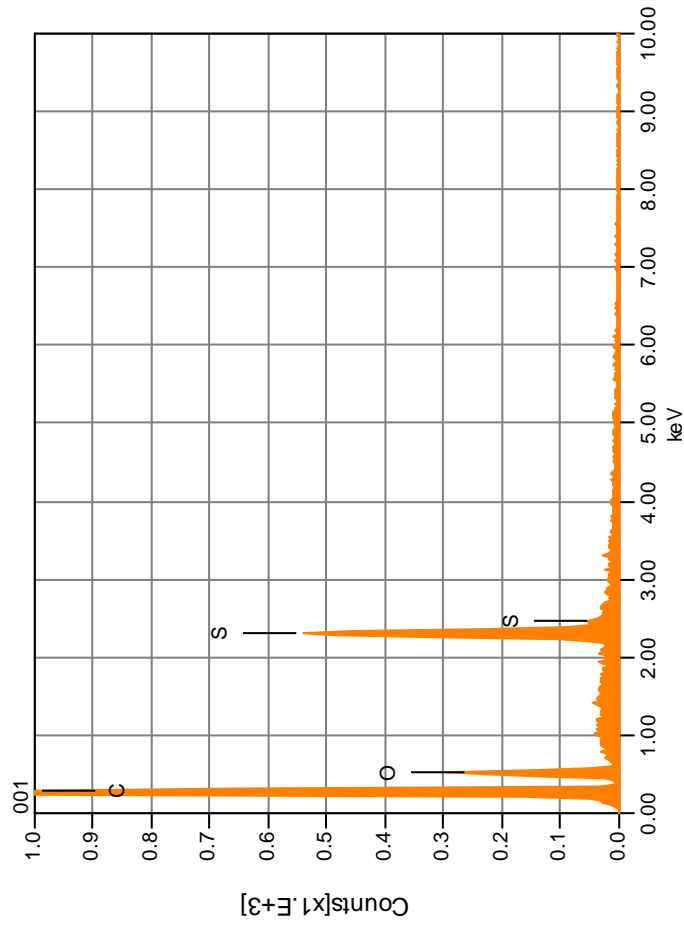
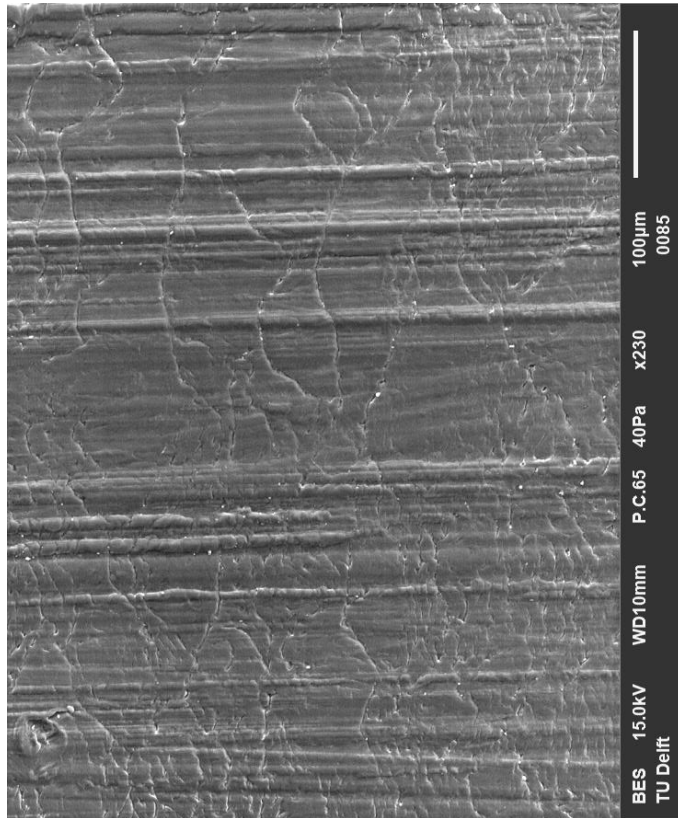


Figure D.12: SEM 600x magnification of the surface of PSU exposed to KOH 30wt% at 90 °C for 61 days. The small white dots are KOH precipitates.

PSU 61 days KOH 30wt% 90 °C

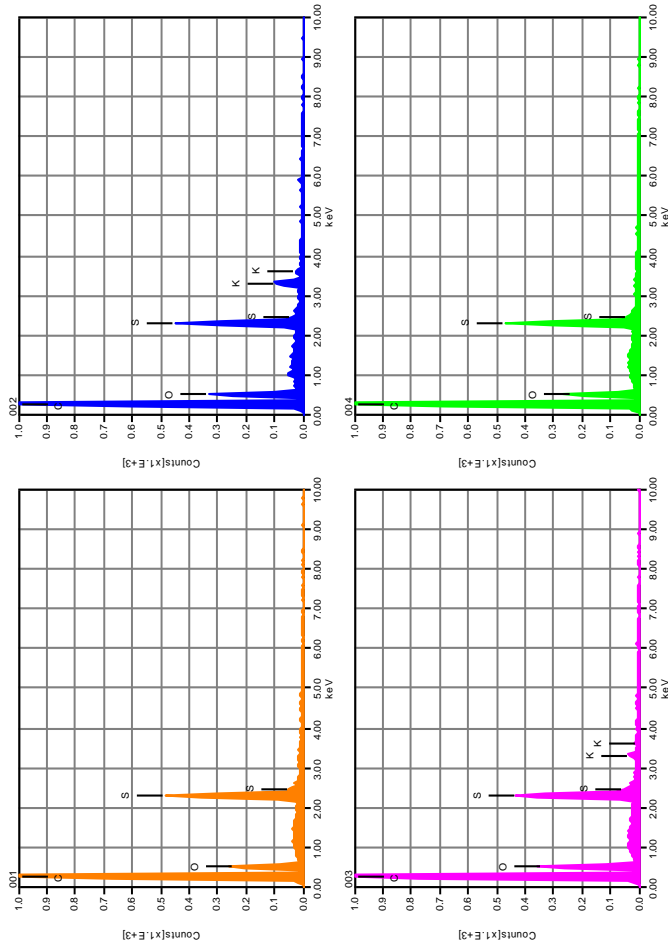
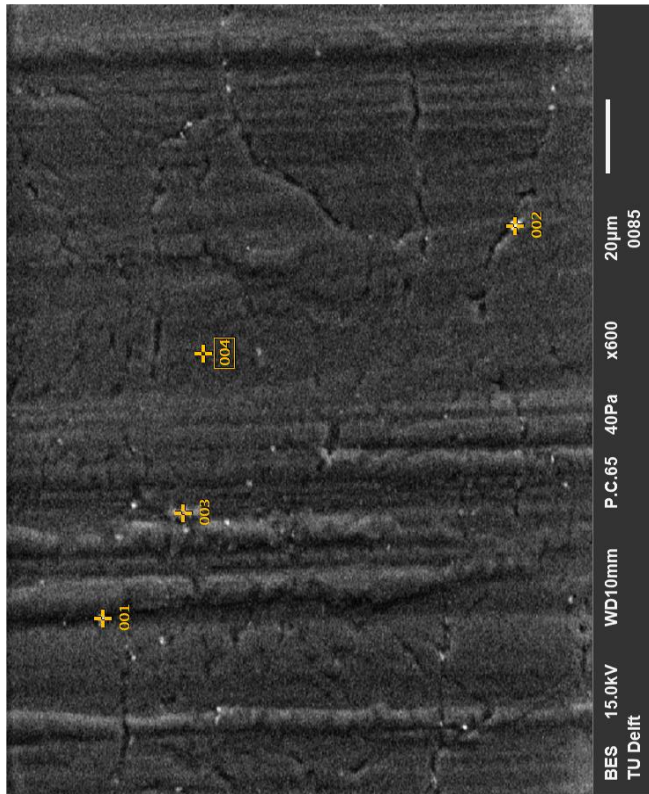


	mass%	Atom%	Sigma	Net	K ratio	Line
C	75.10	82.43	0.07	53012	0.0155911	K
O	17.76	14.63	0.16	6977	0.0071392	K
S	7.14	2.94	0.06	23088	0.0151733	K
Total	100.00	100.00				

	Formula
C	C
O	O
S	S
Total	Total

Volt : 15.00 kV
 Mag. : x 230
 Date : 2019/09/10
 Pixel : 960
 Instrument : IT100LA
 Volt : 15.00 kV
 Current : ---
 Process Time : T4
 Live time : 30.00 sec.
 Real Time : 30.78 sec.

PSU 61 days KOH 30wt% 90°C with KOH precipitation on surface



	K	O	C	S
Volt	15.00 kV			
Mag.	x 600			
Date	2019/09/10			
Pixel	640 x 480			
Instrument	ITI00LA			
Volt	15.00 kV			
Current	---			
Process Time	T4			
Live time	30.00			
Real Time	30.75			
Acquisition Condition				
	2.11	22.89	69.06	5.95
	0.38	20.87	73.07	5.68
	18.50	75.06	6.45	
	18.08	75.40	6.51	

D.3 PSU unaged and after 12 weeks

Figure D.13 shows the stress-strain curve of PSU unaged and unaged after 12 weeks in ambient conditions. It is clear that the curves are very similar. The UTS is in both cases 62.2 ± 1 , the strain at UTS is both 5.5 ± 0.1 and the toughness is for both cases 2.3 ± 0.1 . The Young's modulus is 2.07 ± 0.05 for the unaged case and 2.09 ± 0.05 for the unaged after 12 weeks case. Thus, no physical ageing has occurred for the PSU samples, which is expected for the relatively short time period of 12 weeks.

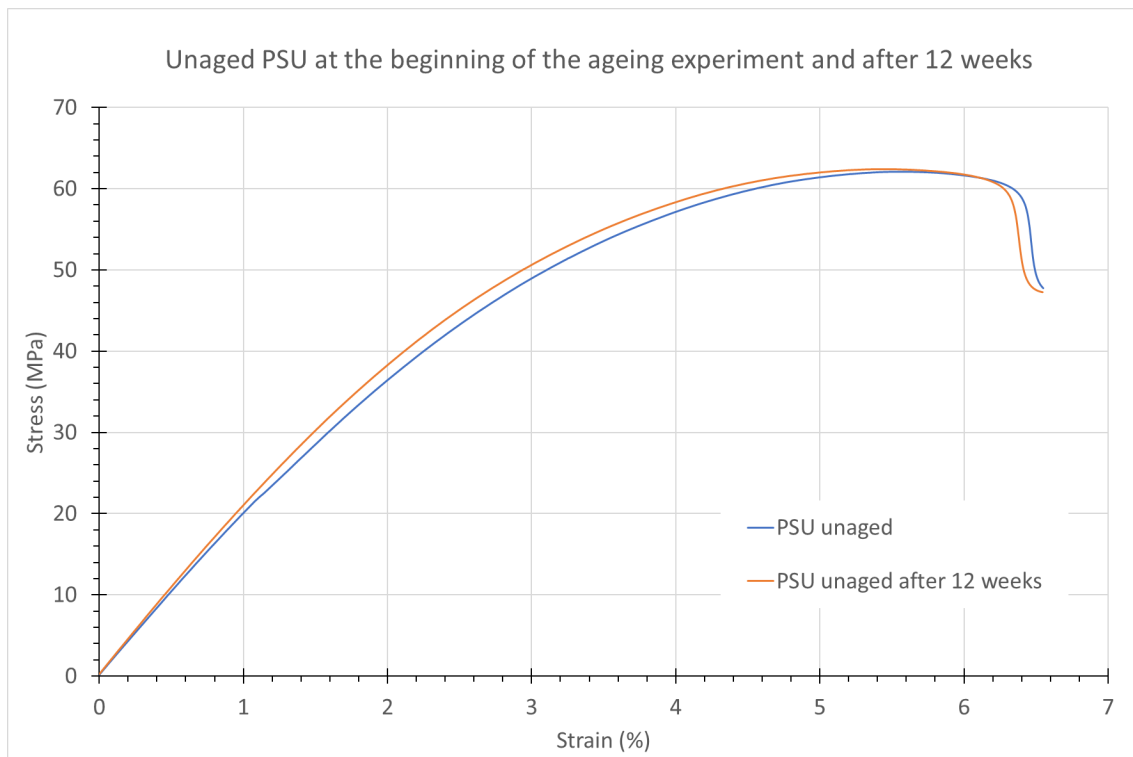


Figure D.13: Stress-strain curves of unaged PSU.